



NOAA Technical Memorandum OAR ARL-247



**ISSUES AFFECTING DISPERSION NEAR HIGHWAYS: LIGHT WINDS, INTRA-URBAN
DISPERSION, VEHICLE WAKES, AND THE ROADWAY-2 DISPERSION MODEL**

R. P. Hosker, Jr.
K. S. Rao
R. L. Gunter
C. J. Nappo
T. P. Meyers

Atmospheric Turbulence and Diffusion Division
Oak Ridge, Tennessee

K. R. Birdwell
J. R. White

Oak Ridge Associated Universities
Oak Ridge, Tennessee

Air Resources Laboratory
Silver Spring, Maryland
February 2003

**Reproduced from
best available copy.**



**PROTECTED UNDER INTERNATIONAL COPYRIGHT
ALL RIGHTS RESERVED
NATIONAL TECHNICAL INFORMATION SERVICE
U.S. DEPARTMENT OF COMMERCE**

REPRODUCED BY: **NTIS**
U.S. Department of Commerce
National Technical Information Service
Springfield, Virginia 22161

NOAA Technical Memorandum OAR ARL-247

**ISSUES AFFECTING DISPERSION NEAR HIGHWAYS: LIGHT WINDS, INTRA-URBAN
DISPERSION, VEHICLE WAKES, AND THE ROADWAY-2 DISPERSION MODEL**

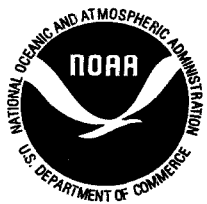
R. P. Hosker, Jr.
K. S. Rao
R. L. Gunter
C. J. Nappo
T. P. Meyers

Atmospheric Turbulence and Diffusion Division
Oak Ridge, Tennessee

K. R. Birdwell
J. R. White

Oak Ridge Associated Universities
Oak Ridge, Tennessee

Air Resources Laboratory
Silver Spring, Maryland
February 2003



**UNITED STATES
DEPARTMENT OF COMMERCE**

**Donald L. Evans
Secretary**

**NATIONAL OCEANIC AND
ATMOSPHERIC ADMINISTRATION**

**VADM Conrad C. Lautenbacher, Jr.
Under Secretary for Oceans
and Atmosphere/Administrator**

**Oceanic and Atmospheric
Research Laboratories**

**David L. Evans
Director**

NOTICE

Mention of a commercial company or product is for information purposes only, and does not constitute an endorsement by NOAA's Oceanic and Atmospheric Research Laboratories. Use for publicity or advertising purposes of information from this publication concerning proprietary products or the tests of such products is not authorized.

ATDD Contribution File No. 01-08

TABLE OF CONTENTS

List of Figures	vi
List of Tables	x
Abstract	1
1. Introduction	2
1.1 Urban Dispersion Issues	2
1.2 Dispersion Near Roadways	5
1.3 Vehicle Wake Issues	9
1.4 Guide to this Report	11
2. Characteristics of Light Winds	12
2.1 Introduction	12
2.2 Study Areas	13
2.2.1 Southern Appalachians	13
2.2.2 Snake River Plain, Idaho	14
2.2.3 Cape Canaveral, Florida	16
2.3 Method of Research	17
2.3.1 Analysis of Wind Rose Change with Respect to Low Wind Speeds	17
2.3.2 Change in Wind Direction and Speed with Respect to Winds Aloft	17
2.3.3 Wind Rose Computation by Site and Time of Day and Subsequent Site to Site Comparisons	20
2.3.4 Wind Speed Distribution with Respect to Time of Day	21
2.3.5 Duration of Calm Winds	21
2.4. Analysis of Wind Rose Changes at low wind speeds: ETOS Network	21
2.4.1 Mountain Sites: T223 (Cove Mountain) and T224 (Buffalo Mountain) ..	22
2.4.2 Ridge Top Sites: T110 (Pine Ridge) and T119 (Walker Branch)	24
2.4.3 Valley Bottom Sites: T001 (NOAA Office) and T004 (Scarboro)	25
2.4.4 Plateau Sites: T330 (Allardt) and T331 (Spencer)	27
2.4.5 Knoxville McGhee-Tyson ASOS Site	28
2.5 Analysis of Wind Rose Changes for Low Wind Speeds: INEEL Network	28
2.5.1 Mountain Valley Site: BLU (Blue Dome)	28
2.5.2 High Valley Sites: ARC (Arco), CRA (Craters of Moon Monument), and EBR (Lava Zone)	29
2.5.3 Low Valley Sites: BLA (Blackfoot), and IDA (Idaho Falls)	30
2.6 Analysis of Wind Rose Changes for Low Wind Speeds: Cape Canaveral	31
2.7 Changes in Wind Direction and Speed with respect to Winds Aloft	32
2.7.1 Comparison of Site T110 (Pine Ridge) with Site T224 (Buffalo Mountain)	32
2.7.1.1 During light winds (< 1.5 m/s) at site T224 (Buffalo Mountain)	33

2.7.1.2	During moderate winds (1.5 to 3.5 m/s) at site T224 (Buffalo Mountain)	33
2.7.1.3	During stronger winds (> 3.5 m/s) at site T224 (Buffalo Mountain)	34
2.7.1.4	Summary of comparison of T110 (Pine Ridge) winds with T224 (Buffalo Mountain) winds	36
2.7.2	Comparison of Site T003 (Oak Ridge Municipal Building) with Site T110 (Pine Ridge)	36
2.7.2.1	During light winds (< 1.5 m/s) at site T110 (Pine Ridge)	36
2.7.2.2	During moderate to strong winds (\geq 1.5 m/s) at site T110 (Pine Ridge)	37
2.8	Wind Rose Computation by Site and Time of Day and Subsequent Site-to-Site Comparisons	37
2.8.1	ASOS Comparison: Site KTYS Knoxville McGhee-Tyson Airport and Site KOQT Oak Ridge	37
2.8.2	ASOS /ETOS Comparison: Oak Ridge ASOS, T001 (NOAA Office), and T005 (Melton Hill Lake)	38
2.9	Wind Speed Distribution with respect to Time of Day	39
2.9.1	Mountain Zones: Sites T223 (Cove Mtn) and T224 (Buffalo Mtn)	39
2.9.2	Ridge Top Zone: Sites T110 (Pine Ridge) and T119 (Walker Branch)	39
2.9.3	Valley Bottom Zone: Sites T001 (NOAA Office) and T004 (Scarboro)	40
2.9.4	Plateau Zone: Sites T330 (Allardt) and T331 (Spencer)	40
2.10	Durations of Calm and Light Winds	40
2.11	Conclusions	41
2.12	Recommendations	41
3.	Urban Turbulence Field Studies	42
3.1	Introduction	42
3.2.	Urban Site Characteristics	42
3.2.1	Knoxville, TN	42
3.2.2	Nashville, TN	46
3.3	Turbulence Instrumentation	48
3.4	Urban Turbulence Results	50
3.5	Conclusions	53
4.	Vehicle Wake Turbulence Field Studies	55
4.1	Introduction	55
4.2	Site	55
4.3	Instrumentations and Apparatus	55
4.4	Data Processing Method for TKE	57
4.5	Results	58
4.6	Contours of Wake Turbulent Kinetic Energy	75
4.7	Mean Flow Vectors in the Wake	78
4.8	Sources of Errors	82
4.9	Summary	95

5. Modeling of Pollutant Dispersion near Highways	97
5.1 Introduction	97
5.2 ROADWAY-2 Formulations	98
5.2.1 ABL model	99
5.2.1.1 Initial Profiles	101
5.3 Vehicle Wake Parameterizations	102
5.3.1 Extension to multiple vehicles	105
5.4 Numerical Solution	106
5.4.1 Eddy diffusivities	106
5.4.2 Initial dispersion	107
5.4.3 ROADWAY-2 user's guide	107
5.5 ROADWAY-2 Evaluation	108
5.5.1 GM experiment	108
5.5.2 Data classification	110
5.5.3 Evaluation results	110
5.6 Conclusions and Recommendations	114
6. Summary, Conclusions, and Recommendations	115
6.1 Light Winds	115
6.2 Intra-Urban Wind Data	117
6.3 Vehicle Wakes	118
6.4 ROADWAY-2 Dispersion Model	119
6.5 Suggestions for Future Research	119
7. Acknowledgments	121
8. References	122
Appendix A: Wind Rose Analysis With Respect to Low Wind Speeds	
Part 1: Analysis of Wind Rose Changes with Respect to Low Wind Speeds	
Plots	A-1
Appendix B: Wind Rose Analysis With Respect to Low Wind Speeds	
Part 2: Changes in Wind Direction and Speed with Respect to Winds Aloft Plots	B-1
Appendix C: Wind Rose Analysis With Respect to Low Wind Speeds	
Part 3: Wind Rose Computation by Site and Time of Day and Subsequent Site-to-Site	
Comparison Plots	C-1
Appendix D: Wind Rose Analysis With Respect to Low Wind Speeds	
Part 4: Wind Speed Distribution with Respect to Time of Day Plots	D-1
Appendix E: Wind Rose Analysis With Respect to Low Wind Speeds	
Part 5: Duration of Calm and Light Winds Plots	E-1

LIST OF FIGURES

Figure 2.1 ETOS sites used in the low wind analysis	13
Figure 2.2 INEEL sites used in the low wind analysis	15
Figure 2.3 Location of Cape Canaveral with respect to the Central Florida Peninsula	16
Figure 2.4 Sites used for analysis in Wind Rose Computation by Site and Time of Day and Subsequent Site to Site Comparisons.	20
Figure 2.5 Percent of valley bottom winds within 22.5° of local ridge axes with respect to valley width.	26
Figure 2.6 Idealized zones of positive forcing for four wind forcing mechanisms with respect to wind above and within the Great Valley	35
Figure 3.1 Aerial view of Knoxville site, looking from the west (top); north (bottom)	43
Figure 3.2 Aerial view of Knoxville site, looking from the southeast. Parking garage is visible at center	44
Figure 3.3 View of equipment installation on Knoxville parking garage roof, looking to the south	45
Figure 3.4 View of equipment installation on Knoxville parking garage roof, looking west. Equipment is visible at lower center	45
Figure 3.5 Aerial view of Nashville, looking east. The experimental site is to the north (left), just out of the picture	46
Figure 3.6 Aerial view of Nashville site, looking south. The experimental site is within the parking lot south of the large, low flat-roofed building located just east (left) of Bicentennial Park	47
Figure 3.7 Ground level view of installation in Nashville, looking south-southwest	47
Figure 3.8 View of installation at the Lebanon airport near Nashville	48
Figure 3.9 Figs. a, b, c, d are scatterplots of observations of mean wind speed, standard deviation of mean wind speed, wind direction, and standard deviation of wind direction, respectively, for the urban Knoxville and the Sharp's Ridge sites	51
Figure 3.10 As for Figure 3.9, but for the urban Nashville site and the rural Lebanon airport site	52
Figure 3.11 Turbulent kinetic energy (TKE, in m^2/s^2) at urban Knoxville site and the nearby rural University of Tennessee agricultural campus	53
Figure 3.12 As for Figure 3.11, but for the urban Nashville site vs. the rural Lebanon airport site	54
Figure 4.1 Van and trailer configuration for wake turbulence study. Top photo depicts the trailer/sonic setup; lower picture shows view facing northeast	56
Figure 4.2 Power spectral density of TKE for Configurations 1-5, Day 322. The inertial subrange slope is shown on Configuration 1, Run 1. Ambient data are also shown.	61
Figure 4.3 Power spectral density of TKE for Configuration 1, Runs 1-6, Day 335, with the inertial subrange slope shown on Run 1. Ambient data are also shown.	63
Figure 4.4 Power spectral density of TKE for Configuration 2, Runs 1-6, Day 335, with the inertial subrange slope shown on Run 1. Ambient data are also shown.	64
Figure 4.5 Power spectral density of TKE for Configuration 3, Runs 1-6, Day 335, with the inertial subrange slope shown on Run 1. Ambient data are also shown.	65

Figure 4.6 Power spectral density of TKE for Configuration 4, Runs 1-6, Day 335, with the inertial subrange slope shown on Run 1. Ambient data are also shown.	67
Figure 4.7 Power spectral density of TKE for Configuration 5, Runs 1-6, Day 335, with the inertial subrange slope shown on Run 1. Ambient data are also shown.	68
Figure 4.8 Power spectral density of TKE for Configuration 6, Runs 1-6, Day 335, with the inertial subrange slope shown on Run 1. Ambient data are also shown.	69
Figure 4.9 Power spectral density of TKE for Configuration 6, Runs 7 and 8, Day 335, with the inertial subrange slope shown on Run 7. Ambient data are also shown.	70
Figure 4.10 Power spectral density of TKE for Configuration 1, Runs 1-6, Day 336, with the inertial subrange slope shown on Run 1. Ambient data are also shown.	72
Figure 4.11 Power spectral density of TKE for Configuration 2, Runs 1-6, Day 336, with the inertial subrange slope shown on Run 1. Ambient data are also shown.	73
Figure 4.12 Power spectral density of TKE for Configuration 3, Runs 1-6, Day 336, with the inertial subrange slope shown on Run 1. Ambient data are also shown.	74
Figure 4.13 Power spectral density of TKE for Configuration 3, Runs 7 and 8, Day 336, with the inertial subrange slope shown on Run 7. Ambient data are also shown.	75
Figure 4.14 Vertical profiles of turbulent kinetic energy (TKE) in near-wake of vehicle ($x = 2, 9, 16$ ft from rear of vehicle) for road speeds of 30 (13.4 m/s) and 50 mph (22.4 m/s) ...	76
Figure 4.15 Contours in vertical-cross-axis plane of constant values of turbulent kinetic energy (TKE, in m^2/s^2) for three along-wake positions behind a vehicle with a road speed of 30 mph (13.4 m/s) and 50 mph (22.4 m/s).	76
Figure 4.16 Contours in vertical-along-axis plane of constant values of turbulent kinetic energy (TKE, in m^2/s^2) along the wake centerline, for vehicle speeds of 30 (13.4 m/s) and 50 mph (22.4 m/s)	77
Figure 4.17. Vehicle wake flow vectors, cross-section view at $x= 2$ ft (0.61 m), $x= 9$ ft (2.74 m), $x = 16$ ft (4.88 m), respectively, behind vehicle, for speed = 30 mph (13.4 m/s), looking from front to rear, vehicle width = 6.2 ft (1.9 m), height = 6.9 ft (2.1 m), scale for vectors on plots: 1 unit = 2 m/s.	79
Figure 4.18. Vehicle wake flow vectors, cross-section view at $x= 2$ ft (0.61 m), $x= 9$ ft (2.74 m), $x = 16$ ft (4.88 m), respectively, behind vehicle, for speed = 40 mph (17.9 m/s), looking from front to rear, vehicle width = 6.2 ft (1.9 m), height = 6.9 ft (2.1 m), scale for vectors on plots: 1 unit = 2 m/s.	80
Figure 4.19 Vehicle wake flow vectors, cross-section view at $x= 2$ ft (0.61 m), $x= 9$ ft (2.74 m), $x = 16$ ft (4.88 m), respectively, behind vehicle, for speed = 50 mph (22.4 m/s), looking from front to rear, vehicle width = 6.2 ft (1.9 m), height = 6.9 ft (2.1 m), scale for vectors on plots: 1 unit = 2 m/s.	81
Figure 4.20. Vehicle wake flow vectors, cross-section view at $z = 6$ ft (1.83 m), $z= 7$ ft (2.13 m), $z = 8$ ft (2.44 m), respectively, above ground, for speed = 30 mph (13.4 m/s), looking from above, vehicle width = 6.2 ft (1.9 m), height = 6.9 ft (2.1 m), scale for vectors on plots: 1 unit = 2 m/s.	83
Figure 4.21. Vehicle wake flow vectors, cross-section view at $z = 9$ ft (2.74 m), $z= 11$ ft (3.35 m), $z = 12$ ft (3.66 m), respectively, above ground, for speed = 30 mph (13.4 m/s), looking from above, vehicle width = 6.2 ft (1.9 m), height = 6.9 ft (2.1 m), scale for vectors on plots: 1 unit = 2 m/s	84

Figure 4.22. Vehicle wake flow vectors, cross-section view at $z = 6$ ft (1.83 m), $z = 7$ ft (2.13 m), $z = 8$ ft (2.44 m), respectively, above ground, for speed = 40 mph (17.9 m/s), looking from above, vehicle width = 6.2 ft (1.9 m), height = 6.9 ft (2.1 m), scale for vectors on plots: 1 unit = 2 m/s	85
Figure 4.23. Vehicle wake flow vectors, cross-section view at $z = 9$ ft (2.74 m), $z = 11$ ft (3.35 m), $z = 12$ ft (3.66 m), respectively, above ground, for speed = 40 mph (17.9 m/s), looking from above, vehicle width = 6.2 ft (1.9 m), height = 6.9 ft (2.1 m), scale for vectors on plots: 1 unit = 2 m/s.	86
Figure 4.24. Vehicle wake flow vectors, cross-section view at $z = 6$ ft (1.83 m), $z = 7$ ft (2.13 m), $z = 8$ ft (2.44 m), respectively, above ground, for speed = 50 mph (22.4 m/s), looking from above, vehicle width = 6.2 ft (1.9 m), height = 6.9 ft (2.1 m), scale for vectors on plots: 1 unit = 2 m/s.	87
Figure 4.25. Vehicle wake flow vectors, cross-section view at $z = 9$ ft (2.74 m), $z = 11$ ft (3.35 m), $z = 12$ ft (3.66 m), respectively, above ground, for speed = 50 mph (22.4 m/s), looking from above, vehicle width = 6.2 ft (1.9 m), height = 6.9 ft (2.1 m), scale for vectors on plots: 1 unit = 2 m/s.	88
Figure 4.26. Vehicle wake flow vectors, cross-section view at $y = -3$ ft (-0.91 m), $y = 0$ ft (0 m), $y = 3$ ft (0.91 m), respectively, from centerline, speed = 30 mph (13.4 m/s), looking from side, vehicle width = 6.2 ft (1.9 m), height = 6.9 ft (2.1 m), scale for vectors on plots: 1 unit = 2 m/s.	89
Figure 4.27. Vehicle wake flow vectors, cross-section view at $y = -2$ ft (-0.61 m), $y = 0$ ft (0 m), $y = 2$ ft (0.61 m), respectively, from centerline, speed = 30 mph (13.4 m/s), looking from side, vehicle width = 6.2 ft (1.9 m), height = 6.9 ft (2.1 m), scale for vectors on plots: 1 unit = 2 m/s.	90
Figure 4.28. Vehicle wake flow vectors, cross-section view at $y = -3$ ft (-0.91 m), $y = 0$ ft (0 m), $y = 3$ ft (0.91 m), respectively, from centerline, speed = 40 mph (17.9 m/s), looking from side, vehicle width = 6.2 ft (1.9 m), height = 6.9 ft (2.1 m), scale for vectors on plots: 1 unit = 2 m/s	91
Figure 4.29. Vehicle wake flow vectors, cross-section view at $y = -2$ ft (-0.61 m), $y = 0$ ft (0 m), $y = 2$ ft (0.61 m), respectively, from centerline, speed = 40 mph (17.9 m/s), looking from side, vehicle width = 6.2 ft (1.9 m), height = 6.9 ft (2.1 m), scale for vectors on plots: 1 unit = 2 m/s	92
Figure 4.30. Vehicle wake flow vectors, cross-section view at $y = -3$ ft (-0.91 m), $y = 0$ ft (0 m), $y = 3$ ft (0.91 m), respectively, from centerline, speed = 50 mph (22.4 m/s), looking from side, vehicle width = 6.2 ft (1.9 m), height = 6.9 ft (2.1 m), scale for vectors on plots: 1 unit = 2 m/s	93
Figure 4.31. Vehicle wake flow vectors, cross-section view at $y = -2$ ft (-0.61 m), $y = 0$ ft (0 m), $y = 2$ ft (0.61 m), respectively, from centerline, speed = 50 mph (22.4 m/s), looking from side, vehicle width = 6.2 ft (1.9 m), height = 6.9 ft (2.1 m), scale for vectors on plots: 1 unit = 2 m/s	94
Figure 5.1 Schematic diagram of the wake-aligned (s, n, z) coordinate system and its relation to the (x, y, z) coordinate system	102
Figure 5.2 (a) Layout plan of instrumented towers in the GM experiment in relation to the traffic lanes; (b) Elevational view of meteorological towers and instrument locations.	109
Figure 5.3 Schematic diagram of wind direction classification of GM data	110

Figure 5.4 Comparison of predicted and observed concentrations for perpendicular winds . . .	111
Figure 5.5 Comparison of predicted and observed concentrations for parallel winds	111
Figure 5.6 Comparison of predicted and observed concentrations for oblique winds	111
Figure 5.7 Comparison of predicted and observed concentrations for all wind directions . . .	113
Figure 5.8 Cumulative frequency distribution of modeled and observed concentrations	114

LIST OF TABLES

Table 2.1 ETOS meteorological sites used in the low wind analysis	14
Table 2.2 INEEL meteorological sites used in the low wind analysis	16
Table 2.3 Meteorological Sites Used in Wind Rose Analysis for Light Winds (0 to 5 m/s)	18
Table 2.4 Sites used for comparisons in Part 2.3.3.	21
Table 4.1 Sonic anemometer array configurations and positions for Day 322.	59
Table 4.2 Sonic anemometer array configurations and positions for Day 335.	62
Table 4.3 Sonic anemometer array configurations and positions for Day 336	71
Table 5.1 ROADWAY-2 evaluation statistics	112
Table 5.2 Model evaluation statistics	113

ISSUES AFFECTING DISPERSION NEAR HIGHWAYS: LIGHT WINDS, INTRA-URBAN DISPERSION, VEHICLE WAKES, AND THE ROADWAY-2 DISPERSION MODEL

R. P. Hosker, Jr., K. S. Rao, R. L. Gunter, C. J. Nappo, T. P. Meyers,
K. R. Birdwell, and J. R. White

ABSTRACT. The research described in this report is a collaboration between the National Oceanic and Atmospheric Administration's (NOAA) Atmospheric Turbulence and Diffusion Division (ATDD) and the Federal Highway Administration (FHWA). The FHWA must perform assessments of the likely impacts of traffic-related air pollutants near highways. Urban highways are a particular concern, and introduce a range of complications, particularly uncertainties about the wind and turbulence information needed to drive the air quality models. This research covered several tasks. The first was a thorough study of light wind data, stratified by wind speed category and time of day, using observations from a number of research-grade meteorological networks in different locations around the U.S. The instruments in these networks could resolve winds down to about 0.5 m/s. Data from the humid and vegetation-covered southeastern U.S., the arid northwest, and a coastal environment were those considered in the most detail. The results are covered in considerable detail. Winds and turbulence within urban regions are of considerable interest, but relatively few measurements are available. Data were therefore collected using 3-D sonic anemometers in Knoxville and Nashville, TN, as well as at nearby rural sites. The mean and turbulence quantities and spectra were compared, to examine the ability to use data from airports or other rural observing locations in lieu of intra-urban data. There are few data available on the wakes of vehicles, which are known to affect the initial dispersion of vehicular effluents, especially under light wind conditions. Most available data are from wind tunnels. To provide real-world data, a special towable apparatus was constructed, which supported six 3-D sonic anemometers for simultaneous measurements at different locations within the wake of the tow vehicle. Turbulent kinetic energy (TKE) was calculated at a number of locations in the near wake, and contours of TKE were plotted. Flow vectors for various cross-sections of the wake were determined. A new near-highway dispersion model was developed, called ROADWAY-2. The model is based on the U.S. Environmental Protection Agency's (EPA) ROADWAY model, but it uses a TKE closure formulation for a time-varying atmospheric boundary layer to provide the mean wind and temperature profiles from input meteorological data. It allows the use of on-site turbulence data, which is increasingly feasible given recent instrumentation advances and lower costs. The parameterization of vehicle wake effects is also new, based on canopy flow theory and wind tunnel measurements. Comparisons of predicted and observed concentrations from the General Motors field study are generally good. More than 80% of the model predictions were within a factor of two, and 95% were within a factor of five. Suggestions for future research are provided.

1. INTRODUCTION

The central problem at hand can be simply phrased: how to make the best estimates of the impacts of motor vehicle emissions on urban air quality. Our initial analysis suggested that the greatest impacts might be expected, as in most dispersion modeling, during periods of light or calm winds, and/or in stable conditions. A first task therefore was to determine how often calm winds might occur in various parts of the country, and to estimate how accurately the data from currently operational wind monitoring sites could be extrapolated to the low wind case. This becomes especially important when the only available wind measurements are not local, but are acquired at a distant airport.

Successful modeling of pollution from vehicle emissions within urban areas requires information on the winds and turbulence within urban areas. There are relatively few urban-scale meteorological observations, and very few observations of turbulence within the urban area. Thus one of the first objectives of our study was to evaluate the differences between urban and rural flow fields and turbulence. This was done for two "targets of opportunity", the nearby cities of Knoxville and Nashville, Tennessee. These studies showed consistent and significant differences exist between rural and urban flow and turbulence fields, and that the use of rural wind and turbulence measurements to model urban diffusion may lead to erroneous predictions.

During calm or very light wind conditions, the initial dispersion of motor vehicle effluents will be controlled by the vehicle wake. At later times, the wake region represents a source configuration for urban scale dispersion models. Thus it is essential to be able to model not only the mean structure of the wake, but also the turbulence or mixing in the wake. Relatively few observations of the turbulence within vehicle wakes have been made, and these have been done in wind tunnels. These facts led to a unique program in which the turbulence and its spatial evolution in the near wake of a real moving vehicle were directly measured. An initial finding of this study is that an inertial subrange of turbulence is not present in the near wake region. This is significant because almost all dispersion theories and models assume the existence of an inertial subrange.

In addition to examining the turbulence behind moving vehicles, we briefly examined the effects of moving vehicles on the turbulence near a roadway. This experiment showed that the passing vehicles could be detected not only by enhanced horizontal momentum flux, but also by signatures of water vapor and carbon dioxide. However, it appears that the vehicle-produced turbulence had little effect on the ambient turbulence, because we observed an inertial subrange not only in the ambient turbulence spectra, but also in the CO₂ spectrum. Individual issues of particular interest are discussed in the following paragraphs.

1.1 Urban Dispersion Issues

Dispersion of pollutants within urban areas has been a concern for a very long time. Until relatively recently, most efforts to model such dispersion dealt mainly with a few important scenarios: dispersion of air pollutants over the city as a whole; dispersion of toxic, hazardous, or annoying effluents near individual buildings; and dispersion of traffic-related pollutants near

roadways. In recent years, there has also been increased attention to what can be called neighborhood-scale dispersion, to estimate the problems which may result from releases of toxic or hazardous materials from specialized local sources such as accidental chemical releases (as at Bhopal) or terrorist releases of chemical or biological weapons. Despite decades of work and extensive literature, there are still many unknowns and uncertainties in predicting both the trajectories and diffusion of gaseous pollutants within an urban region.

Many of these are due to the complex flows which result when winds pass over a collection of buildings of various sizes, shapes, and spacings. The resulting flow deflections, vortex generation, and turbulence production combine to make the intra-urban dispersion problem a very site-specific one. Laboratory (wind tunnel and water channel) and a modest number of field studies have particularly helped to elucidate the phenomena influencing the transport and dispersion processes. In the last few years, the rapid emergence of inexpensive super-computers has now made possible greatly increased use of computational fluid dynamics (CFD) with sufficient spatial resolution to predict the main features of flow near specific building complexes. This situation continues to improve. In particular, the concerns about local releases of and resulting exposures to toxic or harmful materials seem to be spurring new laboratory, field, and numerical studies.

The intent of this discussion is not to provide an extensive review of the literature on flow and dispersion near buildings or groups of buildings; there are several of these already available (see for example, Meroney, 1982; Hosker, 1984 and 1985; Robins et al. 1997). Instead, we will discuss briefly some of the urban dispersion scenarios that are reasonably well understood, and those that still remain as problems.

From decades of wind tunnel and theoretical research, and a modest number of field tests, the basic characteristics of the flow of a turbulent boundary layer wind past a simple isolated building perpendicular to the wind can be fairly well quantified. These characteristics include the distance upwind where the flow begins to be strongly displaced by the building, the height on the front face where the incident flow reattaches, whether or not the rooftop and side flows reattach to those surfaces, and the length of the recirculation zone behind the structure. The general behavior of the far turbulent wake is also known, and in fact was used by Eskridge and Hunt (1979) to help deduce the behavior of the far wake of a vehicle, as discussed below. The situation is not so straightforward when the wind is at an angle to the building, partly because the angled approach flow can result (depending on the building and roof shapes) in a pair of rooftop trailing vortices that will affect the wake flow and effluent dispersion processes.

Things become even more complex when there are multiple buildings. The complicated deflected and wake flows begin to interact as the buildings are placed increasingly closer together. Hussain and Lee's (1980) wind tunnel tests on simple arrays of uniform model buildings brought out the notion of three distinct flow regimes: the "isolated roughness" case where the buildings are far enough apart that their flow fields do not strongly interact; the "wake interference" case where the buildings are close enough that the flow fields do interact strongly; and the "skimming flow" regime, where the buildings are so close that the mean wind no longer penetrates down into the gaps between buildings, but instead skims over the rooftops. In this case, the flows within the gaps often consist of recirculating vortices driven by the flow aloft. These three regimes have become widely

accepted in the literature (e.g., Oke, 1988; Grimmond and Oke, 1999), and there are increasingly quantitative estimates (e.g., Hosker, 1985; Grimmond and Oke, 1999) for when the various regimes can be expected, given the dimensions and spacing of the buildings.

The skimming flow regime often characterizes the urban street canyon, one of the most widely studied aspects of an urban area. In a long street canyon with the wind aloft normal to the canyon axis, a recirculating vortex occurs along the street axis. Albrecht (1933) is usually recognized as the first to report this phenomenon. Georgii et al. (1967), Johnson et al. (1971, 1973), DePaul and Sheih (1984), Nakamura and Oke (1988), Johnson et al. (1996), and many others have reported related field observations. There have been numerous laboratory studies as well (e.g., Hoydysh et al., 1974; Wedding et al., 1977; Hoydysh and Dabberdt, 1988, 1994; Dabberdt and Hoydysh, 1991; Kastner-Klein and Plate, 1999; and many others). These have helped define and test a large number of numerical models aimed at better understanding the mean flow fields, turbulence characteristics, and resulting concentration patterns for air pollutants emitted into street canyons of varying geometry. Some of the better known model studies include Johnson et al. (1973), Hotchkiss and Harlow (1973), Nicholson, (1975), Yamartino and Weigand (1986), Yamartino et al. (1989), Hunter et al. (1992), Sini et al. (1996), Karim and Matsui (1998), and Baik and Kim (1999). In recent years the emphasis has been on computational fluid dynamics approaches newly made possible because of the enormous advances in computer power, and this is likely to continue.

Despite all this effort, there are still many uncertainties in intra-urban flow and dispersion modeling, largely because the local flow patterns and turbulence depend on the detailed geometry and spatial inter-relationships of the local buildings. For example, street canyon flows, which are probably among the best understood, can be significantly altered from the ideal case by the presence of street intersections or by the presence of larger or shorter buildings among those of more uniform size. Tall buildings in particular can divert air from aloft down into a street canyon, and greatly affect the expected concentration fields. Outside of street canyons, in less regular arrays of buildings of mixed heights and sizes, the nature of the mean flow and turbulence is still poorly understood, and it is not possible to assess the accuracy of model predictions. A recent monograph by Hanna and Britter (2000) tries to provide some guidance on estimating a characteristic mean wind speed below roof height in terms of the aerodynamic roughness, the turbulent shear measured above the rooftops, and the neighborhood building morphology. Hanna and Britter (2000) note that the shape of the vertical wind speed profile down amongst the buildings is uncertain (in fact it is probably site-specific), and suggest that a uniform profile or perhaps an exponential form similar to those seen in vegetation canopies (e.g., Cionco, 1972) may be a practical estimate. There is some evidence that the mean turbulence characteristics (e.g., the standard deviations of the u , v , and w velocity components) may be fairly uniform in the vertical within the urban canopy, and so might be determined in terms of their values above the rooftops.

Additional detailed field studies and laboratory observations of models of specific urban regions are needed to provide additional understanding. For example, Rotach (1993, 1995) reported detailed work in Zurich with measurements both above and within a street canyon, as well as a detailed and thorough analysis of the results. Recent laboratory work by Brown et al. (2000) and Lawson et al. (2000) is also aimed in this direction. Brown et al. (2000) reported the results of detailed mean flow and turbulence measurements around a two-dimensional array of model

buildings. They observed that a rooftop separation and recirculation zone was only present on the first (upwind) building in the array, and that recirculating vortices were found in all the street canyons. The street canyon vertical velocity profiles achieved an equilibrium state after only 3 or 4 street canyons, but it took more than 7 buildings before equilibrium was achieved above the rooftops. Lawson et al. (2000) reported on similar measurements around a three-dimensional array of model buildings. They found that the approach flow decelerated more slowly than for the 2-D case, and that there was a rooftop separation and recirculation zone only on the first building (as for the 2-D case, but shallower). The street canyon velocity profiles were nearly identical. Downstream of the building array, the flow returned to ambient-like conditions somewhat more quickly than for the 2-D case; beyond 5 or 6 building heights downwind, there was little difference between the 2-D and 3-D cases. The results of these new studies will be used to assist and verify CFD modeling of the flow over 2-D and 3-D arrays.

1.2 Dispersion Near Roadways

Dispersion of air pollutants near roadways is a long-standing problem. Federal, State, and local environmental regulations now require that air quality impacts of transportation-related projects be analyzed and quantified. However, modeling and measurements of air contaminant concentrations near highways are still poorly understood in areas where there are major influences on air flows near and passing over highways due to large structures, highway site geometry, and large topographic effects. For such sites, including complex urban road intersections, it is important to gain better understanding because of potential air pollution impacts on human health and regulatory decision-making. Thus far, only rather general guidance has been possible for evaluation of the air quality effects of highways. These effects are considered during the location, design, and operation of highways. However, guidance for sites with complex geometry and low wind speeds has not been adequate.

Carbon monoxide has been the primary highway-related air pollutant addressed in monitoring and modeling. However, carbon monoxide and selected tracers such as SF₆ can also serve as surrogates for other contaminants which are inert for at least short distances. In fact, over short distances, the dispersion and transport of dilute concentrations of gases appreciably different in density from carbon monoxide can also be treated similarly. For example, the same principles of atmospheric transport and turbulent mixing applicable to carbon monoxide apply to the dispersion and nearby impacts of aldehydes and very fine particles of less than roughly 1 μm in size.

Experimental data and estimations of concentrations of vehicle-source air pollutants for numerous highway sites have been obtained through wind tunnel simulations, analytical modeling based primarily on general concepts from fluid mechanics, and field measurements. Collectively, these have been employed in the development of air pollutant models, whether they be simple Gaussian formulations for open areas with established boundary layers, simple confined flow models such as TUNVEN and various street canyon models, complex numerical models (based on the fundamental conservation equations of fluid dynamics), or other appropriate algorithms. The models have been applied for worst case scenarios and for more probabilistic estimates.

Worse case assessments are based on using a combination of highly congested or "packed" vehicle traffic (and hence a high pollutant source strength), and atypically persistent direction low wind speeds (1-2 m/s) under thermally stable atmospheric conditions, for nearby and/or vulnerable receptor locations. On the other hand, probabilistic estimates are based on the expected variations of source strengths, wind speeds and directions, thermal stability, and receptor locations. Problems with the above approaches include:

1. Some of the available data have been collected at non-generic or very specific locations, and their applicability to other places or for model development is very limited. Examples include the dispersal of highway air contaminants from a highway tunnel (even at sites of simple geometry), and patterns of concentrations for a specific site or complex of buildings within an urban area, where the site geometry and wind patterns are unique and extremely irregular.
2. The effects on the initial entrainment and dispersion of air contaminants of the presence of one or more highway vehicles, the effective source heights for pollutants, and the movements of vehicles have not been well described and quantified.
3. Often there is no well-established flow or boundary layer upwind or downwind of a highway site. Such a well-established flow would be expected for an at-grade highway across open flat-to-undulating terrain, with no significant obstructions greater than the general surface roughness factor near the highway. In principle, for a two-dimensional isolated obstruction of height H , major perturbations (gross flow deflections and separated flows) of an established atmospheric boundary layer flow can be expected to occur within about 10 to 15 H downwind and perhaps 4 or 5 H upwind of the obstruction. Lesser perturbations (reductions in mean wind speed and changes in turbulence structure and intensity) can be expected to occur at even greater distances. Application of idealized air quality models then requires that the source and receptors must at least be outside these strongly perturbed regions, and perhaps even further away. These distances are considerably reduced to perhaps 1 to 1.5 H upwind and several H downwind (depending on the obstacle width and along-wind length) for the three-dimensional case.
4. Simple along-and cross-canyon box models have treated the dispersion of air contaminants for confined roadways in street canyons or deep open cuts. Qualitative concepts have been given for three-dimensional flows. Some of this work has been described above, in relation to urban dispersion issues.
5. In the atmospheric boundary layer, even over rather idealized terrain, the observed wind speed is generally not uniform with height, and often neither is the direction. The associated turbulence often does not follow the simple distributions assumed in many models. Many simple models (e.g., Gaussian) assume conditions most appropriate to steady strong winds over open terrain and elevated steady sources. Extrapolation of these models to non-flat highway sites, locations with unsteady traffic, and highway locations within the complex geometry of an urban area will therefore often lead to erroneous or misleading results.

6. Previous approaches to highway dispersion modeling frequently have combined deductive reasoning about what should be expected from Gaussian plume dispersion models with data from highway sites on reasonably flat topography away from nearby tall structures, and then have made empirical adjustments in the values of effective source heights and the values of the plume dispersion coefficients ("sigmas").

7. Without adequate consideration of and modification for locally non-uniform and unsteady air flows, problems can be anticipated in applying Gaussian dispersion models, street canyon models, and even so-called higher-order numerical models for the following circumstances:

- a. Highway sites where time-varying traffic patterns, particularly at exchanges and intersections, result in sizeable differences in source locations and strengths during a given time period.
- b. Locations and times when wind velocities are highly variable and accompanied by sizeable vertical air flows, especially during periods of "calms" -- slow and poorly defined wind velocities.
- c. Highway site locations which do not have well-established local boundary layer flows due to the presence of topographical features, complex highway configurations, or large structures, all of which can cause the superposition of locally-generated convergent or divergent flows, horizontal or vertical jets, vortices, and complex wake patterns.

The dispersion of pollutants under low wind-speed conditions is of particular interest in highway dispersion models. There has been some work over the past 20 years in this area, though most of it was aimed at modifying the Gaussian models to obtain agreement with rather limited data. Among recent studies, Sharan et al. (1995) discussed various estimates of dispersion parameters for low wind speeds, and intercompared them using a concentration formula obtained from steady-state advection-diffusion equation. Their results show that, with high-frequency data of wind velocity and standard deviation of horizontal wind direction (σ - θ), schemes based on segmented plume and short-term averaging simulate the observations much better, especially in terms of the multiple peak nature of the concentration distribution, than the traditional methods. Additional work on this topic is needed.

Concentration fields at urban intersections are poorly understood, but are important because of air pollution implications to human health and regulation. Hoydysh and Dabberdt (1994) studied concentrations at an urban intersection and nearby environment using an atmospheric boundary-layer wind tunnel. A regular array of uniform, low-rise rectangular urban blocks was modeled using both flow visualization and quantitative gas tracer techniques. The ratio of building height-to-street width was 0.75, and avenues were about 50% wider than streets. Pedestrian-level concentrations varied widely throughout the intersection and also with ambient wind direction. Emissions from sources in the street contribute more to intersection concentrations than do equivalent emissions in the avenue for nearly all wind directions. Surface concentrations are greatest for ambient winds parallel to the street, and roughly equal for the other wind directions studied. The concentration

fields aloft indicate that vertical dispersion is an important determinant of the surface concentration and its variability.

FHWA requires that air quality effects should be considered during planning, siting, and construction of highway projects, so that highway decisions are consistent with State Implementation Plans (SIPS) for complying with ambient air quality standards; for example, CO concentration associated with a highway impact should not exceed 35 ppm for 1 hour and 9 ppm for 8 hours more than once a year. This requires estimation of CO concentrations on both local and area-wide scales. A number of models of varying sophistication and complexity, ranging from simple line-source-oriented Gaussian models to elaborate numerical models, are used to estimate the CO concentrations. Martinez et al. (1981) described a comprehensive methodology for evaluating the performance of highway air-pollution dispersion models. Other objectives of their study were to compile and document a database to be used to assess model performance, and to perform a preliminary evaluation of selected models. The evaluation methodology encompasses: (a) accuracy analysis, which measures the predictive performance of the model; (b) diagnostic analysis, which identifies conditions associated with inaccuracies in the model's predictions; and (c) sensitivity analysis, which quantifies the model's response to uncertainty in the model input data.

Rao et al. (1980) presented an evaluation of some commonly used highway dispersion models, using the tracer data collected in the General Motors experiment (Cadle et al., 1977). Of these models, four are Gaussian (GM, HIWAY, AIRPOL-4, CALINE-2) and three are numerical (DANARD, MROAD 2, ROADS). Various statistical techniques were employed to quantify the predictive capability of each of these models. In general, the three numerical models performed rather poorly compared to the Gaussian models. For the GM data set, the model with the best performance in accurately predicting the measured concentrations was the GM model, as expected; however, it was skewed towards underprediction. The authors conclude that the HIWAY model would be useful as a screening tool for regulatory purposes, since this model has the highest percentage of overprediction of concentration data in the range of 50th to 100th percentiles. The tested version of the HIWAY model warranted modifications to improve its predictive capability for stable and parallel wind-road conditions.

Air quality models are a key component in determining pollution control requirements. Modeling guidance must be flexible and include better techniques as they become available. Revisions to modeling guidance require an assessment of the scientific basis, a model performance evaluation using observed data, sensitivity analysis for impact on design concentrations and data input requirements, and public review and comment before formal adoption in regulatory programs. Touma et al. (1995) discussed the procedures used in reviewing new techniques and, as an example, examined the appropriateness of adopting a new method for modeling area sources characterized by low-level releases with little buoyancy. The authors argue that the lengthy review process they describe ensures that decisions on potentially costly pollution controls are based on full public participation and sound scientific developments.

1.3 Vehicle Wake Issues

As indicated above, both ambient wind flows and vehicle wake-induced flows can influence the transport and dispersion of air pollutants near roadways. It is clear that vehicle wake flows will be most significant for light ambient winds and close to the roadway. Since the winds within the built-up portion of a city will often be reduced in speed, and people are often in proximity to roadways within cities, it follows that vehicle wake effects may be of considerable interest within urban areas in determining concentrations of vehicle emissions.

A seminal paper on vehicle wakes was presented by Eskridge and Hunt (1979), who considered a vehicle wake as a pure momentum wake (i.e., the effect of longitudinal trailing vortices that occur behind a vehicle which generates lift was explicitly neglected). They assumed the eddy viscosity in the wake would vary with distance along the wake but would be constant with height, and they assumed that the wake would be of "self-preserving form" sufficiently far behind the vehicle. Given their assumptions, they found that the maximum velocity perturbation in the wake should decay as $(x/H)^{-3/4}$ where x is the distance behind the vehicle and H is the vehicle height, that the vertical length scale of the wake should grow as $(x/H)^{1/4}$, and that the components of the turbulent kinetic energy in the wake should decay as $(x/H)^{-3/2}$.

Eskridge and Thompson (1982) carried out wind tunnel studies of a simple block (i.e., a non-lifting shape) model of a vehicle to test the Eskridge and Hunt theory. They found that the velocity deficit in the wake did indeed decay as $(x/H)^{-3/4}$, and the vertical scale length grew as $(x/H)^{1/4}$, but that the turbulent kinetic energy components died off more slowly, as $(x/H)^{-1.2}$. They also found that the Eskridge-Hunt assumption that the lateral and vertical length scales were identical did not describe the lateral spread of the observed wake very well. They therefore developed a revised theory which allowed for two length scales (vertical and horizontal) and vertically variable eddy viscosity, and this theory fits the wind tunnel data better. The lateral scale length in this theory grows as $(x/H)^{0.4}$, and the eddy viscosity reaches its maximum value, according to their observations, at about $z/H = 1.25$, where z is the height above the surface,

Eskridge and Rao (1986) described wind tunnel studies of dispersion behind a block-type vehicle model; they used a block model on the grounds that the observed wake concentrations were either the same as for a more realistic model (typically for $z < H$), or were greater than for the realistic model (when $z > H$), and so were conservative. They used the results to develop improvements in the ROADWAY model, which incorporates vehicle wake theory as well as ambient turbulence information to estimate concentrations near highways.

In 1987, Thompson and Eskridge described wind tunnel studies of the wakes and pollutant dispersion behind scale models of real vehicles, as well as a simple block-shaped vehicle. In this case the lift generated by the streamlined shape of the vehicles results in a pair of counter-rotating vortices aligned more or less along the vehicle axis. The inward and downward rotation of these two vortices carries higher speed, less turbulent air from above the wake down into the center of the vehicle wake. As a result, the mean velocity at the wake centerline is somewhat higher than observed for the pure momentum wake behind the simple block model. The observed wake cross-sections of velocity deficit and turbulence intensity, both of which for the block model tend to be

fairly symmetric bell-shaped curves with their peaks at the wake centerline, instead have local minima at the wake centerline for the streamlined realistic models, with two maxima located more or less symmetrically outboard of the centerline, near $|y/H| \sim O(1)$, where y is the lateral distance from the centerline. Because of the influx of clean air along the wake centerline, the trailing vortices also had a noticeable impact on the distribution of pollutant (tracer material) in the wake at heights above the top of the vehicle, but not much effect was seen below the vehicle top.

It should be noted that virtually all of the above work was conducted at relatively large distances behind the vehicle (generally $10 \leq x/H \leq 60$), and in principle does not apply in the wake zone immediately behind the vehicle, where flow recirculation zones and bluff-body effects such as vortex shedding may be important.

Measurements of the wake characteristics behind real vehicles seem to be unavailable. This is no doubt due to the difficulty of making such measurements; one needs to be able to deploy fast-response instruments at various locations in the x , y , and z directions within the wake of a moving vehicle, without interference from other vehicles or flow perturbations introduced by nearby buildings. In the wind tunnel such measurements are accomplished with hot film anemometers, pulsed wire anemometers, or perhaps a laser Doppler velocimeter. While it would be conceptually feasible to use these methods outdoors, there are practical considerations such as flying particles or insects that would damage the instruments quickly. To perform such measurements in the wake of a real vehicle on a real road, more robust sensors are needed. Chapter 4 describes an effort to acquire such data using an array of 3-D sonic anemometers mounted on a pipe rack framework above an open framework trailer. These fast-response anemometers could be quickly moved without tools to new wake locations in the x , y , and z directions, so that a reasonable number of measurements could be performed under essentially the same synoptic conditions. The tow vehicle and trailer were operated at various road speeds on a nearly unused runway at a local airport, well away from buildings or other vehicles. These data were all taken within the near wake, rather than the far wake, extending out to roughly $x/h = 2.5$; however, some of the wake characteristics just described for the far wake seem to occur within the near wake as well.

Besides the real world vehicle wake studies described, an effort was made to conduct additional detailed wake studies behind scale models of several different characteristic vehicle types. A moving roadway simulator was constructed for the ATDD wind tunnel, to properly simulate the air flow of a vehicle driving along a highway in a calm wind. After all the preliminary engineering, model building, and testing was successfully accomplished, the primary measurement apparatus (hot film anemometers) suffered a major failure. Attempts to repair the equipment locally were unsuccessful, and the equipment is obsolete and no longer supported by its manufacturer. Funds were unavailable to purchase an expensive new replacement system. Attempts to move the wind tunnel studies to a tunnel at the EPA's Research Triangle Park facility were also unsuccessful due to the shutdown of the Fluid Modeling Facility (FMF) because of a budget shortfall there. The FMF has since reopened on a limited basis, but is engaged in a study of intra-urban dispersion modeling funded by another agency, limiting its availability for other use. It is hoped that it will be feasible to borrow or purchase suitable anemometry for the ATDD tunnel in the not-too-distant future, to make use of all the setup and testing effort already expended.

1.4 Guide to This Report

The research reported here has centered on four areas. Chapter 2 discusses detailed analyses of wind roses, segregated by wind speed classes, for a variety of real-world sites equipped with high quality meteorological networks. The data from these sites extend to significantly lower wind speeds than can usually be routinely recorded. The wind roses were analyzed to see whether their shape persists as the winds become progressively weaker, and to look for common factors across the various sites. Chapter 3 presents field studies of turbulence observations within the central urban area of two small cities. The urban data are compared to simultaneously acquired data from nearby rural areas, as well as to airport data. Chapter 4 describes what is believed to be a unique effort to measure mean and turbulent flow components within the wake of a real vehicle operating over a range of normal highway speeds. The technique described can easily be extended to other vehicles. Chapter 5 presents a revision of the well-known ROADWAY model, which has been improved to reflect current boundary layer understanding and to correct some errors. The revised model is called ROADWAY-2. It has been compared to concentration data from the famous GM experiment, and it appears to predict the concentrations quite well. Chapter 6 summarizes our results, and suggests some areas for additional research.

2. CHARACTERISTICS OF LIGHT WINDS

Kevin Birdwell

2.1 Introduction

In recent years, air quality modeling and research have acquired major attention because of growing concerns over air pollution. The accuracy of air quality modeling is highly dependent on input parameters, particularly wind direction and wind speed. However, there are a number of concerns regarding wind measurements that must be considered in the assessment of model accuracy.

Historically, weather observations related to real-time use (such as for aviation, weather forecasting, and the like) have been conducted manually by on-site observers. Over the last several years, however, Automated Surface Observing Systems (ASOS) have come into use as a primary source of real-time meteorological data. Although most ASOS stations report a wide array of detailed meteorological information, wind measurements (as with most of the previous manual observations) are generally limited to an approximate 1.5 m/s (3 knots) threshold. Winds below this threshold are reported as calm. While wind measurements at such low speeds may be of little concern for airport or general use, they create a great deal of uncertainty when modeling for air quality concerns. Usually the forecasting of pollutant transport is a prime objective of air quality models, and such forecasting requires accurate wind data. There is extra concern when the winds are light because pollutant concentrations are often highest in such cases. Yet these are precisely the conditions when readily available data become the least reliable.

Another challenge to air quality modeling is that of terrain. Generally speaking, in areas of level terrain, winds near the surface tend to parallel those aloft as high as 3000 m above ground (700 mb pressure level) except during circumstances involving some active pressure systems. However, seldom can a region be classified as truly non-complex. In mountainous regions and other areas of complex terrain (such as river valleys, coastlines, and urban environments), the effects of the terrain or local features on air flow can significantly modify what might otherwise be straightforward measurements that would be representative of a broad area. For accurate predictions, air quality models must properly consider terrain effects, especially their influence on meteorological observations which can affect the applicability of those observations even to nearby sites.

The situation is most serious during periods of very light winds (near-calm conditions). Under very light winds, the influence of terrain features located close to the meteorological site(s) used for input becomes much greater. Although these effects are usually obscured during periods of moderate to strong winds, they can become the dominant effects under light or nearly calm winds. Local influences could include a wide array of both man-made and natural perturbations of the local wind flow patterns.

The analysis that follows assesses the extent and characteristics of the above factors with respect to changes in wind direction and speed under light wind conditions. Since every locale is unique, it would be impossible to fully assess all the possible effects that winds might have on input

parameters to an air quality model. The sites chosen for study represent several examples of differing complex terrain (a humid region containing multiple terrain types, an arid mountainous region, and a flat coastal environment). Through the choice of these geographical areas of complex terrain, it should be possible to identify a number of major influences on wind inputs that would also be applicable to other areas and situations.

2.2 Study Areas

Three study areas comprise the backdrop for this research. They include: (1) a portion of the Southern Appalachian Mountains including the Great Valley of Eastern Tennessee and its surroundings, (2) a portion of the Snake River Plain and associated mountains in Southern Idaho, and (3) the coastal environment of Cape Canaveral, Florida. The Southern Appalachian region is typical of much of the humid southeastern United States, with vegetation ranging from grassy meadows to forests. The Snake River Plain is an arid northern region with sparse vegetation. Both environments were chosen for their variety of complex terrain as well as for the presence of meteorological networks which could provide wind data at both greater precision and lower thresholds than that available from typical ASOS sites. The Cape Canaveral, Florida site was included for the purpose of analyzing light winds in a coastal environment. Much of the U.S. population lives within a coastal environment.

2.2.1 Southern Appalachians

The National Oceanic and Atmospheric Administration (NOAA) operates a meteorological network associated with the East Tennessee Ozone Study (ETOS) in the Southern Appalachian Mountains. This network is especially suited to the purpose of this study since the area covered by ETOS includes a wide variety of complex terrain land forms such as mountain, valley, ridge-and-valley, and plateau land-forms. Additionally, the ETOS meteorological network uses air-quality-standard wind monitors that have a very low wind speed threshold (0.3 m/s). This is far less than the 1.5 m/s available with ASOS wind monitors. Figure 2.1 shows the various ETOS meteorological sites used in the study; specific information concerning the sites is given in Table 2.1.

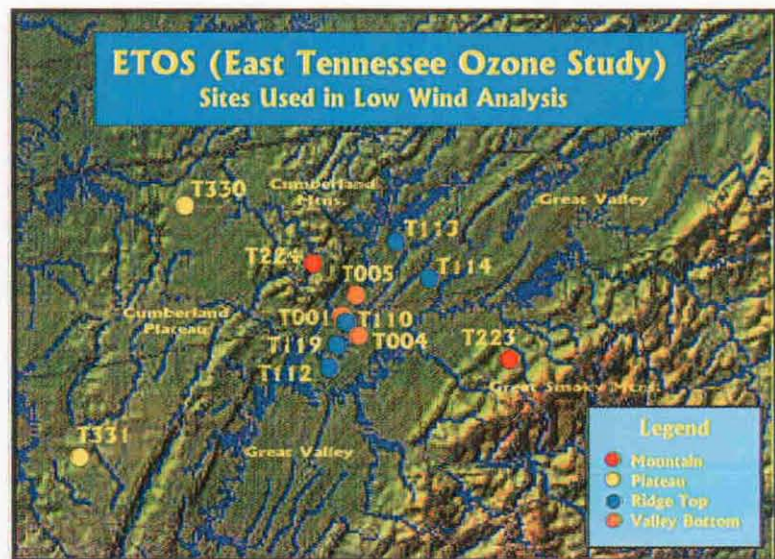


Figure 2.1 ETOS sites used in the low wind analysis.

Table 2.1 ETOS meteorological sites used in the low wind analysis.

<i>Site</i>	<i>Location</i>	<i>Nearest City</i>	<i>Altitude (m)</i>	<i>Tower Ht (m)</i>	<i>Topography</i>
T001	36°00' N, 84°15' W	Oak Ridge, TN	267	17	Valley Bottom
T003	36°01' N, 84°15' W	Oak Ridge, TN	271	17	Valley Bottom
T004	35°59' N, 84°13' W	Oak Ridge, TN	248	10	Valley Bottom
T005	36°02' N, 84°12' W	Oak Ridge, TN	243	10	Valley Bottom
T110	36°00' N, 84°15' W	Oak Ridge, TN	343	10	Ridge Top
T112	35°51' N, 84°20' W	Lenoir City, TN	381	27	Ridge Top
T113	36°08' N, 84°04' W	Heiskell, TN	402	28	Ridge Top
T114	36°00' N, 83°57' W	Knoxville, TN	415	22	Ridge Top
T119	35°58' N, 84°17' W	Oak Ridge, TN	340	45	Ridge Top
T223	35°42' N, 83°37' W	Gatlinburg, TN	1243	24	Mountain Top
T224	36°08' N, 84°20' W	Frost Bottom, TN	1031	10	Mountain Top
T330	36°23' N, 84°54' W	Allardt, TN	520	25	Plateau
T331	35°40' N, 85°29' W	Spencer, TN	572	25	Plateau

Sites were chosen based on their topographical settings (valley-bottom, ridge top, mountain, and plateau). An important benefit of the proximity of so many diverse topographical land forms in east Tennessee was that it permitted better analysis of the winds with respect to each other, for similar upper level wind conditions. The Great Valley of east Tennessee is oriented in a NE-SW direction (see sites in Figure 2.1) and is approximately 80 km wide and 300 km long. It is bordered by the Cumberland Plateau and Mountains to the northwest (approximately 400 - 800 m higher than the Great Valley floor) and by the Great Smoky Mountains to the southeast (800 - 1800 m higher). The Cumberland and Great Smoky Mountain zones represent very rugged terrain while that of the Cumberland Plateau is best described as a relatively level, high-elevation surface with a number of gorges and canyons occasionally interrupting the otherwise level terrain. Within the Great Valley are a series of 80-to-100-m high ridges running parallel to the Great Valley's orientation axis and spaced about 1 to 5 km apart. Such ridge-valley terrain is usual in much of the eastern U.S. along the Appalachian Mountains. The blue-dotted sites in Figure 2.1 are located on such ridges and the orange-dotted sites are located in local nearby valley bottoms. One of the valley bottom sites (T005) is located next to a large river. A number of major highways cross or run along the Great Valley (including I-40, I-75, I-81, US-11E, US-11W, US-25E, US-25W, US-27, and US-127).

Data from two ASOS sites (Knoxville's McGhee-Tyson Airport, and Oak Ridge) were also analyzed. These sites are located in proximity to some ETOS sites, thus allowing good comparison of the two data sets. Information on the ASOS sites is provided in Table 2.4.

2.2.2 Snake River Plain, Idaho

The second study area, a portion of the Snake River Plain in Southern Idaho, is similar to the Great Valley of Eastern Tennessee in that its major feature is that of a large valley bordered on both

sides by more or less continuous higher terrain (see Figure 2.2); however, there are a few major differences. These include: (1) the absence of ridge-and-valley terrain within the primary valley, (2) the presence of smaller mountain valleys which open into the primary valley, roughly

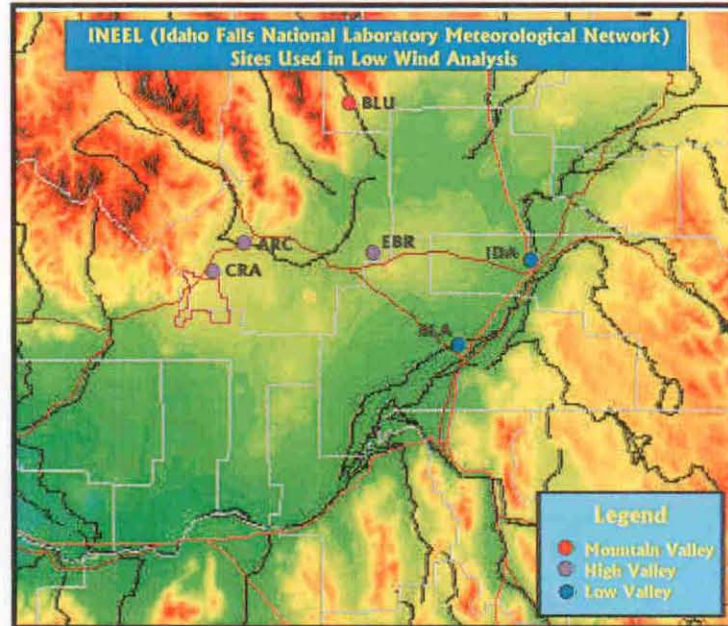


Figure 2.2 INEEL sites used in the low wind analysis.

perpendicular to that of the primary valley, (3) a much greater range of altitude differences within the primary valley including a few isolated mountains, and (4) an arid rather than humid climate (which could affect atmospheric circulation via differences in the effect of water vapor flux). The topographical features allowed the low wind analysis done with the ETOS data to be expanded to include some additional scenarios for complex terrain.

The Idaho National Engineering and Environmental Laboratory (INEEL) meteorological sites measure winds with similar precision to that of the ETOS network. INEEL sites were selected for analysis based on three broad categories of terrain. These included: (1) mountain valleys opening into the primary valley, the Snake River Plain; (2) higher terrain within the Snake River Plain; and (3) lower terrain within the Snake River Plain. It was also desirable that the selection of sites include some sites located on opposite sides of the Snake River Plain. Note that sites “CRA”, “ARC”, and “BLU” are located on the northwest side of the Snake River Plain while sites “BLA” and “IDA” are located near the southeastern side (see Figure 2.2). Specific details about the six sites used in the low wind analysis for the Snake River Plain study area are provided in Table 2.2. Major highways through this area include I-15, I-84, I-86, US-20, US-26, and US-93.

Table 2.2. INEEL meteorological sites used in the low wind analysis.

<i>Site</i>	<i>Location</i>	<i>Nearest City</i>	<i>Altitude (m)</i>	<i>Tower Ht (m)</i>	<i>Topography</i>
ARC	43°38' N, 113°18' W	Arco, ID	1637	15	High Valley
BLA	43°16' N, 112°24' W	Blackfoot, ID	1369	15	Low Valley
BLU	44°04' N, 112°50' W	Blue Dome, ID	1750	15	Mountain Valley
CRA	43°25' N, 115°33' W	Arco, ID	1817	15	High Valley
EBR	43°36' N, 112°39' W	Atomic City, ID	1561	10	High Valley
IDA	43°31' N, 112°04' W	Idaho Falls, ID	1438	15	Low Valley

2.2.3 Cape Canaveral, Florida

Data for a single National Weather Service (NWS) site in Cape Canaveral, Florida were analyzed for changes in low wind speed patterns. This area is a region of complex terrain from the standpoint that it has land/ocean interface characteristics rather than strictly land characteristics. The winds in the Cape Canaveral area are significantly affected by diurnal land and sea breezes that form in response to the differential heating of the Florida Peninsula and the Atlantic Ocean (see Figure 2.3). The strength of the land/sea breeze is often determined by the intensity of synoptic scale systems affecting the Florida Peninsula. Thus, the land/sea breeze influence becomes greater as synoptic forcing of wind flow becomes weaker.



Figure 2.3 Location of Cape Canaveral with respect to the Central Florida Peninsula.

Although the available wind data from Cape Canaveral were not of equivalent accuracy to the ETOS and INEEL meteorological sites, the data were somewhat superior to standard ASOS measurements. Some measurements as low as 0.6 to 1.0 m/s were available; however, response of the equipment to changes in wind speed was not as good as that of the wind monitors used for the other types of data analyzed. This resulted in a limited number of data points under 1 m/s. The data site is located within 3 km of the coast at an elevation of about 3 m above sea level. Major highways in the Cape Canaveral area include I-4, I-95, US-1, and Florida 528.

2.3 Method of Research

A variety of analyses was performed on the various data sets but the majority of the research focused on the ETOS data in the Southern Appalachian Mountains. The amount of data used in each analysis varied with the period of record of the available sites, which varied from as little as nine months to as much as four years. Most analysis was based on either 15-minute or one-hour vector sums of wind direction and mean wind speed. The analysis of wind characteristics focused on several themes: (1) wind rose change with respect to low wind speeds; (2) change in wind direction and speed with respect to winds at higher altitudes or to those aloft; (3) wind rose computation by site and time of day and subsequent comparison with other nearby sites; (4) wind speed distribution with respect to time of day; and (5) the calculation of the duration of calm winds. These were not conducted uniformly on all sites, rather the analyses conducted depended on the overall need for each type of analysis, the location of each site with respect to other sites, and any associated complex terrain. Procedures used are provided below .

2.3.1 Analysis of Wind Rose Change with Respect to Low Wind Speeds

Analysis of wind roses for light winds constituted the primary effort of this research. The motivation for this task was to examine the possibility of extrapolating wind rose data measured at higher wind speeds to wind speeds below the typical ASOS-type instrument thresholds so that air quality models might be applied at lower speeds than normally available. A total of 16 sites were analyzed using such methods (eight from ETOS, six from INEEL, one from Cape Canaveral, and one ASOS site at Knoxville McGhee-Tyson Airport). Information for each site analyzed for wind rose change is given in Table 2.3.

In most cases, wind data were segregated by wind speed into intervals every one-half meter per second. Larger intervals (usually 1 m/s) were sometimes used when less data were available. Winds were analyzed for the range of speeds from 0 to 5 m/s. For each one-half meter per second interval, wind roses were calculated for all early morning (midnight to 6 am), late morning (6 am to noon), afternoon (noon to 6 pm), and evening winds (6 pm to midnight). Particular attention was given to changes in wind patterns with respect to the given terrain type and location. Plotted wind roses identify the frequency of wind directions, overall vector wind, overall average wind speed, percent calm winds, and number of data points.

2.3.2 Change in Wind Direction and Speed with Respect to Winds Aloft

It has been suggested by Whiteman and Doran (1993) that at least four major wind forcing mechanisms affect the steering of winds within an area such as the Great Valley of Eastern Tennessee (the ETOS study area). Briefly, these wind forcing mechanisms are: (1) pressure-driven channeling, (2) downward momentum transport, (3) forced channeling, and (4) thermal forcing. Since these forces affect winds at the surface to varying degrees (depending on the meteorological circumstances), the resultant measured wind patterns (wind roses) may exhibit unexpected results. Although the research here focuses on these effects as observed in and near the Great Valley of

Eastern Tennessee, it should be noted that the aforementioned wind forcing mechanisms may also apply in varying degrees to the wind flow found in many other areas of complex terrain (including the INEEL study area in the Snake River Plain).

Table 2.3 Meteorological Sites Used in Wind Rose Analysis for Light Winds (0 to 5 m/s)

<i>Site</i>	<i>Location</i>	<i>Network</i>	<i>Topography</i>	<i>Period of Data Record</i>
T001	36°00'N 84°15'W	ETOS	Valley Bottom	01/94 - 03/97
T004	35°59'N 84°13'W	ETOS	Valley Bottom	03/94 - 06/96 01/97 - 09/97
T110	36°00'N 84°15'W	ETOS	Ridge Top	08/94 - 03/97
T119	35°58'N 84°17'W	ETOS	Ridge Top	01/94 - 06/97
T223	35°42'N 83°37'W	ETOS	Mountain Top	10/94 - 04/97
T224	36°08'N 84°20'W	ETOS	Mountain Top	03/94 - 03/97
T330	36°23'N 84°54'W	ETOS	Plateau	05/99 - 02/00
T331	35°40'N 85°29'W	ETOS	Plateau	05/99 - 02/00
ARC	43°38'N 113°18'W	INEEL	High Valley	01/94 - 12/97
BLA	43°16'N 112°24'W	INEEL	Low Valley	01/94 - 12/97
BLU	44°04'N 112°50'W	INEEL	Mountain Valley	01/94 - 12/97
CRA	43°25'N 115°33'W	INEEL	High Valley	01/94 - 12/97
EBR	43°36'N 112°39'W	INEEL	High Valley	01/94 - 12/97
IDA	43°31'N 112°04'W	INEEL	Low Valley	01/94 - 12/97
Cape	28°00'N 80°36'W	None	Coast	01/91 - 08/93
Knoxville	35°49'N 83°59'W	ASOS	Valley Bottom	01/98 - 02/00

Eckman (1998) defined pressure-driven channeling with respect to the Great Valley as the imbalance resulting from the Coriolis force between winds within and above the Great Valley. This phenomenon occurs as a result of the component of winds perpendicular to the axis of the Great Valley. Flow entering the valley decelerates and is deflected by the valley walls; consequently, the associated Coriolis force within the Great Valley is reduced. The result is an imbalance between winds within the valley and those winds in the surrounding environment. In the Northern Hemisphere, the imbalance causes a leftward deflection of wind flow. For the central portion of the Great Valley, which has an along-valley axis of about 55°/235°, the effect produces winds within the valley from headings of approximately 55° or 235°. The nature of these two flows depends upon the winds above the valley. When winds aloft vary from 55° clockwise to 235°, resultant valley winds are 55°. Valley winds are from 235° for the balance of winds aloft.

A second wind forcing mechanism, downward momentum transport, occurs when winds within the Great Valley couple with those aloft. As the name suggests, the horizontal momentum of winds is transferred downward through the lower atmosphere to levels within the Great Valley (Doran and Whiteman, 1992). This definition suggests that turbulent mixing and stability parameters are important for the occurrence of the mechanism. By definition, stable air masses inhibit downward momentum transport. Consequently, downward momentum transport is more likely to be a significant factor when the atmosphere is well mixed vertically. Winds within the

Great Valley resulting from downward momentum transport tend to be from approximately the same heading as the winds above the valley, less minor deflections due to the Coriolis force upon descent. For winds filtering down into the Great Valley of Tennessee, Whiteman and Doran (1993) determined that this Coriolis adjustment is leftward and less than 25°.

Forced channeling represents another possible component of resultant winds within the Great Valley. This forcing mechanism is defined as the direct deflection of air flow by the valley walls (not related to Coriolis parameters). As for pressure-driven channeling, air flow resultant from forced channeling flows either up- or down-valley; however, wind reversals occur when wind directions above the valley cross perpendicular to the valley's axis. Thus, wind shifts within a valley resulting from forced channeling would occur at points 90° from those for pressure-driven channeling (Doran and Whiteman, 1992). The characteristics of forced channeling suggest that pressure-driven channeling might be a more significant wind forcing mechanism for locations near ridges or valley walls that run perpendicular to the mean wind. It is also likely that forced channeling would be more significant for smaller scale ridges and valleys where pressure driven channeling would have insufficient scale for the Coriolis differences to be very great.

Fourthly, the thermal forcing parameter may produce resultant winds within a large valley when pressure differences occur along the valley axis as a consequence of uneven heating of various portions of the valley. Thus, thermal forcing as a wind forcing mechanism is not directly dependent upon wind flow above the valley. As before, wind flow resulting from thermal forcing yields either up-valley or down-valley winds since these directions provide the least amount of resistance. This type of forcing mechanism would likely be more significant at night because daytime vertical mixing would inhibit horizontal forcing of air resulting from thermal effects.

The identification of the influence of various forcing mechanisms on complex terrain wind flow is difficult since these forcing mechanisms typically act simultaneously upon the mean wind, and the strength of each forcing mechanism varies with conditions such as synoptic systems, cloud cover, stability, and time of day. It is important to determine the contribution of major wind forcing mechanisms to the mean wind (especially in complex terrain) in order to properly model the air quality of a region. The wind resulting from the combined influence of wind forcing mechanisms may be either light or strong. It is not uncommon for such a resultant wind to be light (frequently even less than the ASOS-threshold of 1.5 m/s) and from a direction unlikely to be expected by a model not designed to deal with such complex terrain. Thus, the primary goal of the analysis conducted here addresses some of the effects of wind forcing mechanisms on surface winds in an area of complex terrain (on scales of approximately 3 to 300 km). The four sites used to identify the primary wind forcing mechanisms affecting the Great Valley of Eastern Tennessee are shown in Figure 2.4.

The ETOS network of towers is well suited to an analysis of wind forcing mechanisms due to the varied locations and altitudes of towers in and around the Great Valley of Eastern Tennessee. The availability of mountain, ridge-top (within valley), valley bottom (within valley), and plateau locations made it possible to measure winds simultaneously above and within the Great Valley (see Table 2.3). It was also possible to analyze local variations caused by wind forcing mechanisms due to the proximity of several ridge-top and valley bottom sites in the Oak Ridge area (see Figure 2.1).

The specific analysis of wind forcing mechanisms focused on the ridge-top site (T110). Winds at this site were compared with those measured concurrently at the mountain top site T224 (located 15 km west-northwest of T110 and 678 m higher). Similarly, winds at the valley bottom site T003 (located 2 km north of T110 and 72 m lower) were compared to those at the ridge-top site T110. The first analysis was to detect large scale effects such as those affecting the Great Valley in general. The second analysis used local effects such as those that might be observed between local ridges and valley bottoms. As in Part 1 of the analysis, the calculation of wind roses played an important role in the observations; however, in this case, wind roses were calculated based on wind direction and speed at a comparison site so that wind patterns could be observed for a given site for each wind direction or speed range at another site. Wind speed values for the site serving as the independent variable in analysis were divided into three categories based on the overall wind speed patterns of the given site. Wind speed categories were: (1) light (< 1.5 m/s), (2) moderate (1.5 to 3.5 m/s), and (3) high (> 3.5 m/s). Note that it was necessary to consider high winds at the independent variable site even though we are primarily studying light winds, since the forcing mechanisms involved might still result in a low wind speed at the dependent variable site.

2.3.3 Wind Rose Computation by Site and Time of Day and Subsequent Site to Site Comparisons

The purpose of this analysis was twofold. First, a comparison of two ASOS sites positioned differently with respect to complex terrain was desired. Secondly, a comparison of wind data for an ASOS site with that of a research grade site (such as an ETOS site) was needed. The Knoxville - Oak Ridge area served this purpose well since the Knoxville McGhee-Tyson Airport ASOS and the Oak Ridge ASOS are both located within the Great Valley only 40 km apart. Two ETOS towers (Site T001 - Oak Ridge NOAA/ATDD and Site T005 - Melton Hill Lake in Oak Ridge) are located in proximity to the Oak Ridge ASOS (about 2 km south and north, respectively). The validity of the comparison is further established by the fact that all four sites are located in local valley bottoms with respect to the area's 100-m parallel ridge lines. The differences between measuring winds to a threshold of 1.5 m/s versus 0.3 m/s should be particularly evident in this comparison. It is also true that local users of wind data have often used Knoxville data as a proxy for Oak Ridge data (even for model input). This analysis should provide valuable insight into the

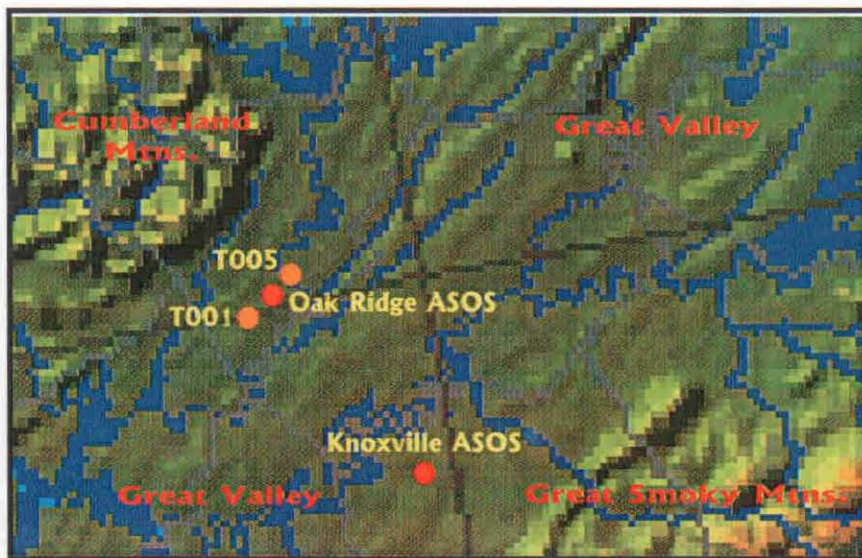


Figure 2.4 Sites used for analysis in Wind Rose Computation by Site and Time of Day and Subsequent Site to Site Comparisons. ASOS sites are shown in red; ETOS sites in orange.

wisdom of such a procedure. Wind roses were calculated for each of the four sites overall and with respect to time of day (early morning, late morning, afternoon, and evening). A summary of the sites analyzed appears in Table 2.4. Figure 2.4 depicts the locations of the four analyzed sites with respect to each other as well as the regional terrain.

Table 2.4. Sites used for comparisons in Part 2.3.3.

<i>Site</i>	<i>Location</i>	<i>Nearest Town</i>	<i>Network</i>	<i>Data Record</i>
T001	36°00' N, 84°15' W	Oak Ridge, TN	ETOS	Jan 98 - Feb 00
T005	36°02' N, 84°12' W	Oak Ridge, TN	ETOS	May 99 - Feb 00
Knoxville	35°49' N, 83°59' W	Knoxville, TN	ASOS	Jan 98 - Feb 00
Oak Ridge	36°01' N, 84°14' W	Oak Ridge, TN	ASOS	Nov 98 - Feb 00

2.3.4 Wind Speed Distribution with Respect to Time of Day

The time of day when light wind speeds occur is also of interest when considering the construction of an air quality model. While it is generally a foregone conclusion that winds tend to be lighter at night (except in the presence of strong synoptic systems), this is not entirely the case in some complex terrains. Wind speed with respect to time of day is also important since differing stability parameters tend to be associated with different times of day. As a result, the goal in this part was to provide the frequency distribution of wind speed at each of the eight ETOS meteorological sites used in the low wind speed analysis (see Part 2.3.1; see also Table 2.1 for site specifics). Sites T001, T004, T110, T119, T223, T224, T330, and T331 were plotted in the same way up to a wind speed threshold of 8.0 m/s.

2.3.5 Duration of Calm Winds

The duration of calm or light winds was analyzed for the Knoxville McGhee-Tyson ASOS site. Duration frequencies were calculated as the numbers of hours winds typically remained below a given wind speed threshold. Durations were calculated for 0.5, 2.0, and 3.5 m/s thresholds. It has been previously noted that current ASOS measurements at Knoxville McGhee-Tyson report winds as calm if they are under 1.5 m/s. Thus, in order to analyze the duration of calm/light winds less than 0.5 m/s, older data from 1991 - 1993 were analyzed, which included some manual measurements made at somewhat lower wind speed thresholds.

2.4. Analysis of Wind Rose Changes at Low Wind Speeds: ETOS Network

Four major topographical zones are represented in this portion of the analysis: (1) mountain; (2) ridge-top (within the Great Valley); (3) valley bottom (within the Great Valley); and (4) (Cumberland) Plateau. Measurements from two sites within each zone were conducted. In addition, the Knoxville McGhee-Tyson Airport ASOS site was analyzed for comparison purposes with the

other sites located within the Great Valley. Complete plots for all nine sites discussed in this section can be found in Appendix A.

2.4.1 Mountain Sites: T223 (Cove Mountain) and T224 (Buffalo Mountain)

The mountains sites used in the analysis were strategically chosen for their respective locations on opposite boundaries of the Great Valley (see Figure 2.1). Computer simulations of flow in and near topography such as the Great Valley have suggested that flow is dependent upon both the width and depth of such a valley (Eckman, 1998). Thus, it is possible that wind observations may be somewhat different from one side of the Great Valley to the other, even for mountain altitudes.

Wind roses for Cove Mountain (site T223) suggest a clear change in direction patterns as wind speeds increase from near calm to 5 m/s. Winds less than 0.5 m/s reveal a strong bias toward being from the east and northeast; however, this may be inconsequential since such winds represent only about 1% of all measured winds at the site. More significant is the strong tendency for winds from northerly directions from wind speeds of about 0.5 m/s thru 2 m/s. This feature was dominant in this wind speed range during all times of day. The 0.5 m/s to 2 m/s range of wind speeds represents about 20% of all winds at Cove Mountain. A northerly range of wind flows (327° to 33°) dominated about 30% of that time for those wind speeds. This finding is significant in light of the recent problems in the Great Smoky Mountains National Park (GSMNP) with respect to air quality. Winds in this range of speeds (0.5 to 2 m/s) are more frequent during summer months when the air quality in the GSMNP tends to be at its worst levels. Since Cove Mountain is located at the interface of the Great Valley and the Great Smoky Mountains (Great Valley to the north of Cove Mountain), it is quite probable that transport of pollutants from the Great Valley toward the Great Smoky Mountains occurs frequently in these situations. While it is still uncertain how much of the pollutants in the Great Valley are locally generated, such pollutants are present and would be transported toward the GSMNP during light northerly wind conditions.

Winds in the 0.5 to 2.5 m/s range at the Cove Mountain site (T223) also showed a tendency for south-easterly flow (102° to 168°) during the early morning hours (midnight to 6 am). This characteristic represented about 15% of wind flow in this range. While the exact cause of such flow is unknown, it may be related to nighttime effects of the higher Great Smoky Mountain Divide about 15 km south of Cove Mountain. The divide is about 500 to 800 meters higher than Cove Mountain (1243 m MSL).

Another notable aspect of the wind rose analysis at Cove Mountain was the shift from a dominance of northerly winds up to 2.5 m/s to a dominance of southwesterly winds (192° to 258°) above 2.5 m/s. This dominance continues up to the 5 m/s threshold of this study. Southwesterly flow dominated approximately 35% of wind speeds from 2 to 5 m/s. With respect to pollutant transport, this might suggest that during moderate winds, different source region of pollutants might be important than when the area is under the influence of lighter winds. The frequency of southwesterly flow did not seem to be affected greatly by time of day considerations except that westerly winds (238° to 303°) were more significant during the afternoon hours (12 to 6 pm) for winds of 2 to 4.5 m/s. This may be the result of increased mixing of the atmosphere during

afternoon hours, which would have the effect of mixing the dominant westerly winds aloft down to lower levels.

The other mountain site (Site T224, Buffalo Mountain) exhibited some expected significant differences from Cove Mountain, but also a significant number of similarities. The dominance of northerly winds at Buffalo Mountain continued up to about 3 m/s. This is notable since the range of winds from 0 to 3 m/s represents 40% of all winds at Buffalo Mountain. Thus, northerly winds during light winds (0 to 3 m/s) seem to be even more significant with respect to pollutant transport than at Cove Mountain. It is also notable that any pollutant transport affecting Buffalo Mountain from the north would not likely have originated or flowed from the Great Valley since Buffalo Mountain is situated west and north of the Great Valley; therefore, air quality problems affecting Buffalo Mountain from the north would have to come from other more distant sources. Another difference between the observed northerly wind flow at Cove Mountain and that observed at Buffalo Mountain is that such flow at Buffalo Mountain showed more diurnal change. In particular, winds during the afternoon (12 - 6 pm) tended to be somewhat more generalized (not having a preferred wind direction). In similar fashion to Cove Mountain, winds at Buffalo Mountain exhibited a preference for northerly flow (327° to 33°) for lighter winds (0 to 2 m/s). Such flow represented about 35% of winds at speeds less than 2 m/s.

Above 3 m/s, winds at Buffalo Mountain (T224) were dominated by flow from the southwest to the northwest (214° to 326°). This represented about 40-45% of all wind flow from 3 to 5 m/s. The dominant flow at Buffalo Mountain had both a broader nature and higher frequency of northwest winds than those at Cove Mountain; however, as was the case with Cove Mountain, a different source region for pollutant transport seems implicated for higher wind speeds than that for lower speeds.

Another interesting feature of winds at Buffalo Mountain was a small increase in easterly winds (89° to 101°) for winds above 2.5 m/s. This tendency represented only about 5 to 10% of flow but is noticeably higher than the frequency of flow either clockwise or counterclockwise of the those easterly winds. Again, the exact cause of this anomaly is not known but it is suggested that it is related to easterly winds that set up in the Great Valley quite frequently. Buffalo Mountain is lower (1031 m MSL) than Cove Mountain (1243 m MSL) and thus may be more influenced by easterly wind flow within the Great Valley. This idea is supported by the observation that the tendency for easterly winds disappears during the afternoon (12 - 6 pm) when vertical mixing of the atmosphere tends to be strongest, and flow induced by the Great Valley tends to be weakest.

Perhaps the most notable aspect of both the Cove Mountain and Buffalo Mountain sites is the shift in dominant wind direction that occurs as wind speeds change at the given sites. Certainly there are implications for pollutant transport. Another very important observation is the wind speed threshold at which the shifts in wind direction occur. The shift takes place at about 2.5 m/s for Cove Mountain and about 3 m/s for Buffalo Mountain. Thus, if measurements at these sites were being performed by ASOS units having a minimum wind speed threshold of 1.5 m/s, it is likely that this significant shift in wind direction pattern at both sites would be observed. This is fortunate since ASOS sites serve as wind data sites for a significant portion of air quality model input. Findings for other complex terrain sites (discussed later) showed less positive results.

2.4.2 Ridge Top Sites: T110 (Pine Ridge) and T119 (Walker Branch)

Sites T110 (Pine Ridge) and T119 (Walker Branch) are located on similarly elevated (approximately 100-m) parallel ridges (343 m and 340 m MSL respectively) within 10 km of one another in Oak Ridge, Tennessee; however, they do differ fairly significantly in tower height. Pine Ridge is located on a 10-m tower and Walker Branch is positioned atop a 45-m tower. Thus, the two sites measure wind properties vertically displaced. Since both locations are within the Great Valley, the focus of the discussion will be more localized than that of the previously discussed mountain sites, which naturally would be exposed to a larger scale flow.

Wind patterns at the Pine Ridge site exhibit a great deal of variation with respect to wind speed. Unlike the aforementioned mountain locations, the overall wind pattern at this ridge top site seems to show a gradual evolution from 0 to 5 m/s. There is no identifiable, consistent pattern throughout a set of wind speed intervals. For winds between 0 - 1 m/s, the overall wind pattern shows no favored direction. Winds from the southern quarter of the compass (about 135° to 225°) are much less frequent than other directions. Winds in the northwestern quadrant of the compass (258° to 33°) make up the bulk of the wind flow (about 55%). As wind speeds increase, patterns become more bi-directional, generally from the southwest (210° to 240°) and northeast (30° to 60°). These directions roughly coincide with the northeast-southwest orientation of the local parallel ridges underlying both the sites. It would seem that for lighter winds (approximately 0 - 1 m/s), the local terrain has little influence on wind direction, but it gradually increases its influence so that winds are strongly aligned with the local ridges by the time wind speeds increase to 1.5 to 2 m/s; however, the wind direction patterns again diverge from local ridge structure for wind speeds of about 3 to 5 m/s. This suggests that for higher wind speeds, downward momentum transport is a significant factor at Pine Ridge. This conclusion is based on the general alignment of winds from 3 to 5 m/s with dominant flow during the approach and passage of synoptic systems. Prefrontal southerly flow is quite common aloft and post-frontal west to west-northwest winds are common. The wind roses at 3 to 5 m/s show that there is a strong preference for these wind directions (about 15-20% of winds for southerly directions and 30-35% for westerly winds). These wind direction preferences are observed with a high degree of consistency for all times of day. There is also a weaker maximum in wind direction from the north-northeast and northeast which represents about 20 to 25% of measurements between 3 to 5 m/s. The latter maximum in wind direction does show some weakness during the afternoon hours (noon - 6 pm). There is also a common post-frontal tendency for winds to become northeast in the Great Valley as high pressure areas approach from the north and northwest. This may account for the north-northeast winds at Pine Ridge.

Walker Branch (T119) shows a similar overall trend in wind characteristics when compared to the data collected at Pine Ridge (T110); however, the Walker Branch data reveal a somewhat smoother transition from one type of pattern to another. This is reasonable since Walker Branch is located about 35 m higher than Pine Ridge which places it above the influence of many possible nearby obstructions.

For lighter winds (0 to 1 m/s), Walker Branch exhibited no significant preference for wind direction. Winds tended to be less frequent from northwesterly and northerly directions (303° to 33°). Note that Pine Ridge showed less frequent flow at these wind speeds from the south. Thus,

the two ridge top sites differ in this respect for wind speeds of 0 to 1 m/s. This result suggests that the sites in question may exhibit some influence from local terrain although this influence appears significantly reduced for light winds (0 to 1 m/s). Above 1 m/s, Walker Branch winds begin to exhibit dominant wind flow that is closely aligned with the local underlying ridge (about 245°/65°). This characteristic occurs gradually as wind speed increases and it doesn't become pronounced until winds have increased above 2 m/s.

For stronger winds (3 to 5 m/s), Walker Branch winds do not diverge from the axis of the underlying ridge as much as those of Pine Ridge; they continue to remain strongly aligned with the local ridge. As with Pine Ridge, there is an increased tendency for west-northwest winds (again possibly associated with post-frontal downward momentum transport).

Unlike the previously discussed mountain locations (Cove and Buffalo Mountains), Pine Ridge and Walker Branch exhibit a more gradual change in wind pattern as winds increase from 0 to 5 m/s. With respect to the 1.5 m/s threshold of a typical ASOS system, this could represent a difficulty in detection of wind patterns with winds less than 1.5 m/s. When winds are above 1.5 m/s, both sites exhibit flow roughly parallel to their respective underlying ridge axes; however, as winds lessen below this speed, the associated wind direction patterns gradually become more generalized. Thus, an air quality model using an ASOS-based measurement in a setting such as Pine Ridge and/or Walker Branch might calculate a significantly different result for air flow and pollutant transport than would actually be the case. This is an especially important consideration since winds between 0 and 1.5 m/s represent 20% of all wind flow at both of these ridge top sites.

2.4.3 Valley Bottom Sites: T001 (NOAA/ATDD Office) and T004 (Scarboro)

Site T001 (NOAA/ATDD, Oak Ridge, TN) is located in a local valley bottom between two parallel ridges about 80 m high. The local valley (City of Oak Ridge) is about 4-5 km wide, and the site is located approximately 500 m northwest of a ridge with an approximate 200-m gap. The other valley bottom site at Scarboro (T004) is located in adjacent Bethel Valley between two parallel ridges. Unlike the Oak Ridge valley, Bethel Valley is about 2 km wide. The Scarboro site is positioned about midway between the ridges that border Bethel Valley. Both valley areas are oriented in an east-northeast to west-southwest axis with the neighboring ridges.

The most notable observation regarding wind patterns at the NOAA/ATDD site is the pronounced shift in pattern that occurs around 0.5 m/s. Winds at 0.5 m/s and below tended to be dominated by an east to southeast flow (57° to 168°), being more easterly during the morning hours and more southeasterly during the afternoon/evening hours. The gap in the ridge 500 m to the southeast may be responsible for much of this wind pattern.

Winds above 0.5 m/s at the NOAA/ATDD site exhibited a good alignment with the local ridge. Winds were dominated by flow from the east-northeast to east and from the west and west-southwest under these circumstances. This pattern remained fairly consistent for all times of day and for all wind speeds up to 5 m/s. A minor exception to this rule was that of afternoon winds (12 -

6 pm) from speeds of 0.5 to 1.5 m/s where the flow pattern remained somewhat more generalized. This probably represents the localized effects of afternoon mixing of the surface layer.

Winds at the Scarborough site also show general alignment with the local ridge-and-valley axis (although the winds were aligned roughly with a northeast to southeast axis due to the slightly different angle of the local ridges in that area). Unlike the NOAA site, Scarborough showed significant alignment with the local ridge-and-valley axis even for light winds less than 0.5 m/s. This is likely due to the effect caused by the narrower valley containing Scarborough than that containing the NOAA/ATDD site. During daytime hours (6 am to 6 pm), the flow at Scarborough tended to be more generalized (again, probably due to localized mixing of the surface layer).

It was noted that the winds at Scarborough were aligned with the local ridge-and-valley axis to an even higher degree than those at NOAA/ATDD. Birdwell (1996) has shown that there seems to be an approximate exponential relationship between local valley width and wind direction at a given valley location within ridge-and-valley terrain (see Figure 2.5) for valleys up to 6 km wide. Consideration of this effect by air quality models might also help improve calculations in ridge-and-valley terrain.

Perhaps the most notable observation of the wind analyses for valley bottom sites is the high percentage of wind speeds measured that fall below the 1.5 m/s threshold common to most ASOS-type systems. Over 50% of winds at the NOAA/ATDD site (T001) fall below this threshold and over 55% fall below it at the Scarborough site (T004). This strongly suggests that air quality modeling would be difficult in ridge-and-valley terrain using the currently available ASOS-type wind data since these measurements would miss over half of the light but still important wind flow. Another factor to consider is the abrupt change in wind pattern observed at the NOAA/ATDD site. This change in flow would be absent in ASOS data since it occurred well below the 1.5 m/s threshold.

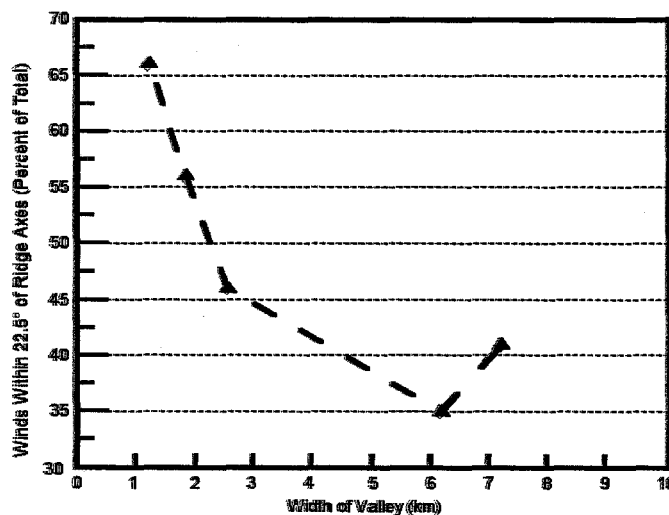


Figure 2.5 Percent of valley bottom winds within 22.5° of local ridge axes with respect to valley width.

Perhaps this effect is less important when measurements are made in the central portion of a valley bottom (note that there were fewer abrupt changes in the wind pattern at Scarborough, located in the center of its valley bottom with respect to NOAA/ATDD, located near the southeastern edge of its valley bottom). Since valley bottom sites represent one of the higher concentration areas of both people and vehicles with respect to topography, it would be prudent to take note of such wind pattern effects when devising new modeling techniques.

2.4.4 Plateau Sites: T330 (Allardt) and T331 (Spencer)

Sites T330 (Allardt) and T331 (Spencer) are located on the Cumberland Plateau (see Figure 2.1). With respect to air flow, the Cumberland Plateau represents a fairly level, elevated surface. The analysis of these sites provides an interesting comparison of winds on nearly level terrain to that of the non-level terrain discussed in the last three sections. Additionally, these observation sites are located in the same region as those previously analyzed (they are generally under the influence of similar upper level winds).

Winds for Allardt are basically general in nature with no consistent dominant wind direction when wind speeds are from 0 to 1.5 m/s. A number of individually high preferences of wind direction are evident but these appear to be more associated with the limited nature of the data set rather than any meteorological effect. At wind speeds above 1.5 m/s, the availability of data increases significantly. At ranges of 1.5 to 3 m/s, wind flow remains fairly generalized except that winds from the southeast to south (124° to 191°) begin to be more dominant, accounting for about 25 to 30% of total flow. This south-southeasterly flow seems to be more significant during the morning hours (midnight to noon). As wind speeds continue to increase (ranges of 3 to 5 m/s), the south-southeasterly component of wind flow begins to dominate evening hours as well (6 pm to midnight), accounting for as much as 40% of all wind flow. Afternoon winds (12 to 6 pm) from 3 to 5 m/s are equally dominated by northwesterly flow (282° to 348°). As noted previously, the northwest flow could probably be associated with the effects of downward momentum transport during the afternoon hours, when the atmosphere is sometimes, but not always, coupled with wind flow aloft.

Spencer exhibited much the same wind flow characteristics as those observed at Allardt. One minor difference observed was a preference for northwesterly flow (282° to 348°) in about 35% of the winds at speeds of 1 to 2.5 m/s; compared to values at Allardt that were only about 20%. Spencer showed the same tendencies for increasingly prevalent south-southeasterly flow as wind speeds increased. Spencer also showed the same tendency for northwesterly flow during the afternoon at wind speed ranges of 3 to 5 m/s.

The similarity of wind observations at Allardt and Spencer was expected since both are located on a relatively level plateau at similar altitudes. This suggests that wind characteristics were influenced more by regional influences rather than local terrain or even nearby mountain ranges. It is notable that even at these relatively flat terrain sites, wind patterns change with respect to speed. Unlike the complex terrain sites previously discussed, these sites exhibit most of their change in

wind pattern at speeds above 1.5 m/s (about 2 to 3 m/s); therefore, it is likely that the pattern change for lighter winds would be detectable by ASOS-type wind monitors having thresholds of 1.5 m/s.

2.4.5 Knoxville McGhee-Tyson ASOS Site

The Knoxville ASOS is located at the McGhee-Tyson Airport near Alcoa, Tennessee, in the central portion of the Great Valley. The site could be classified as “valley bottom” although it is somewhat more open than the valley bottom locations discussed previously. Since ASOS sites generally have a wind speed threshold of 1.5 m/s, winds analysis started at that level and continued up to 5 m/s. The “Calm” designation given to the winds below 1.5 m/s by the ASOS system resulted in almost 21% of all winds reported at the site. This is clearly unacceptable for air quality modeling purposes. An additional 10% of winds from 1.5 to 3 m/s were reported as “Variable”, resulting in an additional set of data that would be a problem for model input. Of the data having both a reported wind direction and speed, the site shows a clear preference for winds from the northeastern quadrant of the compass (349° to 101°) when wind speeds were from 1.5 to 2.5 m/s; however, for winds at or above 2.5 m/s, southwest to westerly flow (214° to 281°) were prevalent. Winds from the northwest or southeast quadrant were about 10% of total observations. Thus, the site shows a good approximate alignment with the axis of the Great Valley (about 45°/225° at this location). What are notably absent from the observations at the Knoxville ASOS are the more interesting localized features observed at the NOAA/ATDD and Scarboro. This is probably the result of the ASOS’ lack of the reporting of wind direction and speed below 1.5 m/s.

2.5 Analysis of Wind Roses for Low Wind Speeds: INEEL Network

Three significant topographical zones are identified and represented in this portion of the analysis: (1) mountain valley, adjacent to the Snake River Plain; (2) high valley within the Snake River Plain; and (3) low valley, within the Snake River Plain. Measurements from the sites within each zone are reviewed here. Complete plots for all 6 sites discussed in this section can be found in Appendix A.

2.5.1 Mountain Valley Site: BLU (Blue Dome)

Site BLU (Blue Dome) exhibits a great deal of wind pattern variation both with respect to wind speed and time of day. It certainly fails the aforementioned ASOS threshold “test” of 1.5 m/s. The variations are more dramatic than those observed with sites associated with the ETOS network in the Southern Appalachian region. The reason for this effect is easier to see when one considers the relief of the Snake River Plain compared to the Southern Appalachians. The difference in altitude between valley floor and surrounding mountains is several times greater in the area of the Snake River Plain compared to that of the Great Valley and the surrounding Cumberland Plateau /Mountains and Great Smoky Mountains.

With respect to wind speed, the Blue Dome site exhibits a gradual change in wind pattern from one that is completely generalized (at 0 to 0.5 m/s) to one that is strongly aligned with the axis of the local valley (about 340°/160°). This change seems to occur primarily between 1 to 1.5 m/s; therefore, it would be unlikely that an ASOS-type system would detect the significantly different wind pattern for very light winds (0 to 1 m/s).

Another characteristic wind pattern observed at the Blue Dome site was not significantly noted in any of the ETOS network sites in the Southern Appalachians. This site appears to be influenced by a well established mountain-valley breeze (the highland equivalent of a sea-breeze environment). This is similar to the previously discussed thermal wind forcing mechanism and results in very pronounced up-valley flow (from the south-southeast in this case) during daytime hours (6 am to 6 pm) and the reverse at night (6 pm to 6 am). The mountain-valley breeze appears to account for 80 to 85% of all winds at Blue Dome when winds are from 2 to 5 m/s; however, under lighter wind conditions (1 m/s or below), the wind patterns are very generalized. This is another characteristic that would be missed if these measurements had been made using a 1.5 m/s threshold.

2.5.2 High Valley Sites: ARC (Arco), CRA (Craters of Moon Monument), and EBR (Lava Zone)

Each of the three sites are located within the main portion of the Snake River Plain at elevated levels within the basin but differ in altitude by as much as 250 meters. Arco and Craters of the Moon are located near the north-northwestern side of the Snake River Plain, with Arco located just outside the mouth of a mountain valley. The Lava Zone site is located closer to the center of the Snake River Plain (see Figure 2.2 and Table 2.2).

Wind patterns at Arco exhibited some characteristics similar to those observed for the ridge top sites in the ETOS network. The overall wind pattern changes from one of a general nature (at 0 to 0.5 m/s) to an alignment with the mountain valley to the north of Arco at speeds of 1 to 3 m/s. The alignment with the mountain valley is similar to that observed at Blue Dome, with similar north-northwest and south-southeast winds, although the Arco site seems affected more by the down-valley flow (NNW) of this phenomena than the corresponding up-valley (SSE) flow. From about 3 m/s upward, overall wind patterns also exhibit a lesser but significant degree of alignment with the Snake River Plain axis (about 60°/240°).

Wind patterns with respect to time of day tended to be fairly complex. The down-valley component of the mountain-valley breeze dominates or is significant in nearly all night time measurements (6 pm to 6 am) but also was evident during the day time when the mountain-breeze should reverse. This suggests that the observed down-valley wind may be a mixture of mountain-valley breeze flow and that of downward momentum transport from winds aloft during the day. There is a significant flow observed in daytime winds (6 am to 6 pm) from the SSE that probably represents the real affect of the mountain-valley breeze during the daytime. It is interesting that even though Arco is located outside of the nearby mountain valley and within the Snake River Plain (by about 30 km), the site still experiences significant flow associated with the mountain valley. This flow appears more dominant than that associated with the up and down valley winds of the Snake River Plain.

Most of the observed wind patterns at Arco would be observable with an ASOS-type system, with one important exception. Winds less than or equal to 0.5 m/s (and to some extent those less than 1 m/s) show a very generalized pattern. This phenomenon would be unknown if measurements were made only at 1.5 m/s or above, as on a typical ASOS system. In this case, these type winds represent about 8 to 10% of the total wind flow.

Site CRA (Craters of the Moon National Monument) is also located near the northern side of the Snake River Plain but it is positioned further from the mouth of the mountain valley that is close to Arco (see Figure 2.2). Overall wind patterns at Craters of the Moon show a somewhat generalized flow for very light winds (0 to 0.5 m/s) although not as much as for Arco. Even with such a light wind speed range, there is evidence for alignment of winds with the up and down valley components of the Snake River Plain. This feature is most evident during the daytime hours (6 am to 6 pm). The overall alignment of winds with the axis of the Snake River Plain is evident throughout the entire range of wind speeds from 0 to 5 m/s although this phenomena grows significantly stronger with increasing wind speed. For night time winds from 1 to 5 m/s, the down valley (northeasterly) component winds seem somewhat skewed toward the north. This is likely an influence from the mountain valley affecting Arco. Inspection of the topography in Figure 2.2 seems to support this possibility.

The change in wind patterns for winds under 1.5 m/s exists for the CRA site as for the Arco site, although the differences are less pronounced than at Arco. A system that doesn't measure winds under 1.5 m/s would have some difficulty resolving accurate wind flow for Craters of the Moon.

The Lava Zone site (EBR) is situated on high ground near the middle of the Snake River Plain with respect to the sides of the basin (see Figure 2.2) and shouldn't be influenced by mountain valleys near the sides of the basin. As expected, wind roses show good agreement with the axis of the Snake River Plain except, below 1 to 1.5 m/s, the winds become very generalized. Again, this presents a problem for systems with high wind speed thresholds. Little change in wind distribution occurs with respect to time of day. As overall speeds increase from 1.5 to 5 m/s, the prevailing northeasterly (down valley) winds gradually become dominated by southwesterly (up valley) winds. For higher wind speeds (3 to 5 m/s), an anomalous south to south southeast wind becomes dominant during the evening hours (6 pm to midnight). No obvious reason for this flow was observed.

2.5.3 Low Valley Sites: BLA (Blackfoot), and IDA (Idaho Falls)

Both the Blackfoot (BLA) and Idaho Falls (IDA) sites are located near the southeastern side of the Snake River Plain at similar altitudes (see Figure 2.2 and Table 2.2). The Idaho Falls site is a little further from the side of the basin (about 30 to 40 km) and is perhaps more exposed to the northeastern end of the Snake River Plain.

Blackfoot exhibits fairly consistent and predictable wind patterns as compared to the previously discussed analyses. As before, wind patterns were very generalized (no particular wind direction) for winds less than 1.5 m/s. Above 1.5 m/s, wind flow aligns well with the axis of the

Snake River Plain and becomes more pronounced as wind speed increases to 5 m/s. Little anomalous behavior was observed with respect to time of day. Even though the site exhibits fairly predictable wind patterns, it still would present problems for an ASOS-type system having a wind speed threshold of 1.5 m/s.

Idaho Falls shows a more complex set of wind patterns than that of Blackfoot. Generalized wind flow is still evident for winds of 0 to 0.5 m/s or 1 m/s, yet instead of having a northeast-southwest alignment with the Snake River Plain as for other sites, Idaho Falls exhibited what appears to be a north-south alignment of winds. This flow begins to be evident at winds as low as 0.5 to 1 m/s and persists up to wind speeds of at least 3 m/s. Above 3 m/s, up valley (southwesterly) flow becomes more evident and a northeast flow does not develop at any time of day. Northwesterly winds become prevalent as well for wind speeds of 2.5 to 5 m/s during nighttime hours (6 pm to 6 am). Although it is difficult to explain some of the discrepancies observed at the Idaho Falls site, it is probable that they are related to the long northwest fetch of the site with respect to the Snake River Plain as well as the northeastern terminus of the basin (see Figure 2.2). The former characteristic might explain the northwesterly flow observed for higher wind speeds (2.5 to 5 m/s) and the latter factor perhaps explains the more northerly aspect of down valley flow observed for wind speeds of 1 to 3 m/s. It is clear that Idaho Falls exhibits a number of wind characteristics not observed at Blackfoot. This is somewhat surprising due to the two sites' apparent proximity to each other and with respect to their similar locations in the Snake River Plain (see Figure 2.2 above).

Although an ASOS-type system could observe most of the anomalous tendencies in wind patterns at Idaho Falls, patterns for light winds would again be difficult to resolve due to the overall change in wind patterns observed for winds of 1 m/s or less. In most cases, such light wind periods cannot be discounted because they comprise a small but significant percentage of winds at the site.

2.6 Analysis of Wind Roses For Low Wind Speeds: Cape Canaveral

The Cape Canaveral, Florida, site is operated by the National Weather Service (NWS). Since data were collected prior to the implementation of ASOS, the measurements include some wind speeds as low as 0.6 to 1.0 m/s that were taken by manual observation. Such low wind speed data were sparse and wind speed increments were not as precise as those used for both ETOS and INEEL; therefore, the data analyzed represent an accuracy somewhere between the ASOS systems and the ETOS and INEEL research meteorological networks. Due to the less accurate wind speed increments used at Cape Canaveral, wind speed measurements were divided into 1 m/s intervals instead of 0.5 m/s intervals. Complete plots for the site discussed in this section can be found in Appendix A.

The winds observed at Cape Canaveral exhibit a somewhat more complex pattern than might be expected. Although the sea breeze has a major effect at the site, other factors strongly influence winds there as well. This includes large scale pressure systems moving from the major part of the North American continent from the north and northwest. One notable consistency in the data set is that winds from almost every direction are observed to occur with about 5% frequency or better

for all wind speeds from 0 to 5 m/s. Significantly higher overall frequencies occur for winds from the north (8 to 13%) and from easterly directions (20 to 25%).

Wind patterns vary significantly with respect to time of day. This is to be expected in a diurnally driven sea breeze environment. Winds from east to southeasterly directions were observed frequently during the nighttime hours (6 pm to 6 am). They are fairly consistent with respect to all wind speeds and comprise about 40% of all winds. Daytime winds reveal a variety of patterns with wind direction maxima frequently from the northwestern quadrant; however, wind from the east were also frequent during the daytime. These patterns probably reflect a combination of sea breeze flow with that of other factors such as winds associated with pressure systems or downward momentum transport. A positive aspect about the wind patterns at Cape Canaveral is that they remained fairly consistent with respect to wind speed, despite the fact that there are differing patterns with respect to time of day. It seems likely that interpolating winds for winds less than 1.5 m/s using those measured above 1.5 m/s might work in this particular case.

2.7 Changes in Wind Direction and Speed with respect to Winds Aloft

In order to assess when light winds might be more likely to occur at ridge top and valley bottom sites within the Great Valley of Tennessee, winds at three significant altitudes (corresponding to major topographic features) were compared. Site T110 (Pine Ridge), a ridge top location within the Great Valley, was compared with Site T224 (Buffalo Mountain), a mountain site perched near the western side of the Great Valley. Pine Ridge is separated from Buffalo Mountain by about 750 m in altitude and is located about 15 km east. In addition, local effects were analyzed by a comparison of the Oak Ridge Municipal Building site (T003) with the Pine Ridge site. The Municipal Building site is positioned in the middle of a 4-5 km wide local valley within the Great Valley that contains Oak Ridge, Tennessee, at an altitude about 65 m lower and is located 1 km north of Pine Ridge. The influence of several wind forcing mechanisms (discussed previously) should be identifiable. It is desirable, where possible, to identify the relative influence of each of these forcing mechanisms on wind measurements in the Great Valley in order to assess their influence with respect to light winds.

2.7.1 Comparison of Site T110 (Pine Ridge) with Site T224 (Buffalo Mountain)

The wind roses (see Appendix B) show that resultant wind direction at Pine Ridge varied considerably from that simultaneously measured at Buffalo Mountain. Generally speaking, Buffalo Mountain represents the regional wind flow over the Great Valley (in the vicinity of Oak Ridge) whereas Pine Ridge represents the resultant flow within the Great Valley. As discussed previously, the various major wind forcing mechanisms provide an influence upon the winds in the Great Valley in various ways. Figure 2.6 summarizes these flow influences with respect to a valley axis of about 55°/235° (the approximate axis of the Great Valley in the area of investigation). The figure will provide a reference for positive wind forcing mechanism features in the discussions of wind rose comparisons that follow.

2.7.1.1 During light winds (< 1.5 m/s) at site T224 (Buffalo Mountain)

See Appendix B to view the plots discussed in this section. During periods of light NE and ENE winds (0 to 1.5 m/s) at Buffalo Mountain, wind direction at Pine Ridge were similar in wind direction at Buffalo Mountain. It is suspected that during such circumstances, the down valley (approximately northeast) flow in the Great Valley was deep enough vertically to affect Buffalo Mountain. When light winds at Buffalo Mountain were from the E through SSE, winds at Pine Ridge continued to favor a down valley flow within the Great Valley. This effect would seem best explained by pressure driven channeling, forced channeling, or some combination of the two (see Figure 2.6). Winds from the south through the west at Buffalo Mountain corresponded to a wide variety of wind flows at Pine Ridge. These wind flows at Pine Ridge tended to focus on the directions of roughly NNE to NE, SSE, and W to WNW. For such winds, none of the wind forcing mechanisms discussed here seem to be particularly dominant on Pine Ridge winds (based on criteria in Figure 2.6, as well as by definition). Winds at Pine Ridge showed strong correlation with those at Buffalo Mountain when Buffalo Mountain winds were from the WNW. During NW or NNW flows at Buffalo Mountain, Pine Ridge winds agreed much of the time; however, there were also significant periods of northeast to easterly flows at Pine Ridge when Buffalo Mountain showed NW or NNW flow.

Overall, it appears that the influence of a particular wind forcing mechanism at Pine Ridge (within the Great Valley) was difficult to ascertain when winds were light above the valley; however, there is one notable factor. When winds at Buffalo Mountain were less than 1.5 m/s, winds at Pine Ridge averaged twice the speed, yet the overall winds at Buffalo Mountain average twice that of Pine Ridge. This result seems to suggest that important wind flows might occur within the terrain of the Great Valley that do not have a significant dependence on overall flow aloft. Thus, it may be necessary to develop better methods for accounting for local terrain effects with respect to air quality and air flow models.

2.7.1.2 During moderate winds (1.5 to 3.5 m/s) at site T224 (Buffalo Mountain)

In contrast to the light wind comparisons (< 1.5 m/s) between Buffalo Mountain and Pine Ridge, the effects of pressure driven channeling as a wind forcing mechanism became evident when winds at Buffalo Mountain ranged from 1.5 to 3.5 m/s. There is also some evidence for downward momentum transport for W to NW winds at Buffalo Mountain. When Buffalo Mountain winds were from the N through SSE, the corresponding winds at Pine Ridge showed a strong alignment with down valley (northeasterly) flow in the Great Valley. This is indicative of pressure driven channeling (see Figure 2.6). Winds from the S through SW at Buffalo Mountain resulted in both down valley and up valley flow within the Great Valley (at Pine Ridge). This is expected if pressure driven channeling is a major forcing influence, since these directions represent the zone where winds in the Great Valley would reverse with respect to pressure driven channeling. For winds at Buffalo Mountain from the W and WSW, winds at Pine Ridge roughly corresponded to up-valley (southwesterly) flow in the Great Valley, again suggesting pressure driven channeling as the dominant wind forcing mechanism. However, for W through N winds at Buffalo Mountain, winds from the W and WNW were prevalent at Pine Ridge. This flow does not correspond to the axis of

the Great Valley and thus suggests the influence of downward momentum transport. It is notable that the dominant W to NW flow at Pine Ridge varied from the corresponding direction at Buffalo Mountain leftward by about 10° to 50°. However, it was previously noted that a leftward Coriolis force adjustment needed to be taken into account for downward momentum transport causes. This would account for about 25° of the discrepancy.

Overall, pressure driven channeling and downward momentum transport account for most of the wind pattern relationships between Buffalo Mountain and Pine Ridge when winds were between 1.5 and 3.5 m/s. The pressure driven mechanism was dominant in the eastern half of the compass and the southwestern quarter of the compass with respect to Buffalo Mountain. The northwestern quarter of the compass was dominated by downward momentum transport. Review of the data suggested that this latter phenomenon is frequently associated with the aftermath of the passages of large scale synoptic system and/or frontal systems. It is also notable that the shift of winds from up valley to down valley flow with respect to pressure driven channeling should occur at about 55° with respect to the Great Valley axis and instead the shift occurred at about 10°. A possible explanation for this could be the irregular shape of the northwestern side of the Great Valley just northwest and north of the study area (see Figure 2.1). It is clear from these conclusions that wind forcing mechanisms must be taken into account when modeling winds in a complex terrain environment such as the Great Valley, and that the placement of meteorological sites (even if using a lower wind speed threshold than the typical ASOS system) may have an impact on the accuracy of wind modeling.

Unlike the wind speed relationship observed for light winds at Buffalo Mountain, wind speeds at Pine Ridge averaged slightly less than those at Buffalo Mountain when winds (at Buffalo Mountain) were from 1.5 and 3.5 m/s. This is a reversal of the trend observed during light winds (< 1.5 m/s) at Buffalo Mountain.

2.7.1.3 During stronger winds (> 3.5 m/s) at site T224 (Buffalo Mountain)

Wind comparisons for stronger winds (> 3.5 m/s) between Buffalo Mountain and Pine Ridge showed a greater influence of pressure driven channeling at Pine Ridge. The overall patterns were similar to those for moderate winds (1.5 to 3.5 m/s) at Buffalo Mountain with a few notable differences. The transition zone from WNW flow at Pine Ridge to down-valley flow with respect to when winds were between N and NNE aloft was pronounced. Moreover, the transition from down- valley to up-valley flow at Pine Ridge was more distinct, and occurred when winds at Buffalo Mountain were between the SSW and SW. The WNW flow at Pine Ridge associated with downward momentum transport continued to be evident when Buffalo Mountain winds were from the W to N; however, there was also evidence for some up-valley flow associated with pressure driven channeling.

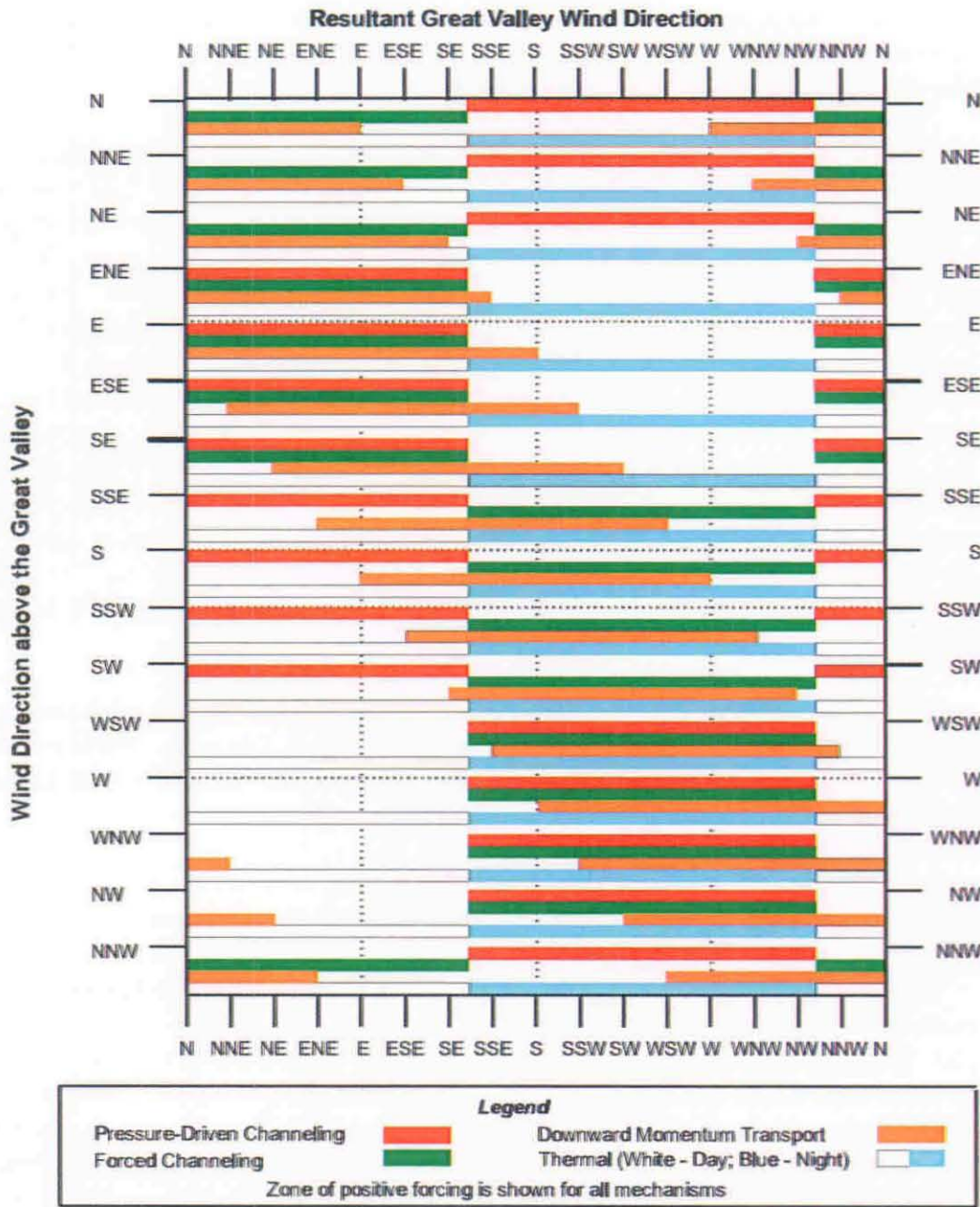


Figure 2.6 Idealized zones of positive forcing for four wind forcing mechanisms with respect to wind above and within the Great Valley.

2.7.1.4 Summary of comparison of T110 (Pine Ridge) winds with T224 (Buffalo Mountain) winds

In summary, it would appear that for lighter winds above the Great Valley (< 1.5 m/s at Buffalo Mountain), undefined local terrain effects play an important role in wind flow within the Great Valley. Pressure driven channeling, downward momentum transport, and other factors seemed to explain little of the resulting flow in the Great Valley at Pine Ridge; however, for stronger winds (> 1.5 m/s), flow within the Great Valley was explained well by pressure driven channeling and downward momentum transport. Pressure driven channeling seems to become the more dominant wind forcing mechanism when winds above the Great Valley were strongest (winds > 3.5 m/s) at Buffalo Mountain. It is important to keep in mind that most of the aforementioned forcing mechanisms act simultaneously to varying degrees on resultant winds within the Great Valley, although it is not uncommon for one particular mechanism to dominate conditions.

An additional and somewhat surprising finding of the study concerned light winds at Pine Ridge. Observations confirmed that winds less than 1 m/s occurred with an 8 to 10% frequency regardless of how strong the winds were at Buffalo Mountain. This phenomena could suggest fairly frequent decoupling of the atmosphere within the Great Valley from that above it.

2.7.2 Comparison of Site T003 (Oak Ridge Municipal Building) with Site T110 (Pine Ridge)

The wind roses (see Appendix B) comparing Sites T003 (Oak Ridge Municipal) and T110 (Pine Ridge) provided a means of analyzing localized effects of complex terrain more than that discussed for the comparison of winds above and within the Great Valley as a whole (Pine Ridge compared to Buffalo Mountain). Specifically, this portion of the analysis noted the effects of local parallel ridges on valley bottom winds (keeping in mind that valley bottoms tend to have higher concentrations of transportation-related activity). It was observed that ridge top winds (such as measured at Pine Ridge) approximately correlate to the general flow of the Great Valley. Thus, it is important to determine any observed variation of the flow in a valley bottom setting from that at a nearby ridge top setting. Due to the lighter nature of the winds at Pine Ridge and the Oak Ridge Municipal Building Sites, the comparisons conducted here were divided into two categories instead of three (winds < 1.5 m/s and winds ≥ 1.5 m/s at Pine Ridge).

2.7.2.1 During light winds (< 1.5 m/s) at site T110 (Pine Ridge)

For light winds (< 1.5 m/s) at Pine Ridge, winds at the Oak Ridge Municipal Building showed a strong correlation with the forced channeling mechanism (the wind direction characteristics of forced channeling in the Great Valley shown in Figure 2.7 would approximately apply here as well) for most wind directions at Pine Ridge. However, for wind direction at Pine Ridge of west, west northwest, northwest, and north northwest, there was a dominant tendency for winds at the Oak Ridge Municipal Building to approximate those at Pine Ridge. This is best explained by downward momentum transport. Overall, wind speeds at both Pine Ridge and the Oak Ridge Municipal Building were similar.

2.7.2.2 During moderate to strong winds (≥ 1.5 m/s) at site T110 (Pine Ridge)

For moderate to strong winds (≥ 1.5 m/s) at Pine Ridge, winds at the Oak Ridge Municipal Building continued to show a significant correlation with the forced channeling mechanism. More significant, however, was the evidence for downward momentum transport. In a majority of cases, winds at Oak Ridge Municipal were within 25° of corresponding flow at Pine Ridge. This suggests that as winds increase at ridge top level, winds in the valley bottom tend to become coupled with the ridge top winds. Thus, downward momentum transport appears to become more important as winds increase. Overall wind speeds at Pine Ridge for moderate to strong winds (≥ 1.5 m/s) tended to be higher than the corresponding valley bottom flow at Oak Ridge Municipal Building by a factor of about two.

2.8 Wind Rose Computation by Site and Time of Day and Subsequent Site-to-Site Comparisons

Complete plots for the four sites (See Table 2.4 and Figure 2.5) in the comparison are in Appendix C. The analysis first compares two ASOS sites in proximity but in different locations with respect to the width of the Great Valley. The second portion of the analysis compares winds measured at ETOS sites (having higher precision wind measurements) with those measured at one of the ASOS sites.

2.8.1 ASOS Comparison: Site KTYS Knoxville McGhee-Tyson Airport and Site KOQT Oak Ridge

A question of concern with respect to data input for atmospheric models is that of instrument location, and is particularly important with respect to complex terrain, where winds in one location may not be as representative of an area as another. In order to address this concern, the sites that were analyzed had to meet two major criteria: (1) they were located in an area of complex terrain (the Great Valley in this case), and (2) they were ASOS-grade towers (the data type that is currently used for input into an atmospheric model). The Knoxville and Oak Ridge ASOS sites meet both of these criteria.

As expected, both sites exhibited a general preference for winds associated with flow moving up and down the axis of the Great Valley; however, significant differences existed in a couple of areas. First, wind speeds at the Knoxville location averaged about 60% higher than those in Oak Ridge. This phenomena may be related to an effect demonstrated by Eckman (1998), who modeled wind flow in and around the Great Valley and showed that the pressure driven channeling has the strongest effect on the eastern half of the Great Valley. The Knoxville ASOS is located in the southeastern side of the Great Valley while the Oak Ridge ASOS is located closer to the northwestern border of the Great Valley.

Another notable difference between the Knoxville and Oak Ridge sites was the percentage of variable and calm winds. Variable winds (rapidly changing wind directions designated in ASOS-type data) occurred in 4.2% of the Knoxville data but represented 15.0% of the Oak Ridge data. Since no specific wind direction is given in a "variable" wind designation, these data would

probably be unusable as air quality model input. Also, 20.8% of winds at Knoxville were designated as “calm” (all winds under 1.5 m/s in ASOS data) and 44.5% of the data at Oak Ridge registered as “calm”.

Although the overall wind patterns at the Knoxville and Oak Ridge ASOS sites have similar relative frequencies, the differences are significant in major ways including: (1) magnitude of the wind direction frequencies, (2) frequency of variable winds, and (3) frequency of calm winds. These effects could have significant effects on model input, depending on the area of interest and the data site used.

2.8.2 ASOS /ETOS Comparison: Oak Ridge ASOS, T001 (NOAA Office), and T005 (Melton Hill Lake)

In order to better illustrate the loss of data between currently used ASOS-type wind equipment and that of air-quality-grade wind equipment, the Oak Ridge ASOS site was compared with data from Sites T001 (NOAA/ATDD site) and T005 (Melton Hill Lake) of the ETOS network, that are located only 1 to 2 km north and south of the Oak Ridge ASOS site, respectively. Also, all of the sites are located in valley bottom terrain. The NOAA/ATDD and the Oak Ridge ASOS sites are located in different parts of the same valley bottom while the Melton Hill Lake site is located in a valley bottom (near Melton Hill Lake) that is only partially separated from that containing the Oak Ridge ASOS site.

Overall wind speed averages for measured winds (excluding those reported as “calm”) were similar for all three sites. Also, all three showed a preference for wind directions associated with up and down valley flow with respect to the axis of the Great Valley. Both the Oak Ridge ASOS site and Melton Hill Lake showed a preference for generally northeasterly and southwesterly winds. The NOAA/ATDD site, however, showed a tendency for east northeasterly and westerly winds. These differences may be associated with the proximity of a local ridge or the minor deviation of local ridges from the angle of the main axis of the Great Valley.

The frequency of wind direction values was much lower at the Oak Ridge ASOS as compared to either NOAA/ATDD or Melton Hill Lake. This is largely due to winds at the ASOS site being reported as “calm” when they were under 1.5 m/s. It was noted previously that as much as 50% of all winds occur at speeds under 1.5 m/s in this area. Thus, the Oak Ridge ASOS site misses much of the ambient wind flow while the ETOS sites do not since ETOS sites have a 0.3 m/s threshold. This factor would obviously cause major concern regarding the accuracy of model performance if the local ASOS data were used for model input.

All of the above factors suggest that a higher density network of meteorological sites would be useful to an atmospheric or air quality model. There are currently four ASOS sites in the Great Valley of Eastern Tennessee. This is probably inadequate for modeling purposes there or any similar area with complex terrain.

2.9 Wind Speed Distribution with respect to Time of Day

When conducting this type of analysis, it is useful to understand the wind distribution of a given site with respect to wind speed. Plots of wind speed distribution can help put into perspective the percentage of winds that occur below or above a particular wind speed and how the bulk of observed wind flow changes with respect to the time of day. Of particular interest is the percentage of wind observations that fall above or below the important 1.5 m/s threshold.

Wind speed distribution plots were calculated for the eight ETOS sites used in the wind rose analysis. The plots can be found in Appendix D and show the frequency of wind (in percent) in 0.5 m/s intervals of wind speed.

2.9.1 Mountain Zones: Sites T223 (Cove Mtn) and T224 (Buffalo Mtn)

The distribution of wind observations with respect to wind speeds were similar at Cove Mountain (T223) and Buffalo Mountain (T224). Both sites exhibited a broad overall peak in wind speed of approximately 2 to 4 m/s. Both also revealed a higher peak of about 2 m/s during the afternoon (12 to 6 pm), with a slightly higher peak at Cove Mountain (14%) than at Buffalo Mountain (12%). Another notable observation was that winds at both sites tended to be slightly higher at night (6 pm to 6 am), which is the reverse of the trend seen at lower altitudes. This effect is probably due to the lack of vertical mixing at night.

Since observations below a 1.5 m/s threshold occurred in about 10% of all observations, ASOS-grade measurements probably would suffice for Cove and Buffalo Mountains. The average was lowest at night (5%) and higher (about 15%) in the day.

2.9.2 Ridge Top Zone: Sites T110 (Pine Ridge) and T119 (Walker Branch)

At Pine Ridge, about 30% of winds occurred at or below 1.5 m/s. This is a significant proportion of the total winds. Unlike the data in the valley bottom sites, the peak in observations remained fairly constant with respect to wind speed for all times of day. Observations at Walker Branch showed higher wind speed averages than at Pine Ridge. Only 19% of winds fell at or below 1.5 m/s and this average remained fairly constant with respect to time of day. Also, peaks in observations remained approximately the same during the day and at night.

Overall, air quality modeling attempts using an ASOS-grade wind threshold of 1.5 m/s would probably be able to resolve ridge top conditions better than valley bottom; however, a significant proportion of wind measurements (about 20% overall) would be missed. It should also be noted that such ridge top measurements do not necessarily reflect conditions in nearby valley bottoms, where most of the population and transportation activity tends to occur.

2.9.3 Valley Bottom Zone: Sites T001 (NOAA Office) and T004 (Scarboro)

The most notable effect observed with respect to winds at the NOAA/ATDD site is the high percentage of winds (about 65%) that occur at or below the 1.5 m/s ASOS-threshold. For night time winds (6 pm to 6 am), 75 to 80% of winds occur at speeds below 1.5 m/s. This suggests that attempts to model air quality at night at this site would be largely useless using a system with a 1.5 m/s wind speed minimum threshold. Even for day time measurements (6 am to 6 pm), over 40% of winds occurred below this threshold. Measurements at Scarboro showed much the same result although afternoon (12 to 6 pm) measurements showed a somewhat lower percentage of winds below 1.5 m/s (about 30%).

2.9.4 Plateau Zone: Sites T330 (Allardt) and T331 (Spencer)

Allardt and Spencer showed similar wind distributions with respect to wind speed. Peak observations occurred near 3 m/s. Less than 10% of overall winds occurred at or below 1.5 m/s so this suggests these ASOS-type sites could yield fairly good results if used as input to an air quality or other model. Conditions at either site did not vary significantly with respect to time of day.

2.10 Duration of Calm and Light Winds

The duration of calm and light winds (with respect to a 1.5 m/s threshold) can be significant in an area of complex terrain. The Knoxville McGhee-Tyson Airport ASOS site was used for this analysis since it is currently used for dispersion model input more than other locations in the area. The duration of calm or light wind periods was analyzed for three wind speed categories: (1) winds less than 0.5 m/s, (2) winds less than 2 m/s, and (3) winds less than 3.5 m/s. In order to obtain realistic data for the 0.5 m/s threshold, observations from 1991 to 1993 were used. This was a period when manual observations were being taken and the data contained some wind speed measurements below 1.5 m/s. Plots are in Appendix E.

Information for winds less than 0.5 m/s showed that these near calm periods seldom exceeded a few hours, being almost non-existent for periods longer than 5 hours. Approximately 17% of observations show a period of one hour having winds less than 0.5 m/s and about 8% of the data revealed two-hour periods of such winds.

Knoxville showed a prevalence for winds under 2 m/s, with an occurrence of about 35% for one-hour periods, two hour periods about 23% of the time, and 3 hour periods with a frequency of about 15%. Most of the wind during such periods would be unobservable using ASOS-type systems and thus unknown to a model using such input.

Using 3.5 m/s as a threshold for light winds revealed that winds remain below this threshold at the Knoxville site much of the time. One-hour periods occurred over 80% of the time, six-hour periods occurred over 55% of the data, and 12-hour periods represented about 35% of the data set.

2.11 Conclusions

The definition of complex terrain goes beyond just that of mountainous regions. It is important to note that most landscapes would fall into the category of complex terrain. Cities, buildings, lakes, forests, rivers, etc. can all add features that could cause an area to be classified as complex terrain. We have focused mostly on that type of terrain in order to illustrate the influence that a number of factors can have on wind in a locale; however, much work still needs to be done in such areas. We have focused on some known atmospheric effects within complex terrain and applied them to a real world situation. It is by sorting out such factors that we can show what remains to be identified and quantified.

With respect to current air quality measurement techniques, analysis shows that available meteorological parameters are often inadequate. Mountain and plateau locations showed the most promise with respect to the ability to correctly model local air flow; however, since most population and transportation centers tend to be located in lower terrain, such modeling capability may be of limited utility. Clearly, the higher terrain locations are important to modeling techniques in terms of establishing a general or regional flow of air or pollutants; however, sub-regional or local effects are equally important.

It has been shown that air quality modeling using wind data from current National Weather Service ASOS-type monitoring stations is apt to miss local scale effects. More importantly, currently available ASOS stations fail to measure important low speed wind cases. This work has demonstrated clearly that these missed winds often behave differently than stronger wind, and that they vary spatially within complex terrain. Therefore, not only is it important to devise means of making better measurements at current observation sites, it is also important to account for the lack of representativeness of some sites with respect to nearby surrounding areas.

2.12 Recommendations

First, it is important to improve the quality of measurements at existing meteorological sites that are used for air quality model input. It would be technically feasible to provide wind monitors at ASOS-type stations to measure winds as low as 0.3 to 0.5 m/s at relatively modest cost at each location, but it may not be permissible to do this. If light wind cases are to be handled properly, it means that a separate independent monitoring station will be needed.

Second, the addition of numerous sites for use in model input should be considered. This is particularly true for areas of significantly complex terrain. New measurement locations could be outfitted with real-time communication capability in order to expedite the modeling process. Current technology exists to place and outfit meteorological systems of this sort with modest cost (far below the cost of many existing ASOS-type systems).

3. URBAN TURBULENCE FIELD STUDIES

R.P. Hosker, Jr., R.L. Gunter, J.R. White, C.J. Nappo, T.P. Meyers

3.1 Introduction

It has always been difficult to obtain and interpret turbulence data within urban areas, partly because of the limitations of instrument systems, and partly because of the difficulty of making representative measurements within the crowded urban region. Such information would be useful for understanding and modeling intra-urban pollutant dispersion, especially near ground level. Most previous urban measurements reported in the literature seem to have been taken in somewhat idealized configurations such as urban street canyons, or from towers and other high points well above the building roofs. However, idealized geometries are not common, especially in cities where urban renewal has resulted in a mix of older low buildings (typically three or four levels) and newer office buildings (ten or more stories tall), with a scattering of parking lots, open garages, and pedestrian thoroughfares. Furthermore, measurements well above roof level do not address the near-ground dispersion question. As part of this collaboration between FHWA and NOAA, portable turbulence and flux measurement systems were installed to obtain turbulence data within a built up urban area. This chapter reports on turbulence measurements within the urban canopy regions of two small U.S. cities.

3.2. Urban Site Characteristics

3.2.1 Knoxville, Tennessee

Knoxville, with a city population of about 169,000, is located in the southeastern U.S., about 40 km west of the Great Smoky Mountains, within the Great Valley of eastern Tennessee, in a region of broad valleys separated by long low ridges. A site was established on the open flat roof of a multi-level parking garage built into the side of a slope, so the roof is only about 6 m above street level on the west side of the structure, just above the traffic and small ornamental trees bordering the adjacent street. The garage is roughly in the midst of the built-up urban center, east of a more-or-less north-south array of tall office buildings, so that westerly winds place the measurement system in the composite wake of these structures. The site is about 0.5 km from the nearest building, not within the immediate wake of any individual structure. The top picture on Figure 3.1 shows an aerial view of the downtown Knoxville area, looking from the west. The parking garage site is nearly hidden from view behind the tall buildings at the rear of the photo. The bottom picture in Figure 3.1 is an aerial view from the north. The site is visible to the left of center, just west of the roadway. Figure 3.2 is an aerial view from the southeast where the parking garage is clearly visible near the center of the photo.



Figure 3.1 Aerial views of the Knoxville site. The top picture is looking from the west; the bottom picture is looking from the north.



Figure 3.2 Aerial view of the Knoxville site, looking from the southeast. Parking garage is visible at center.

The parking structure is rather open; each level has walls about 1.1 m high on all four sides, with open space above the walls. The entire center of the structure, where a common up-down driveway is located, is open from the lowest level to the roof. This rather porous structure, with its capability for pressure equalizations, seems unlikely to result in extensive roof flow separation and recirculation zones, except close to the low wall on the upwind edge. The instruments were positioned as far from this wall as possible, close to the open central region. Figure 3.3 shows the turbulence measurement system on the roof of the parking garage, looking to the south. The batteries are in the large plastic box on the ground, and the sonic anemometer is clearly visible on the top of the tripod. Figure 3.4 shows the turbulence system, looking to the west, with the Knoxville buildings in the background.

For contrast with the urban data, mean wind measurements were made on a 22 m fire spotter's tower on Sharp's Ridge, about 3.8 km NW of the parking garage site, outside the urban area. After the first few experiments, a full turbulence measurement site was also established at the University of Tennessee's Agricultural Campus, a farm about 8 km SSW of the city center. Additional meteorological data are available from Knoxville McGhee-Tyson Airport, about 18 km SSW of the city center.



Figure 3.3 View of equipment on Knoxville garage roof, looking south.

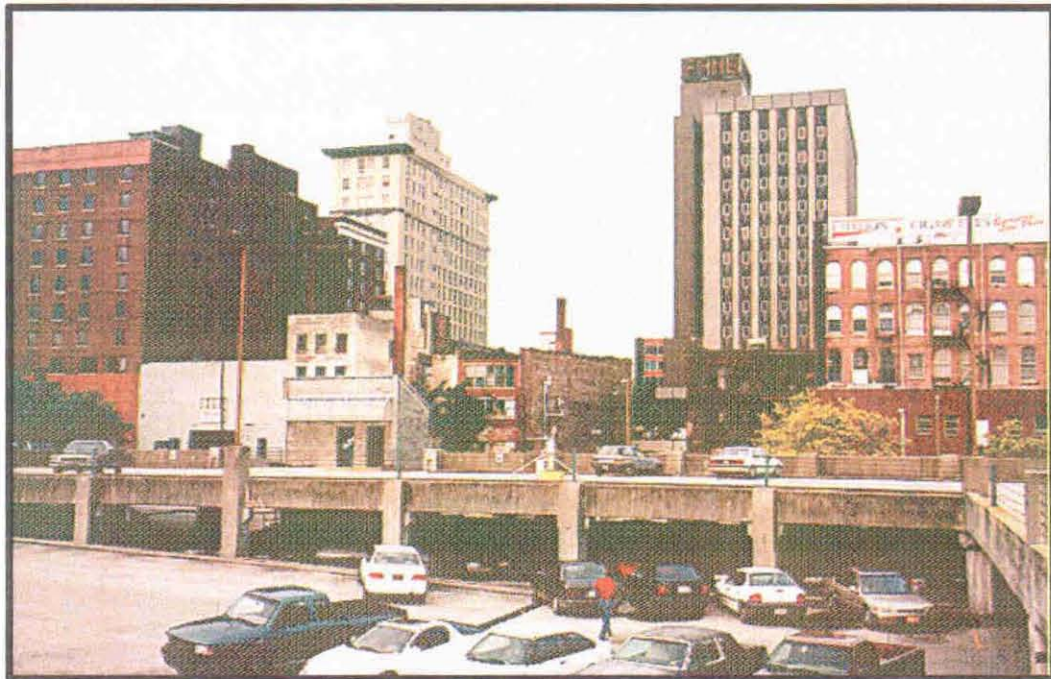


Figure 3.4 View of equipment on the Knoxville garage roof, looking west. Equipment is visible at lower center.

3.2.2 Nashville, Tennessee

Nashville, with a city population of about 488,000, is located in the Central Basin of middle Tennessee, near the escarpment of the Highland Rim. The Rim rises about 100 m above the Basin floor, encircling the city like a horseshoe from SW through N to SE. The southern region is more or less open, in undulating terrain.

A site was established just north of the built-up downtown area, in a very large parking lot near the Bicentennial Capitol Mall State Park. SE winds blow through the highest portions of the downtown area to reach the instruments, but winds from the S and SW must also traverse the built-up area. The site is at least 1 km from the nearest buildings, not in the wake of any individual structure. Figure 3.5 shows an aerial view of Nashville looking to the east. Figure 3.6 is another aerial view, looking to the south; the instrument site was on a grassy strip within the large parking lot south of the low, flat-roofed building and just east of Bicentennial Park. Figure 3.7 shows the turbulence measuring system at ground level, looking roughly south-southwest, with the Nashville buildings in the background.



Figure 3.5 Aerial view of Nashville, looking east. The experimental site is to the north (left), just out of the picture.

For contrast, a second turbulence site was set up in a flat grassy area beside the runway at the rural Lebanon airport, about 40 km E of the Nashville city center. Our instruments are located next to the National Weather Service's Lebanon Automated Weather Observing System (ASOS). Meteorological data from the Nashville Airport, about 10 km ESE of the city center, are also available. Figure 3.8 shows the Lebanon site.



Figure 3.6 Aerial view of Nashville site, looking south. The experimental site is within the parking lot south of the large, low flat-roofed building located just east (left) of Bicentennial Park.



Figure 3.7 Ground level view of equipment in Nashville, looking SSW.



Figure 3.8 View of equipment at the Lebanon Airport near Nashville.

3.3 Turbulence Instrumentation

A compact and readily portable turbulence measurement system developed at our laboratory over a period of several years and refined during a number of field programs has made these urban measurements possible. The measurement system is based on commercially available omnidirectional 3-D sonic anemometers mounted on sturdy, lightweight, easily disassembled aluminum pipe tripods. The mean and fluctuating wind vector components are determined with Solent sonic anemometers (Gill Instruments, Hampshire, England). Both the 10.4 Hz "R2" model and the 4 Hz "Windmaster" were used.

Traditionally the eddy covariance method (e.g., Businger, 1986; Baldocchi *et al.*, 1988), used to calculate momentum and heat fluxes, has been constrained to short term intensive field campaigns. Improvements in instrument design, stability, and power requirements during the last few years now permit nearly continuous measurements of sensible and latent energy fluxes using the eddy covariance technique. Using this method, the average vertical turbulent eddy fluxes of sensible and latent heat flux and other scalars are determined, for example, as

$$\overline{w' \chi'} = \frac{\sum_{i=1}^n (w_i - \langle w \rangle) (\chi_i - \langle \chi \rangle)}{n}$$

where w is the vertical velocity component of the wind vector, and χ is any scalar of interest (e.g., water vapor concentration). Here, the bracketed quantities denote an average or "mean" that is subtracted from the instantaneous values to obtain the fluctuating component. Average vertical turbulent fluxes $\overline{w'\chi'}$ were computed in real time using a digital recursive filter (200-s time constant) for the determination of a "running mean" from which the instantaneous values are subtracted. An averaging period of 30 min (denoted by the overbar) was used and is considered large enough for statistical confidence in the covariance quantity but short enough to resolve the structure of the diurnal cycle. In addition to the averaged results, the raw data were also recorded for later analysis.

It is well known that wind vector measurements made at experimental sites that are not perfectly flat can result in non-zero vertical wind velocities as measured from a gravitationally vertical coordinate system (e.g., Kaimal and Haugen, 1969; Hyson *et al.*, 1977). At first glance, this would seem to be true in urban areas, where the complex flow fields around buildings and the flow patterns over a roof where instruments are located are bound to result in streamline curvatures. If the city is located on hilly terrain, as is Knoxville, for example, the situation is even more complex. Therefore, at the end of each 30-min averaging period, vertical turbulent fluxes perpendicular to the mean streamwise wind were obtained by mathematically rotating the coordinate system of the measurement frame of reference to obtain a zero mean vertical and transverse velocity (i.e., $\overline{w} = \overline{v} = 0$). Details of this procedure, described by Wesely (1970) and Hyson *et al.* (1977), were outlined by Businger (1986) and Baldocchi *et al.* (1988); the program used here was based on McMillen (1986). However, second thoughts about such coordinate rotation within urban regions have emerged. Lee (1998) has discussed the probability of non-zero mean vertical winds occurring in forests, and it is likely that these will also be experienced within the urban canopy layer because of flow deflections and building wake effects. Future work should include analyses of the effects of such coordinate rotation on the data. The analysis below represents a mixed approach where most of the results are from coordinate-rotated data, but the spectra and TKE are not.

The three components of the wind vector were determined with Solent sonic anemometers (Gill Instruments, Hampshire, England). Both the 10.4 Hz "R2" model and the 4 Hz "Windmaster" anemometers were used in this study. The stable long-term operational characteristics of this instrument and its ability to continue measurements during cold weather and light rain events (Yellard *et al.*, 1994), as well as its low power consumption, were important considerations in its selection. The symmetric head design of the R2 (the Windmaster is nearly identical) with its slender support structure produces little flow distortion (Grelle and Lindroth, 1994).

A 486-class laptop computer was configured in a multi-tasking mode. For the first and main task, measurements of the three components of the wind vector along with the speed of sound (from which the virtual temperature can be derived) were sent digitally via a RS-232 line from the sonic anemometer to the laptop computer, which was housed on the instrument tripod in a small

environmental enclosure. In the second task, the computer retrieved standard meteorological data such as mean wind speed, direction, and temperature from a Campbell Scientific 21X data logger every 30 minutes, and appended the data to a separate file. Lastly, during extended runs, the covariance data and standard meteorological data files are copied after midnight to new files with a name, year and calendar day header; this feature was used at the rural sites in this study, but not at the urban ones. During long-term continuous studies the computer is usually equipped with a modem and cellular telephone in order to retrieve the data and conduct system checks from the comfort of the laboratory. However, during this urban experiment, where there was some concern for the safety of the equipment, an on-site observer was continually present, and periodically verified that the data were being captured and that the system components were functional. During more extended experimental periods, data are generally retrieved from the laptop computer about once every two days.

Measurements were made in each case about 3 m above the local surface. The entire system operates on 12 VDC power, so it operates on standard deep-cycle batteries. In rural areas, battery recharging is usually accomplished with solar panels and in urban regions, a trickle charger powered by the AC mains is usually feasible.

3.4 Urban Turbulence Results

Figure 3.9a shows a scatterplot of the mean wind speed measured within the Knoxville urban canopy layer vs. the mean wind measured from the fire tower on Sharp's Ridge, outside the city. It is clear that the winds are greatly reduced in speed in the city, and nearly uncorrelated with the speed observed outside the city center. Figure 3.9b shows a scatterplot of the standard deviation of wind speed within and outside Knoxville. Figure 3.9c is a scatterplot of wind direction within and outside Knoxville and, if the point at 0° on Sharp's Ridge is mapped to 360° , the correlation is quite reasonable. Wind direction within the city does track that observed outside, but with a good bit of scatter. Figure 3.9d shows the scatterplot of σ_θ within Knoxville compared to that outside the city. There is a much wider range of σ_θ within the city, and the values are not correlated with the rural data.

We interpret these results as indicating that the direction of the mean wind within Knoxville is related to the wind aloft, but the wind speed is significantly reduced and rather independent of the wind speed aloft. Fluctuations in wind speed within the city are about as large as the mean speeds. And the fluctuations in wind direction are very large, reflecting the expected influence of locally directed flows and wakes. These results are important for dispersion modeling, which often must utilize airport data from outside the city to characterize intra-urban conditions. It is clear that there are substantial differences between the urban and rural data.

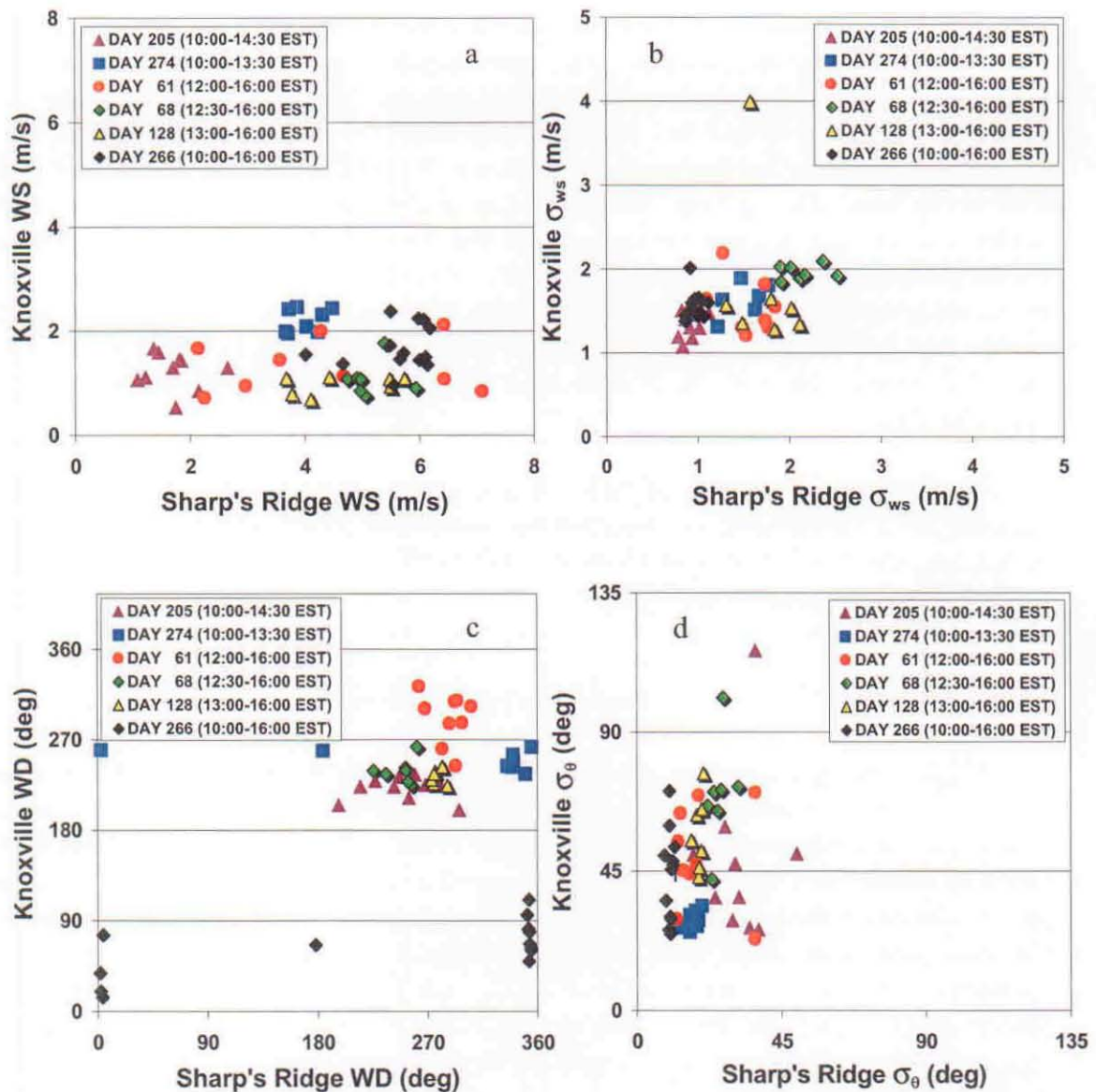


Figure 3.9 Figs. a, b, c, d are scatterplots of observations of mean wind speed, standard deviation of mean wind speed, wind direction, and standard deviation of wind direction, respectively, for the urban Knoxville and the Sharp's Ridge sites.

Figure 3.10 is much like Figure 3.9, but for Nashville and the rural site near Lebanon. Figure 3.10a is a scatterplot of the wind speed measured within Nashville vs. the wind measured at the rural Lebanon Airport. The Nashville winds are only somewhat reduced in speed relative to the rural airport, and they are moderately correlated with the speeds observed outside the city center. This is different than observed in Knoxville, and may be due to the more open exposure of the Nashville site. Figure 3.10b shows a scatterplot of the standard deviation of wind speed within and outside Nashville. The wind speed fluctuations seem to be somewhat greater within the city. The reason for the small cluster of high urban values on two days is still unknown. Figure 3.10c is a scatterplot

of wind direction within and outside Nashville. As in Knoxville, wind direction in Nashville does track that observed outside, but with a good bit of scatter. Figure 3.10d shows the scatterplot of σ_θ within Nashville compared to that at Lebanon. As in Knoxville, there is often a much wider range of σ_θ within the city, and the values are not well correlated with the rural measurements.

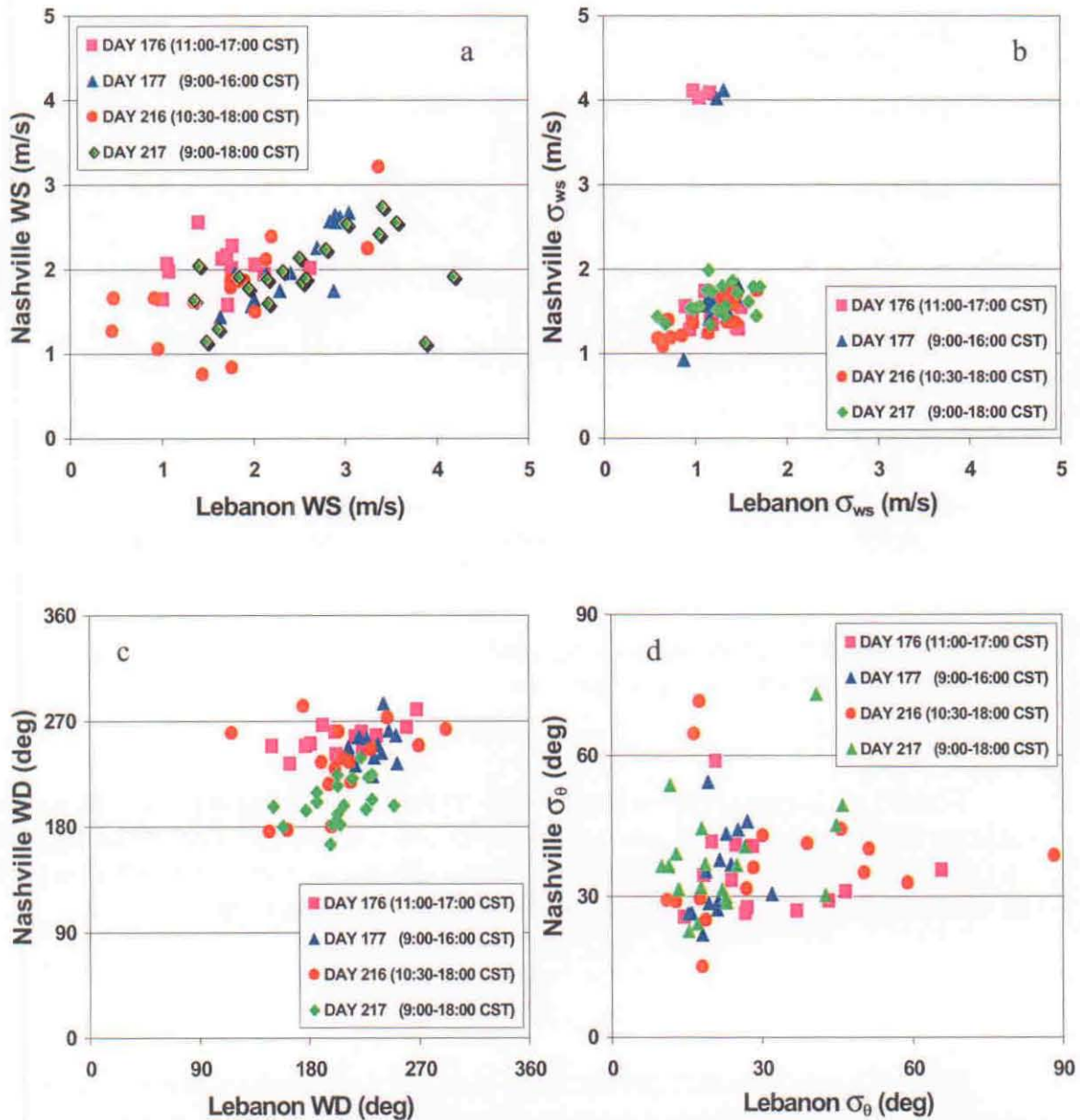


Figure 3.10 As for Figure 3.9, but for the urban Nashville site vs. the rural Lebanon airport site.

Figure 3.11 shows the urban and rural (UT Agricultural Campus) turbulent kinetic energies (TKE) as functions of time for one day in Knoxville. The Knoxville data did not begin until about noon, and the TKE is somewhat lower than the rural value at that time. After about 1230 hrs, the urban TKE is larger than the rural value, and this persists until about 1330 hrs. After that, the urban and rural values are similar until the rural site shut down with a computer power problem.

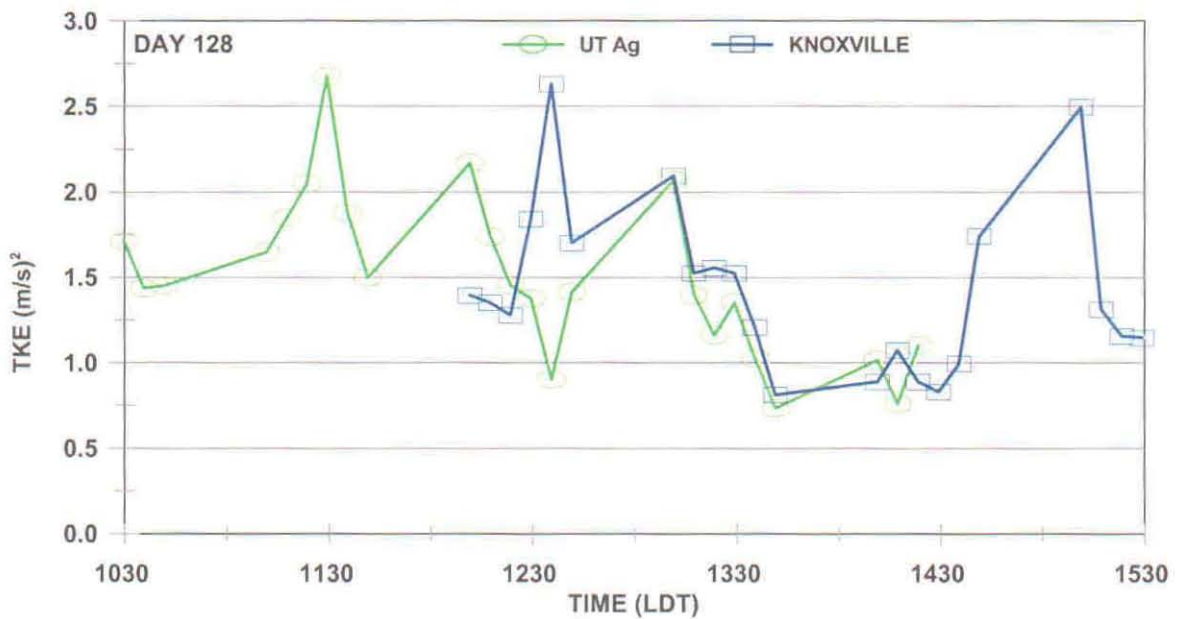


Figure 3.11 Turbulent kinetic energy (TKE, in m^2/s^2) at urban Knoxville site and the nearby rural University of Tennessee agricultural campus.

Figure 3.12 is akin to Figure 3.11, but for Nashville. It shows the time-wise behavior of the turbulent kinetic energy for the urban and rural site, for a single day. TKE values for both sites are very close in the early morning, but diverge quickly after sunup, with higher values in the urban area for nearly the entire day. Late in the day the values again become close.

3.5 Conclusions

For both Knoxville and Nashville, it was observed that the intra-urban mean wind speeds were significantly lower than observed in nearby rural areas. The mean wind directions within the cities tend to track those observed in nearby rural areas if terrain influences are not strong (e.g., directions at the Nashville Airport are often different than those seen elsewhere around and within Nashville; this is ascribed to the influence of terrain near the airport). The standard deviations of the wind direction, which are a measure of turbulence and can be useful in local plume or puff dispersion

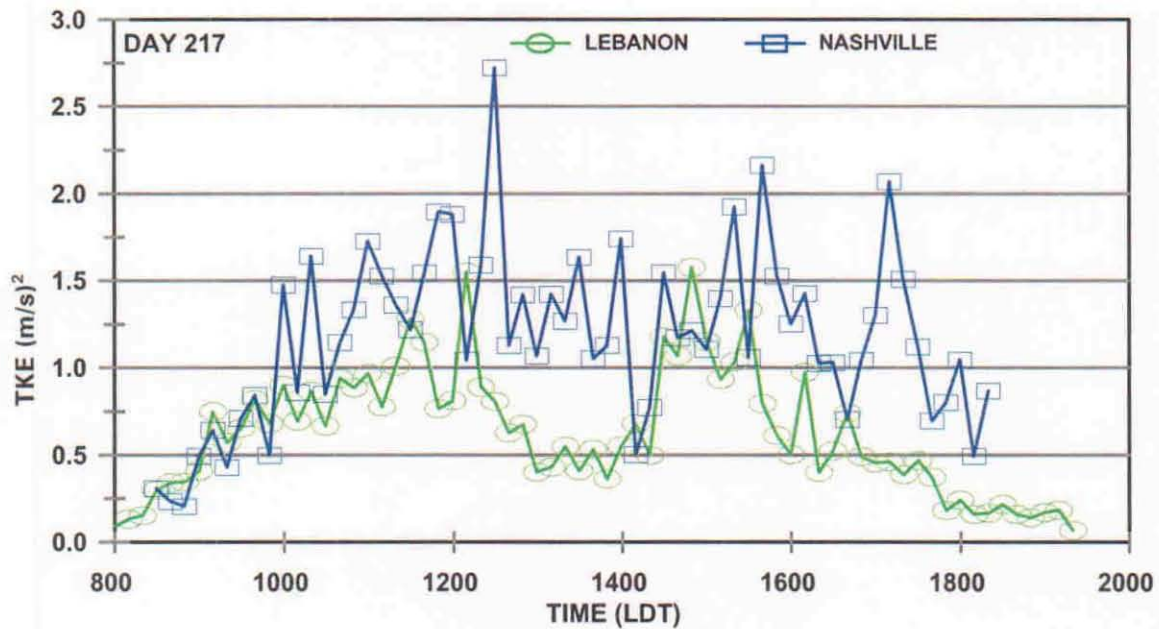


Figure 3.12 As for Figure 3.11, but for the urban Nashville site and the rural Lebanon airport site.

modeling, tend to be much larger within the city than outside. None of these results is very surprising. They do bring out the fact that it may be quite inappropriate to use data from an airport, typically located in open rural surroundings, to model atmospheric pollutant transport and dispersion within a city.

Measurements of turbulent kinetic energy (TKE) indicate that daytime TKE values tend to be higher within the city than in nearby rural areas. The additional turbulence within a city is generated by the wind passing amongst the buildings, and as well as by the changes in local energy budget and local zones of solar heating and shading.

Additional intra-urban data are needed. In a separate study not related to this project, ATDD staff recently performed wind and turbulence measurements from a sonic anemometry system mounted in the bed of a pickup truck. This system could be driven to a location of interest (e.g., the median strip of an urban arterial), oriented to north, and used to take measurements for several hours or days. A system such as this makes exploratory measurements possible.

Wind data within the urban canopy but above ground level are very difficult to obtain. Portable tower systems or mounting locations on buildings or other structures are needed for turbulence measurements since remote sensing techniques may be able to provide mean wind data above the ground. This remains one of the least known features of wind behavior in a city, despite its importance to local air quality issues.

4. VEHICLE WAKE TURBULENCE FIELD STUDIES

R.P. Hosker, Jr., R.L. Gunter, J.R. White, C.J. Nappo, T.P. Meyers

4.1 Introduction

Vehicles emit exhaust and evaporative gases that impact urban environments. If the vehicles are moving, their wakes affect the initial dispersion of these effluents; therefore, vehicle wake turbulence information is necessary to accurately predict pollutant transport and dispersion. Few models parameterize vehicle wake effects with empirical relationships. It would be useful to be able to accurately describe the effect of mixing by vehicles; however, turbulence behind a moving vehicle has generally not been measured. The high cost and complexity of turbulence measuring instruments, (e.g., the sonic anemometer) precluded feasible multi-instrument operation. Recent improvements in technology have led to relatively low-cost sonic anemometers, which are simpler to operate than earlier instruments. This has permitted an examination of the wake behind a single moving vehicle.

Measurements of the along-axis u , cross-axis v , and vertical w wake velocity components were taken behind a moving vehicle in a rather idealized environment to help characterize the 3-D flow field in the wake of one type of vehicle. The objective was to take fast-response measurements in a variety of configurations in conjunction with various vehicle speeds. We chose days that had relatively light winds, to lessen the effect of crosswind interference and ambient turbulence on the measurements.

4.2 Site

In order to avoid the effects of nearby buildings or other urban interference during sampling, we utilized the runway at the Rockwood, TN Airport. The airport is located in a rural setting about 30 miles (48 km) west of Knoxville, TN, on the Cumberland Plateau. There is a single runway approximately 5000 feet (1.5 km) long, oriented in a NE/SW direction. During the week there is only occasional aircraft traffic, providing virtually interference-free sampling conditions.

4.3 Instrumentation and Apparatus

Six commercially available 3-D sonic anemometers ("sonics"; Gill Instruments, Hampshire, England) were used for the measurements. Three sonics had a design sampling rate of 10 Hz, and three sampled at 10.4 Hz. Data were transmitted by serial cables to six laptop computers.

The six anemometers were mounted in a horizontal and vertical array (3 across x 2 high) on an adjustable aluminum pipe scaffolding mounted on an open framework lightweight trailer 17 ft (5.2 m) long x 6.7 ft (2.0 m) wide. To minimize the impact of the platform of the wake airflow, the trailer flooring was removed, leaving only the main support structural members. In the experiments reported here, the trailer was towed by a standard full-size van (see Figure 4.1), but the apparatus

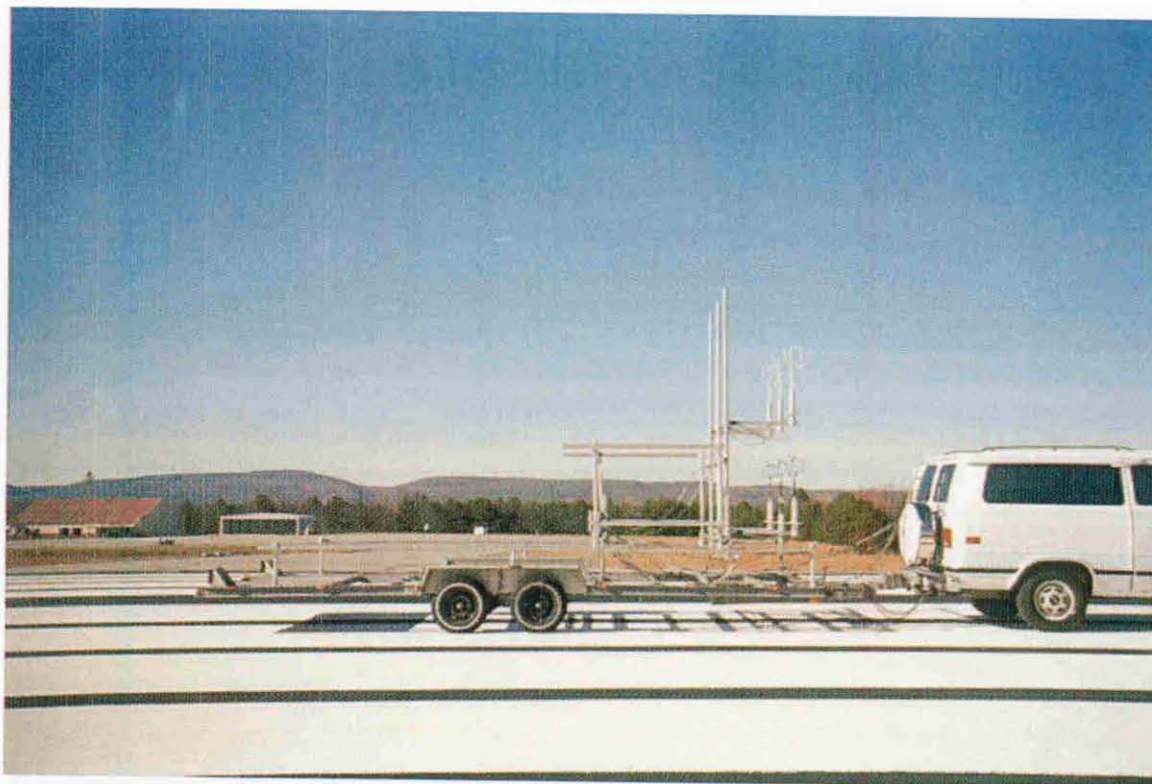


Figure 4.1 Van and trailer configuration for wake turbulence study. Top picture depicts the trailer/sonic setup; bottom picture shows view facing NE.

is light enough that it could easily be towed by a variety of vehicles. Facing the trailer from the rear of the van, the bottom tier of sonics were labeled "a", "b", "c" (left to right), and the top tier were "d", "e", "f" (left to right). The sonics were aligned so that the u component was along the trailer, with u positive as air flows from front to rear. The scaffolding was designed so that sampling positions could be changed in 1 ft (0.3 m) increments along each of the three axes. There were 15 possible positions from front to back, 9 in the vertical, and 4 to the left and right from center. The rearmost possible position was 18 feet (5.5 m) from the rear of the van.

At all times there was one anemometer in the center, both on the top and bottom levels of the array. The maximum possible distance to the left and right from center was 3 feet (0.91 m), although longer pipes can be added to the scaffolding to extend the lateral reach. The height range that could be sampled went from close to ground level (with the lower row of anemometers mounted inverted) up to 14 ft above ground (4.27 m) with the present apparatus, although this maximum height could also be increased. The position of the anemometers could be adjusted fairly quickly, without tools, using latching pins. After making simultaneous measurements at six locations within a given x-y plane, the box-like pipe array could be slid back along the pipe rails to another location along the trailer axis. The fixed rails minimized the risk of angular misalignments during a given set of measurements. During this series of experiments, the top three sonics (10.4 Hz units) were intentionally placed higher than the top of the van to provide measurements that would be above the wake cavity zone of the van. For each array setting, there was usually a run toward the NE and then toward the SW, plus one or more ambient condition samples with the vehicle not moving. Each run (depending, of course, on the speed of the vehicle) took approximately one minute.

The data collection system consisted of the six sonic anemometers with serial data cables, six laptop computers, a bank of four 12 VDC deep-cycle marine batteries wired in parallel, and several DC to AC inverters to power the computers. The battery pack provided a very stable source of power for the anemometers and computers. A hand-held voltage source was used to send a voltage signal simultaneously to each sonic anemometer that indicated the vehicle speed or other special condition. This signal was then digitized by the sonic anemometer and reported to the laptop computer recording the data from that unit. In addition to indicating the vehicle speed or other special condition for that run, the step change in the signal voltage provided to each anemometer provided a convenient means to synchronize all the data records for each run. The voltage "tags" were as follows: 0.1 V = "ignore", 0.5 V = ambient (non-moving) data, 1.0 V = 10 mph (4.5 m/s), 2.0 V = 20 mph (8.9 m/s), 3.0 V = 30 mph (13.4 m/s), etc.

4.4 Data Processing Method for TKE

The turbulence kinetic energy (TKE) was calculated to use as an indicator of the energy associated with the wake turbulence of the vehicle. Calculation of TKE utilized the raw data

$$\text{TKE} = 0.5 * (u'^2 + v'^2 + w'^2)$$

where u' , v' , and w' are the fluctuating components of the along-axis u component, the cross-axis v component, and the vertical w component measured by the sonic anemometers. The fluctuating components are calculated from the measured u , v , and w by subtracting the mean values, \bar{U} , \bar{V} , and \bar{W} : $u' = u - \bar{U}$; $v' = v - \bar{V}$; $w' = w - \bar{W}$.

Spectra of the TKE were calculated to determine if the size and the production (or dissipation) of the turbulent eddies could be resolved based on energy levels.

A power spectral density routine from a commercially available computing software package (MatLab by MathWorks, Inc.) was used to produce the spectra of TKE. The function PSD produces the power spectral density estimate. The following description is taken from the MatLab manual, to describe the processing procedure.

$P_{xx} = \text{PSD}(X, \text{NFFT}, F_s, \text{WINDOW})$ estimates the Power Spectral Density of a discrete-time signal vector X using Welch's averaged, modified periodogram method.

X is divided into overlapping sections, each of which is detrended (according to the detrending flag, if specified), then windowed by the WINDOW parameter, then zero-padded to length NFFT [number of points for the Fast Fourier Transform]. The magnitude squared of the length NFFT DFTs [Discrete Fourier Transforms] of the sections are averaged to form P_{xx} . P_{xx} is length NFFT/2+1 for NFFT even, (NFFT+1)/2 for NFFT odd, or NFFT if the signal X is complex. If you specify a scalar for WINDOW, a Hanning window of that length is used. F_s is the sampling frequency which doesn't affect the spectrum estimate but is used for scaling the X-axis of the plots.

The default values for the parameters are NFFT = 256 (or LENGTH(X), whichever is smaller), NOVERLAP = 0, WINDOW = HANNING(NFFT), $F_s = 2$, $P = .95$, and DFLAG = 'none'.

For the spectra of TKE presented here, the input parameters were $X = \text{TKE}$ (during the specified run); $\text{NFFT} = 128$; $F_s = k = \text{wavenumber}$, calculated from the sampling frequency of either 10 or 10.4 Hz, depending on the particular anemometer used; and the default Hanning window. The NFFT of 128 was chosen because the sample was small (approximately one minute), and 128 yielded an overlapping section of about 13 seconds. Since data were collected at several vehicle speeds, using frequency on the x-axis didn't allow direct comparison over the same distances. The frequency was converted to the wavenumber by assuming a direct mapping of frequency, f to wavenumber, k by $k = f/u$, where u is the total velocity as measured by each sonic. The spectra were then plotted on a logarithmic scale.

4.5 RESULTS

There were three days of sampling: 18 November 1999, and 1 and 2 December 1999:

18 November 1999 (Julian Day 322): On this day there were five anemometer configurations with six runs total, and all data were taken at a nominal vehicle speed of 40 mph (17.9 m/s). Table 4.1 lists the configurations and sonic positions for Day 322.

Table 4.1. Sonic anemometer array configurations and positions for Day 322.

Day 322												
	Configuration 1 Runs 1, 2, and ambient						Configuration 2 Run 1					
sonic	a	b	c	d	e	f	a	b	c	d	e	f
X (ft from rear of van)	16	16	16	16	16	16	13	13	13	13	13	13
Y (ft from centerline)	-3	0	3	-3	0	3	-3	0	3	-3	0	3
Z (ft AGL)	6	6	6	9	9	9	6	6	6	9	9	9
	Configuration 3 Run 1						Configuration 4 Run 1					
sonic	a	b	c	d	e	f	a	b	c	d	e	f
X (ft from rear of van)	10	10	10	10	10	10	6	6	6	6	6	6
Y (ft from centerline)	-3	0	3	-3	0	3	-3	0	3	-3	0	3
Z (ft AGL)	6	6	6	9	9	9	6	6	6	9	9	9
	Configuration 5 Run 1											
sonic	a	b	c	d	e	f						
X (ft from rear of van)	2	2	2	2	2	2						
Y (ft from centerline)	-3	0	3	-3	0	3						
Z (ft AGL)	6	6	6	9	9	9						

Sampling began with the sonic array at the far end of the trailer (16 feet back, 4.9 m), with vertical positioning of the bottom three sonics at 6ft (1.8 m) above ground level (AGL), and the top three sonics at 9 ft (2.7 m) AGL. The crosswise positions for both the top and bottom row were the centerline ("b" sonic), and the outmost positions of ± 3 feet (± 0.9 m; for "a" and "c"). For this configuration, we performed two runs and one ambient reading. The next four runs were with the sonic array moved forward to 13 ft (4.0 m), 10 ft (3.0 m), 6 ft (1.8 m), and 2 ft (0.6 m) from the rear of the van, respectively. In each of these runs, the horizontal and vertical settings were the same.

Average wind speed for this day calculated from all six sonics during the sampling period was approximately 1.5 m/s, with a wind direction from the SSW (approximately 190°). These

calculations agree with wind speed and wind direction measurements from the National Weather Service (NWS) Automated Surface Observing System (ASOS) located at Crossville, TN (about 20 miles WNW of the Rockwood Airport) and a National Oceanic and Atmospheric Administration (NOAA), Air Resources Laboratory (ARL), Atmospheric Turbulence and Diffusion Division (ATDD) East Tennessee Ozone Study (ETOS) meteorological station at Jamestown, TN (approximately 30 miles NW of Rockwood Airport) during the same time frame. The spectra for ambient conditions show that the energy level is small and fairly consistent, i.e., that the light wind speed produces only weak turbulence; therefore, TKE values during the runs were not adjusted by the ambient TKE.

Figure 4.2 illustrates the spectra of TKE for all six sonics for each run, configuration, and vehicle heading for Day 322. The ambient data taken under Configuration 1 conditions are also shown with the top two figures that depict Configuration 1 (Runs 1 and 2). The inertial subrange indicator is shown on the spectra of TKE for Configuration 1, Run 2, and on Configuration 2. In the inertial subrange there is no production of energy, there is only transfer from larger-scale eddies. On a log-log scale, TKE vs. wavenumber in the inertial subrange follows a $-5/3$ slope (Stull, 1988). The ambient TKE for Day 322 follows the same slope, as do all the ambient data taken during the three days of sampling. Note that sonics "d", "e", and "f" (the top three) show energy spectra similar to that for the ambient case. Since the vehicle speed was kept constant across all runs on this day, sonics "a", "b", and "c" show about the same level of TKE. The center sonic on the lower tier ("b") almost always shows higher energy levels than the outer edge sonics. This is expected because it is receiving the maximum contribution of the turbulence created by the motion of the van.

It is evident that different headings and different configurations change the TKE seen by each sonic. On Configuration 1, Run 2 (with the sonic array at the far end of the trailer), it can be seen that by heading into the wind (Hdg SW), the TKE appears organized and increases slightly, with the center sonic clearly experiencing increased turbulence.

On Configuration 2, Run 1, when the vehicle was heading to the NE, there was a small tailwind, almost a crosswind. Sonic "c" shows decreased TKE under these conditions. Sonics "a" and "b" under this configuration saw about the same turbulence. An explanation for the decreased TKE for "c" could be that the wake was shifted slightly due to the tailwind/crosswind so that sonics "a" and "b" both saw the higher energy that "b" usually saw. On the next run to the SW, even with a different configuration (Configuration 3), the energy pattern is similar to the previous SW heading run, i.e., with the center sonic detecting the higher energy, and the two outer sonics sampling about the same.

On the last two runs, with the sonics increasingly closer to the van, (Configuration 4 was 6 ft (1.8 m) back; then Configuration 5 at 2 ft (0.6 m) from the rear of the van) the TKE exhibits the same separation with slightly varying energy values. There could be several explanations for having the same pattern with changing direction. It could suggest wind direction shifted slightly causing the difference with direction, or it could indicate that as in Configuration 2, Run 1, the ambient winds displaced the wake off to one side.

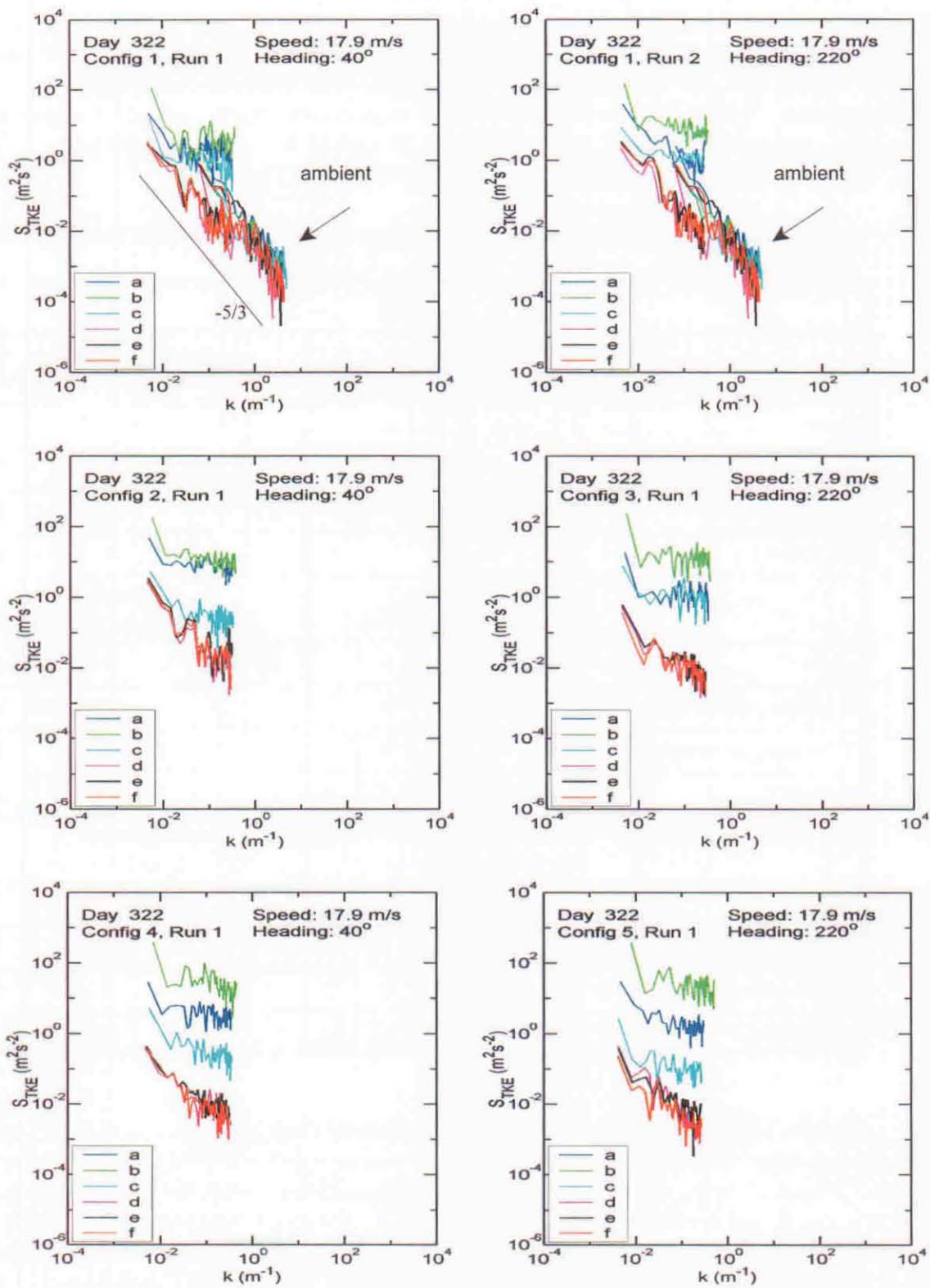


Figure 4.2 Power spectral density of TKE for Day 322, Configurations 1-5. The inertial subrange slope is shown on Configuration 1, Run 1. Ambient data are with Configuration 1.

1 December 1999 (Julian Day 335): This day saw a more consistent sampling pattern. There were multiple runs with the same configuration, varying only the vehicle speeds (30, 40, and 50 mph [13.4, 17.9, 22.4 m/s]). Each configuration had six runs (three to the NE, three to the SW), along with one ambient reading. For this day there were six anemometer configurations. With the last configuration, there were two additional ambient readings (one facing NE, and one facing SW), followed by one 10-mph (4.5 m/s) and one 20-mph (8.9 m/s) run. Table 4.2 lists the configurations and sonic positions for Day 335.

Table 4.2. Sonic anemometer array configurations and positions for Day 335.

Day 335												
	Configuration 1 Runs 1-6, and ambient						Configuration 2 Runs 1-6, and ambient					
sonic	a	b	c	d	e	f	a	b	c	d	e	f
X (ft from rear of van)	2	2	2	2	2	2	9	9	9	9	9	9
Y (ft from centerline)	-3	0	3	-3	0	3	-3	0	3	-3	0	3
Z (ft AGL)	6	6	6	9	9	9	6	6	6	9	9	9
	Configuration 3 Runs 1-6, and ambient						Configuration 4 Runs 1-6, and ambient					
sonic	a	b	c	d	e	f	a	b	c	d	e	f
X (ft from rear of van)	16	16	16	16	16	16	16	16	16	16	16	16
Y (ft from centerline)	-3	0	3	-3	0	3	-3	0	3	-3	0	3
Z (ft AGL)	6	6	6	9	9	9	8	8	8	12	12	12
	Configuration 5 Runs 1-6, and ambient						Configuration 6 Runs 1-8, and 3 ambients					
sonic	a	b	c	d	e	f	a	b	c	d	e	f
X (ft from rear of van)	9	9	9	9	9	9	2	2	2	2	2	2
Y (ft from centerline)	-3	0	3	-3	0	3	-3	0	3	-3	0	3
Z (ft AGL)	8	8	8	12	12	12	8	8	8	12	12	12

Figure 4.3 shows all the runs at the various speeds for Configuration 1 on Day 335, along with the ambient data. This configuration had the sonic array 2 ft (0.6 m) back from the van, with the sonics "a" and "c" at the outer edges (± 3 ft (0.9 m) from center), with the lower tier in the array 6 ft (1.8 m) AGL and the higher tier at 9 ft (2.7 m) AGL. Figures 4.4 and 4.5 show the TKE for data taken with the same horizontal and vertical configurations with the difference only in the distance back from the van; Configuration 2 (Fig. 4.4) was 9 ft (2.7 m) back and Configuration 3 (Fig. 4.5) was back 16 ft (4.9 m). Ambient data are also shown.

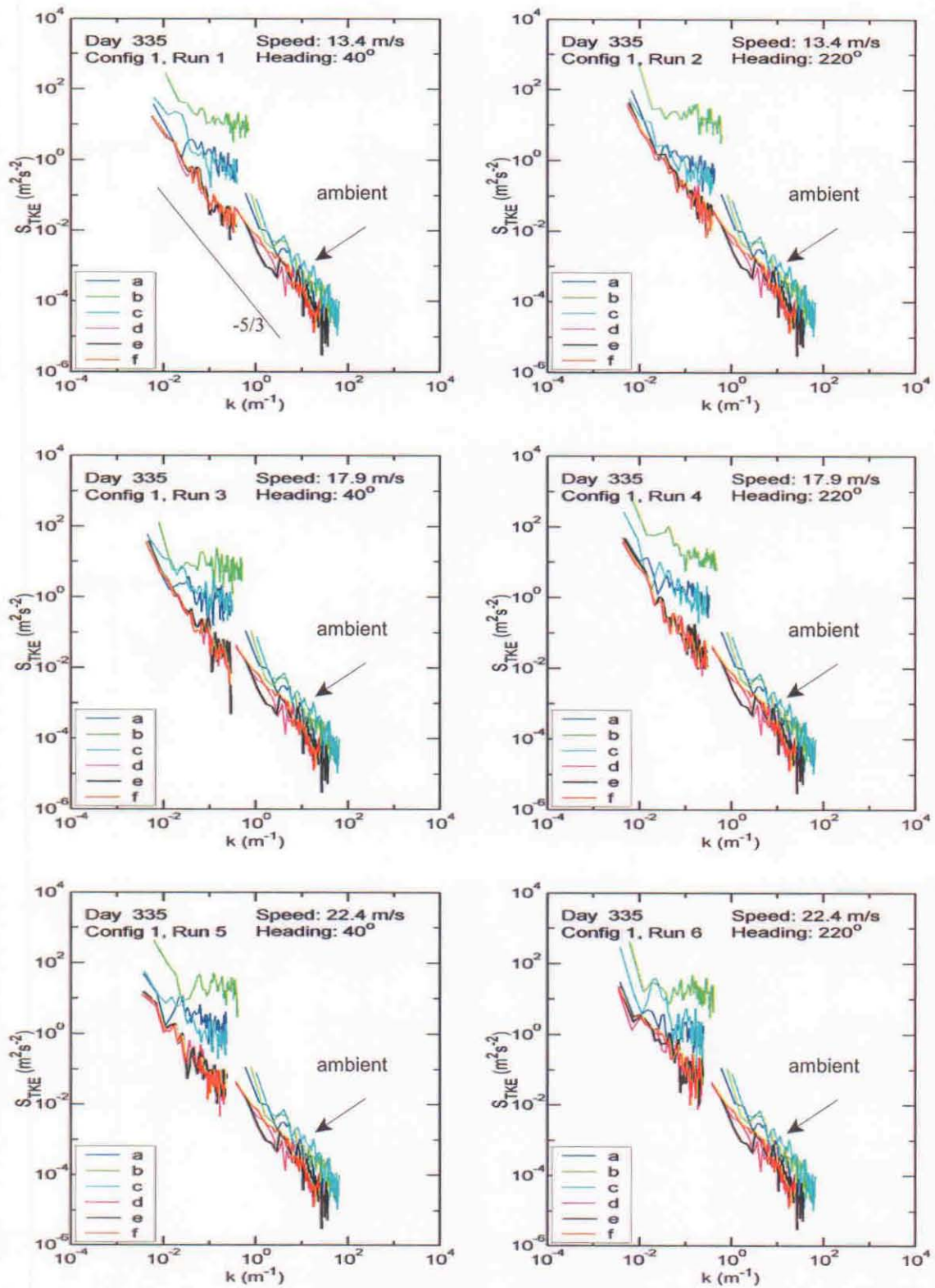


Figure 4.3 Power spectral density of TKE for Day 335, Configuration 1. The inertial subrange slope is shown on Run 1. Ambient data are with each run.

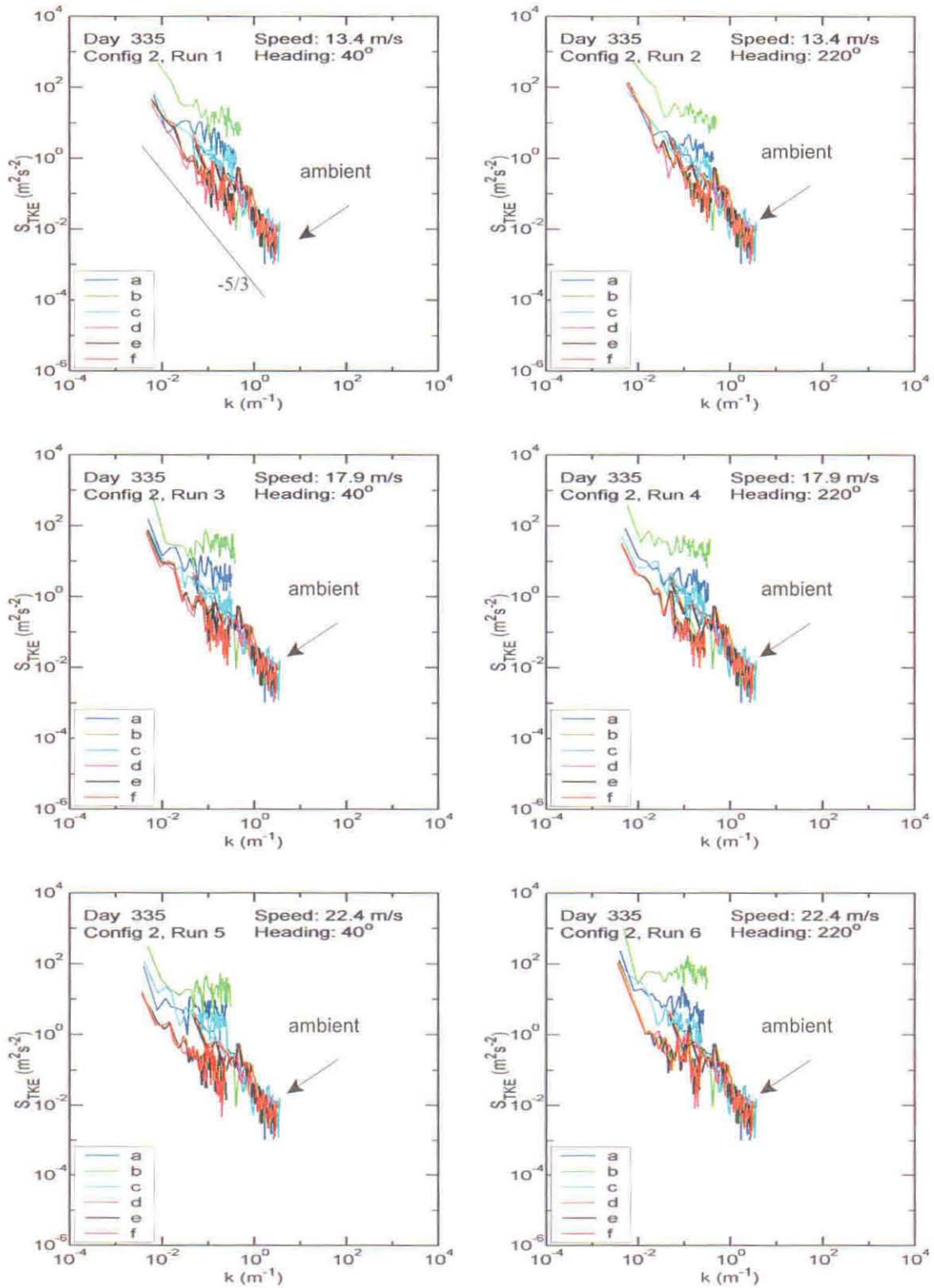


Figure 4.4 Power spectral density of TKE for Day 335, Configuration 2. The inertial subrange slope is shown on Run 1. Ambient data are with each run.

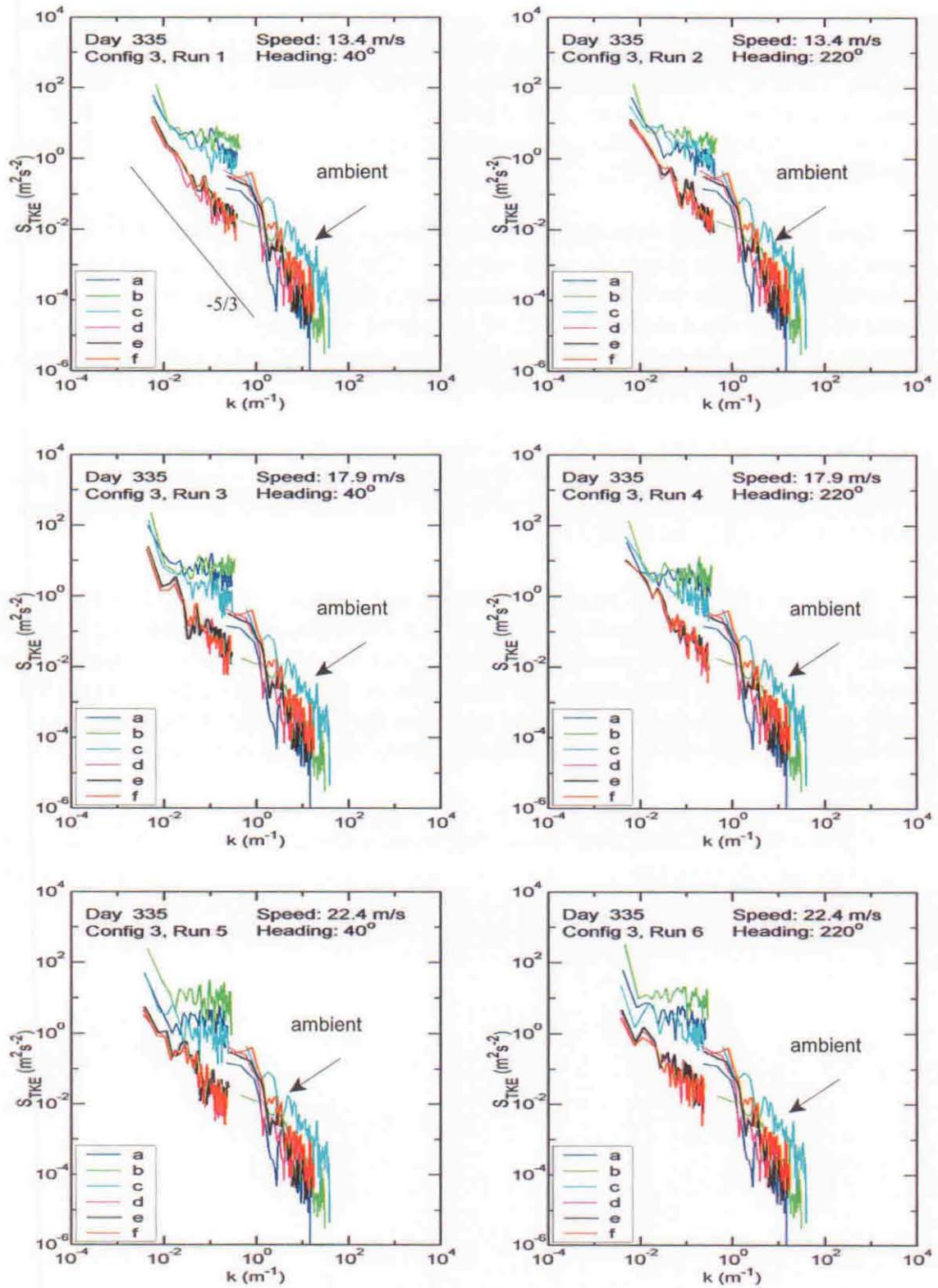


Figure 4.5 Power spectral density of TKE for Day 335, Configuration 3. The inertial subrange slope is shown on Run 1. Ambient data are with each run.

The winds were calmer than on Day 322 as is evidenced by the lower TKE. Except for one ambient sampling period, average wind speeds ranged from 0.4 to 1.0 m/s. During the one exception (Configuration 2), the average wind speed was about 2.3 m/s, and the TKE shows the increase. Local wind direction on the average was ESE, approximately 130°. One sampling period showed a direction of 80°, but the winds were only about 0.3 m/s. Wind speed and direction for the two verifying stations (Crossville and Jamestown) showed light and variable winds, predominately ESE (75° to 150° at about 1.0 to 1.5 m/s).

Note again, that the three top sonics show only a slight increase in TKE over ambient, and generally stay the same as vehicle speed increases. The center sonic on the bottom tier consistently shows the most energy, and the energy increases as vehicle speed increases. The two outer sonics appear to receive about the same level of turbulence, and these also increase as vehicle speed increases. The direction of travel in these three configurations does not seem to influence the TKE much, due, most likely to the light ambient wind conditions.

The next set of runs had all the sonics up higher, but in the same horizontal positions, i.e., the center position and the outer edges at ± 3 ft (0.9 m). The lower tier of sonics was moved to 8 ft (2.4 m) AGL, and the higher tier was moved to 12 ft (3.7 m) AGL. Configuration 4 in these settings was at 16 ft (4.9 m) back on the trailer.

Figures 4.6 through 4.8 show the TKE for Configuration 4 through 6, with ambient data, as the sonic array is moved forward from the 16 ft (4.9 m) back position, to 8 ft (2.4 m), then to 2 ft (0.6 m). As before, the TKE seen by the top three sonics does not change much either with vehicle speed or configuration. The center sonic on the bottom ("b") continued to see more TKE, slightly increasing with vehicle speed. The outer sonics on the bottom tier change TKE values as before with respect to heading of the vehicle, although not as obviously as when the ambient wind speeds were higher.

Figure 4.9 shows Configuration 6, with ambient readings at 10-mph (4.5 m/s) and 20-mph (8.9 m/s). Wind speeds were about 0.5 m/s with wind direction of 150°. The 10-mph and the 20-mph runs (both heading SW) are interesting because they show that even at very low vehicle speeds, there is organized flow that sets up, and the TKE can be used to distinguish it.

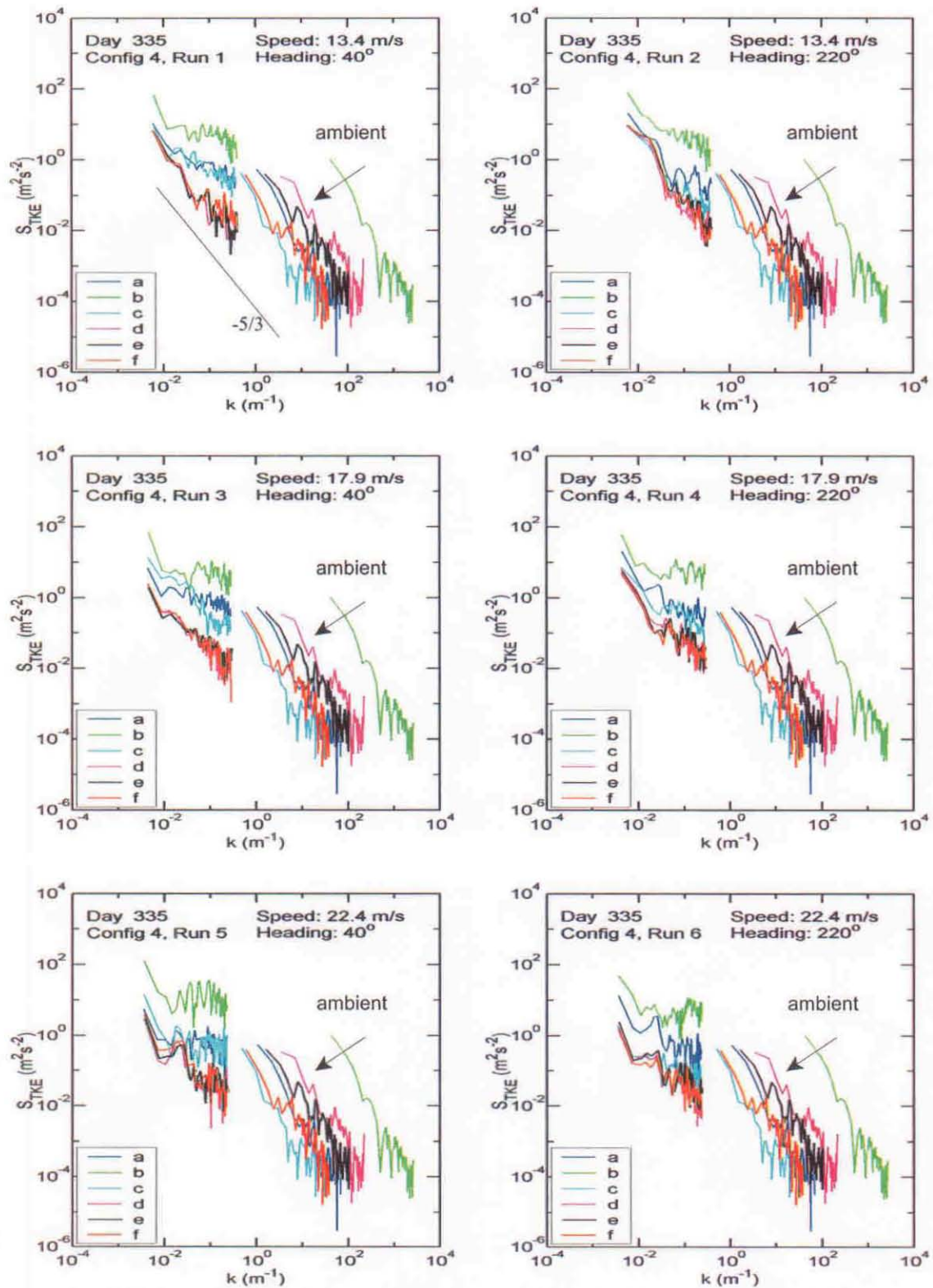


Figure 4.6 Power spectral density of TKE for Day 335, Configuration 4. The inertial subrange slope is shown on Run 1. Ambient data are with each run.

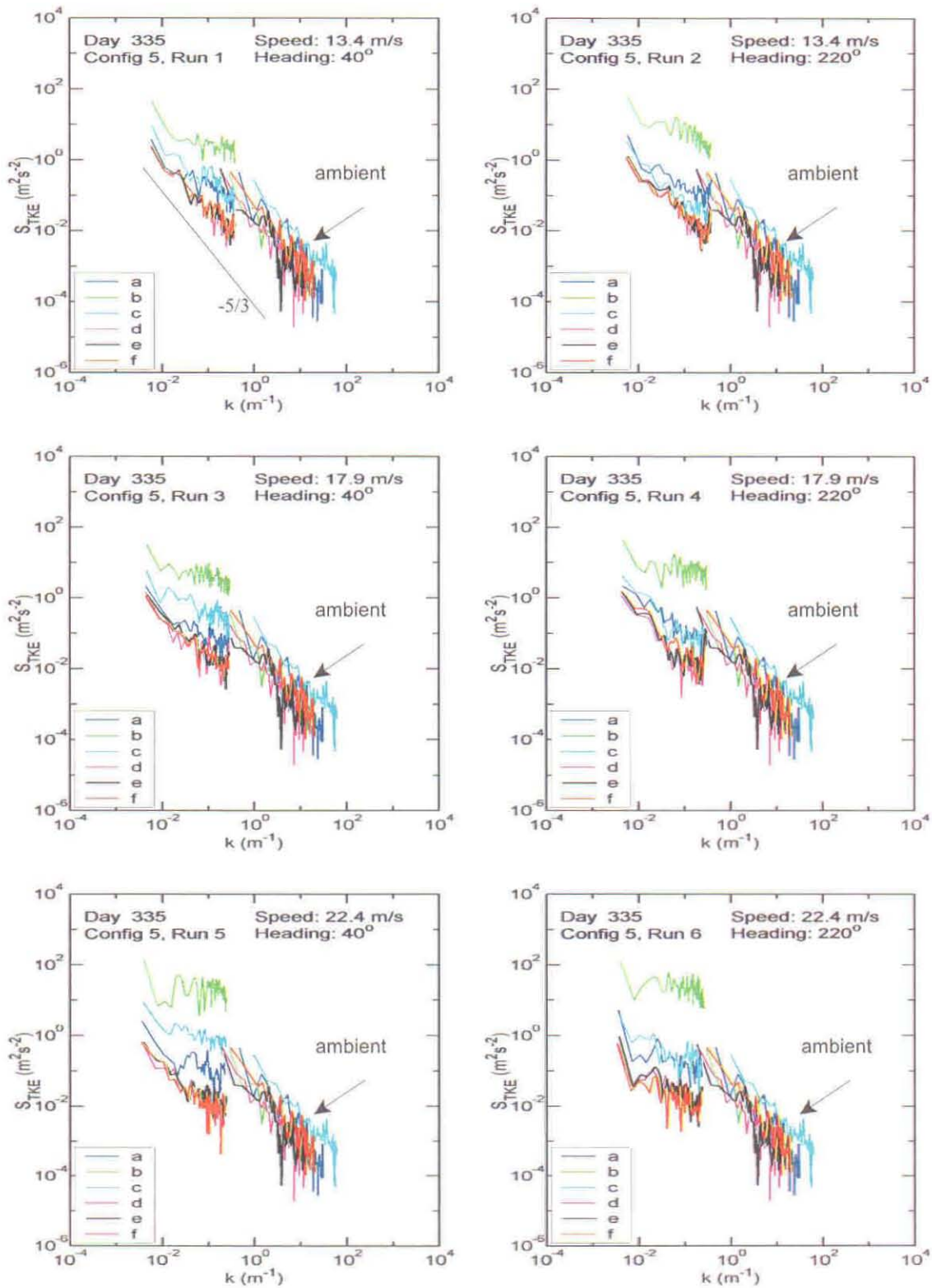


Figure 4.7 Power spectral density of TKE for Day 335, Configuration 5. The inertial subrange slope is shown on Run 1. Ambient data are with each run.

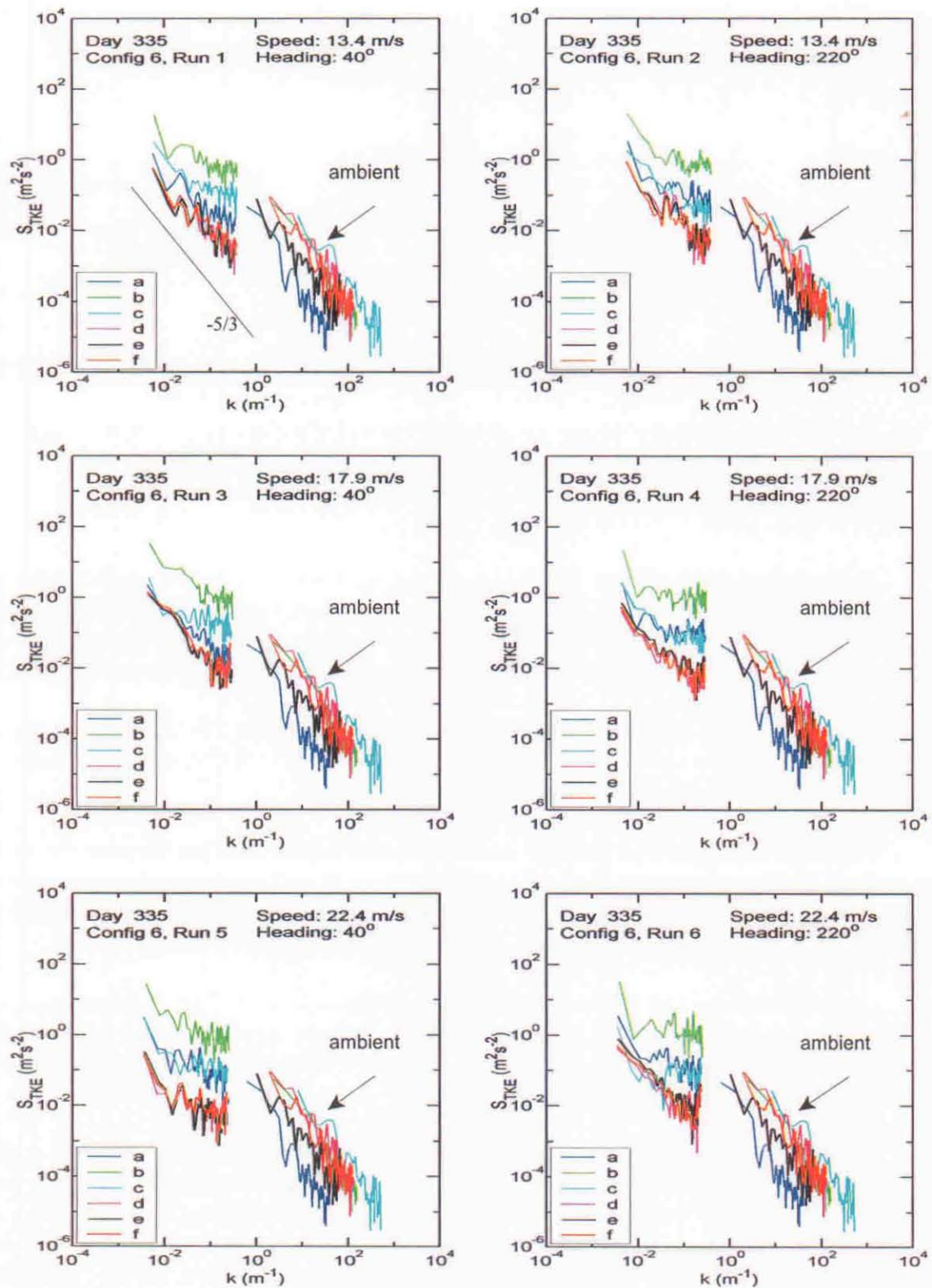


Figure 4.8 Power spectral density of TKE for Day 335, Configuration 6, Runs 1-6. The inertial subrange slope is shown on Run 1. Ambient data are with each run.

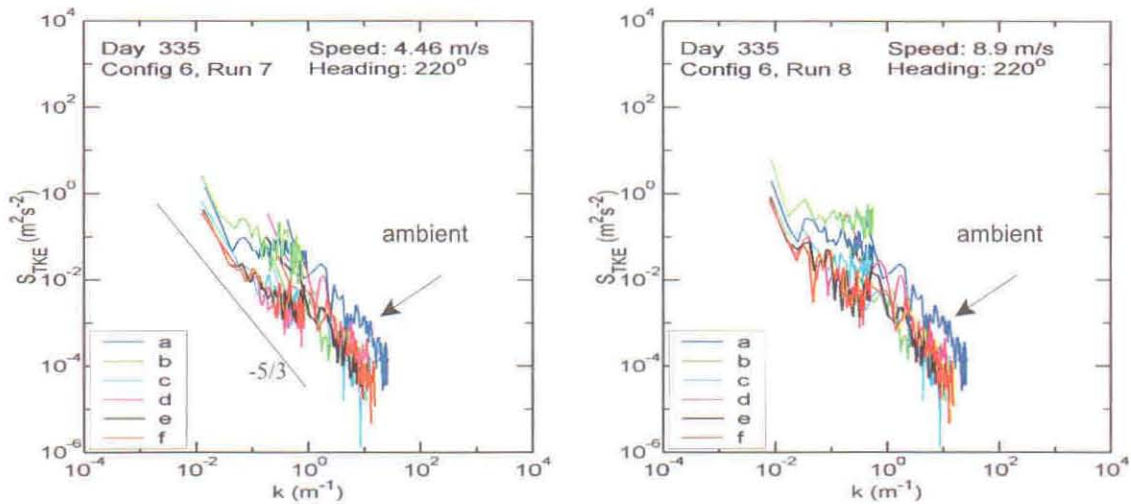


Figure 4.9 Power spectral density of TKE for Day 335, Configuration 6, Runs 7 and 8. The inertial subrange slope is shown on Run 7. Ambient data are with each run.

2 December 1999 (Julian Day 336): Sampling was conducted as on Day 335 (i.e., same speeds, and same number of runs and ambient samples per configuration), except there were fewer configurations (three). For the last configuration we took two ambient readings and a 10-mph (4.5 m/s) and a 20-mph (8.9 m/s) run. Table 4.3 lists the configurations and sonic positions for Day 336.

Sampling began on this day with the sonic array in a position 2 ft (0.6 m) from the van. The lower tier of sonics was at 7 ft (2.1 m) AGL, the higher tier at 11 ft (3.4 m) AGL. Sonics "a", "c", "d", and "f" were only ± 2 ft (0.6 m) from the center.

Ambient wind speed on this day was significantly higher than on the previous two days of sampling. The speeds ranged from 1.5 to almost 3 m/s. Local wind direction was from the SSE, approximately 130° - 180° . Winds at Crossville were 3 m/s from 160° , and at Jamestown, 5 m/s from 180° to 200° .

The runs for Day 336 are shown in Figures 4.10 through 4.13. The first set of runs were with the array at 2 ft (0.6 m) from the van (Configuration 1), then the next six runs were at 9 ft (2.7 m) from the van (Configuration 2), and the next six at 16 ft (4.9 m) back (Configuration 3). All configurations show the ambient data.

Figure 4.10 (Configuration 1) shows that on these runs, with the sonics close to the van, with increased wind speeds, at the lower velocity of 30 mph (13.4 m/s), and heading essentially crosswind, the top and lower tier sonics' energy levels are barely distinguishable. When the van is heading NE, again crosswind, all six sonics see about the same level of energy. As the vehicle speed increases, the TKE for the NE heading doesn't show much difference, but the TKE for the SW heading looks like the energy conditions seen previously.

Table 4.3. Sonic anemometer array configurations and positions for Day 336.

Day 336						
	Configuration 1 Runs 1-6, and ambient					
sonic	a	b	c	d	e	f
X (ft from rear of van)	2	2	2	2	2	2
Y (ft from centerline)	-2	0	2	-2	0	2
Z (ft AGL)	7	7	7	11	11	11
	Configuration 2 Runs 1-6, and ambient					
sonic	a	b	c	d	e	f
X (ft from rear of van)	9	9	9	9	9	9
Y (ft from centerline)	-2	0	2	-2	0	2
Z (ft AGL)	7	7	7	11	11	11
	Configuration 3 Runs 1-8, and 2 ambients					
sonic	a	b	c	d	e	f
X (ft from rear of van)	16	16	16	16	16	16
Y (ft from centerline)	-2	0	2	-2	0	2
Z (ft AGL)	7	7	7	11	11	11

The next set of runs (Configuration 2), shown in Figure 4.11, with the array approximately half-way back on the trailer (9 ft), show discernible differences in the TKE. For both headings and all three velocities, the lower center sonic receives the most energy, and it is clearly apparent with the higher velocities.

With the sonics at the far end of the trailer (Figure 4.12, Configuration 3, at 16 ft back), the separated flow becomes the most evident, with the center sonic receiving the most energy, and the top sonics apparently again sampling outside the wake flow.

The 10-mph (4.5 m/s) and 20-mph (8.9 m/s) runs, as shown in Figure 4.13, were both heading into the wind, and significant differences among the anemometers are not seen until 20 mph (8.9 m/s). By moving the two outer sonics closer to the center line, it is seen that the TKE for the bottom sonics all now nearly match because their placement now puts them in the main turbulent wake.

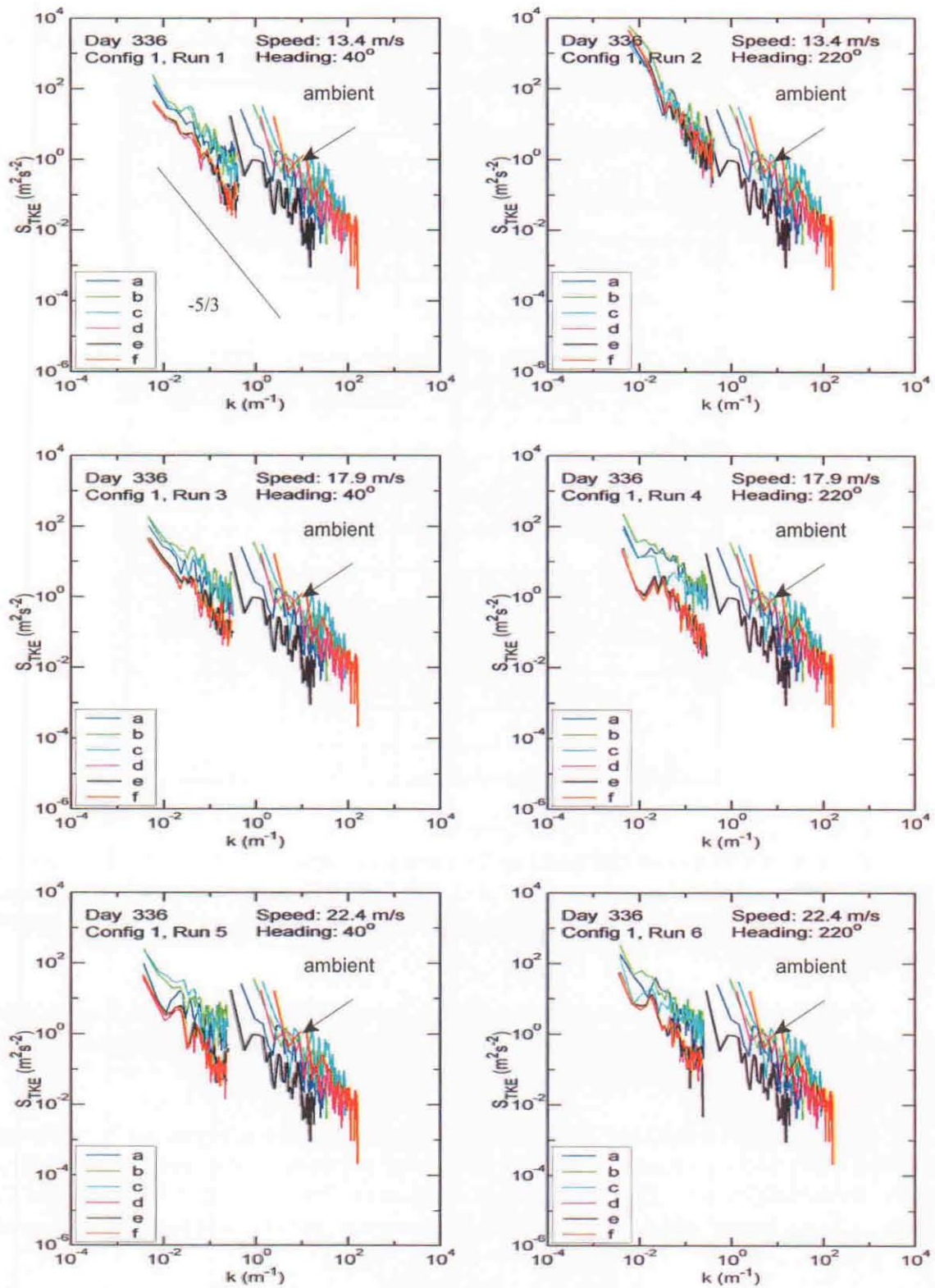


Figure 4.10 Power spectral density of TKE for Day 336, Configuration 1. The inertial subrange slope is shown on Run 1. Ambient data are with each run.

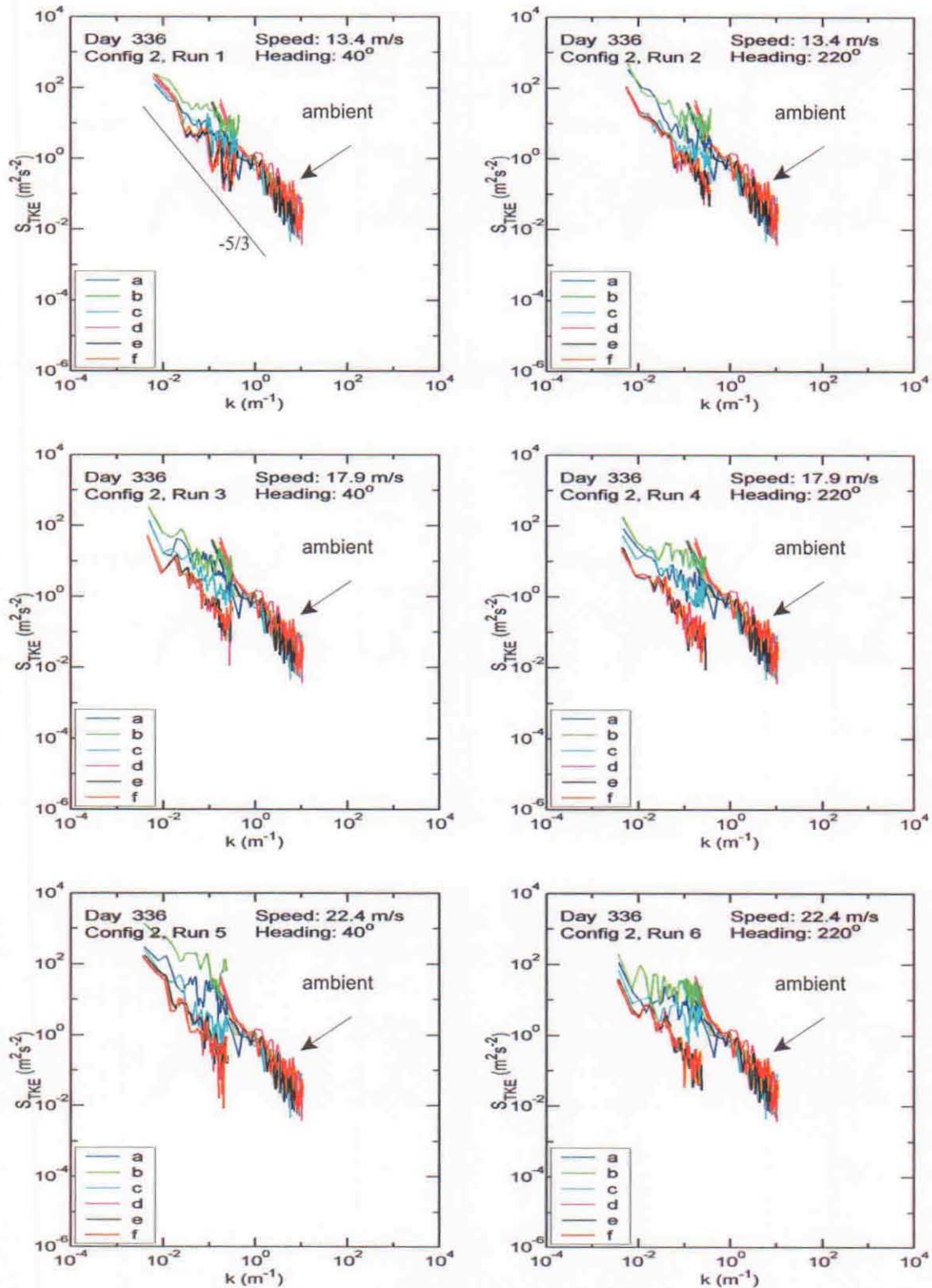


Figure 4.11 Power spectral density of TKE for Day 336, Configuration 2. The inertial subrange slope is shown on Run 1. Ambient data are with each run.

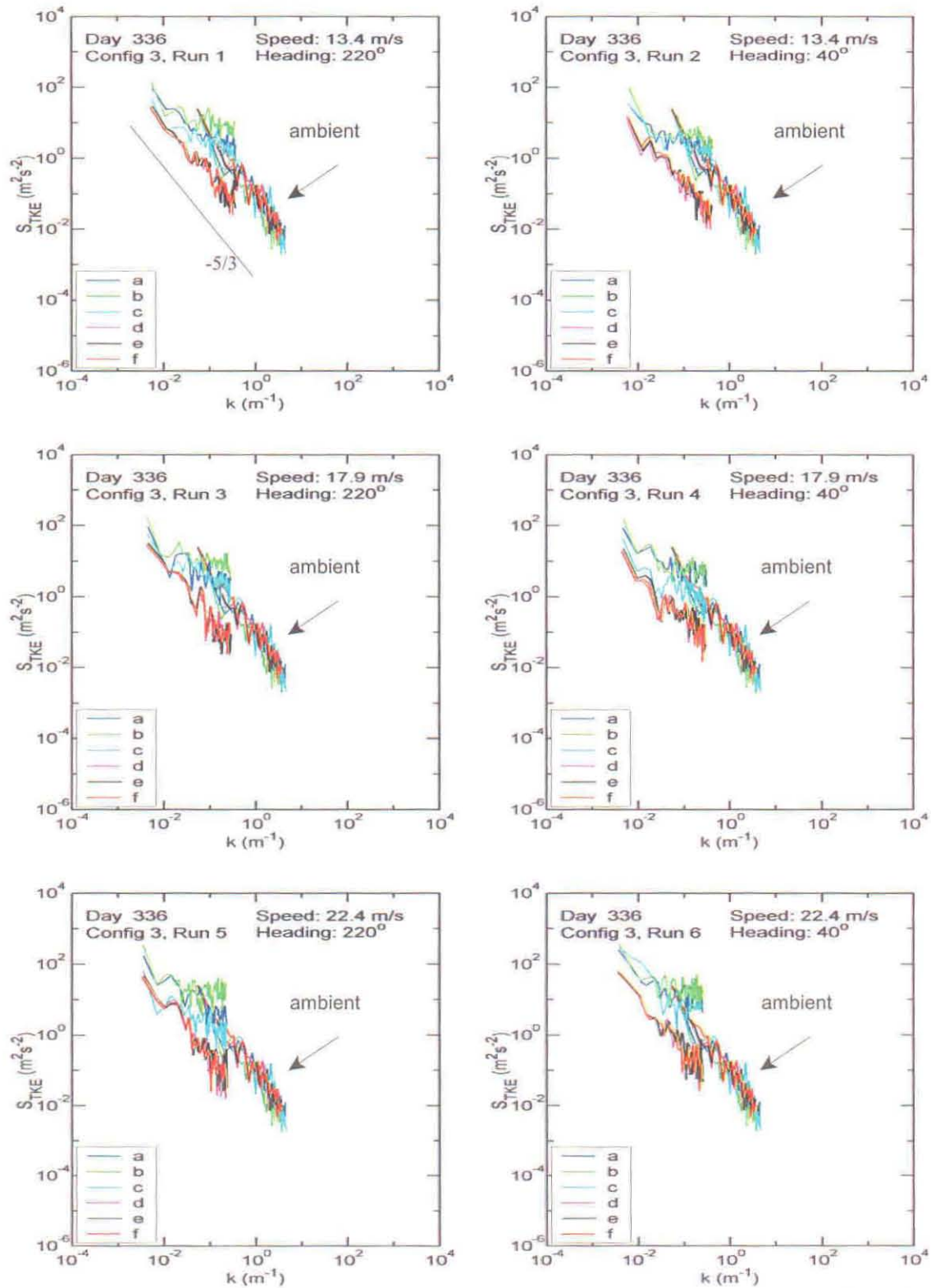


Figure 4.12 Power spectral density of TKE for Day 336, Configuration 3, Runs 1-6. The inertial subrange slope is shown on Run 1. Ambient data are with each run.

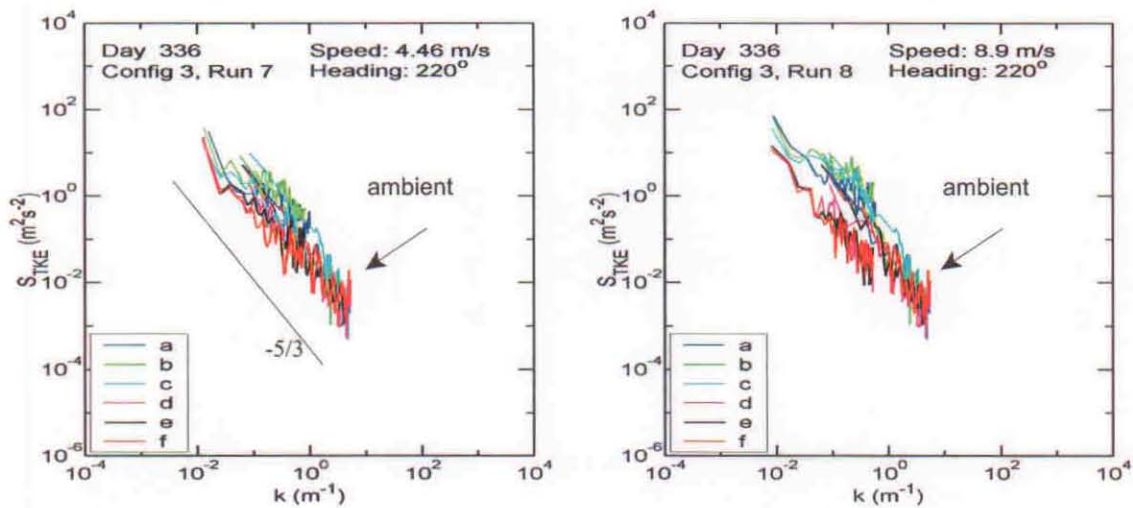


Figure 4.13 Power spectral density of TKE for Day 336, Configuration 3, Runs 7 and 8. The inertial subrange slope is shown on Run 7. Ambient data are with each run.

4.6 Contours of Wake Turbulent Kinetic Energy

The computed values of turbulent kinetic energy at each location in the sampling array were used to generate plots of the spatial variability of the wake TKE. Figure 4.14 shows the vertical variability of TKE between the lowest sampling position (6 ft, 1.8 m) and the highest (12 ft, 3.7 m), for vehicle travel speeds of 30 mph (13.4 m/s) and 50 mph (22.4 m/s), at several locations along the trailer. In both cases the TKE decreases quickly with increasing height until about 7 or 8 ft (2.1 to 2.4 m), and then decreases more slowly until the ambient value is reached near 11 or 12 ft (3.4 to 3.7 m).

Figure 4.15 shows the vertical-horizontal (Z-X) cross-sections along the wake centerlines for vehicle speeds of 30 mph (13.4 m/s) and 50 mph (22.4 m/s). The plotting package required data values at the surface, which were arbitrarily set to zero, and the contours below the minimum observing height of 6 ft (1.8 m) are suspect. Ignoring this portion of the plots, the contours suggest the greatest TKE occurs at a downwind distance of about 9 ft (2.7 m) from the rear of the van, about 1.4 vehicle heights downwind. A bit above the vehicle roof, at about 7 ft (2.1 m), the TKE values seem rather uniform with along-axis distance, and decrease with increasing height, to near-ambient values at about 11 or 12 ft (3.4 to 3.7 m).

Figure 4.16 shows the lateral-vertical (Y-Z) cross-sections at three locations along the wake for vehicle speeds of 30 (13.4 m/s) and 50 mph (22.4 m/s), in units of m^2/s^2 . These contours were generated by a software package (Surfer) that requires data at locations where none were observed (below 6 ft, 1.8 m, AGL), so these values were arbitrarily set to zero at ground level. This means that the contours are suspect below the minimum observation height of 6 ft (1.8 m). However, above this level, the contours have enough data to be credible. They

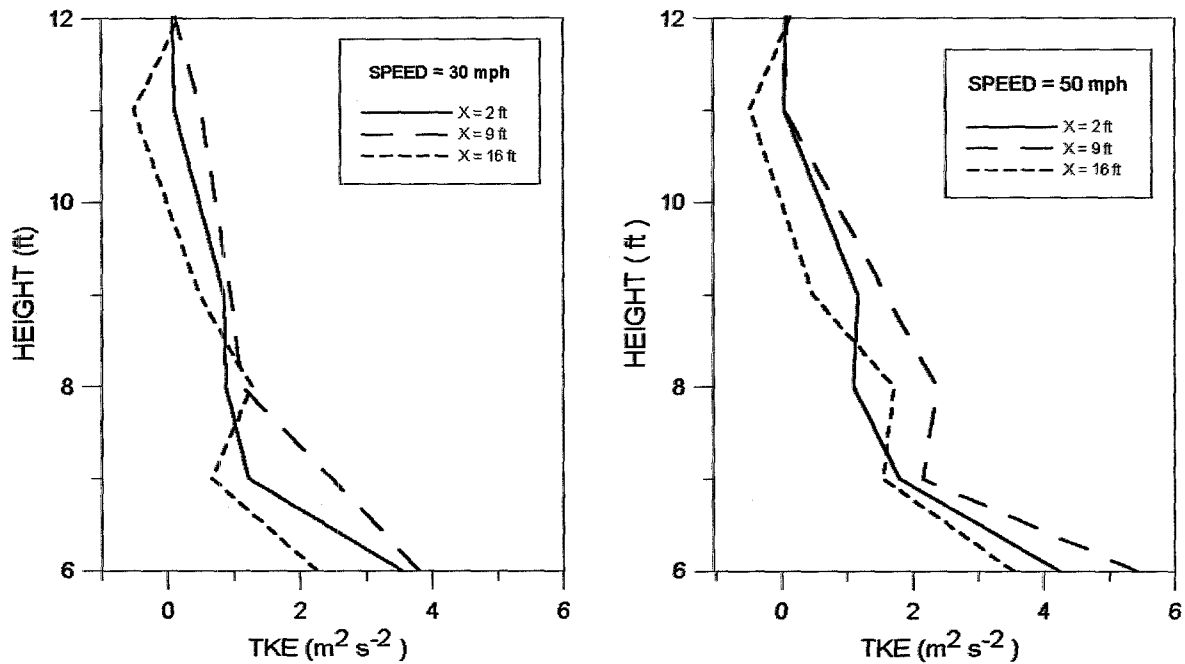


Figure 4.14 Vertical profiles of turbulent kinetic energy (TKE) in near-wake of vehicle ($x = 2, 9, \text{ and } 16 \text{ ft}$ from rear of vehicle for road speeds of 30 and 50 mph.

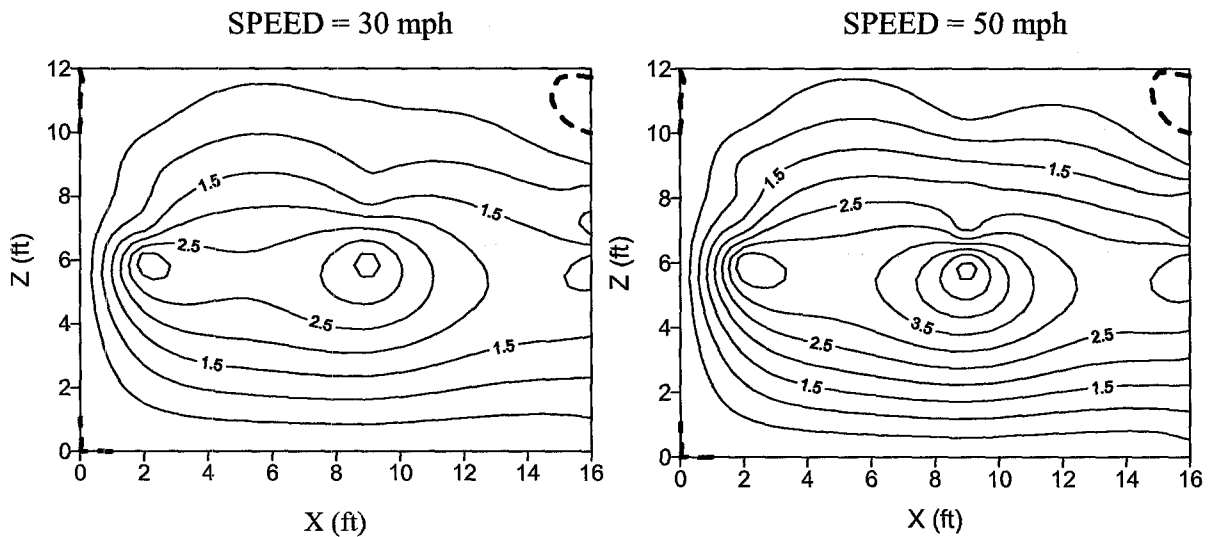


Figure 4.15 Contours in vertical-along-axis plane of constant values of TKE (m^2/s^2) along the wake centerline, for vehicle speeds of 30(13.4 m/s) and 50 mph (22.3 m/s).

are roughly symmetric about the $Y=0$ axis, and show the expected of higher wake TKE for the 50 mph (22.4 m/s) speed. The contours also suggest that the maximum TKE at each speed occurs a little below the minimum observing height of 6 ft (1.8 m).

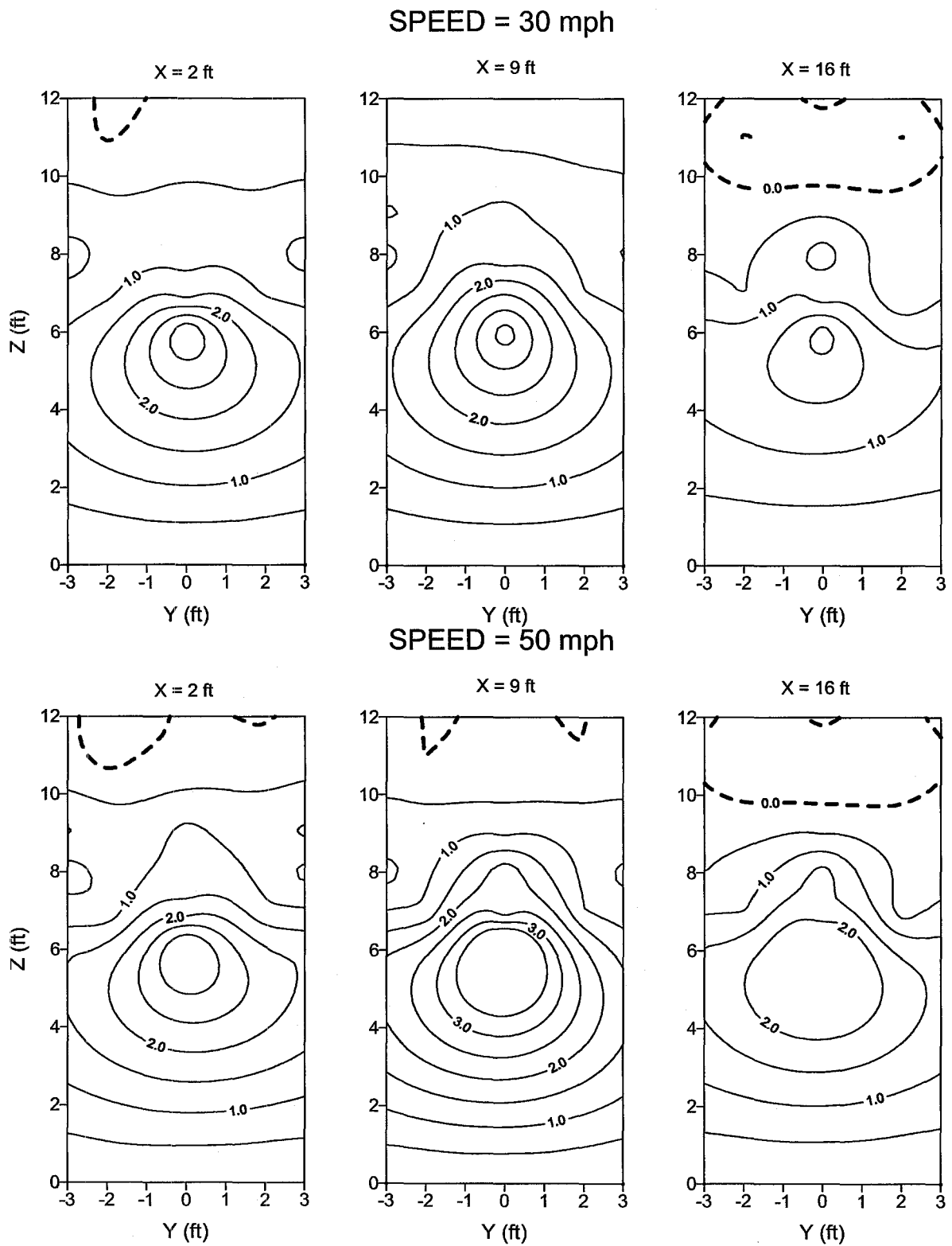


Figure 4.16 Contours in vertical-cross-axis plane of constant values of TKE in m^2/s^2 for three along-wake positions behind a vehicle with road speed of 30 mph (13.4 m/s; top) and 50 mph (22.4 m/s; bottom).

4.7 Mean Flow Vectors in the Wake

Cross-sectional views were plotted for the X - Y, X - Z, and Y - Z planes to better visualize the airflow field in the near-wake region of vehicle. Figure 4.17, for speed = 30 mph (13.4 m/s), show flow vectors in the Y - Z plane at $x = 2$ ft (0.61 m), $x = 9$ ft (2.74 m), and $x = 16$ ft (4.88 m), respectively. Those plots indicate that flow above $z = 8$ ft (2.44 m) was mostly downward (- "w" component), with very little lateral ("v" component) flow; however, for $z = 8$ ft (2.44 m) or less (i.e., closer to the ground), the magnitude of downflow increased noticeably while the magnitude of lateral flow greatly increased within the projected frontal area of vehicle (below $z = 6.9$ ft, 2.1 m). Note that the "v" component indicates flow toward the center from either side (consistent with vortex formation on each side), as well as the "w" component indicating a vortex from the van roof. As expected, the magnitude of all vectors decreases with increasing heights above the vehicle and increasing distances downwind from the rear of the vehicle. Figures 4.18 and 4.19 show the same qualitative flow characteristics, with greater magnitudes as the nominal vehicle speed was increased to 40 mph (17.9 m/s) and 50 mph (22.4 m/s), respectively.

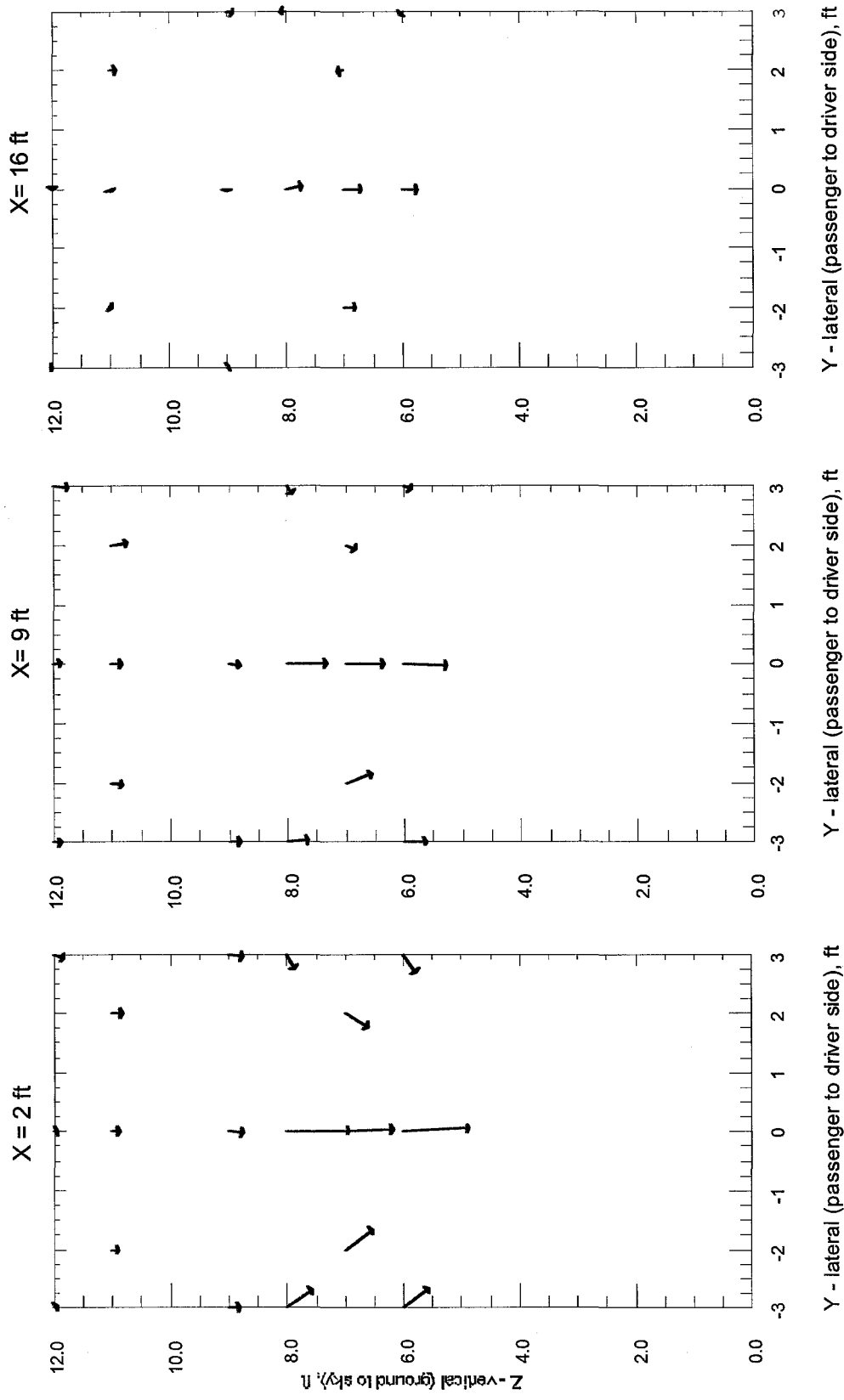


Figure 4.17. Vehicle wake flow vectors, cross-section view at $x = 2$ ft (0.61 m), $x = 9$ ft (2.74 m), $x = 16$ ft (4.88 m), respectively, behind vehicle, for speed = 30 mph (13.4 m/s), looking from front to rear, vehicle width = 6.2 ft (1.9 m), height = 6.9 ft (2.1 m), scale for vectors on plots: 1 unit = 2 m/s.

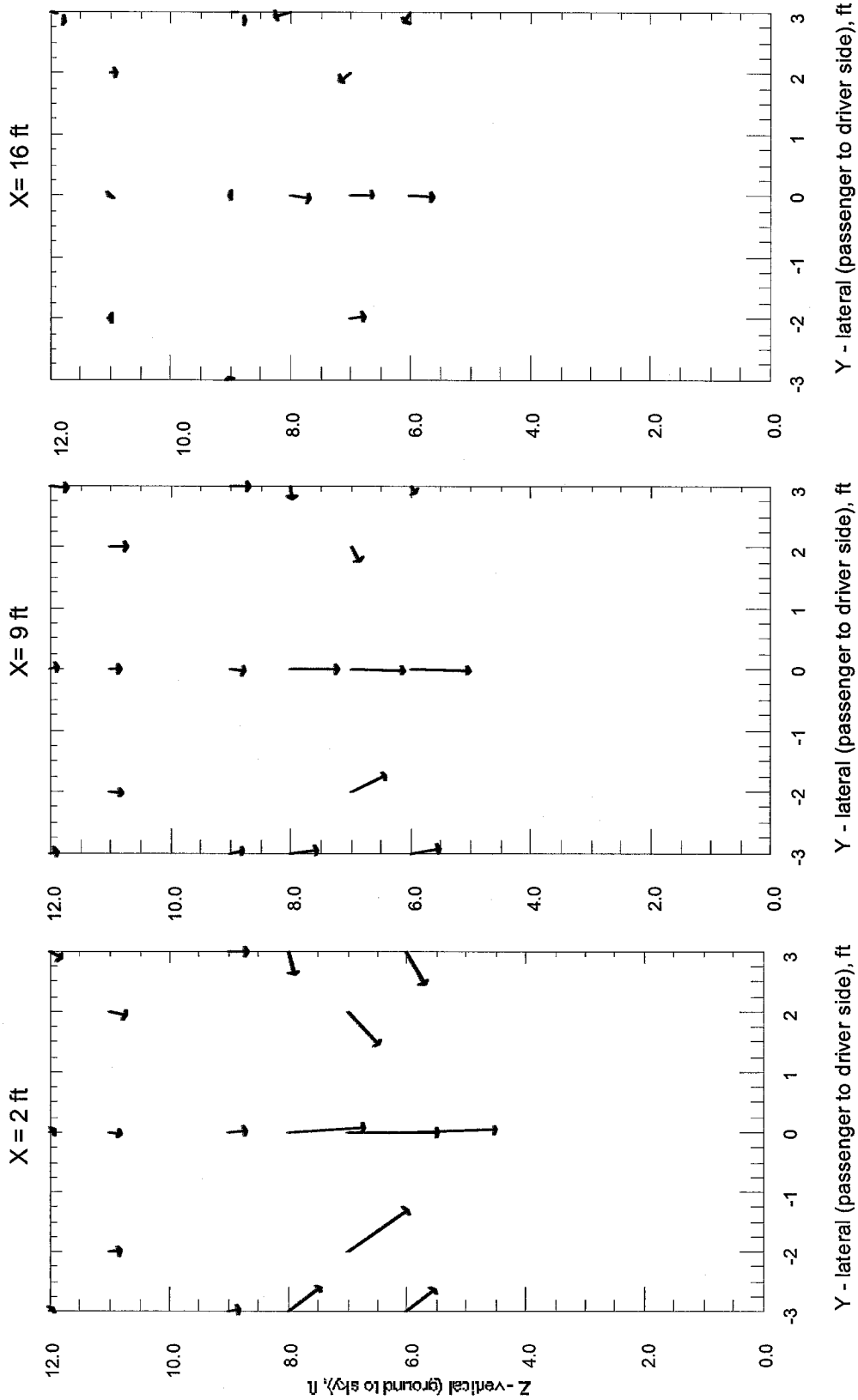


Figure 4.18. Vehicle wake flow vectors, cross-section view at $x = 2$ ft (0.61 m), $x = 9$ ft (2.74 m), $x = 16$ ft (4.88 m), respectively, behind vehicle, for speed = 40 mph (17.9 m/s), looking from front to rear, vehicle width = 6.2 ft (1.9 m), height = 6.9 ft (2.1 m), scale for vectors on plots: 1 unit = 2 m/s.

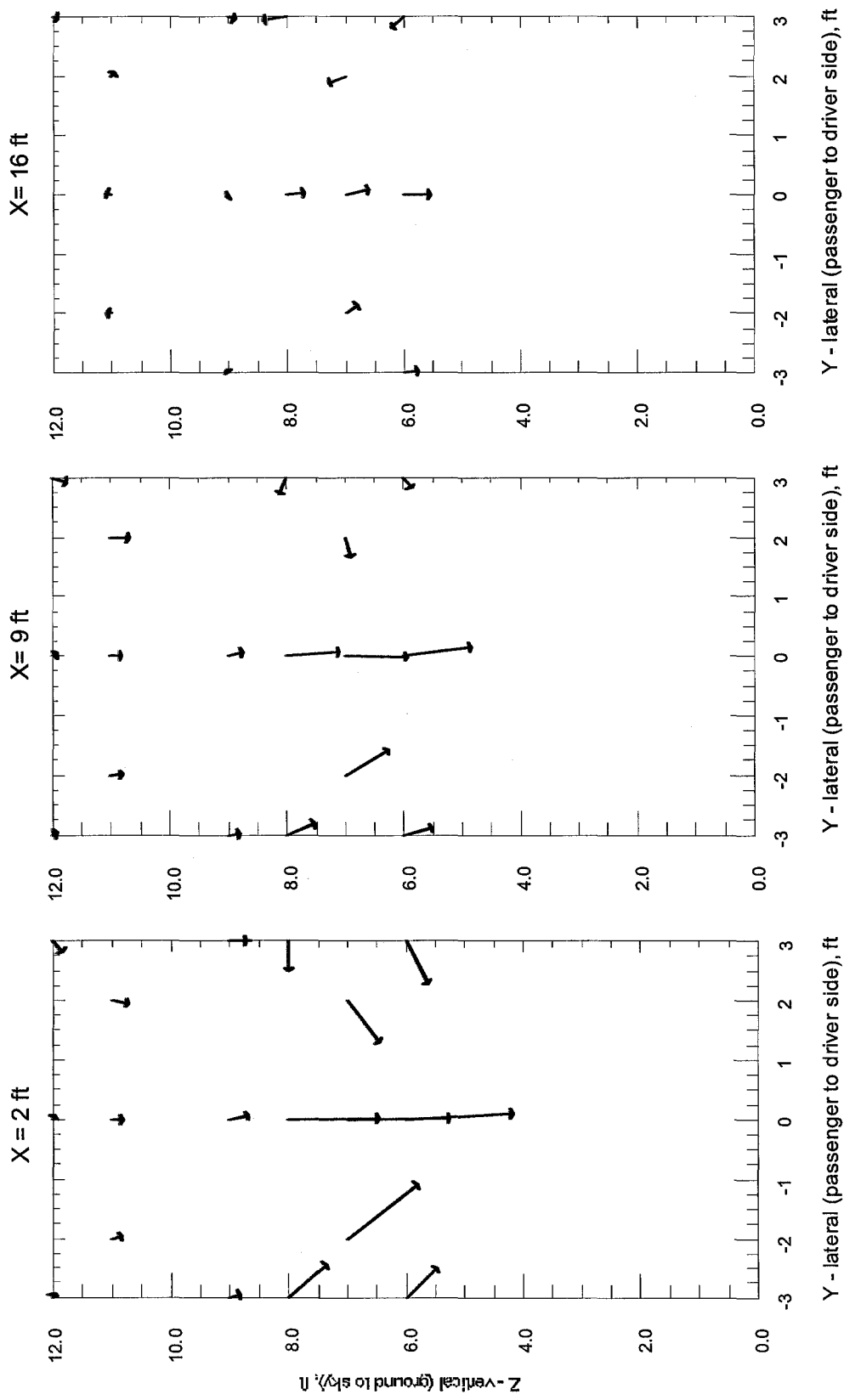


Figure 4.19. Vehicle wake flow vectors, cross-section view at $x = 2$ ft (0.61 m), $x = 9$ ft (2.74 m), $x = 16$ ft (4.88 m), respectively, behind vehicle, for speed = 50 mph (22.4 m/s), looking from front to rear, vehicle width = 6.2 ft (1.9 m), height = 6.9 ft (2.1 m), scale for vectors on plots: 1 unit = 2 m/s.

The vector flow field is viewed from above in Figures 4.20 and 4.21 for X - Y planes at six vertical locations, $z = 6$ ft (1.83m), $z = 7$ ft (2.13 m), $z = 8$ ft (2.44 m), $z = 9$ ft (2.74 m), $z = 11$ ft (3.35 m), and $z = 12$ ft (3.66 m), respectively. Clearly, Figure 4.20 indicates the air was impacted by the vehicle passage up to $z = 8$ ft (2.44 m); however, Figure 4.21 shows little influence on the air from vehicle passage for greater heights. As expected, the magnitude of the flow vectors again decreases with distance above the vehicle and/or increasing downwind distances. Additionally, Figures 4.22, 4.23, 4.24, and 4.25 show the same qualitative flow characteristics, but with greater magnitudes as the nominal vehicle speed increased to 40 mph (17.9 m/s) and 50 mph (22.4 m/s), respectively.

The vector flow field is shown from the side in Figures 4.26 and 4.27 for X - Z planes at various lateral (side to side) locations, $y = -3$ ft (-0.91 m), $y = -2$ ft (-0.61 m), $y = 0$ ft (0 m), $y = 2$ ft (0.61 m), and $y = 3$ ft (0.91 m). In Figure 4.26, differences between $y = 3$ ft and $y = -3$ ft (symmetric points about vertical centerline of vehicle) are rather minor. Likewise, Figure 4.27 shows that flow behavior at $y = -2$ ft and $y = 2$ ft are very similar. In a broader sense, $y = -3$ ft, $y = -2$ ft, $y = 2$ ft, and $y = 3$ ft are very similar; however, the centerline position ($y = 0$) shows vectors with much greater magnitude for heights less than $z = 8$ ft (2.44 m). As noted for the previous plots, the magnitude of the flow vectors decreases with increasing height above the vehicle and/or increasing downwind distances. Additionally, Figures 4.28, 4.29, 4.30, and 4.31 show the same qualitative flow characteristics, with greater magnitudes as the nominal vehicle speed increased to 40 mph (17.9 m/s) and 50 mph (22.4 m/s), respectively.

4.8 Sources of Errors

Any experiment has a number of sources of potential errors or variations which must be addressed and minimized. In this vehicle wake study, the nominal speed of the vehicle was somewhat variable even with the use of cruise control and a relatively flat runway surface, and this affected the speed of the air passing over the vehicle. Likewise, ambient wind conditions affected the actual airspeed by fluctuating during and between individual measurement periods (“runs”). Since one or more sonic anemometers were located in what was believed to be free-stream (non-wake region) air flow, the net effect of ambient and vehicle speed variations could be addressed. Vehicle speed variations could have also been addressed by using a differential Global Positioning System, although this was not used in this study.

The alignment of the individual sonic anemometers at any given location appears to be of greater concern than the previously mentioned variations. Since u , v , and w can be of significantly different magnitudes, apparently minor misalignment of the sonic anemometers can significantly contaminate the other flow component values. During this experiment, the angular differences determined from readings taken during ambient runs were used during post-processing of the data to address any misalignment of the anemometers. The exact anemometer orientation was carefully marked during the installation of each device; however, flexing or sagging of the test platform (trailer) may have slightly contaminated the w component for measurements near the rear of the platform, well aft of the trailer wheels.

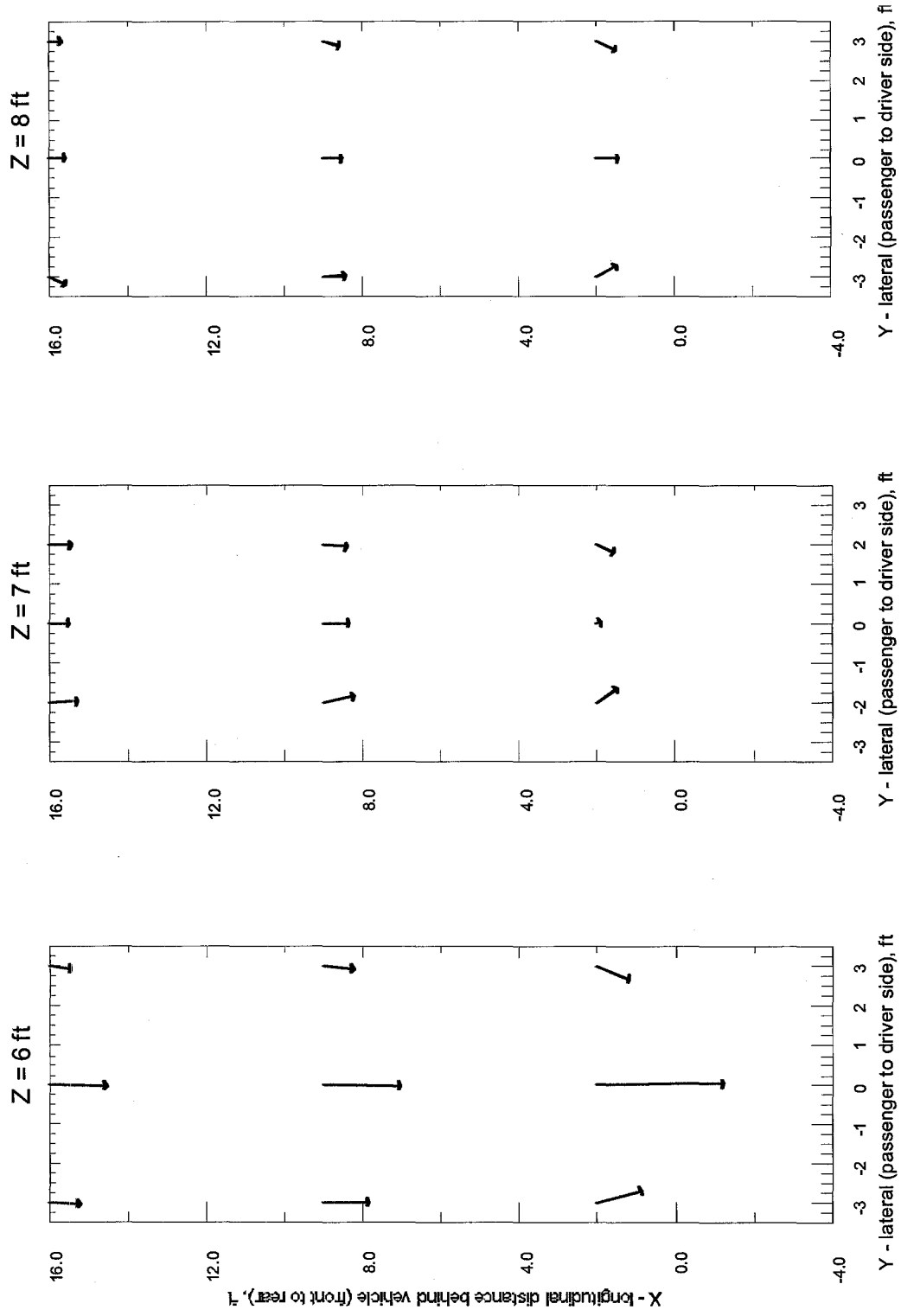


Figure 4.20. Vehicle wake flow vectors, cross-section view at $z = 6$ ft (1.83 m), $z = 7$ ft (2.13 m), $z = 8$ ft (2.44 m), respectively, above ground, for speed = 30 mph (13.4 m/s), looking from above, vehicle width = 6.2 ft (1.9 m), height = 6.9 ft (2.1 m), scale for vectors on plots: 1 unit = 2 m/s.

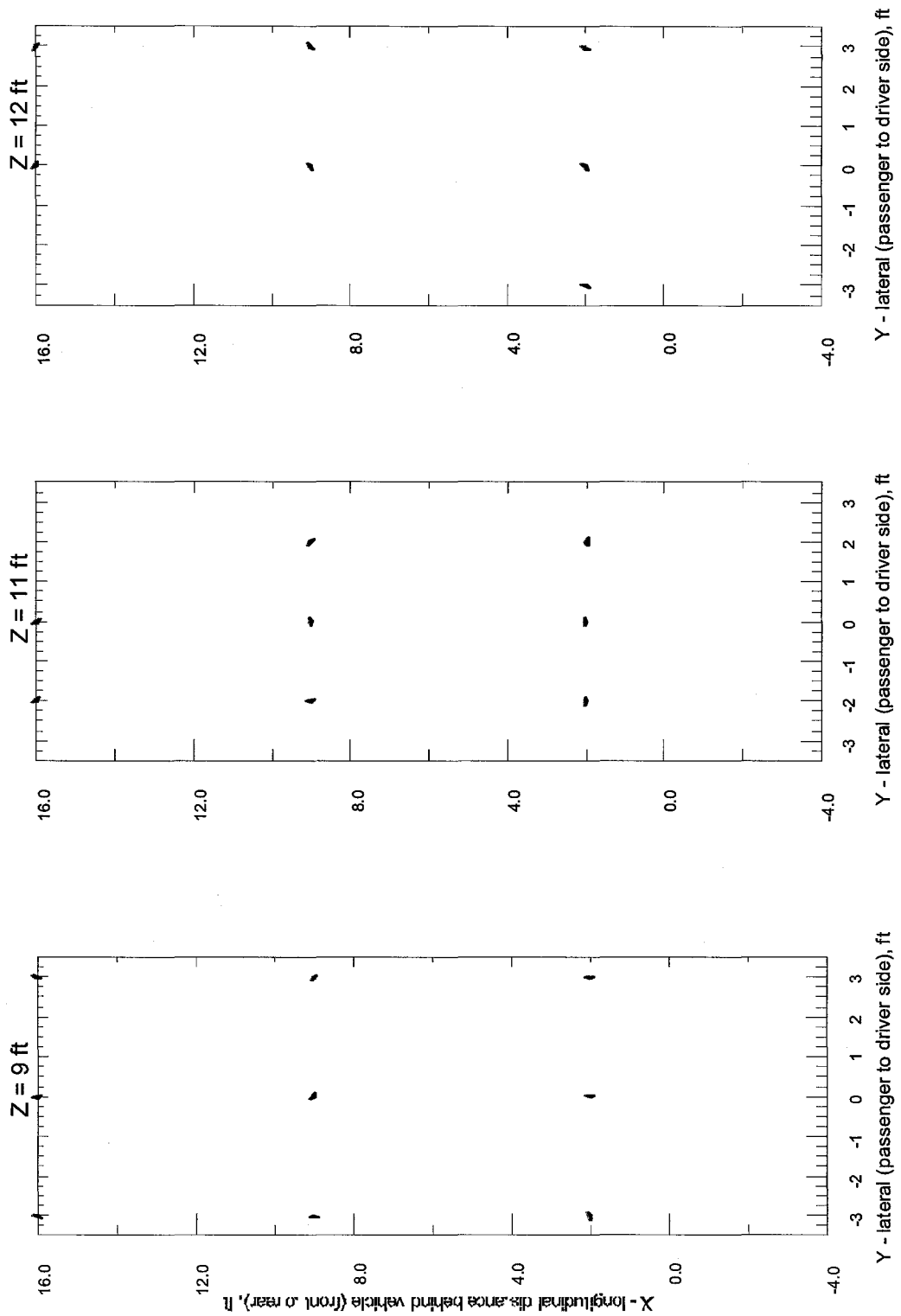


Figure 4.21. Vehicle wake flow vectors, cross-section view at $z = 9$ ft (2.74 m), $z = 11$ ft (3.35 m), $z = 12$ ft (3.66 m), respectively, above ground, for speed = 30 mph (13.4 m/s), looking from above, vehicle width = 6.2 ft (1.9 m), height = 6.9 ft (2.1 m), scale for vectors on plots: 1 unit = 2 m/s.

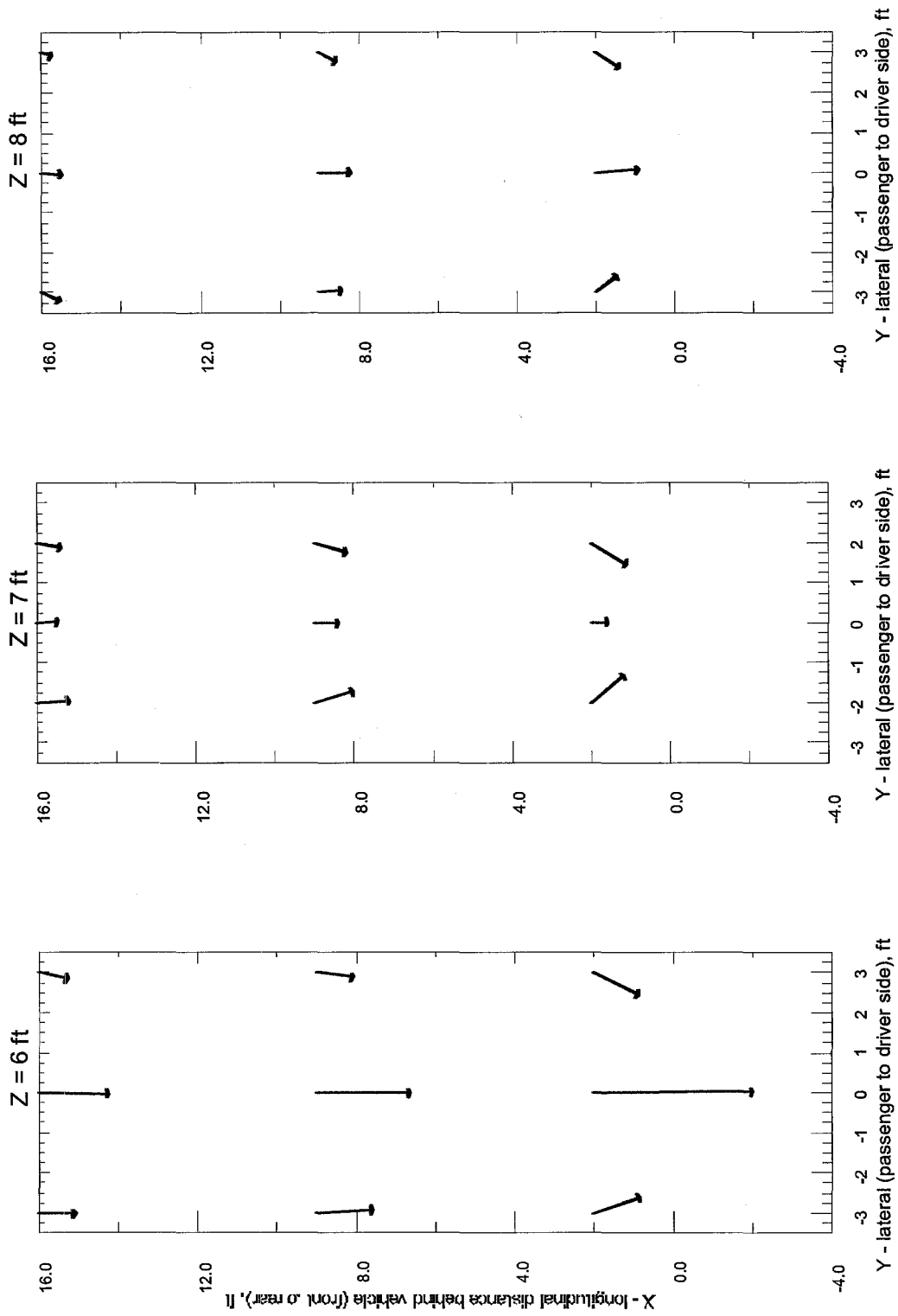


Figure 4.22. Vehicle wake flow vectors, cross-section view at $z = 6$ ft (1.83 m), $z = 7$ ft (2.13 m), $z = 8$ ft (2.44 m), respectively, above ground, for speed = 40 mph (17.9 m/s), looking from above, vehicle width = 6.2 ft (1.9 m), height = 6.9 ft (2.1 m), scale for vectors on plots: 1 unit = 2 m/s.

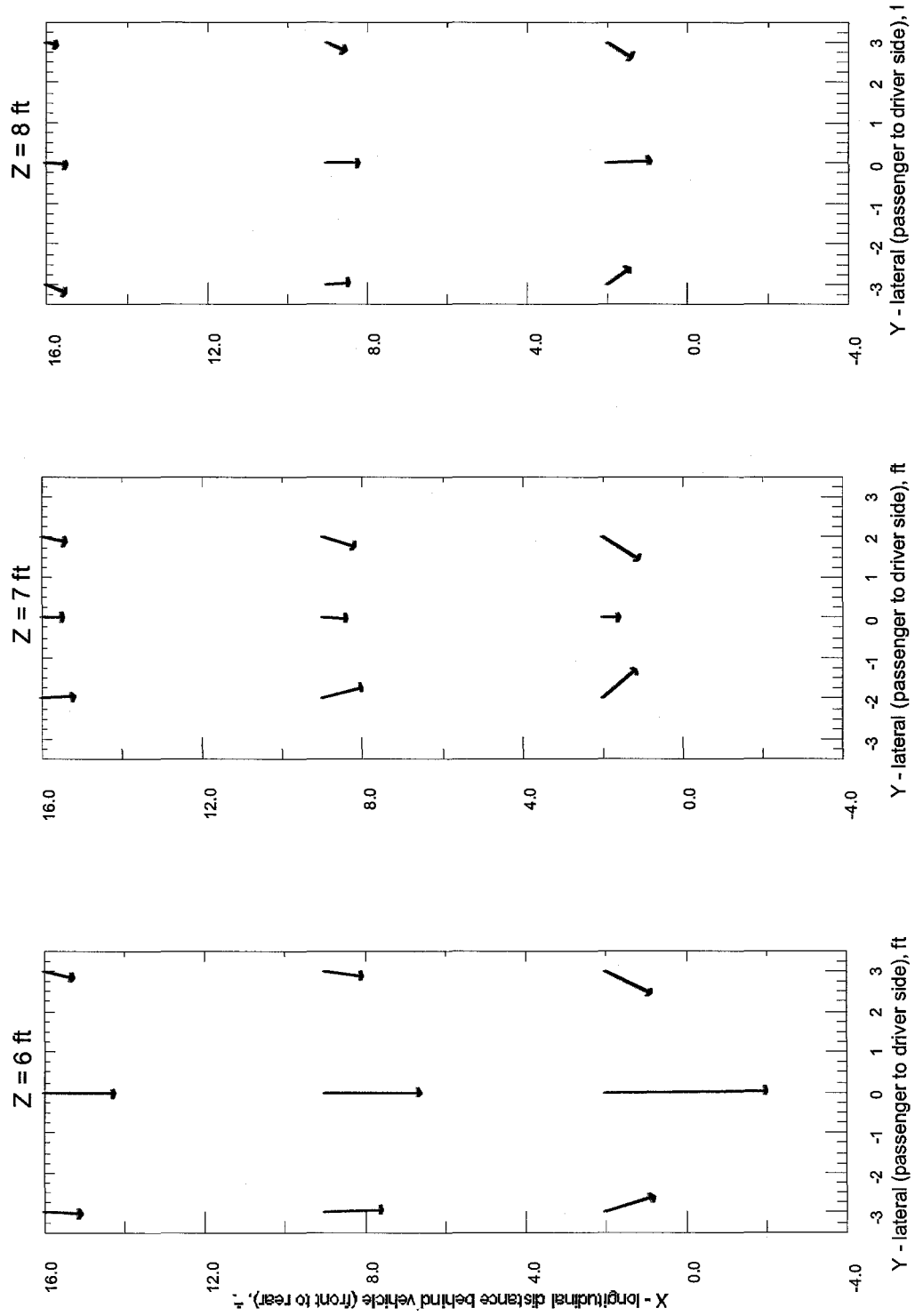


Figure 4.23. Vehicle wake flow vectors, cross-section view at $z = 6$ ft (1.83 m), $z = 7$ ft (2.13 m), $z = 8$ ft (2.44 m), respectively, above ground, for speed = 40 mph (17.9 m/s), looking from above, vehicle width = 6.2 ft (1.9 m), height = 6.9 ft (2.1 m), scale for vectors on plots: 1 unit = 2 m/s.

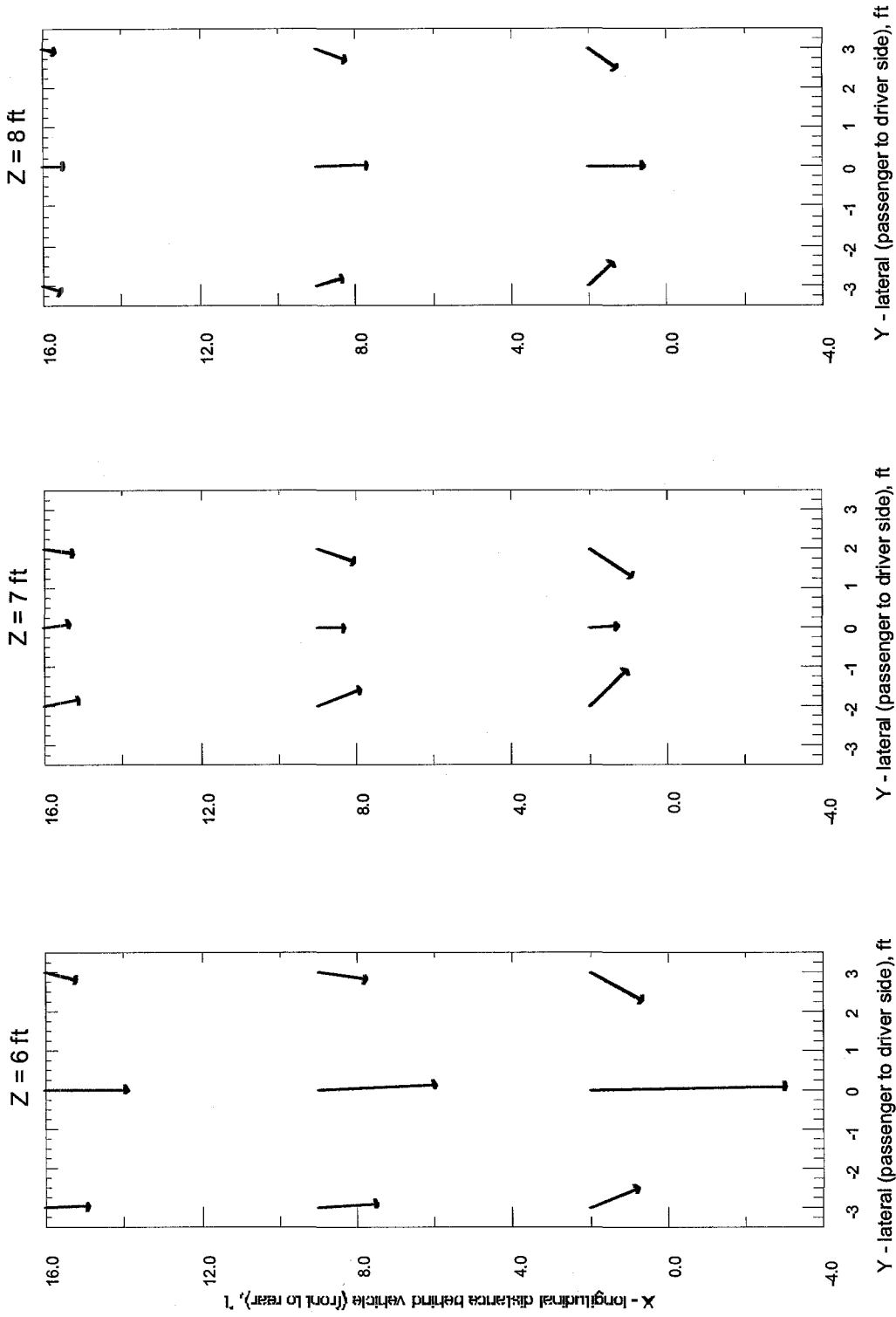


Figure 4.24. Vehicle wake flow vectors, cross-section view at $z = 6$ ft (1.83 m), $z = 7$ ft (2.13 m), $z = 8$ ft (2.44 m), respectively, above ground, for speed = 50 mph (22.4 m/s), looking from above, vehicle width = 6.2 ft (1.9 m), height = 6.9 ft (2.1 m), scale for vectors on plots: 1 unit = 2 m/s.

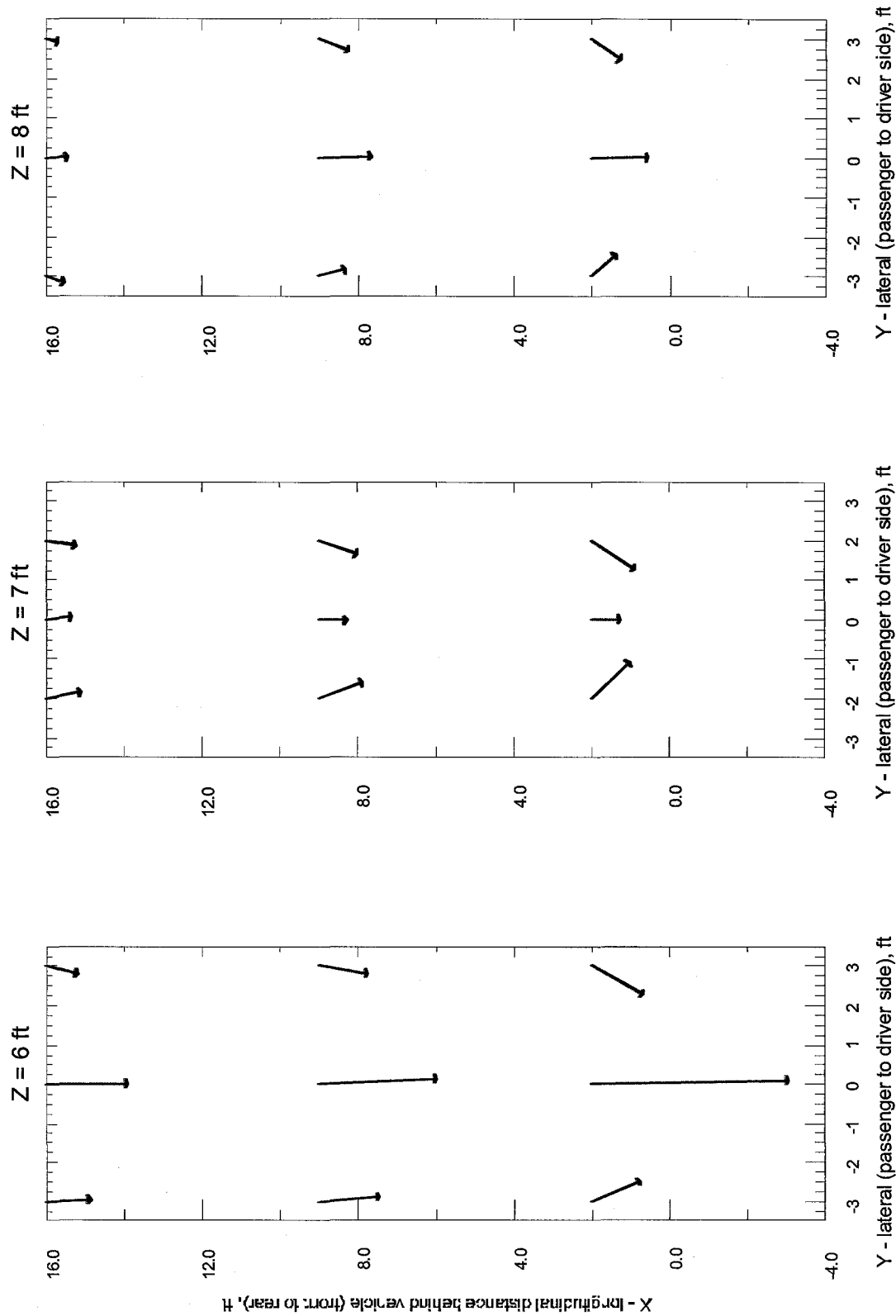


Figure 4.25. Vehicle wake flow vectors, cross-section view at $z = 6$ ft (1.83 m), $z = 7$ ft (2.13 m), $z = 8$ ft (2.44 m), respectively, above ground, for speed = 50 mph (22.4 m/s), looking from above, vehicle width = 6.2 ft (1.9 m), height = 6.9 ft (2.1 m), scale for vectors on plots: 1 unit = 2 m/s.

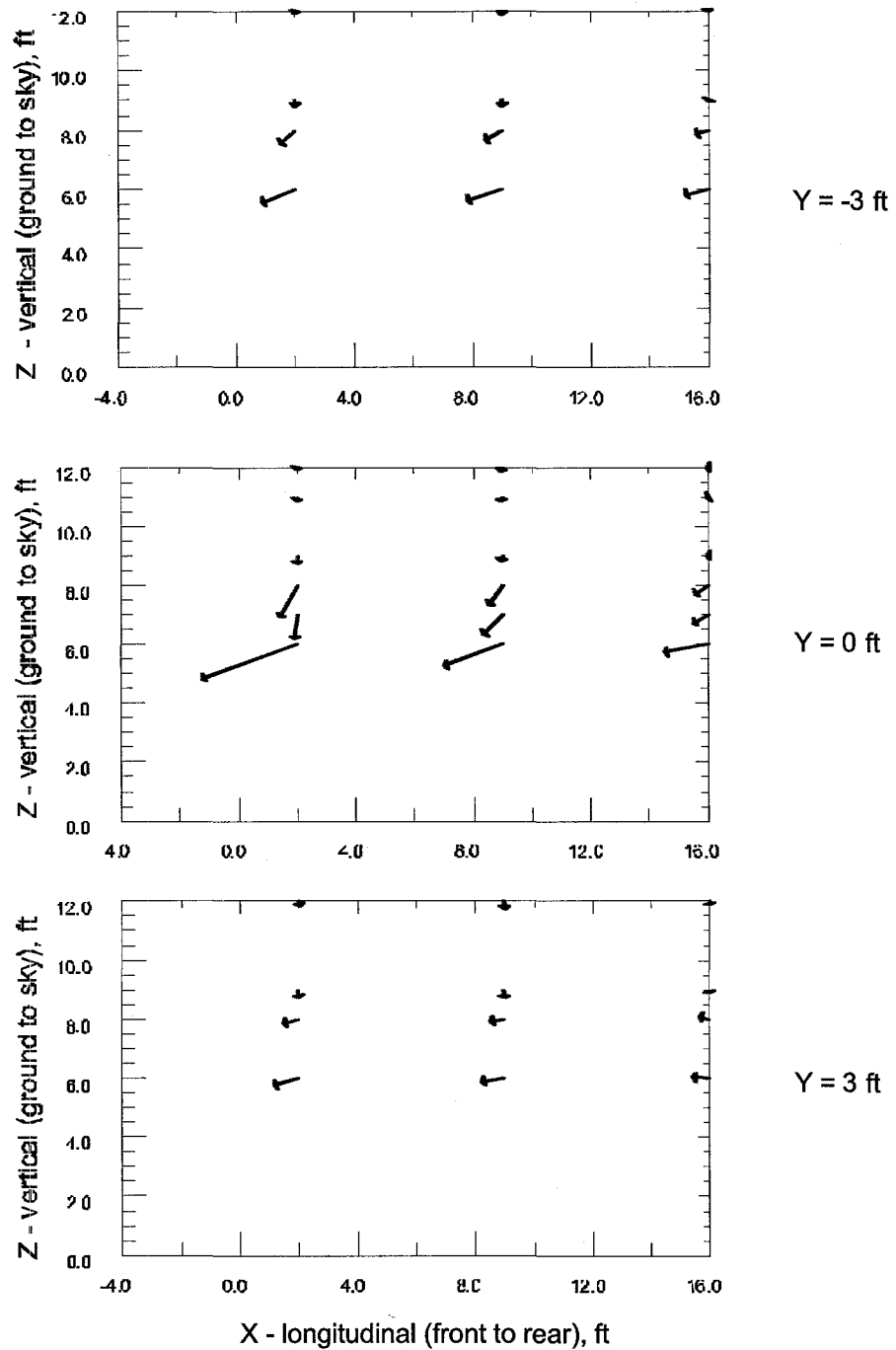


Figure 4.26. Vehicle wake flow vectors, cross-section view at $y = -3$ ft (-0.91 m), $y = 0$ ft (0 m), $y = 3$ ft (0.91 m), respectively, from centerline, speed = 30 mph (13.4 m/s), looking from side, vehicle width = 6.2 ft (1.9 m), height = 6.9 ft (2.1 m), scale for vectors on plots: 1 unit = 2 m/s.

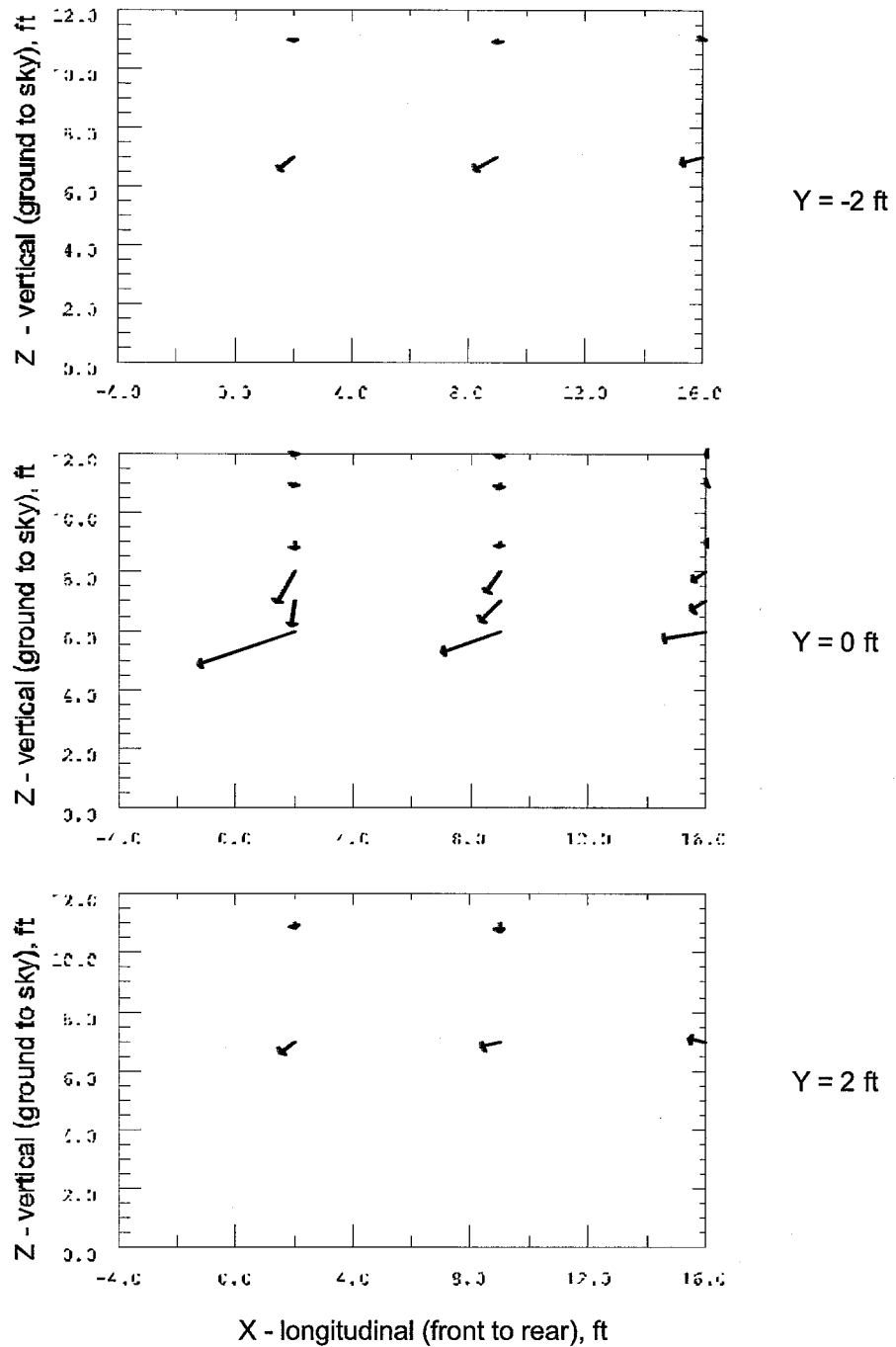


Figure 4.27. Vehicle wake flow vectors, cross-section view at $y = -2$ ft (-0.61 m), $y = 0$ ft (0 m), $y = 2$ ft (0.61 m), respectively, from centerline, speed = 30 mph (13.4 m/s), looking from side, vehicle width = 6.2 ft (1.9 m), height = 6.9 ft (2.1 m), scale for vectors on plots: 1 unit = 2 m/s.

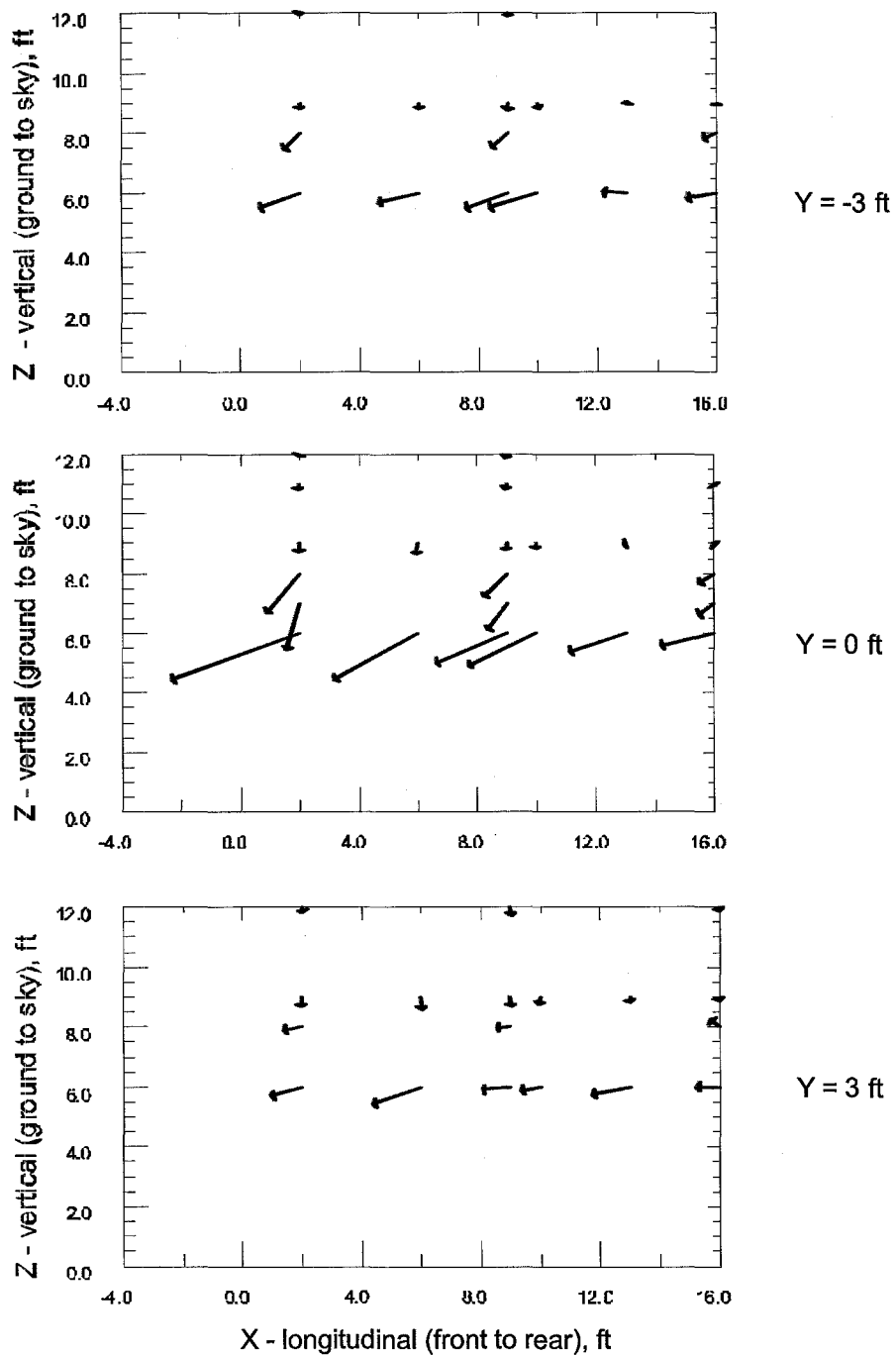


Figure 4.28. Vehicle wake flow vectors, cross-section view at $y = -3$ ft (-0.91 m), $y = 0$ ft (0 m), $y = 3$ ft (0.91 m), respectively, from centerline, speed = 40 mph (17.9 m/s), looking from side, vehicle width = 6.2 ft (1.9 m), height = 6.9 ft (2.1 m), scale for vectors on plots: 1 unit = 2 m/s.

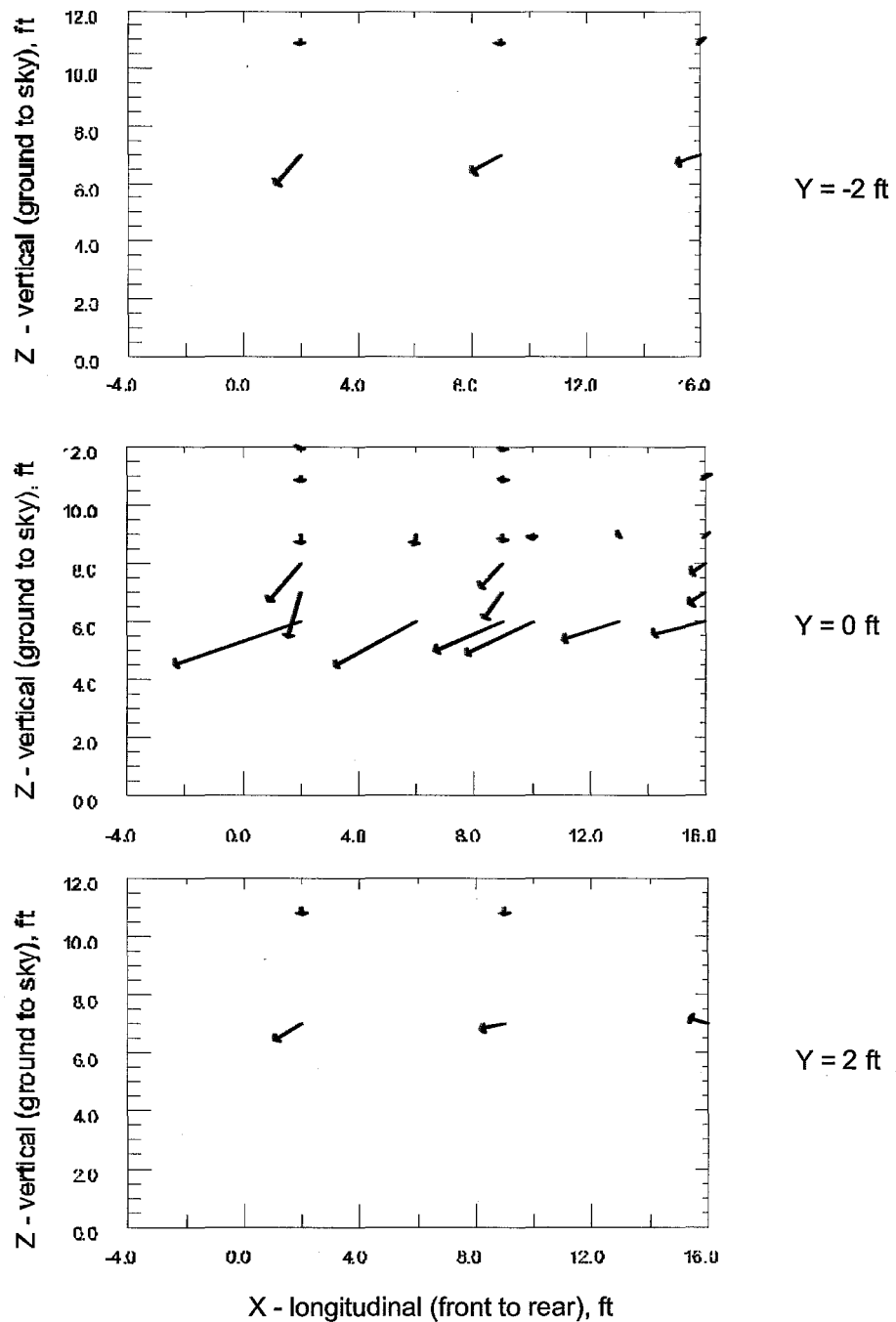


Figure 4.29. Vehicle wake flow vectors, cross-section view at $y = -2$ ft (-0.61 m), $y = 0$ ft (0 m), $y = 2$ ft (0.61 m), respectively, from centerline, speed = 40 mph (17.9 m/s), looking from side, vehicle width = 6.2 ft (1.9 m), height = 6.9 ft (2.1 m), scale for vectors on plots: 1 unit = 2 m/s.

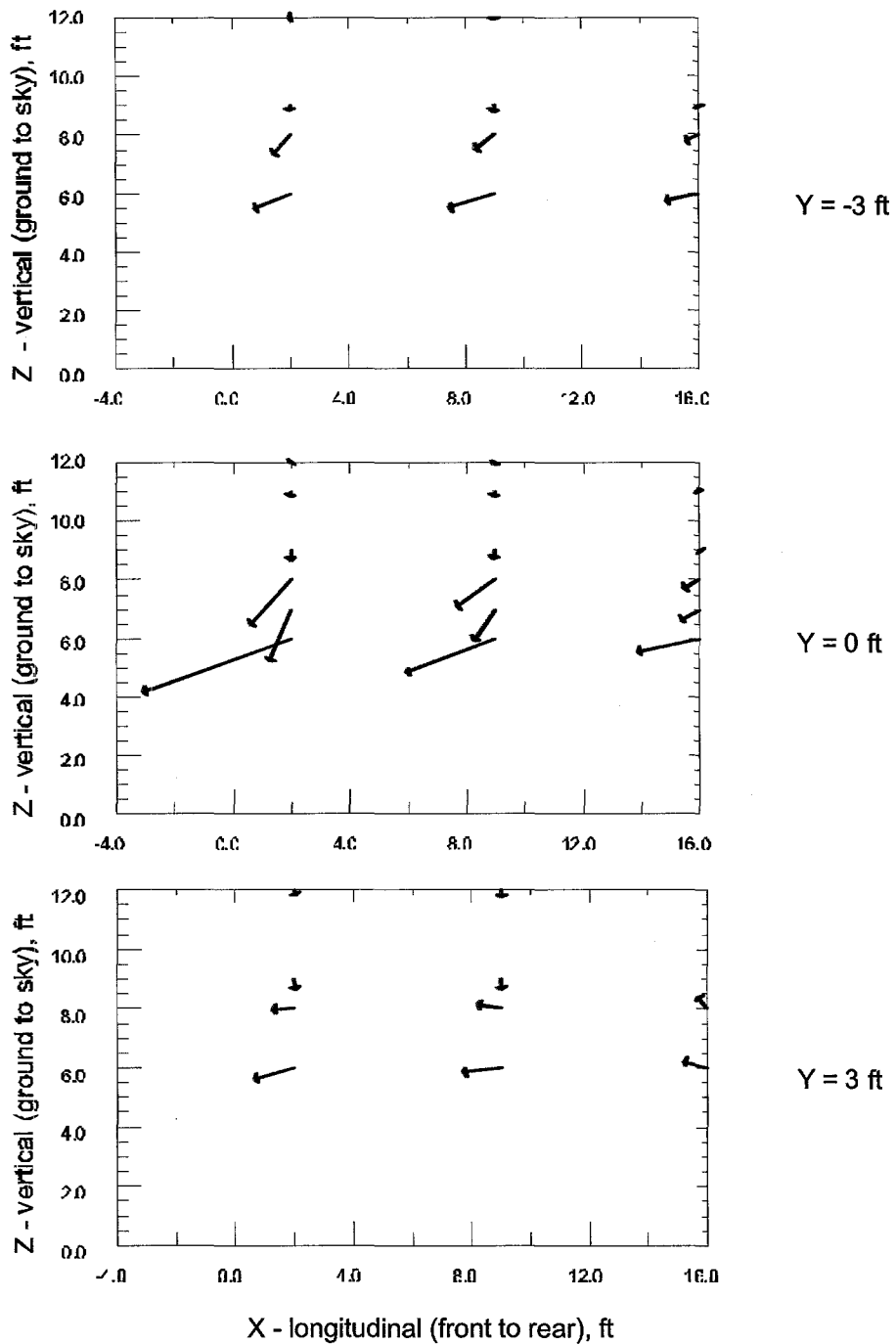


Figure 4.30. Vehicle wake flow vectors, cross-section view at $y = -3$ ft (-0.91 m), $y = 0$ ft (0 m), $y = 3$ ft (0.91 m), respectively, from centerline, speed = 50 mph (22.4 m/s), looking from side, vehicle width = 6.2 ft (1.9 m), height = 6.9 ft (2.1 m), scale for vectors on plots: 1 unit = 2 m/s.

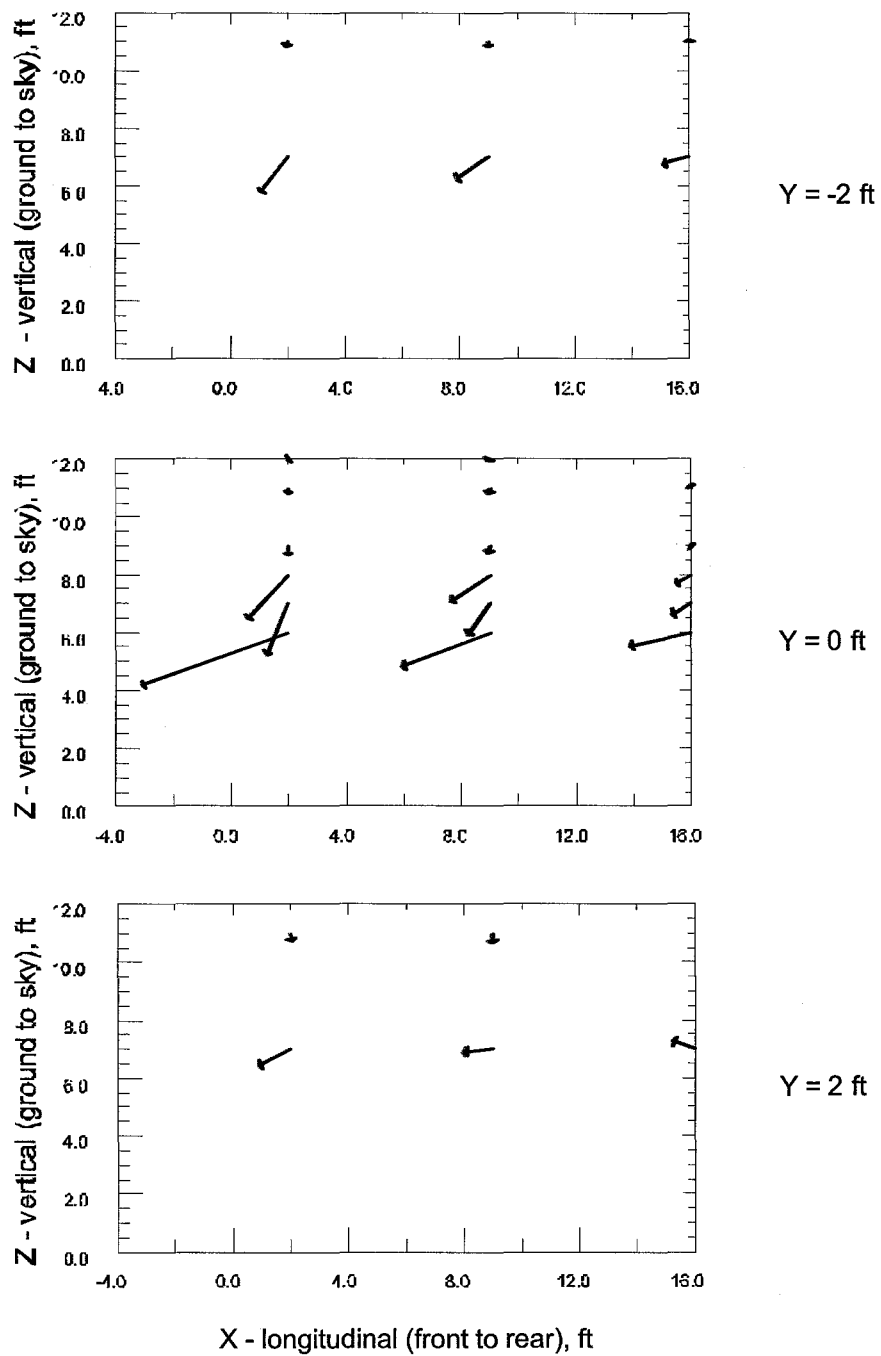


Figure 4.31. Vehicle wake flow vectors, cross-section view at $y = -2$ ft (-0.61 m), $y = 0$ ft (0 m), $y = 2$ ft (0.61 m), respectively, from centerline, speed = 50 mph (22.4 m/s), looking from side, vehicle width = 6.2 ft (1.9 m), height = 6.9 ft (2.1 m), scale for vectors on plots: 1 unit = 2 m/s.

Note the slight “+w” flow at $z=11$ ft (3.35 m) and $x = 16$ ft (4.88 m) in Figures 4.19 and 4.20, as well as a few other “+w” flows in those figures which are suspected to be the result of contamination due to the large u component multiplied by a slight angular pitch. Stiffening of the test platform with one or more I-beams would likely minimize or eliminate this problem in future studies.

4.9 Summary

Six fast-response sonic anemometers were utilized to measure the u , v , and w components of the wind. The objective was to characterize the 3-D flow field in the wake of a vehicle.

TKE was calculated for each run and configuration. Under some conditions it could be seen that TKE spectra from the top tier of anemometers saw an energy drop-off with wavenumber typical of the inertial subrange, and the bottom tier sometimes approached the inertial subrange slope. TKE calculated for times when the vehicle was not moving was useful for determining conditions for comparison with the different configurations for both the top and bottom tier of sonics while the vehicle was moving. The upper tier of sonics compared favorably in energy levels and spectral slope with the ambient readings, which suggests that the top tier of sonics were generally out of the wake turbulence. The bottom tier of sonics generally received increased energy and it was clear that they were sampling the wake turbulence of the vehicle. There was some indication that the ambient winds shifted the wake at times when the direction of travel was crosswind, and it was also seen that when the vehicle was heading into the wind, the energy levels increased, indicating increased wake turbulence. The size or the dissipation rate of the wake eddies could not be determined from the TKE spectra here. The contours of TKE indicated maximum energy along the wake centerline, at a height a little below 6 ft (1.8 m) and about 9 ft (2.7 m) behind the rear of the vehicle. Data closer to the road surface are needed to better determine these contours.

Flow vectors in the wake indicated strong downward flow and strong forward flow (i.e., toward the vehicle) along the centerline, decreasing with increasing height above the ground and increasing distance from the vehicle. The downward centerline flow may indicate the action of a pair of counter-rotating vortices near roof level, moving air aloft down into the wake cavity right behind the vehicle.

In order to fully characterize wake turbulence, it was determined from this series of experiments that there should optimally be a denser configuration of sonic anemometers. The six units available were placed strategically and symmetrically, but they were unable to measure completely what was actually occurring in the wake of the vehicle. Measurements closer to the road surface are essential to better understand the lower portions of the near wake. In particular, what is happening just behind the lower portion of the vehicle, where air passing below the vehicle emerges into the near wake? Video tapes of flow visualization using smoke candles mounted at the sonic anemometer positions and near the vehicle's rear bumper would assist considerably in understanding the wake flow patterns and in interpreting the wind component data.

The lightly used airport runway turned out to be an ideal place to measure, and it is suggested that future measurements be conducted in a similar situation. The number of runs per configuration

should be extended for a better ensemble realization. It was found that intermittent measurements of ambient wind conditions are not really sufficient, and the ambient wind should to be continuously measured, probably at a location halfway along the runway. This would allow for more time to be allocated to data runs, and would allow for better tracking of ambient winds over the entire sample time, but at the expense of needing an additional sonic anemometer.

5. MODELING OF POLLUTANT DISPERSION NEAR HIGHWAYS

K. Shankar Rao

5.1 Introduction

Pollutants emitted from motor vehicles on major highways contribute significantly to the degradation of air quality. Regulatory agency interest in the U.S. has long focused on the potential for large concentrations of carbon monoxide (CO), total suspended particulates (TSP, which also include Pb in countries that use leaded fuels), and other traffic-related pollutants (such as NO, NO₂, and O₃) near busy highways. The Federal Highway Administration (FHWA) requires that potential impacts should be considered during planning and construction of highway projects so that ambient air quality standards are met. For example, CO concentration associated with a highway impact should not exceed 35 ppm for 1 hour and 9 ppm for 8 hours more than once a year.

The regulatory and health concerns have led to the development and application of mathematical dispersion models for estimating the air quality adjacent to existing or proposed roads. These models are of varying sophistication and complexity, ranging from simple line-source Gaussian plume models to elaborate numerical models in two or three dimensions. The open-highway Gaussian models are easy to use, even with modifications for non-ideal situations, and require only simple meteorological input data. The usual limitations of Gaussian modeling apply: inability to deal with complex mean wind fields or near-calm conditions. The grid-based numerical models are capable of handling light winds and accounting for the variability of flow and diffusion conditions near highways, but these models are complex and often require elaborate inputs.

Among the difficulties in highway dispersion modeling are the specification of emissions and meteorological input data. The emission rates are highly variable depending on the vehicle type and its operating mode, and are often approximated in terms of their average values. In addition, many models do not account for vehicle-induced turbulence and buoyancy, though their importance for the prediction of dispersion near highways is well-documented. For example, Rao *et al.* (1979) showed that moving traffic produces an augmentation of energy in the high frequency end of the spectra and cospectra of the velocity components. Only a few field studies were performed near highways where detailed emissions, concentrations, and meteorological data were collected for model evaluation. Among these, tracer release studies such as the General Motors (GM) experiment (Cadle *et al.*, 1976) are particularly useful.

This section describes the near-highway dispersion model, ROADWAY-2, developed at the Atmospheric Turbulence and Diffusion Division (ATDD) under a collaborative research agreement between the National Oceanic and Atmospheric Administration (NOAA) and the FHWA. This work is based on U.S. EPA's ROADWAY (Eskridge and Catalano, 1987) model, which obtained mean velocity and temperature profiles and eddy-diffusivities from formulations based on equilibrium surface layer similarity theory. ROADWAY also incorporated vehicle wake formulations derived by Eskridge and Hunt (1979) from a perturbation solution to the equations of motion. The wake

effects were linearly superposed on the atmospheric wind and eddy diffusivity fields. A major restriction of this model is that the vehicle speed must be much greater than the wind speed. However, this requirement is usually met in most instances of significant pollution impacts.

ATDD's ROADWAY-2 model incorporates a turbulent kinetic energy (TKE) closure model of the atmospheric boundary layer (ABL), with up-to-date surface parameterizations, to derive mean wind and temperature, and turbulence profiles from input meteorological data. There are several reasons for this: First, a time-dependent ABL model avoids the need for making the questionable assumption that equilibrium surface layer relations are applicable near busy highways. Second, the linear superposition of the eddy diffusivities of the atmosphere and the wake employed in ROADWAY is not valid, since the length scales of the atmosphere and the wake are different. However, the eddy energies of the atmosphere and the wake are additive, and the inclusion of a TKE equation facilitates this addition to account for the wake turbulence production. Finally, the TKE closure model offers the flexibility for incorporating on-site turbulence measurements in the input data in future, with only slight modifications to the model. Such measurements are becoming feasible and attractive with the recent advances and affordability of instrumentation.

The atmospheric mean velocity components and TKE in ROADWAY-2 are adjusted to account for velocity deficit and turbulence production in vehicle wakes. The adjusted velocity and turbulence profiles are used in the calculation of pollutant transport and dispersion. The wake parameterizations incorporated in ROADWAY-2 are derived from the vegetation canopy flow theory (Dubov and Bykova, 1974; Kaimal and Finnigan, 1994) and the wind tunnel measurements in vehicle wakes by Eskridge and Thompson (1982).

The ROADWAY-2 model formulations and wake parameterizations are described in §5.2 and §5.3, respectively. The numerical solution and related model details are discussed in §5.4. The evaluation of ROADWAY-2 using the GM data is presented in §5.5. Some conclusions and recommendations are given in §5.6. A User's Guide to ROADWAY-2 will be included in a separate report (under preparation) on the model.

5.2 ROADWAY-2 Formulations

ROADWAY-2 model numerically solves a two-dimensional conservation of species equation:

$$\partial C / \partial t = -\nabla \cdot V C + \nabla \cdot K \nabla C + S_e, \quad (5.1)$$

where C is the concentration of a pollutant species, V is the wind vector, K is the eddy diffusivity, and S_e is the source (emissions) term. The boundary conditions are specified as follows:

$$\partial C / \partial z = 0 \text{ at } z = 0, C = C_B \text{ at inflow and top, } \partial C / \partial x = 0 \text{ at outflow boundary, } (5.2)$$

where z is the height above ground surface, C_B is the ambient background concentration of the species outside the computational grid. The two-dimensional grid varies in size depending on the wind speed and direction, and the number of highway lanes. The grid extends vertically from $z_b = 1$ m at the bottom to $z_t = 70$ m at the top, with logarithmic spacing to provide fine resolution near the ground. The horizontal grid, internally generated by the model to cover all traffic lanes, consists of a set of unevenly spaced points to give a higher resolution near the road. Numerical solution of Eqs. (5.1) and (5.2) is obtained by a fractional step finite-difference method. The advection steps are based on a flux-corrected transport algorithm (Zalesak, 1979; Book et al., 1975) which uses an upstream difference scheme that ensures non-negative values for concentration at every grid point.

5.2.1 ABL model

The mean wind and turbulence profiles used in Eq. (5.1) are obtained from a one-dimensional numerical model of the atmospheric boundary layer based on a turbulent kinetic energy closure. The ABL model equations can be written as follows:

$$\partial u / \partial t = \partial (K_m \partial u / \partial z) / \partial z + f (v - v_g) , \quad (5.3)$$

$$\partial v / \partial t = \partial (K_m \partial v / \partial z) / \partial z - f (u - u_g) , \quad (5.4)$$

$$\partial \theta / \partial t = \partial (K_h \partial \theta / \partial z) / \partial z , \quad (5.5)$$

where u and v are horizontal mean velocity components along x (east-west) and y (north-south) directions, u_g and v_g are the corresponding geostrophic wind components, f is the Coriolis parameter, and θ is the mean potential temperature.

The eddy diffusivities for momentum and heat (K_m and K_h) are calculated from a turbulent kinetic energy closure model described by Rao and Snodgrass (1981):

$$K_{m,h} = \ell_{m,h} (0.2 E)^{1/2} , \quad \ell_{m,h} = k z / \phi_{m,h} . \quad (5.6)$$

Here, E is the TKE, ℓ_m and ℓ_h are turbulent mixing lengths for momentum and heat, $k = 0.4$ is the von Kármán constant, and

$$\begin{aligned} \phi_m &= (k z / u_*) \partial S / \partial z , \quad S = (u^2 + v^2)^{1/2} \\ \phi_h &= (k z / T_*) \partial \theta / \partial z , \end{aligned} \quad (5.7)$$

are nondimensional mean velocity and potential temperature gradients specified according to the similarity theory relations of the atmospheric surface layer:

$$\begin{aligned}\phi_m(z/L) &= (1 - \gamma_m z/L)^{-1/4}, \quad \phi_h(z/L) = Pr_t (1 - \gamma_h z/L)^{-1/2}, \quad \text{for } L < 0, \\ \phi_m(z/L) &= 1 + \beta_m z/L, \quad \phi_h(z/L) = Pr_t + \beta_h z/L, \quad \text{for } L > 0.\end{aligned}\quad (5.8)$$

Here $L = -u_*^3/[k(g/\theta_o)H_o/(\rho c_p)]$ is Monin-Obukhov (—O) stability length ($L < 0$ for unstable and $L > 0$ for stable conditions), u_* is surface friction velocity, $H_o/(\rho c_p)$ is surface temperature flux, θ is surface potential temperature, and Pr_t is the turbulent Prandtl number. The empirical parameter values used in these equations are recommended by Höögström (1996) after a critical examination of several experimental data sets and comparison of their formulations: $\gamma_m = 19.0$, $\gamma_h = 11.6$, $\beta_m = 5.3$, $\beta_h = 8.0$, $Pr_t = 0.95$. The TKE is calculated from the prognostic equation:

$$\begin{aligned}\partial E/\partial t &= \partial(K_m \partial E/\partial z)/\partial z + K_m [(\partial u/\partial z)^2 + (\partial v/\partial z)^2] \\ &\quad - (g/\theta_o) K_h \partial \theta/\partial z - b(0.2E)^2/K_m,\end{aligned}\quad (5.9)$$

where b is a constant of order unity.

At $z = z_b$, the lower boundary conditions are specified as

$$\begin{aligned}S &= u_* F(z_b/L, z_o/L), \quad u = S \cos \beta, \quad v = S \sin \beta, \\ \theta &= \theta_o + T_* G(z_b/L, z_o/L), \quad E = 5u_*^2,\end{aligned}\quad (5.10)$$

where z_o is surface roughness height, $T_* = -H_o/(\rho c_p u_*)$ is the temperature scale, $\beta = \tan^{-1}(v/u)$ is determined at the grid point just above the lower boundary, and the functions F and G are given (Nickerson and Smiley, 1975) by

$$\begin{aligned}F(z/L, z_o/L) &= \int_{z_o}^z (k z')^{-1} \phi_m(z'/L) dz', \\ G(z/L, z_o/L) &= \int_{z_o}^z (k z')^{-1} \phi_h(z'/L) dz' .\end{aligned}\quad (5.11)$$

Nickerson and Smiley (1975) and Benoit (1977) gave the expressions for F and G obtained from Eq. (5.11) for the stable and unstable cases after substituting for ϕ_m and ϕ_h from Eq. (5.8).

At $z = z_p$ the upper boundary conditions are given by

$$\begin{aligned}S &= u_* F(z_t/L, z_o/L), \quad u = S \cos \beta, \quad v = S \sin \beta, \\ \theta &= \theta_o + T_* G(z_t/L, z_o/L), \quad \partial E/\partial z = 0.\end{aligned}\quad (5.12)$$

where β is angle of the mean wind direction relative to the x -axis. Numerical integration of the closed equation set (5.3) to (5.9), subject to boundary conditions (5.10) to (5.12), is performed using a Dufort-Frankel explicit finite difference scheme until a steady state evolves at $t = 3$ or 4 hr. The calculated TKE is partitioned into $\overline{u^2}$, $\overline{v^2}$, $\overline{w^2}$ by using appropriate diagnostic equations. Initial profiles of u , v , θ , and E used to start the integration are obtained as discussed below.

5.2.1.1 Initial profiles

Approximate initial profiles for the mean variables and key surface parameters required in the ABL model are derived from input meteorological data and surface-layer similarity relations, following Eskridge and Catalano (1987). The input data consist of hourly mean wind speeds S_1 and S_2 and temperatures θ_1 and θ_2 measured at heights z_1 and z_2 , respectively, on a meteorological tower (with $z_2 > z_1$) upwind of the highway.

From the input data, a bulk Richardson number is calculated as

$$Ri_b = (g/\theta_m) [\Delta\theta/(\Delta S)^2] \Delta z, \quad (5.13)$$

where $\Delta z = z_2 - z_1$, $\Delta S = S_2 - S_1$, $\Delta\theta = \theta_2 - \theta_1$, and $\theta_m = (\theta_1 + \theta_2)/2$. This permits estimation of M-O length L , using an iterative process, from the equation:

$$L = [\Delta z G / (k F^2 Ri_b)], \quad (5.14)$$

where $F = F(z_2/L, z_1/L)$ and $G = G(z_2/L, z_1/L)$ are computed from Eq. (5.11). The surface parameters are then calculated as

$$u_* = \Delta S / F, \quad T_* = \Delta\theta / G, \quad \theta_o = \theta_1 - T_* G(z_1/L, z_o/L). \quad (5.15)$$

The mean velocity and temperature profiles are then obtained as

$$\begin{aligned} u(z) &= u_* F(z/L, z_o/L) \cos \beta, \quad v(z) = u_* F(z/L, z_o/L) \sin \beta, \\ \theta(z) &= \theta_o + T_* G(z/L, z_o/L). \end{aligned} \quad (5.16)$$

The initial TKE profile is calculated from an equilibrium diagnostic relation derived from Eq. (5.9). Though it is preferable to measure the winds at two heights, the above analysis can also be performed with wind measurement only at height z_2 ; see, *e.g.*, Nickerson and Smiley (1975). ROADWAY-2 model incorporates both options for input data.

5.3 Vehicle Wake Parameterizations

Automobile wakes are characterized as momentum wakes and contain trailing organized vortices aligned with the wake axis, which rapidly mix the pollutants released in the turbulent wake. Because of this mixing, the buoyant plume rise resulting from the heated exhaust gases is expected to be small. Though Chock (1978) included plume rise in his line source model under very stable and light wind conditions, ROADWAY-2 does not consider the buoyancy of vehicle emissions.

Eskridge and Hunt (1979) presented a theory (hereafter referred to as the E-H theory) based on perturbation analysis for a three-dimensional wake behind a moving vehicle in still air. Assuming that the strength of the wake is determined by the overturning moment (or couple) acting on the vehicle rather than the drag, they derived analytical expressions for mean velocity deficit and turbulent velocity variances in the wake. Eskridge and Thompson (1982) investigated the wake behind a block-shaped vehicle fixed in position over a moving surface (no shear in the approach flow) in the wind tunnel; this simulates the wake behind a vehicle traveling along a highway under calm atmospheric conditions.

The momentum wake observed by Eskridge and Thompson (1982) did not have a simple self-preserving form. However, it was possible to collapse the velocity deficit data with one length scale and one velocity scale, and the turbulence data with different length and velocity scales. Figure 5.1 schematically shows the wake-aligned moving coordinate system (s, n, z) and its relation to the (x, y, z)

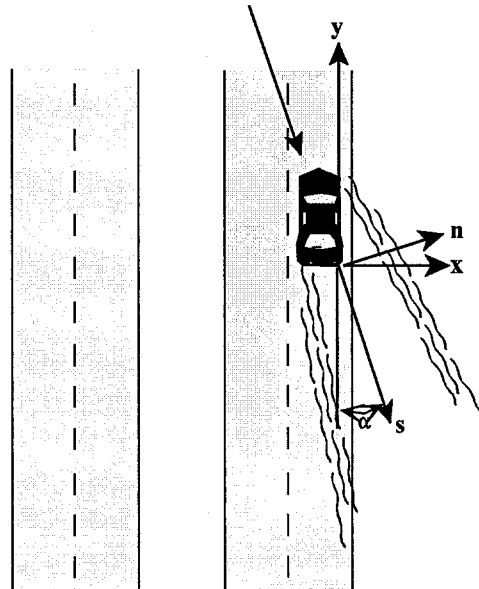


Figure 5.1 Schematic diagram of the wake-aligned (s, n, z) coordinate system and its relation to the (x, y, z) coordinate system.

Cartesian coordinate system, where the y axis is oriented along the highway and the x axis is normal to y in the horizontal plane, and z is in the vertical. Eskridge and Thompson (1982) found that the velocity deficit in the wake behind the vehicle decays as $(s/h)^{-3/4}$ and the length scale grows as $(s/h)^{1/4}$, where s is the downwind distance measured along the axis of the wake from its origin and h is the height of the vehicle. This confirmed the theoretical predictions of Eskridge and Hunt (1979). The TKE components decayed as $(s/h)^{-1/2}$ and the turbulence length scale was found to grow as $(s/h)^{0.4}$.

In the present study, we turn to the classical theory of flow in a vegetation canopy to derive the wake parameterizations for velocity deficit and turbulence production. There are two reasons for this: first, the wakes due to canopy elements are similar to the vehicle wakes with respect to the mechanisms of interest; second, the canopy flows have been studied over a longer time (*e.g.*, Dubov and Bykova, 1974; Shaw and Seginer, 1985; Wilson, 1988; Kaimal and Finnigan, 1994) in both models and measurements, and are therefore better understood. The key difference between the two flows is that the canopy elements are stationary, while the vehicles are moving. The latter requires use of the wind speed relative to the moving vehicle. In a canopy flow, complex energy transformations are caused by viscous and form (pressure) drag on vegetation. The rate of work done by the mean flow against the form drag results in a positive contribution to the TKE, *i. e.*, wake production. Experimental evidence suggests that the rate of wake production of TKE is comparable in magnitude to the shear production rate. However, the wake turbulence is of small scale and dissipates very rapidly. The time-dependent aerodynamic drag force exerted on the canopy per unit volume is equal to the product of the local foliage area density (foliage area per unit volume), a constant drag coefficient, and the square of the local velocity.

In an analogous way, for the vehicle wakes, the aerodynamic drag force can be written as

$$\partial u_D / \partial t \propto C_d A_v Q^2, \quad (5.17)$$

where u_D is the wake velocity deficit, C_d is the drag coefficient,

$$A_v = (\ell_v \sin \alpha + w_v \cos \alpha) h / (\ell_v w_v h) \quad (5.17a)$$

is vehicle area density, and

$$Q = [u_\infty^2 + (v_\infty - V_h)^2]^{1/2} \quad (5.17b)$$

is wind speed relative to the vehicle, which is moving with velocity V_h . In the above, ℓ_v and w_v are length and width of the vehicle, h is its height, u_∞ and v_∞ are the ambient velocity components, α is the angle between the mean wind and the road (y axis) as shown in Fig. 5.1.

Assuming an integral time scale $\tau \propto h/Q$ exists, an expression for the magnitude of u_D can be derived from Eq. (5.17) as

$$u_D \propto C_d A_v Q^2 \tau \propto C_d A_v Q h. \quad (5.18)$$

Incorporating the u_D variations with respect to (s,n,z) determined from wind tunnel measurements of Eskridge and Thompson (1982), this can be written as

$$u_D = C_u C_d A_v Q h (s/h)^{-3/4} Y(\eta) T(\zeta) . \quad (5.19)$$

Here C_u is a constant and the functions Y and T , determined from E-H theory and wind tunnel measurements, were given by Eskridge and Catalano (1987) as

$$Y(\eta) = C_1 \exp(-\eta^2/8) \quad (5.20a)$$

$$T(\zeta) = b_0 + b_1 \zeta + \dots + b_6 \zeta^5 , \quad (5.20b)$$

where $C_1 \approx 1.0$, and $b_p (p = 1, \dots, 6)$ are empirical coefficients listed in Table 2 of Eskridge and Catalano (1987), and η and ζ (are dimensionless lateral and vertical coordinates defined as follows:

$$\eta = n / [\lambda (w_v/h) \ell_D] , \quad \zeta = z / \ell_D , \quad \ell_D = \gamma A h (s/h)^{1/4} . \quad (5.21)$$

In the above, ℓ_D is the length scale for the velocity deficit, $\gamma = 0.095$ and $\lambda = 1.14$ are empirical constants, and $A = [C_d / (32\pi e^{1/2} \lambda \gamma^3)]^{1/4}$ is the constant in the expression for strength of the wake, determined by the overturning moment acting on the vehicle (Eskridge and Hunt, 1979).

Similarly, following the canopy flow parameterizations (e.g., Dubov and Bykova 1974; Shaw and Seginer, 1985), the rate of vehicle wake production of TKE (E_v) can be written as

$$\partial E_v / \partial t \propto C_d A_v Q^3 , \quad (5.22)$$

which leads to

$$E_v \propto C_d A_v Q^3 \tau \propto C_d A_v Q^2 h . \quad (5.23)$$

Incorporating Eskridge and Thompson's (1982) wind tunnel measured variations of E_v with respect to (s,n,z) , this can be written as

$$E_v = C_e C_d A_v Q^2 h (s/h)^{-1.2} F_c(\chi, \omega) , \quad (5.24)$$

where C_e is a constant. Eskridge and Thompson (1982) determined the function $F_c(\chi, \omega)$ as a least-squares orthogonal polynomial fit to wind tunnel data:

$$F_c(\chi, \omega) = \sum_{n=0}^4 \sum_{m=0}^2 \psi_{2m,n} \chi^{2m} \omega^n , \quad (5.25a)$$

$$\chi = (n/w_v) (s/h)^{-0.4} , \quad \omega = (z/h) (s/h)^{-0.4} , \quad (5.25b)$$

such that $F_v > 0$. The coefficients are listed in Table 2 of Eskridge and Catalano (1987). The wake TKE given by Eq. (5.24) is partitioned into its components along (s, n, z) directions as

$$(\overline{u_s^2}, \overline{v_n^2}, \overline{w_z^2}) = (a_1, a_2, a_3) E_v / a_4, \quad (5.26)$$

where $a_1 = 0.048$, $a_2 = 0.040$, $a_3 = 0.030$ based on the wind tunnel data of Eskridge and Thompson (1982), and $a_4 = (a_1 + a_2 + a_3)/2$.

The expressions for vehicle wake velocity deficit and turbulence production, obtained from canopy flow theory and wind tunnel measurements, are analogous to those given by Eskridge and Catalano (1987) based on E-H theory. In principle, the constants C_u and C_e can be independently determined if suitable data are available. In the absence of such data, their values in the present study were determined by equating the expressions for u_D and E_v given by Eqs. (5.19) and (5.24) to the corresponding expressions given by Eskridge and Catalano (1987). This leads to

$$C_u = A/B, \quad C_e = a_4 A^2/B, \quad (5.27)$$

where $B = C_d A_v h$, and A and a_4 are defined above. Thus the expressions for u_D and E_v presently used in ROADWAY-2 are identical to those given by Eskridge and Catalano (1987). This does not however preclude an independent determination of their values later when suitable data become available.

5.3.1 Extension to multiple vehicles

The wake parameterizations given above for a single vehicle can be extended to N vehicles passing an observation point $X_p = (x_p, y_p, z_p)$ near the highway during a given time interval $[-T/2, T/2]$ by summing up the effects of all vehicles, as shown by Eskridge and Catalano (1987). The effective pollutant advection velocity components u and v in x and y directions are then obtained by appropriately adding the ambient velocity components u_∞ and v_∞ determined from the ABL model to the corresponding components of the total wake velocity deficit:

$$\overline{u(X_p, t)} = \overline{u_\infty(z_p, t)} - \text{sign}(u_\infty) \frac{1}{T} \sum_{j=1}^N \int_{-T/2}^{T/2} u_{D_j}(X_p, t) \sin \alpha_j dt, \quad (5.28)$$

$$\overline{v(X_p, t)} = \overline{v_\infty(z_p, t)} + \text{sign}(V_h) \frac{1}{T} \sum_{j=1}^N \int_{-T/2}^{T/2} u_{D_j}(X_p, t) \cos \alpha_j dt, \quad (5.29)$$

where the overbars indicate time averages over the interval $[-T/2, T/2]$. In Eq. (5.28), $\text{sign}(u_\infty) = -1$ when the x component of the ambient surface wind is from the east to west, and $+1$ when it is from west to east, such that the two terms on the right-hand side are of opposite sign. In Eq. (5.29), $\text{sign}(V_h) = -1$ for southbound traffic and $+1$ for northbound traffic. For integrating the above expressions, we set $dt = |dy/V_h|$ and modify the lower and upper integration limits to $-|TV_h/2|$ and $|TV_h/2|$, respectively.

The (x,y,z) components of the turbulence variances produced by multiple vehicle wakes are integrated and added to the corresponding ambient atmospheric values to obtain the total TKE components at X_p , as follows:

$$\overline{u^2(X_p, t)} = \overline{u_\infty^2(z_p, t)} + \frac{1}{T} \sum_{j=1}^N \int_{-T/2}^{T/2} [\overline{u_s^2(X_p, t)} \sin \alpha + \overline{v_n^2(X_p, t)} \cos \alpha] dt, \quad (5.30)$$

$$\overline{v^2(X_p, t)} = \overline{v_\infty^2(z_p, t)} + \frac{1}{T} \sum_{j=1}^N \int_{-T/2}^{T/2} [\overline{u_s^2(X_p, t)} \cos \alpha + \overline{v_n^2(X_p, t)} \sin \alpha] dt, \quad (5.31)$$

$$\overline{w^2(X_p, t)} = \overline{w_\infty^2(z_p, t)} + \frac{1}{T} \sum_{j=1}^N \int_{-T/2}^{T/2} \overline{w_z^2(X_p, t)} dt, \quad (5.32)$$

where $\overline{u_s^2}$, $\overline{v_n^2}$, $\overline{w_z^2}$ are the wake turbulence variances from Eq. (5.26), and the subscript ∞ denotes the ambient atmospheric TKE components determined from the ABL model (see §5.2).

5.4 Numerical Solution

A fractional finite-difference method is employed in the numerical solution of Eq. (5.1), subject to the boundary conditions in Eq. (5.2). The mean wind components (adjusted for vehicle wake effects), given by Eqs. (5.28) and (5.29), are used to advect the pollutants. The calculation of eddy diffusivities used in Eq. (5.1) is described below. The advection steps are based on a flux-corrected transport algorithm (Zalesak, 1979; Book *et al.*, 1975), which was successfully adapted to the logarithmic vertical grid used in ROADWAY-2.

5.4.1 Eddy diffusivities

The vertical eddy diffusivity profile used in Eq. (5.1) is calculated in terms of the total TKE components determined in Eqs. (5.30) to (5.32), as follows:

$$K_z(x, z) = c_k \sigma_{\text{tot}} z = c_k (2.5 E)^{1/2} l_h, \quad (5.33)$$

where the constant $c_k \approx 1.08$ and ℓ_h is the turbulent mixing length for scalar quantities (see §5.2); the latter is limited here such that $\ell_h \leq 1$. The expression given above for K_z is based on the wind tunnel diffusion study of Eskridge and Rao (1986).

The horizontal eddy diffusivity profile is more difficult to specify, but the results are found to be relatively insensitive to the exact expression used. Some investigators used $K_x(x,z) = K_z(x,z)$. In ROADWAY-2, K_x is calculated as

$$K_x(x, z) = c_k [2.5 (\overline{u^2} \cos \beta + \overline{v^2} \sin \beta)/2]^{1/2} \ell_h, \quad (5.34)$$

where β is the angle of the mean wind relative to the x axis.

5.4.2 Initial dispersion

Several previous studies noted the correlation between crossroad wind speed and initial vertical dispersion. These studies concluded that lower wind speeds result in greater initial vertical dispersion (see, *e.g.*, Benson, 1992). In ROADWAY-2, the initial mixing volume (V_i) for the pollutants is modeled as

$$V_i = W z_i |v_1 - V_h| \quad (5.35a)$$

for southbound lanes, and

$$V_i = W z_i |v_1 + V_h| \quad (5.35b)$$

for northbound lanes. Here W is the width of the highway lane, V_h is the vehicle speed, and v_1 is the ambient surface (at $z = 1$ m) wind component along the road; v_1 is positive when it is towards the north (along the positive y -axis), and it is negative otherwise. For the GM tracer data simulation (see §5.5), the height z_i (in meters) of the initial mixing volume is specified as a function of the surface (at $z = 1$ m) wind speed (S_1) in m/s, as follows:

$$\begin{aligned} z_i &= 1.5, \quad S_1 \geq 1.0, \\ &= 1.5 + 4.5(1.0 - S_1)/0.5, \quad 0.5 < S_1 < 1.0, \\ &= 6.0, \quad S_1 < 0.5. \end{aligned} \quad (5.36)$$

This parameterization may vary with climate and experimental conditions, and needs more study.

5.4.3 ROADWAY-2 user's guide

A user's guide to ROADWAY-2 is under preparation and will be included in a separate report on the model. This guide, which includes information on input data file preparation, output data

description, and I/O file listings of an example problem, should be used together with the ROADWAY user's guide by Eskridge and Catalano (1987).

5.5 ROADWAY-2 Evaluation

The ROADWAY-2 model has been evaluated with the General Motors sulfate-dispersion experiment data. This experiment was held in September and October of 1975 at the GM proving grounds in Milford, Michigan. A fleet of 352 automobiles were driven on a north-south track of 10 km length for 17 days during morning hours. A complete description of the experiment, analysis procedures, and data tables can be found in Cadle *et al.* (1976); the data for the model evaluation are taken directly from this report. The model grid was modified to simulate the experimental setup.

5.5.1 GM experiment

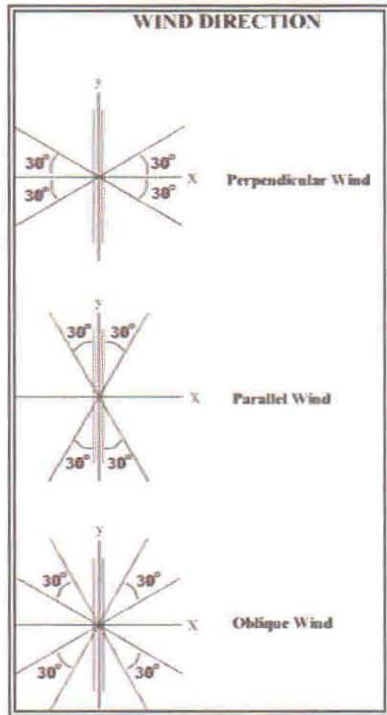
Meteorological instruments and chemical samplers were located on six towers and two stands 2.4 km north of the south end of the test track. Figure 5.2(a) and (b) shows the layout of the instrumented towers relative to the test track, and the height locations of the various instruments. Twenty Gill UVW anemometers were located on the towers at approximate heights of 1.5, 4.5, and 10.5 m above the surface on the six towers, and at 1.5 m on the two stands. The SF₆ syringe samplers were located at heights of 0.5, 3.5, and 9.5 m on the towers, and at 0.5 m height on the stands. Wind speeds from the 20 anemometers were recorded once per second. Temperature data were recorded from towers 1 and 6 every 5 s using platinum resistance thermometers mounted in aspirated temperature shields, which were located at the same heights as the wind instruments.

The fleet consisted of sixteen packs, spaced 300 m apart and 22 cars in each, which traveled at 80 km/hr. The packs passed the instrumented tower every 29 s in the northbound and southbound lanes, leading to a vehicle flow rate of 5462 veh/hr or 1365 veh/hr/lane in each of the 4 lanes. SF₆ tracer gas was released by 8 pickup trucks distributed in the 16 packs of cars, such that the trucks were evenly spaced and staggered to avoid running side-by-side. One truck passed the instrument tower every 58 s, in the northbound and in the southbound lanes, giving a flow rate of 124 veh/hr or 31 veh/hr/lane for the tracer emission.

Tracer sampling began approximately 5 min after the vehicles started around the track. Four sequential samples, each taken over a 30-min period, were analyzed to obtain the 30-min average SF₆ concentration at each observation point. The accuracy of the analysis by a dual-column gas chromatograph was estimated to be within ±6%. Problems occurred with the tracer release on two of the experiment days; the total number of (nominally 30 min) sampling periods, therefore, is 58 instead of 66. For a sampling period numbered as 279080959, for example, 279 was the Julian day, 08 was the hour, and 09 and 59 were the minutes and seconds, respectively, in local time at the end of the sampling period. This notation of GM data (Cadle *et al.*, 1976) has been followed in the present work.

5.5.2 Data classification

Depending on the wind direction and wind speed at the 4.5 m height on the upwind tower, and the observed temperature difference ($\Delta T = T_2 - T_1$ between $z_2 = 4.5$ m and $z_1 = 1.5$) on that tower, the tracer sampling periods in the GM data (Cadle *et al.*, 1976) are classified as follows:



1) Perpendicular wind: wind direction is within 30° of the east-west axis; parallel wind: direction is within 30° of the north-south axis; oblique wind: direction is within the remaining 30° sectors. This is schematically illustrated in Figure 5.3.

2) High wind: $S_2 \geq 2.5$ m/s; moderate wind: $1 < S_2 < 2.5$ m/s; low wind: $S_2 \leq 1$ m/s, where S_2 is the wind speed at $z_2 = 4.5$ m.

3) Unstable atmosphere: $\Delta T < 0$; neutral: $\Delta T = 0$; stable: $\Delta T > 0$.

Four 30-min tests for each of the perpendicular, parallel, and oblique wind cases were selected for ROADWAY-2 evaluation. For each wind direction, half of the tests had unstable conditions and the other half had stable conditions. Several of these tests had low winds; the rest had moderate winds. This allowed for evaluation of the model performance under most of the conditions likely to be encountered in practice.

Figure 5.3 Schematic diagram of wind direction classification of GM data.

5.5.3 Evaluation results

The ROADWAY-2 model predictions are compared to the corresponding 30-min average observed tracer concentrations. Figure 5.4 shows a comparison of the observed and predicted concentrations for the perpendicular wind. The corresponding results for the parallel and the oblique winds are presented in Figs. 5.5 and 5.6. The model evaluation statistics for the three cases are listed in Table 5.1. These statistical measures have been described and widely used in literature (e.g., Tangirala *et al.*, 1992).

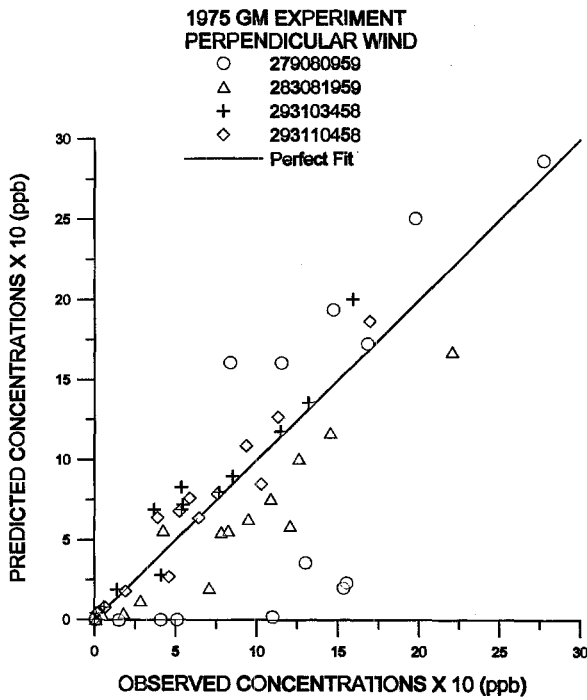


Figure 5.4 Comparison of predicted and observed concentrations for perpendicular winds.

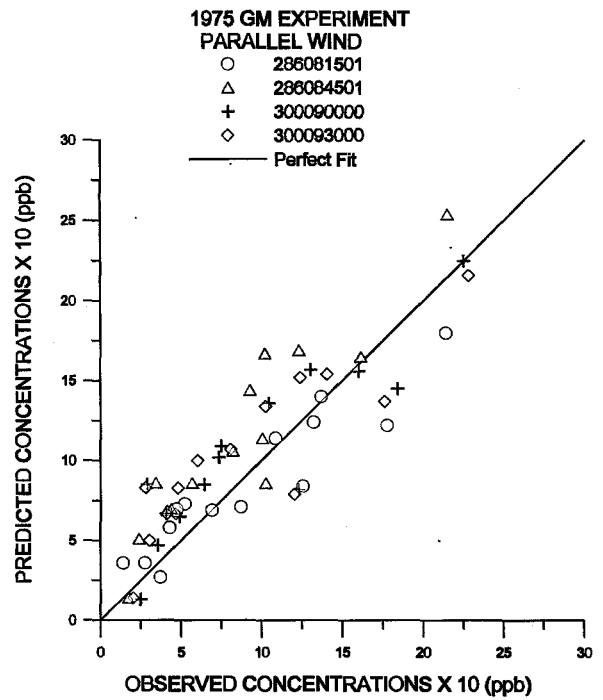


Figure 5.5 Comparison of predicted and observed concentrations for parallel winds.

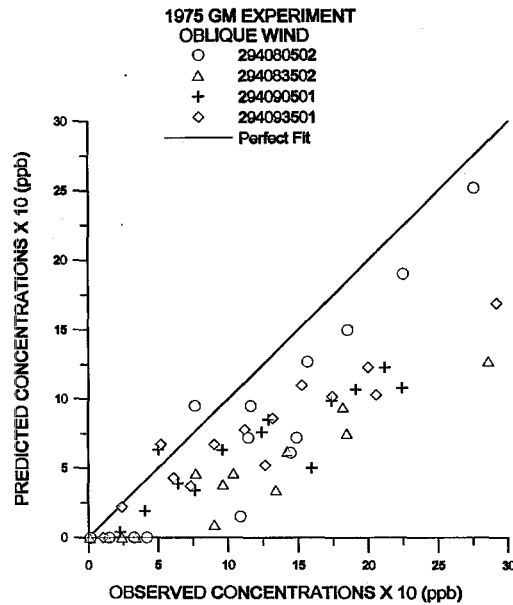


Figure 5.6 Comparison of predicted and observed concentrations for oblique winds.

Table 5.1 ROADWAY-2 Evaluation Statistics†

	Perpend. wind		Parallel wind		Oblique wind	
	Obs.	Pred.	Obs.	Pred.	Obs.	Pred.
Mean	7.96	7.13	8.99	10.18	12.01	6.84
SD	6.27	6.93	5.87	5.28	7.97	5.53
O_i range	0.01 – 27.7		1.39 – 22.8		0.09 – 32.7	
N_s	56		56		55	
R	0.81		0.88		0.88	
FB	0.11		-0.12		0.55	
$NMSE$	0.30		0.10		0.52	

†Concentration units for mean, SD, and O_i range are ppb x 10.
 N_s —sample size, SD—standard deviation, R —correlation coefficient,
 $FB = 2(\bar{O} - \bar{P})/(\bar{O} + \bar{P})$ is fractional bias, $NMSE = (\overline{P_i - O_i})^2 / (\bar{O} \bar{P})$
is normalized mean square error, where \bar{O} and \bar{P} are means of observed
and predicted concentrations over the sample size N_s .

The observed and predicted mean concentrations (ppb x 10) for the perpendicular wind case are 7.96 and 7.13, respectively. The fractional bias (FB) is 0.11 (slight underprediction), the normalized mean square error ($NMSE$) is 0.3, and the correlation coefficient (R) is 0.81. For good model performance, FB and $NMSE$ should be close to 0 and R should be close to 1. The values obtained for the perpendicular wind confirm the good performance of ROADWAY-2 for this case. The parallel wind case, which is generally considered to be more difficult to model, shows even better model performance with $FB = -0.12$ (slight overprediction) and $NMSE = 0.10$ (small scatter), and $R = 0.88$.

The oblique wind case is systematically underpredicted, with a mean observed concentration (\bar{O}) of 12.01 and a mean predicted concentration (\bar{P}) of 6.84; however, the R value is quite high (0.88). Further analysis showed that 84% of the mean squared error is systematic, suggesting that the model performance can be improved by modifying the model parameterizations for this case. This optimization was not attempted however, since all four oblique wind cases are sequential half-hour periods on the same day (Julian day 294) and had wind speeds in the range 1.1 to 1.6 m/s. Further testing of the model with additional data, preferably with higher wind speeds, is desirable before attempting to modify the model for the oblique wind case.

Figure 5.7 shows a comparison of observed and predicted concentrations for all wind cases. The corresponding statistics are shown in Table 5.2. The \bar{O} and \bar{P} are 9.64 and 8.06, respectively. The small values of FB (0.18) and $NMSE$ (0.29), and $R = 0.77$ indicate the good performance of

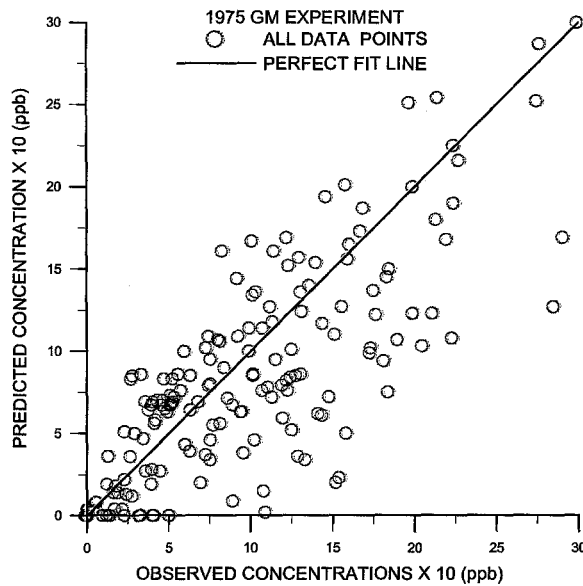


Figure 5.7 Comparison of predicted and observed concentrations for all wind directions.

Table 5.2 Model Performance Measures*.

	All wind directions	
	Obs.	Pred.
Mean	9.64	8.06
SD	6.93	6.11
O_i range	0.01 – 32.7	
N_s	167	
R	0.77	
FB	0.18	
$NMSE$	0.29	

*Units for mean, SD, and O_i range are ppb x 10.

ROADWAY-2 over all types of wind and stability conditions. A cumulative frequency distribution of $F = P/O$ (or $F = O/P$ such that $F > 1$), shown in Fig. 5.8, indicates that over 80% of the model predictions are within a factor of 2 of the corresponding observations, and 95% are within a factor of 5.

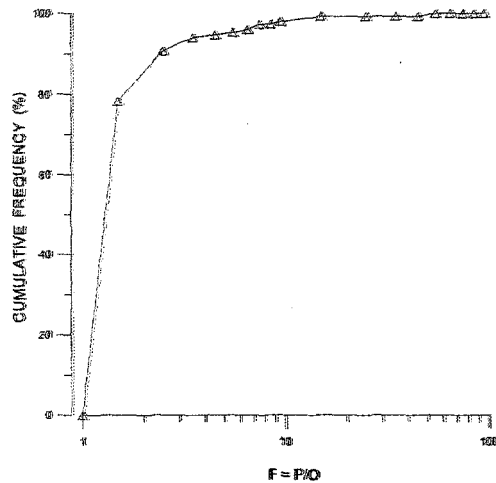


Figure 5.8 Cumulative frequency distribution of modeled and observed concentrations.

5.6 Conclusions and Recommendations

The preliminary evaluation results of ROADWAY-2 are considered quite satisfactory and promising. No direct comparison with EPA's ROADWAY model (Eskridge and Catalano, 1987) has been attempted, because of a coding error found in its WAKE subroutine which was determined to affect its predictions significantly. Further testing of ROADWAY-2 with additional GM data is recommended, especially for the oblique wind case, to check if the model parameterizations need adjustment. Suitable data from field or laboratory studies should be obtained to independently determine the constants C_u and C_e in the wake parameterizations. Direct measurements of mean profiles and turbulence parameters are preferred, whenever feasible, as inputs to the model; the latter can be easily modified to accommodate this.

6. SUMMARY, CONCLUSIONS, AND RECOMMENDATIONS

An important question for the Federal Highway Administration is how to make the best possible estimates of the impacts of motor vehicle emissions on urban air quality. The collaborative research reported here addressed significant components of that question.

6.1 Light Winds

Wind data for air quality modeling of individual sites are generally not available at the sites of interest, and so must be acquired from some (relatively) nearby monitoring location, often a local airport. This use of off-site data introduces two questions: how representative can those data be expected to be, and how well do they represent light wind conditions? The latter question is especially important because most dispersion models predict that the highest ground level concentrations can be expected during periods of light or calm winds, and/or in stable conditions, and because one generally expects to find lower wind speeds within a city than in its rural surroundings. An additional question might be whether the observations reported from a routine monitoring station could credibly be extrapolated to lower wind speeds, so as to extend modeling capability to wind speeds somewhat below the (often rather high) detection threshold of the wind instruments. A first task therefore was to determine how often calm winds might occur in various parts of the U.S., and to estimate how accurately the data from currently operational routine wind monitoring sites (such as the National Weather Service ASOS sites) could be extrapolated to the low wind speed case. To explore these questions, data from a number of research grade networks with lower-than-usual instrument thresholds were collected and analyzed. When selecting sites to study, it is important to realize that most landscapes fall into the category of complex terrain. Complex terrain includes more than just mountainous regions. Because of the availability of high quality data, this research focused mostly on mountainous terrain to illustrate the influence that various factors can have on wind in a particular locale. However, cities, buildings, lakes, forests, rivers, and coastlines can all influence local atmospheric conditions sufficiently that these areas must be considered to be complex terrain.

The research reported here centered on detailed analyses of wind roses, segregated by wind speed classes, for a variety of sites equipped with high quality meteorological networks. The data from these sites was available at wind speeds significantly lower than are usually routinely recorded. The wind roses were analyzed to see whether their shape persisted as the winds became progressively weaker, for changes in wind direction and speed with respect to winds aloft or at stations at higher altitude, for diurnal changes, and for other characteristics. The percentage of calm wind conditions was calculated for each site. Additionally, common factors across the sites were analyzed.

In terms of extrapolation of wind roses to progressively lighter wind speeds, the results were mixed. For higher elevation sites, including plateaus, this approach seemed plausible. The general pattern of the observed winds persisted from easily measurable speeds of about 2 m/s down to less

than 1 m/s for such sites. For a coastal site, the wind pattern persisted down to about 1 m/s. For valley floors, the wind roses began to change shape at wind speeds only slightly below 2 m/s, as local terrain influences began to dominate. To answer the question of whether one might apply measured wind roses to lower than measured wind speeds, thus extending modeling ability to sub-threshold wind speeds, appears not to be a credible technique, although it will work in some locations.

With respect to current air quality measurement techniques, the analysis showed that available meteorological data are often inadequate. Mountain and plateau locations showed the most promise with respect to the ability to correctly model local air flow; however, since most population and transportation centers tend to be located in lower terrain, such modeling capability may be of only limited utility. The higher terrain locations are important to modeling techniques in terms of establishing a general or regional flow of air or pollutants in and out of an area. Sub-regional or local effects are very important, especially for air quality impact assessments, and these are often poorly represented in the normally available data sets.

Air quality modeling based on wind data from current National Weather Service ASOS-type monitoring stations is apt to miss local scale effects, and, perhaps more importantly, currently available ASOS stations fail to measure the important low speed wind cases. For some of the sites examined, the winds were below the ASOS threshold of about 1.5 m/s more than 50% of the time, and so would be reported as "calm". It has been demonstrated clearly that these "missed" winds often behave differently than those observed during stronger measurable winds. The research also verified the well-known result that winds do vary spatially within complex terrain. Therefore, not only is it important for accurate air quality modeling to provide better measurements at current observation sites, it is also important to deal with the lack of representativeness of some reporting sites (such as airports) with respect to nearby areas.

Some recommendations for providing adequate data for light wind dispersion modeling can be given. First, it is important to improve the quality of measurements at existing meteorological sites that are used for air quality models. The existing instrumentation is generally not adequate for dispersion modeling needs, especially for light winds. Many existing systems cannot measure winds below about 1.5 m/s. It would be technically feasible to provide wind monitors at ASOS-type stations to measure winds as low as 0.3 to 0.5 m/s at relatively modest cost at each location, but it may not be permissible to do this. A separate independent monitoring station will be needed if light wind cases are to be handled properly. Second, the addition of multiple observing sites for use in model input should be considered. This is particularly true for areas of significantly complex terrain, where the wind patterns will vary significantly with location. Last, it is now technically feasible to equip new measurement locations with real-time communications capability to expedite the data reporting, data quality control, and modeling processes. The FHWA should consider making use of such supplementary meteorological stations in preparing its assessments, since meteorological systems of this sort can be constructed and installed at modest cost (far below the cost of ASOS-type systems).

6.2 Intra-Urban Wind Data

Successful modeling of pollution from vehicle emissions within urban areas requires information on the winds and turbulence. There are relatively few intra-urban meteorological observations available, and very few observations of turbulence within the urban area. Thus one of the objectives of this study was to evaluate the differences between urban and rural flow fields and turbulence. This was done for two “targets of opportunity”, the nearby cities of Knoxville and Nashville, Tennessee. These studies showed consistent and significant differences exist between rural and urban flow and turbulence fields. They also showed that the use of rural (i.e., “airport”) wind and turbulence measurements to model urban diffusion may lead to erroneous predictions.

For both of these cities, wind data from the city airports was inappropriate for application in the intra-urban region. In particular, for both Knoxville and Nashville, it was observed that the intra-urban mean wind speeds were significantly lower than those observed in nearby rural areas. However, the mean wind directions within the cities tended to track those observed in nearby rural areas if terrain influences were not strong (in practice, it was found that directions at the Nashville Airport were often different than those seen elsewhere around and within Nashville; it is believed that this is due to the influence of terrain features near the airport). The observed standard deviations of the wind direction, which are a measure of turbulence and can be useful in local plume or puff dispersion modeling, tended to be much larger within the city than outside. Also, measurements of turbulent kinetic energy (TKE) indicated that daytime TKE values tended to be higher within the city than in nearby rural areas. The additional turbulence within a city is generated by the wind passing amongst the buildings, and also by the changes in local energy budget and the presence of local zones of solar heating and shading. None of these results are surprising. They do emphasize the fact that it may be quite inappropriate to use data from an airport – typically located in open rural surroundings – to model atmospheric pollutant transport and dispersion within a city.

Additional intra-urban data are needed. However, wind data within the urban canopy are very difficult to obtain, especially above ground level. In a separate study not related to this project, NOAA/ATDD staff recently performed intra-urban wind and turbulence measurements from a 3-D sonic anemometry system on an adjustable mast mounted in the bed of a pickup truck. This system could be driven to a location of interest (e.g., the median strip of an urban arterial) and used to take measurements for several hours or even days. A system such as this would make urban wind and turbulence exploratory measurements possible. Similarly portable tower systems or mounting locations on buildings or other structures are needed to measure vertical profiles of winds and turbulence (see Rotach, 1995, for example). Remote sensing techniques (e.g., sodars or laser Doppler velocimeters) may also be able to provide mean wind data above the ground (e.g., Cionco et al., 1998). Vertical variations remain one of the least known features of wind behavior in a city, despite their importance to local air quality issues.

6.3 Vehicle Wakes

During calm or very light wind conditions, the initial dispersion of motor vehicle effluents will be dominated by the vehicle wake. At later times, the wake region represents a source configuration for urban scale dispersion models. Thus it is essential to be able to model not only the mean structure of the wake, but also the turbulence or mixing in the wake. Relatively few observations of the turbulence within vehicle wakes have been made, and these all seem to have been done in wind tunnels. These facts led to a unique research program in which the turbulence and its spatial evolution in the near wake of a real moving vehicle were directly measured. Six fast-response sonic anemometers were mounted on a moveable array on an open frame trailer to measure the u , v , and w components of the 3-D flow field in the wake of a vehicle. The trailer was towed by a vehicle on an isolated airport runway to eliminate the effect of buildings or other road traffic on the results. Light wind conditions were chosen, minimizing ambient effects on the wake. Three anemometers were located above the roof of the tow vehicle, and three were mounted well within the highly turbulent wake zone immediately behind the vehicle.

TKE was calculated for each run and anemometer configuration. Under some conditions it could be seen that TKE spectra from the top tier of anemometers saw an energy dropoff with frequency typical of the inertial subrange, while the bottom tier sometimes approached the inertial subrange slope. TKE calculated for times when the vehicle was not moving was useful for determining ambient conditions for comparison with the different configurations for both the top and bottom tier of sonics while the vehicle was moving. The upper tier of sonics generally compared favorably in energy levels and spectral slope with the ambient readings, which suggests that the top tier of sonics were generally out of the wake turbulence. The bottom tier of sonics generally recorded increased energy and it was clear that they were sampling the wake turbulence of the vehicle. There was some indication that the ambient winds shifted the wake during periods when the direction of travel was crosswind, as would be expected, and it was also seen that when the vehicle was heading into the wind, the energy levels increased, indicating increased wake turbulence. The size or the dissipation rate of the wake eddies could not be determined from the TKE spectra here. An initial finding of this study is that an inertial subrange of turbulence is generally not present in the near wake region. This is significant because almost all dispersion theories and models assume the existence of an inertial subrange. However, the sampling frequency of the sonics was not sufficient to determine the full turbulence spectrum, and further studies using sonics with higher sampling rates are needed to substantiate this finding. Examination of the 3-D flow vectors observed within the wake indicated a strong downflow along the wake centerline that decreased sharply with lateral distance from the centerline, and also diminished with increasing distance from the rear of the tow vehicle. These observations are consistent with the notion of a pair of trailing vortices originating near the upper rear corners of the vehicle roof, circulating air from above down into the wake cavity zone behind the vehicle.

In addition to examining the turbulence behind moving vehicles, the effects of moving vehicles on the turbulence near a roadway were briefly examined. This experiment showed that the passing vehicles could be detected not only by enhanced horizontal momentum flux, but also by their

signatures of water vapor and carbon dioxide. However, it appears that the vehicle-produced turbulence had only little effect on the ambient turbulence, because we observed an inertial subrange not only in the ambient turbulence spectra, but also in the CO₂ spectrum.

6.4 ROADWAY-2 Dispersion Model

Atmospheric dispersion models are often needed to estimate the impacts of pollutants near existing or proposed roads. In this research, the U.S. EPA's ROADWAY model (Eskridge and Catalano, 1987) was used as the basic framework for a revised model called ROADWAY-2. The new model uses a turbulent kinetic energy closure formulation for the time-varying atmospheric boundary layer, to derive the mean wind and temperature and turbulence vertical profiles from input meteorological data. This approach avoids the questionable assumption that equilibrium surface layer relations are valid near busy highways. It also avoids the questionable linear superposition of eddy diffusivities that was used in the ROADWAY model. And the model allows the direct use of on-site turbulence data, which is potentially of significant operational utility, given the availability of a new generation of (relatively) inexpensive turbulence instrumentation. The parameterization of vehicle wake effects in ROADWAY-2 is also a new approach, derived from canopy flow theory and wind tunnel measurements. The atmospheric wind and turbulence fields are adjusted to account for velocity-deficit and turbulence production due to vehicle wakes.

ROADWAY-2 has been compared to concentration data from the famous GM experiment (Cadle et al., 1976), and it appears to predict the observed concentrations quite well. A number of statistical values (predicted vs. observed mean values, fractional bias, normalized mean square error, correlation coefficient) were calculated. Both the cross-wind and along-wind cases were handled well; the oblique wind case was systematically underpredicted, but with a high correlation. It is believed that improvements in the model parameterizations could improve the performance for this case. A cumulative frequency distribution plot showed that more than 80% of the model predictions were within a factor of two, and 95% were within a factor of five.

6.5 Suggestions for Future Research

Dispersion modeling needs site-specific data. The analysis of light wind observations from a wide variety of locations indicated considerable site-specific effects. Use of off-site data will lead to significant modeling errors, especially in complex terrain. Methods are needed to inexpensively acquire mean and turbulence data at key locations near highways, especially in urban areas, to assure credible dispersion modeling. Current developments in measurement and communications technologies make this goal feasible.

Additional wind and turbulence measurements are needed within urban areas. The latest generation of relatively low cost sonic anemometers overcomes most of the problems previously associated with such measurements. Instruments such as these could be deployed for long periods

of time on new or existing street lamp poles or other targets of opportunity, and could use radio frequency modems or other telemetry to transfer the data to a nearby host computer without the need for data cables (which can be a major nuisance in an urban environment). Mobile systems can now be developed easily and deployed on pickup trucks or on vans equipped with telescoping towers, to provide short term data at key locations, or to determine reasonable wind sampling locations. Mini-sodars, laser Doppler velocimeters, and other remote sensing techniques can be used for additional data up to and above roof height in urban areas.

Additional wake data behind real vehicles are needed to characterize wake turbulence for modeling. The trailer-based apparatus described worked well after some initial problems. It could be used to study the wakes behind a wide variety of vehicle types, since the trailer is relatively light. One useful improvement would be to use a single laptop computer fitted with multiple serial (or perhaps USB) ports, to communicate with the anemometers, rather than using multiple computers. The necessary computer hardware is now available. The vertical and lateral extent of the anemometer support array could easily be increased, and this should be done. No measurements were made close to the ground, in the lower portion of the vehicle wake. Such measurements are needed to better understand the wake of a vehicle moving over a roadway, and could be performed with minimal risk to the instruments, given the smooth runway surface. Additional instruments are needed for continuous measurements of ambient winds and turbulence, and perhaps of the CO₂ and water vapor signatures of the passing vehicle since this can be done at relatively little additional cost. The real-vehicle wake measurements should be supplemented with simple smoke releases using standard low-cost, low-hazard smoke candles; the smoke candles should be mounted close to the sonic anemometer positions, to help visualize exactly what the anemometers were recording. A video camera with electronic image stabilization could be used to capture the visualizations for replay and study. To support and supplement this field study, wind tunnel measurements behind a scale model of each tow vehicle should be performed to provide additional detail and to extend the measurements into the far wake zone. This work must be performed over a moving beltway to properly simulate the flow under the vehicle.

Some improvements to the new ROADWAY-2 model will be needed to better handle the oblique wind case. Additional highway tracer data would be useful, to further test and improve the model.

7. ACKNOWLEDGMENTS

Messrs. J. Duncan, M. Hall, C. Harness, M. Ludwig, and R. Mayhew assisted in the setup and operation of the measurement systems. Ms. K. Hill assisted with graphics. The authors appreciate the interest, support, and patience of Dr. H. Jongedyk of the U.S. Federal Highway Administration. This work was performed under a collaborative agreement between the FHWA and the National Oceanic and Atmospheric Administration.

8. REFERENCES

- Albrecht, F., 1933: Untersuchungen der vertikalen Luftzirkulation in der Grossstadt. *Meteorol. Z.* **50**, 93-98.
- Baik, J-J. and J-J. Kim, 1999: A numerical study of flow and pollutant dispersion characteristics in urban street canyons. *J. Appl. Meteorol.* **38** (11) 1576-1589.
- Baldocchi, D. D. and T. P. Meyers, 1988: A spectral and lag-correlation analysis of turbulence in a deciduous forest canopy. *Bound.-Layer Meteorol.* **45**, 31-58.
- Baldocchi, D. D., B. B. Hicks, and T. P. Meyers, 1988: Measuring biosphere-atmosphere exchanges of biologically related gases with micrometeorological methods. *Ecology* **69**, 1331-1340.
- Benoit, R., 1977: On the integral of the surface layer profile-gradient functions. *J. Appl. Meteor.* **16**, 859-860.
- Benson, P. E., 1992: A review of the development and application of the CALINE3 and 4 models. *Atmos. Environ.* **26B**, 379-390.
- Birdwell, K. R., 1996: A Climatology of Winds Over a Ridge and Valley Terrain within the Great Valley of Eastern Tennessee. Master's Thesis, Murray State University.
- Book, D. L., J. P. Boris, and K. Hain, 1975: Flux-corrected transport II: generalizations of the method. *J. Computational Phys.* **18**, 248-283.
- Brown, M. J., R. E. Lawson, Jr., D. S. DeCroix, and R. L. Lee, 2000: Mean flow and turbulence measurements around a 2-D array of buildings in a wind tunnel. Presented at 11th Joint AMS/AWMA Conference on Applications of Air Pollution Meteorology, Long Beach, CA, Jan. 9-14, 2000.
- Businger, J. A., 1986: Evaluation of the accuracy with which dry deposition can be measured with current micrometeorological techniques. *J. Clim. Appl. Meteorol.* **25**, 1100-1124.
- Cadle, S. H., D. P. Chock, J. M. Heuss, and P. R. Monson, 1976: Results of General Motors sulfate dispersion experiments. GMR-2107, General Motors Research Labs., Warren, MI, 179 pp.
- Cadle, S. H., D. P. Chock, P. R. Monson, and J. M. Heuss, 1977: General Motors sulfate dispersion experiment: experimental procedures and results. *J. Air Poll. Control Assoc.* **27**, 33ff.
- Chock, D. P., 1978: A simple line-source model for dispersion near roadways. *Atmos. Environ.* **12**, 823-829.

- Cionco, R., 1972: A wind-profile index for canopy flow. *Bound.-Layer Meteorol.* **3** (2), 255-263.
- Cionco, R. M., G. Steele, and G. Moran, 1998: Remote sensing of wind profiles within and above an urban domain. Presented at and in Preprints of the Second Urban Environment Symposium, Albuquerque, NM, Nov. 2-6 (Amer. Meteorol. Soc., Boston, MA), 125-128.
- Dabberdt, W. F., and W. G. Hoydysh, 1991: Street canyon dispersion: sensitivity to block shape and entrainment. *Atmos. Environ.* **25A**, 1143-1153.
- DePaul, F. T., and C. M. Sheih, 1984: A Study of Pollutant Dispersion in an Urban Street Canyon. Argonne Nat. Lab. report ANL/ER-84-1. Avail. ANL, Argonne, IL, 84 pp.
- Doran, J. C., and C. D. Whiteman, 1992: The Coupling of Synoptic and Valley Winds in the Tennessee Valley. Pacific Northwest Laboratory, Dept. of Energy.
- Dubov, A. S., and L. P. Bykova, 1974: Turbulence in forest canopies. *Izv. Atmos. Ocean Phys.* **10**, 650-652.
- Eckman, R. M., R. J. Dobosy, and W. R. Pendergrass, 1992: Preliminary Analysis of Wind Data from the Oak Ridge Site Survey. NOAA Technical Memorandum ERL ARL-193.
- Eckman, R. M., 1996: Observations and Numerical Simulations of Winds within a Broad Forested Valley. *J. Appl. Meteor.* **37**, 206-219.
- Eskridge, R. E., and J. A. Catalano, 1987: ROADWAY - A numerical model for predicting air pollutants near highways. User's Guide. EPA/600/S8-87/010, U.S. EPA, Research Triangle Park, NC. Available as *PB 87-171 906*, NTIS, Springfield, VA, 134 pp.
- Eskridge, R. E., and J. C. R. Hunt, 1979: Highway modeling. Part I: prediction of velocity and turbulence fields in the wake of vehicles. *J. Appl. Meteorol.* **18** (4), 387-400.
- Eskridge, R. E., and S. T. Rao, 1986: Turbulent diffusion behind vehicles: experimentally determined turbulence mixing parameters. *Atmos. Environ.* **20** (5), 851-860.
- Eskridge, R. E., and R. S. Thompson, 1982: Experimental and theoretical study of the wake of a block-shaped vehicle in a shear-free boundary layer. *Atmos. Environ.* **16** (12), 2821-2836.
- Georgii, H. W., E. Busch, and E. Weber, 1967: Untersuchung Uber die Zietliche und Raumliche Verteilung der Imissions-Konzentration des Kohlenmonoxid in Frankfurt am Main. Berichte des Institutes fur Meteorol. und Geophys. der Universitat Frankfurt/Main #11, 60 pp. Avail. as NAPCA translation 0477.

- Grelle, A. and A. Lindroth, 1994: Flow distortion by a Solent sonic anemometer: wind tunnel calibration and its assessment for flux measurements over forest and field. *J. Atmos. Oceanic Tech.* **11**, 1529-1542.
- Grimmond, C. S. B., and T. R. Oke, 1999: Aerodynamic properties of urban areas derived from analysis of surface form. *J. Appl. Meteorol.* **38** (9), 1262-1292.
- Hanna, S. R., and R. E. Britter, 2000: The Effect of Roughness Obstacles on Flow and Dispersion at Industrial Facilities. AICHE/CCPS, Vapor Cloud Subcommittee. In press.
- Högström, U. 1996: Review of some basic characteristics of the atmospheric surface layer. *Bound.-Layer Meteor.* **78**, 215-246.
- Hosker, R. P., Jr., 1984: Flow and Dispersion Near Obstacles. Chapter 7 in Atmospheric Science and Power Production (D. Randerson, ed.), U.S. Dept. of Energy Technical Information Center DOE/TIC-27601, DE84005177, pp. 241-326. Avail. NTIS, Springfield, VA.
- Hosker, R. P., Jr., 1985: Flow around isolated structures and building clusters: a review. *ASHRAE Trans.* **1985**, **91**, part 2B (Feb. 1986).
- Hotchkiss, R. S., and F. H. Harlow, 1973: Air Pollution Transport in Street Canyons. US EPA report EPA-R4-73-029.
- Hoydysh, W. G., Y. Ogawa, and R. A. Griffiths, 1974: A scale model study of dispersion of pollutants in street canyons. APCA paper # 74-157, presented at 67th Annual Meeting of Air Poll. Control Assoc., Denver, CO, June 9-13.
- Hoydysh, W. G., and W. F. Dabberdt, 1988: Kinematics and dispersion characteristics of flows in asymmetric street canyons. *Atmos. Environ.* **22**, 2677-2689.
- Hoydysh, W. G., and W. F. Dabberdt, 1994: Concentration fields at urban intersections: fluid modeling studies. *Atmos. Environ.* **28**, 1849-1860.
- Hunter, L. J., G. T. Johnson, and I. D. Watson, 1992: An investigation of three-dimensional characteristics of flow regimes within the urban canyon. *Atmos. Environ.* **26B**, 425-432.
- Hussain, M. and B. E. Lee, 1980: An Investigation of Wind Forces on Three-Dimensional Roughness Elements in a Simulated Atmospheric Boundary Layer Flow. Part II: Flow Over Large Arrays of Identical Roughness Elements and the Effect of Frontal and Side Aspect Ratio Variations. Univ. of Sheffield report BS-56. Avail. Univ. of Sheffield, Dept. of Building Science, Faculty of Architect. Studies, Sheffield, UK, 81 pp.

- Hyson, P., J. R. Garratt, and R. J. Francey, 1977: Algebraic and electronic corrections of measured uw covariance in the lower atmosphere. *J. Appl. Meteorol.* **16**, 43-47.
- Johnson, W. B., F. L. Ludwig, W. F. Dabberdt, and R. J. Allen, 1971: Field Study for Initial Evaluation of an Urban Diffusion Model for Carbon Monoxide. Stanford Research Institute report, project 8563, 144 pp. + Appendices A - R.
- Johnson, W. B., F. L. Ludwig, W. F. Dabberdt, and R. J. Allen, 1973: An urban diffusion simulation model for carbon monoxide. *J. Air Poll. Control Assoc.* **22** (6), 490-498.
- Johnson, G. T., H. A. Cleugh, L. J. Hunter, and J. R. Barnett, 1996: Field evaluation of an urban canyon airflow and scalar dispersion model. *Clean Air* **30**, 31-37.
- Kaimal, J. C., and D. A. Haugen, 1969: Some errors in the measurement of Reynold's stress. *J. Appl. Meteorol.* **8**, 460-462.
- Kaimal, J. C., and J. J. Finnigan, 1994: Atmospheric boundary layer flows. Oxford Univ. Press, New York, 289 pp.
- Karim, M. M., and H. Matsui, 1998: A mathematical model of wind flow, vehicle wake, and pollutant concentration in urban road microenvironments. Part I: model description. *Transportation Research Part D* **3** (2), 81-92.
- Kastner-Klein, P., and E. J. Plate, 1999: Wind-tunnel study of concentration fields in street canyons. *Atmos. Environ.* **33**, 3973-3979.
- Lawson, R. E., Jr., M. J. Brown, D. S. DeCroix, and R. L. Lee, 2000: Mean flow and turbulence measurements around a 3-D array of buildings in a wind tunnel. To be presented at American Meteorological Society's Third Symposium on the Urban Environment, Davis, CA, August 14-18, 2000.
- Lee, X., 1998: On micrometeorological observations of surface-air exchange over tall vegetation. Accepted for *Agric. Forest Meteorol.* (in press).
- Martinez, J. R., H. S. Javitz, R. E. Ruff, A. Valdes, K. C. Nitz, and W. F. Dabberdt, 1981: Methodology for evaluating highway air pollution dispersion models. NCHRP report 245, Transportation Research Board, National Research Council, Washington, DC, 85 pp.
- McMillen, R. T., 1986: A BASIC Program for Eddy Correlation in Non-Simple Terrain. NOAA Technical Memorandum ERL ARL-147 (June, 1986), available NTIS, Springfield, VA.
- Meroney, R. N., 1982: Turbulent Diffusion Near Buildings. Chapter 11 in *Engineering Meteorology* (E. J. Plate, ed.), Elsevier Scientific Publishing Co., Amsterdam, pp. 481-525.

- Nakamura, Y., and T. R. Oke, 1988: Wind, temperature and stability conditions in an east-west oriented urban canyon. *Atmos. Environ.* **22**, 2691-2700.
- Nicholson, S. E., 1975: A pollution model for street-level air. *Atmos. Environ.* **9** (1), 19-31.
- Nickerson, E. C., and V. E. Smiley, 1975: Surface layer and energy budget parameterization for mesoscale models. *J. Appl. Meteor.* **14**, 297-300.
- Oke, T. R., 1988: Street design and urban canopy layer climate. *Energy Bldg.* **11**, 103-113.
- Rao, K. S., and H. F. Snodgrass, 1981: A nonstationary nocturnal drainage flow model. *Bound.-Layer Meteor.* **20**, 309-320.
- Rao, S. T., L. Sedafian, and U. H. Czapski, 1979: Characteristics of turbulence and dispersion of pollutants near major highways. *J. Appl. Meteor.* **18**, 283-293.
- Rao, S. T., G. Sistla, M. T. Keenan, and J. S. Wilson, 1980: An evaluation of some commonly used highway dispersion models. *J. Air Poll. Control Assoc.* **30**, 239-246.
- Robins, A., D. J. Carruthers, and C. A. McHugh, 1997: The ADMS building effects module. *Int. J. Environ. And Poll.* **8**, 708-717.
- Rotach, M. W., 1993: Turbulence close to a rough urban surface. Part I: Reynolds stress. *Bound.-Layer Meteorol.* **65**, 1-28.
- Rotach, M. W., 1995: Profiles of turbulence statistics in and above an urban street canyon. *Atmos. Environ.* **29**, 1473-1486.
- Sharan, M., A. K. Yadav, and M. P. Singh, 1995: A comparison of various sigma schemes for estimating dispersion of air pollutants in low winds. *Atmos. Environ.*
- Shaw, R. H., and I. Seginer, 1985: The dissipation of turbulence in plant canopies. *Seventh Symp. on Turb. and Diff., Boulder, CO, Preprints.* Amer. Meteor. Soc., Boston, MA, 200-203.
- Sini, J.-F., S. Anquetin, and P. G. Mestayer, 1996: Pollutant dispersion and thermal effects in urban street canyons. *Atmos. Environ.* **30**, 2659-2677.
- Stull, R. B., 1988: *An Introduction to Boundary Layer Meteorology.* Kluwer Academic Publishers, Dordrecht, The Netherlands, 666 pp.
- Tangirala, R. S., K. S. Rao, and R. P. Hosker, 1992: A puff model simulation of tracer concentrations in the nocturnal drainage flow in a deep valley. *Atmos. Environ.* **26A**, 299-309.

- Thompson, R. S., and R. E. Eskridge, 1987: Turbulent diffusion behind vehicles: experimentally determined influence of vortex pair in vehicle wake. *Atmos. Environ.* **21** (10), 2091-2097.
- Touma, J. S., J. S. Irwin, J. A. Tikvart, and C. T. Coulter, 1995: A review of procedures for updating air quality modeling techniques for regulatory reforms. *J. Appl. Meteorol.* **34**, 731-737.
- Wedding, J. B., D. J. Lombardi, and J. E. Cermak, 1977: A wind tunnel study of gaseous pollutants in city street canyons. *J. Air Poll. Control Assoc.* **27**, 557-566.
- Wesely, M. L., 1970: Eddy Correlation Measurements in the Atmospheric Surface Layer over Agricultural Crops. Ph.D. dissertation, University of Wisconsin, Madison, WI.
- Whiteman, C. D., and J. C. Doran, 1993: The relationship between overlying synoptic-scale flows and winds within a valley. *J. Applied Meteorol.* **32**: 1669-1682.
- Wilson, J. D., 1988: A second-order closure model for flow through vegetation. *Bound.-Layer Meteor.* **42**, 371-392.
- Yamartino, R. J., and G. Weigand, 1986: Development and evaluation of simple models for the flow, turbulence and pollutant concentration fields within an urban street canyon. *Atmos. Environ.* **20** (11), 2137-2156.
- Yamartino, R. J., D. G. Strimaitis, and T. A. Messier, 1989: Modification of highway air pollution models for complex site geometries. Vol. 1, U.S. Federal Highway Admin report FHWA-RD-89-112, 233 pp.
- Yellard, M. J., P. K. Taylor, I. E. Consterdine, and M. H. Smith, 1994: The use of the inertial dissipation technique for shipboard wind stress determination, *J. Atmos. Oceanic Tech.* **11**, 1093-1108.
- Zalesak, S. T., 1979: Fully multidimensional flux-corrected transport algorithm for fluids. *J. Computational Phys.* **31**, 335-362.

Appendix A

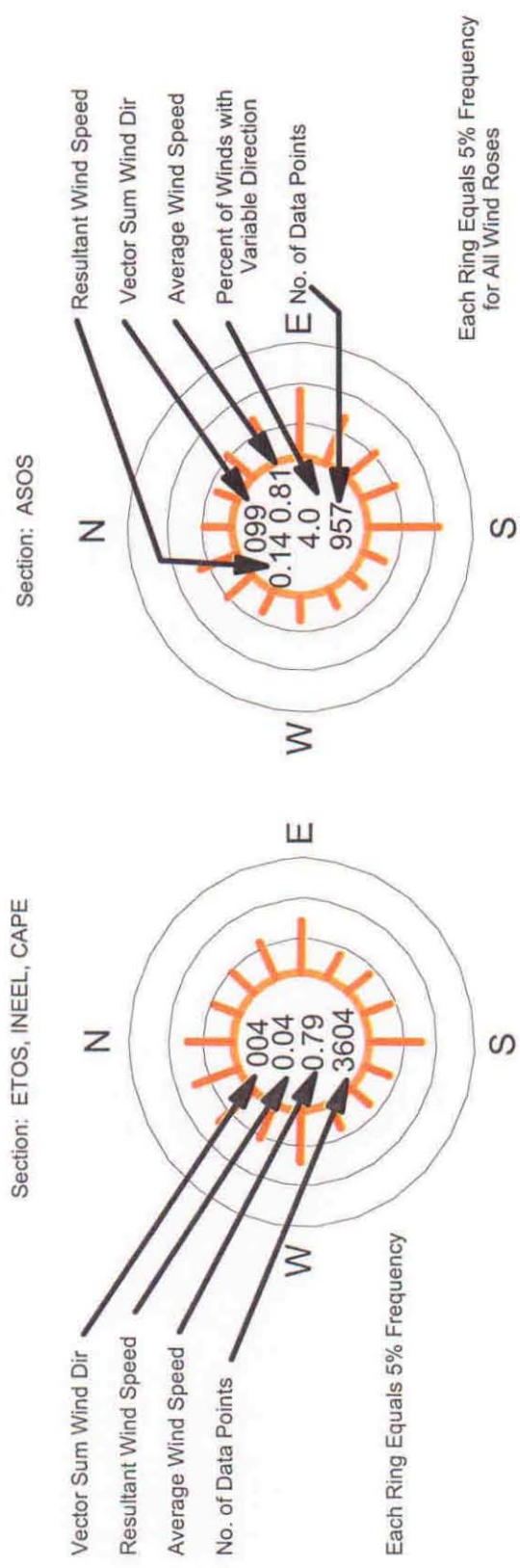
Wind Rose Analysis With Respect to Low Wind Speeds

Part 1: Analysis of Wind Rose Changes with Respect to Low Wind Speeds Plots



Part 1: Analysis of Wind Rose Change with Respect to Low Wind Speeds

KEY TO WIND ROSE INTERPRETATION



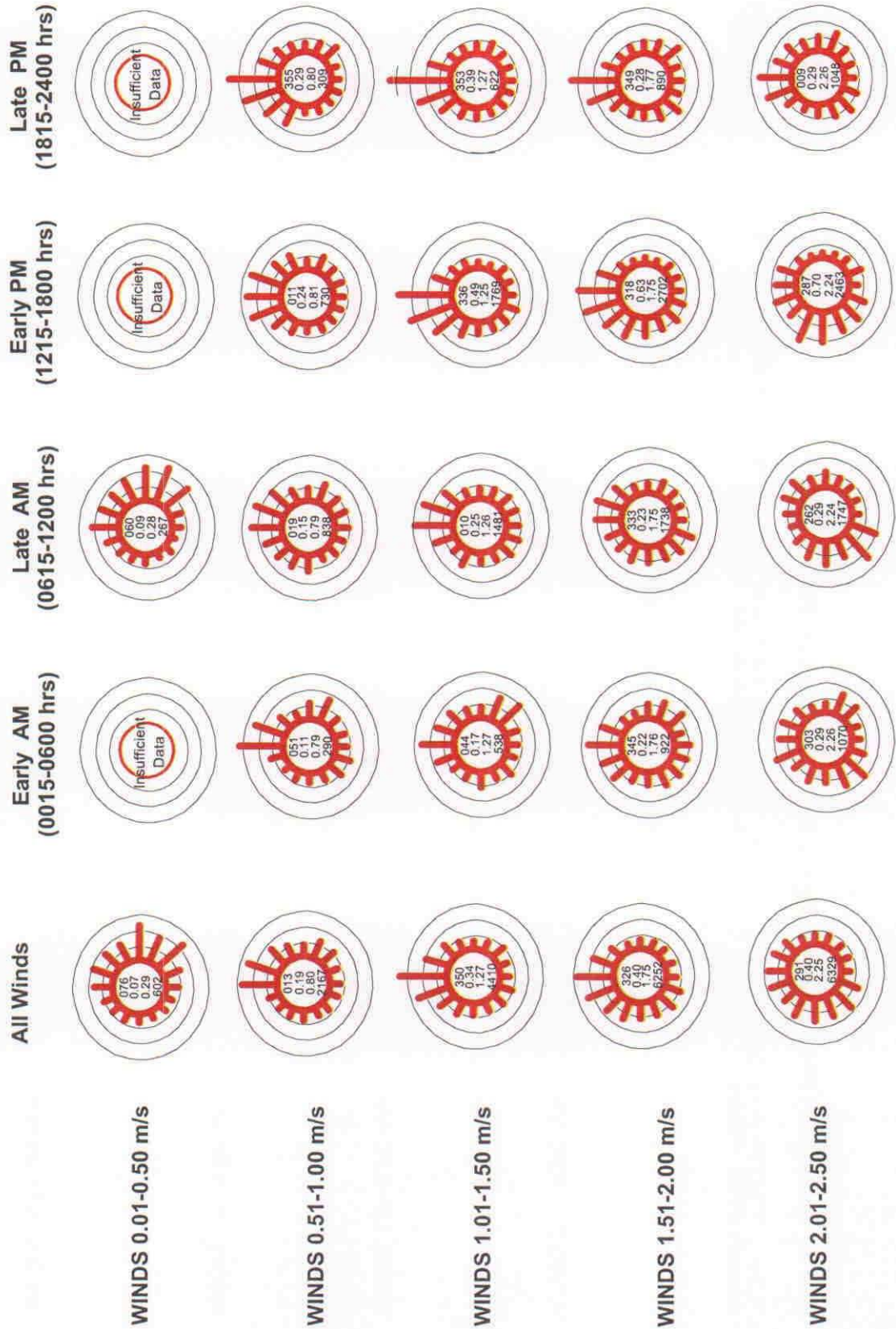
All Wind Direction measurements are given in degrees (0 to 360)

All Wind Speed measurements are given in meters per second (m/s)

Part 1: Analysis of Wind Rose Change with Respect to Low Wind Speeds



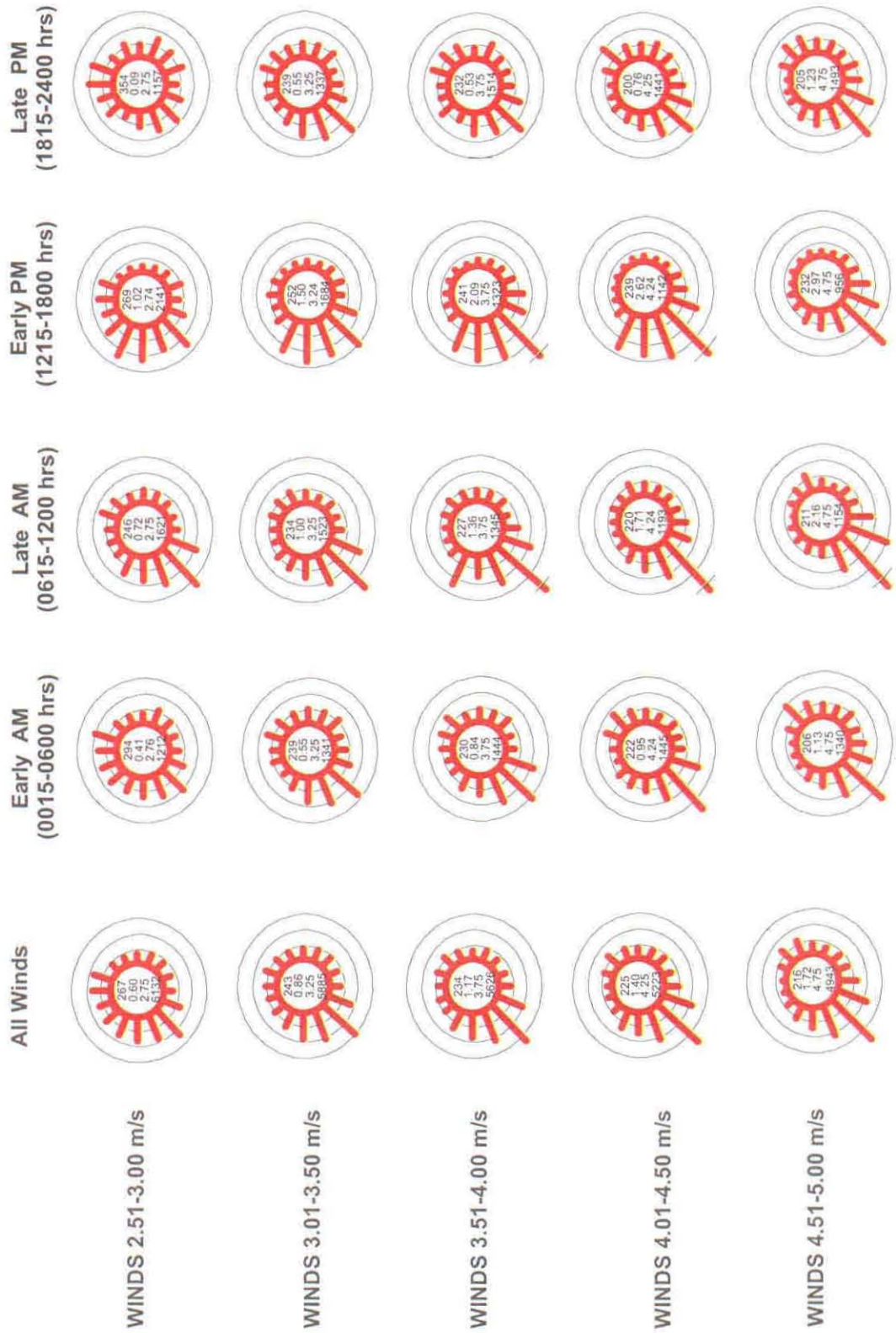
Section: ETOS (Southern Appalachians)
 Topographic Zone: Mountain
 Site: T223, Cove Min, Lat 35 42 N, Long 83 37 W, Altitude 1243 m, Tower Ht 24
 Period of Record: October 1994 - April 1997



Part 1: Analysis of Wind Rose Change with Respect to Low Wind Speeds



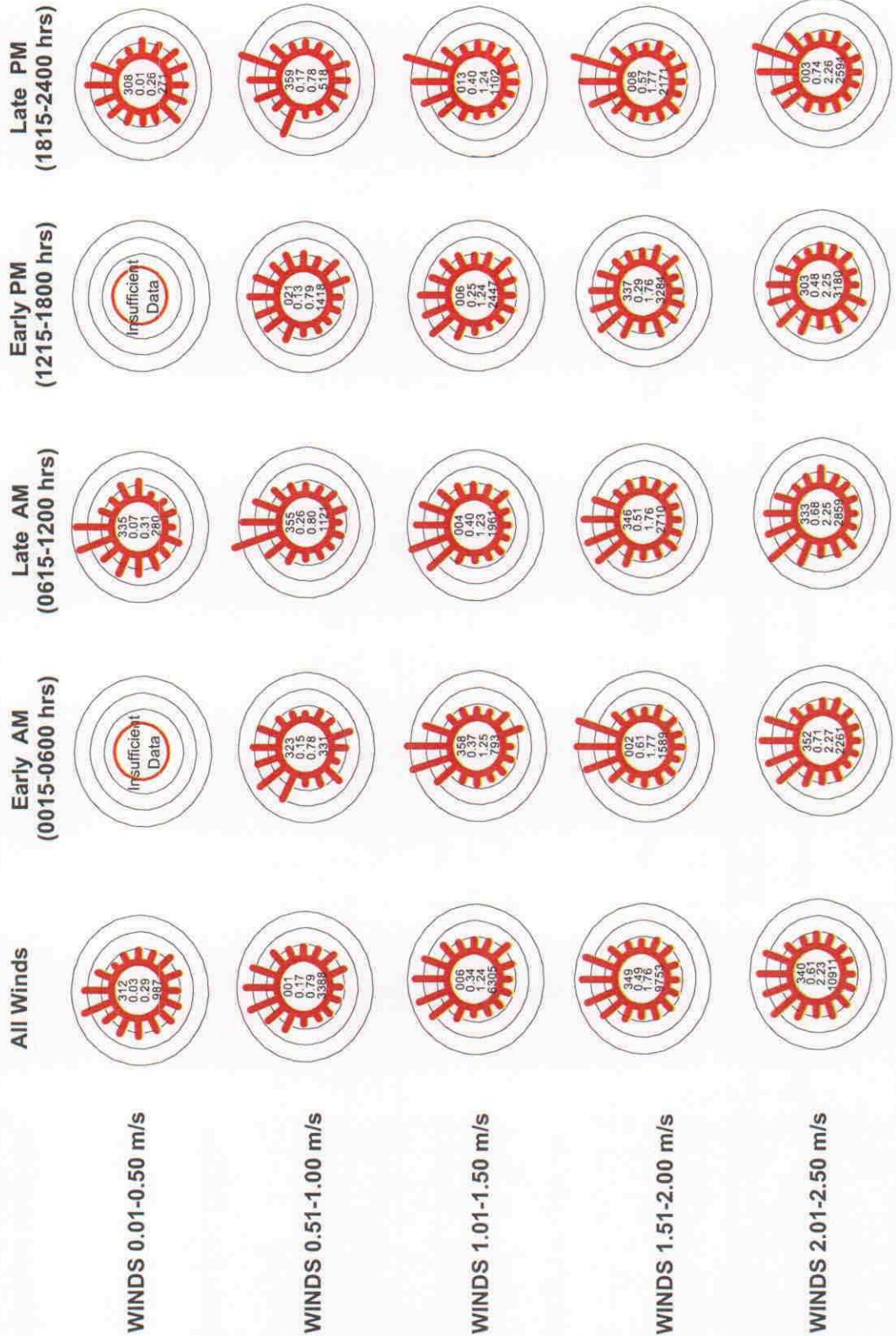
Section: ETOS (Southern Appalachians)
 Topographic Zone: Mountain
 Site: T223, Cove Mtn, Lat 35 42 N, Long 83 37 W, Altitude 1243 m, Tower Ht 24
 Period of Record: October 1994 - April 1997



Part 1: Analysis of Wind Rose Change with Respect to Low Wind Speeds



Section: ETOS (Southern Appalachians)
 Topographic Zone: Mountain
 Site: T224, Buffalo Mtn., Lat 36 08 N, Long 84 20 W, Altitude 1031 m, Tower Ht 10 m
 Period of Record: February 1994 - March 1997

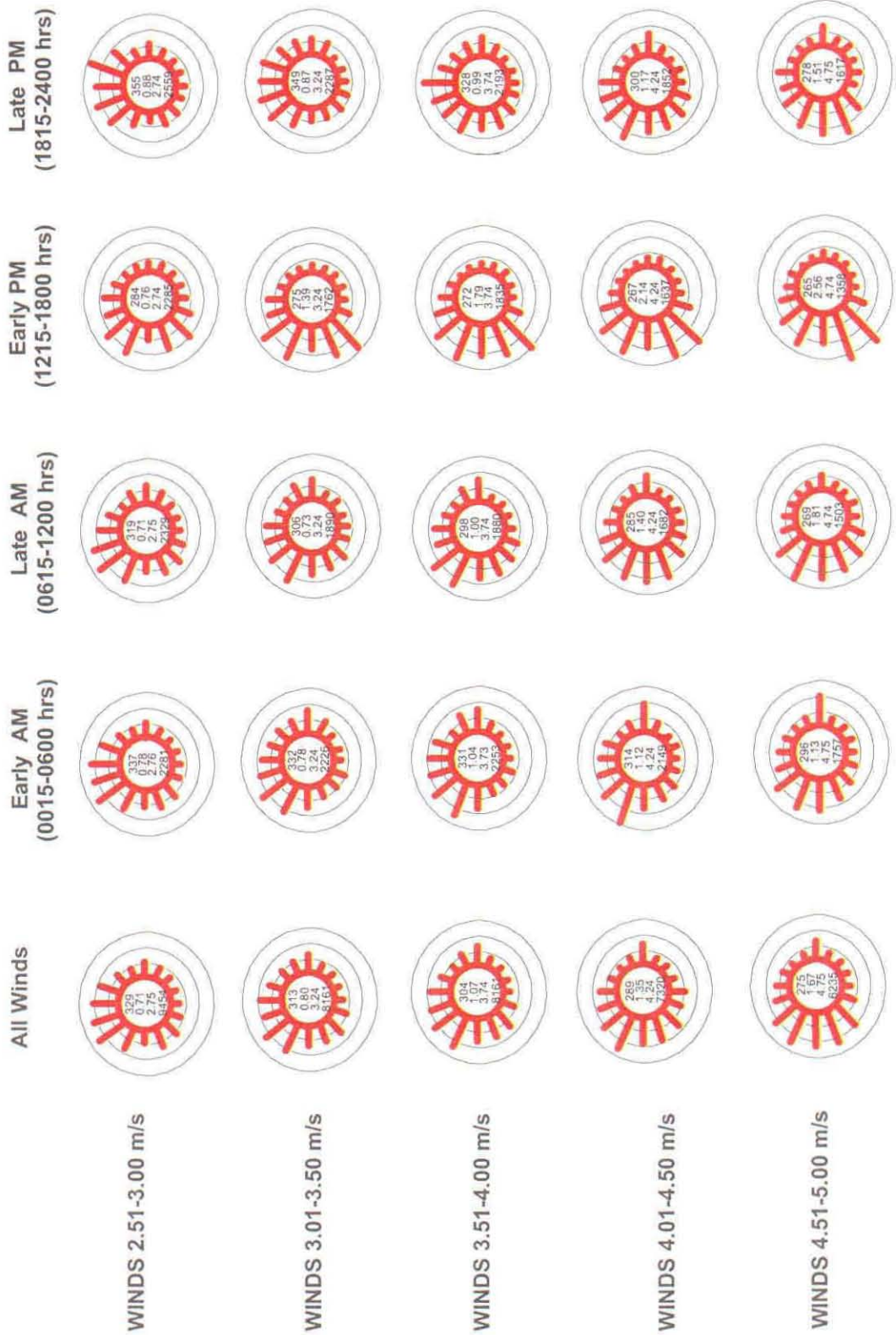


Part 1: Analysis of Wind Rose Change with Respect to Low Wind Speeds



Section: ETOS (Southern Appalachians)
 Topographic Zone: Mountain

Site: T224, Buffalo Mtn., Lat 36 08 N, Long 84 20 W, Altitude 1031 m, Tower Ht-10 m
 Period of Record: February 1994 - March 1997

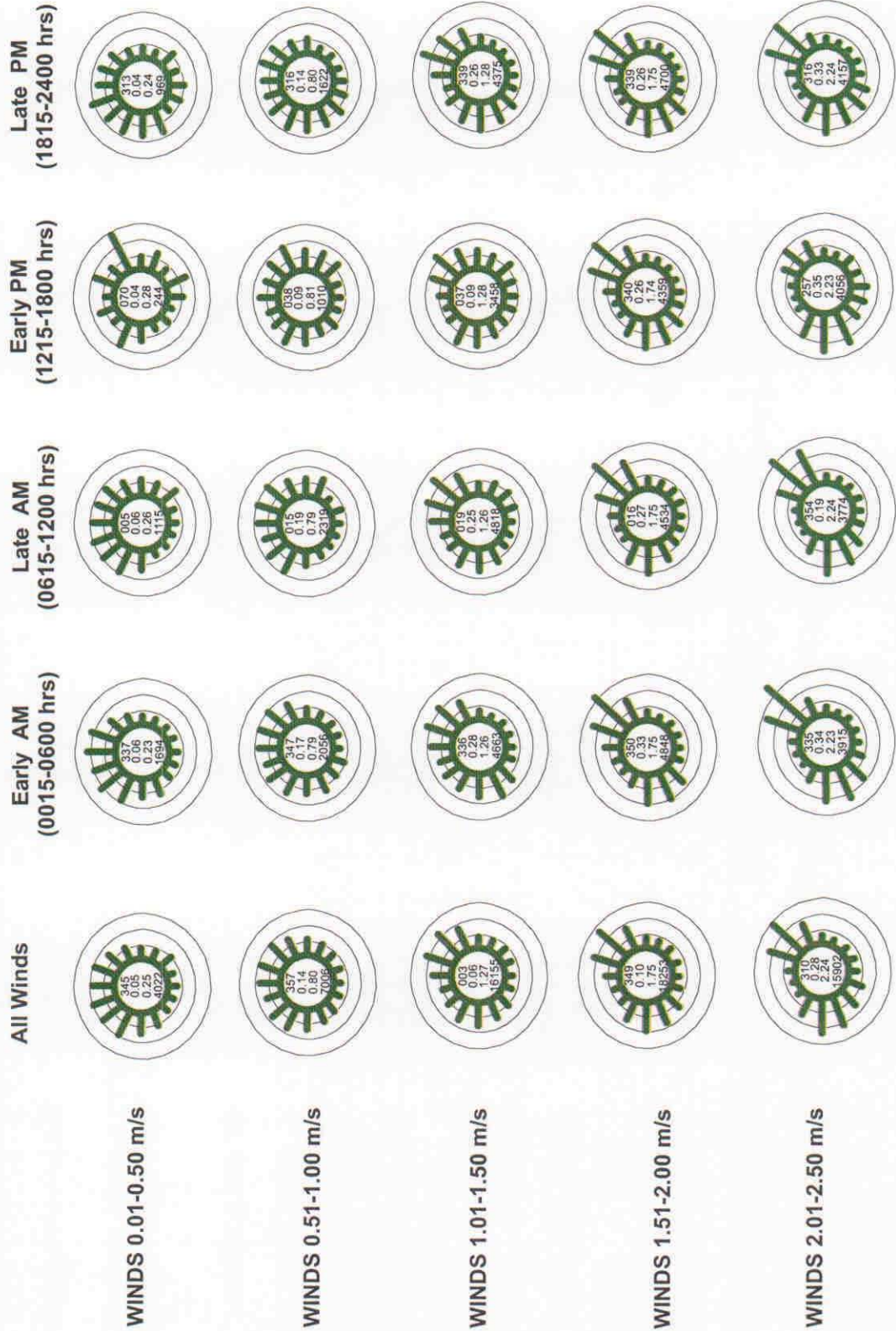


Part 1: Analysis of Wind Rose Change with Respect to Low Wind Speeds



Section: ETOS (Southern Appalachians)
 Topographic Zone: Ridge Top

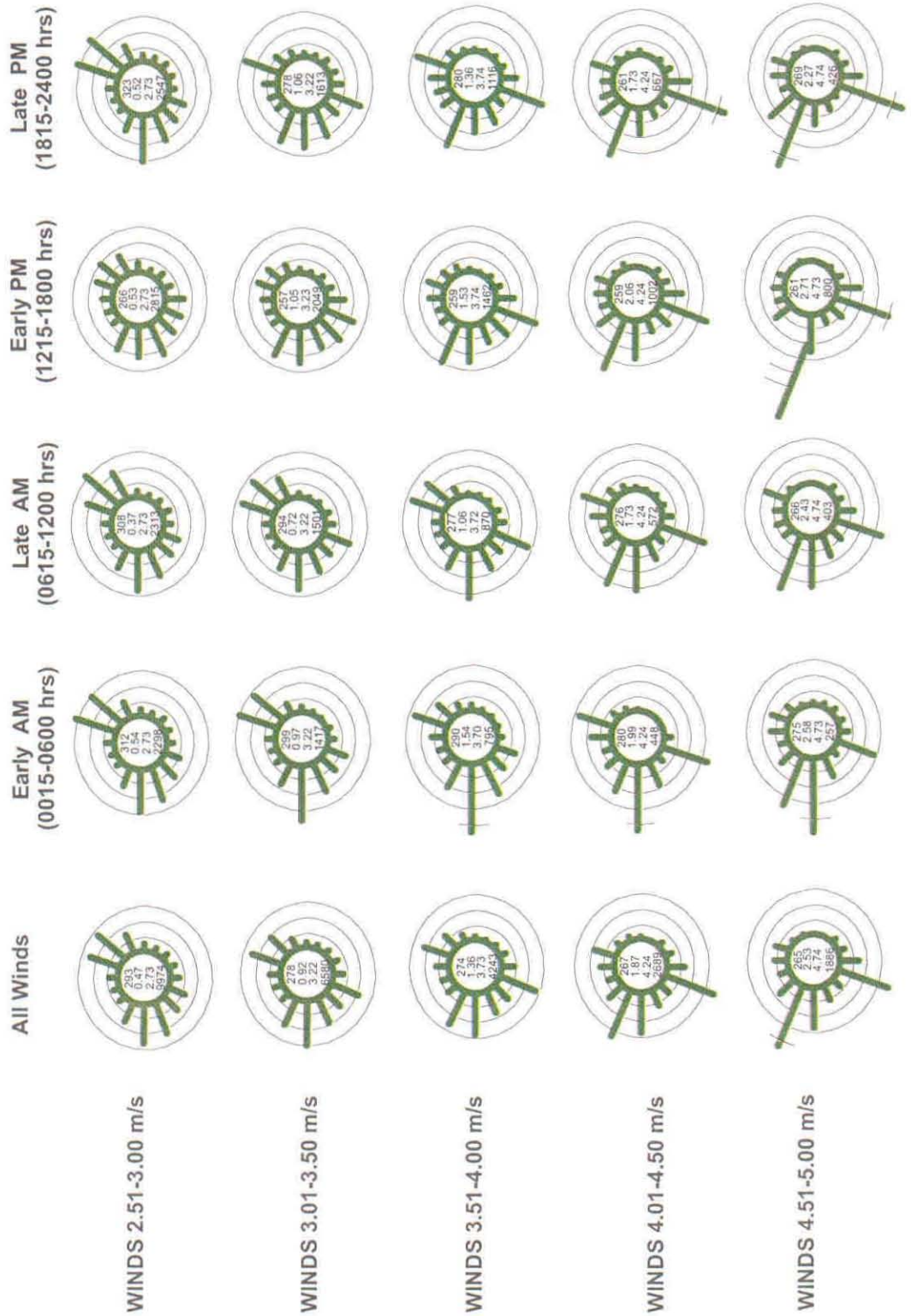
Site: T110, Pine Ridge, Lat 36 00 N, Long 84 15 W, Altitude 343 m, Tower Ht 10 m
 Period of Record: August 1994 - March 1997



Part 1: Analysis of Wind Rose Change with Respect to Low Wind Speeds



Section: ETOS (Southern Appalachians)
 Topographic Zone: Ridge Top
 Site: T110, Pine Ridge, Lat. 36.00 N, Long. 84.15 W, Altitude 343 m, Tower Ht 10 m
 Period of Record: August 1994 - March 1997

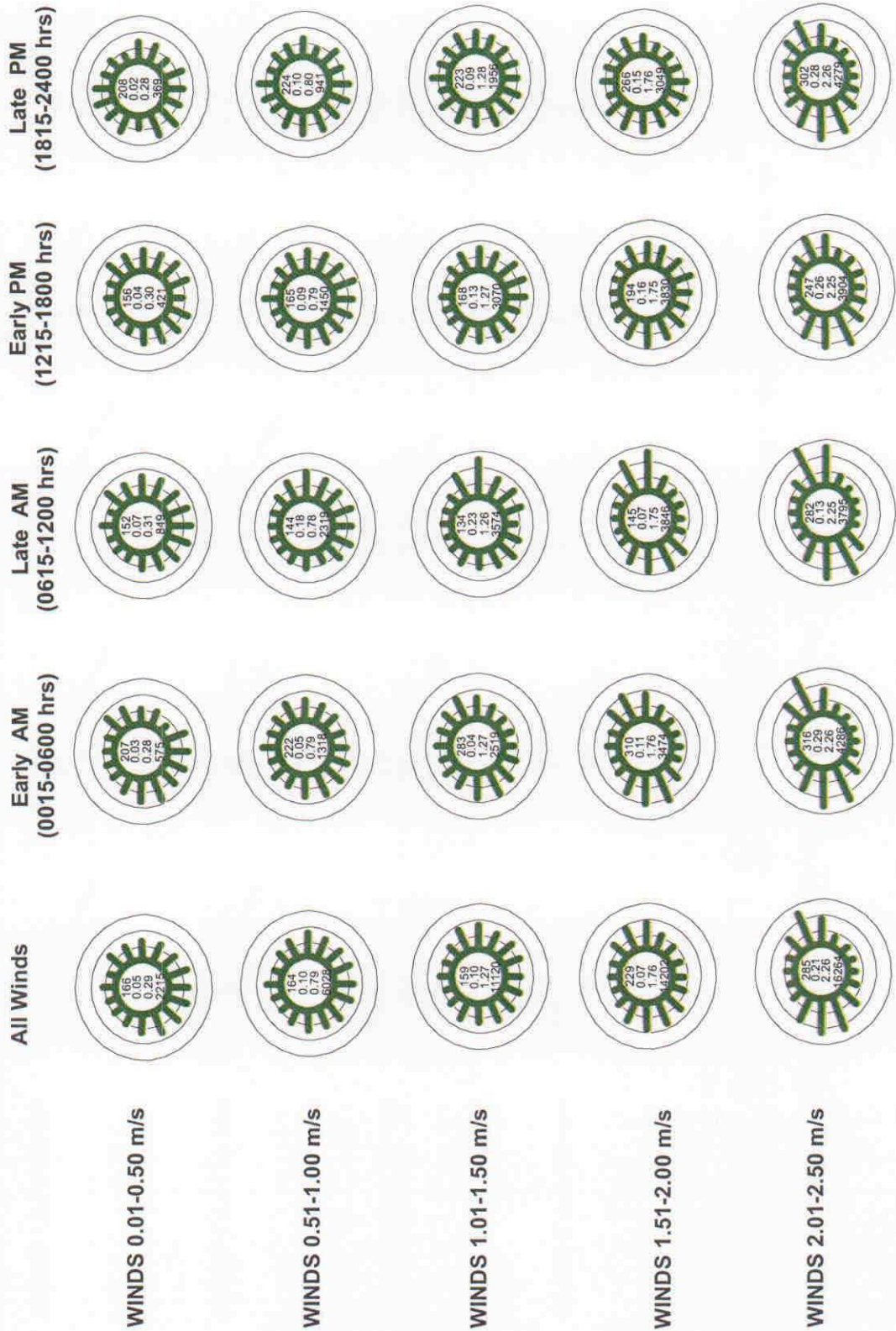


Part 1: Analysis of Wind Rose Change with Respect to Low Wind Speeds



Section: ETOS (Southern Appalachians)
 Topographic Zone: Ridge Top

Site: T119, Walker Branch, Lat 35 58 N, Long 84 17 W, Altitude 340 m, Tower Ht 45 m
 Period of Record: January 1994 - June 1997

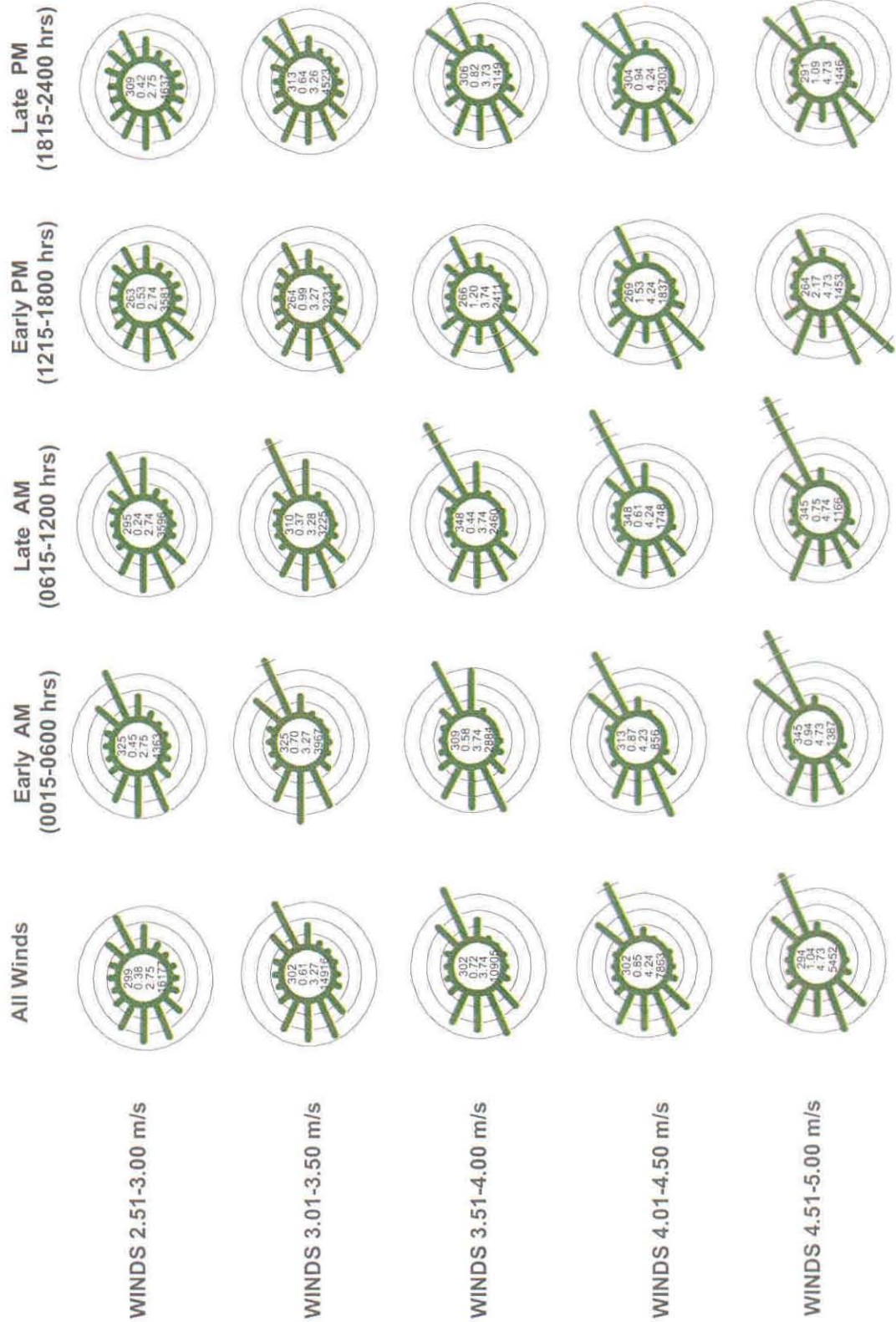




Part 1: Analysis of Wind Rose Change with Respect to Low Wind Speeds

Section: ETOS (Southern Appalachians)
 Topographic Zone: Ridge Top

Site: T119, Walker Branch, Lat 35 58 N, Long 84 17 W, Altitude 340 m, Tower Ht 45 m
 Period of Record: January 1994 - June 1997

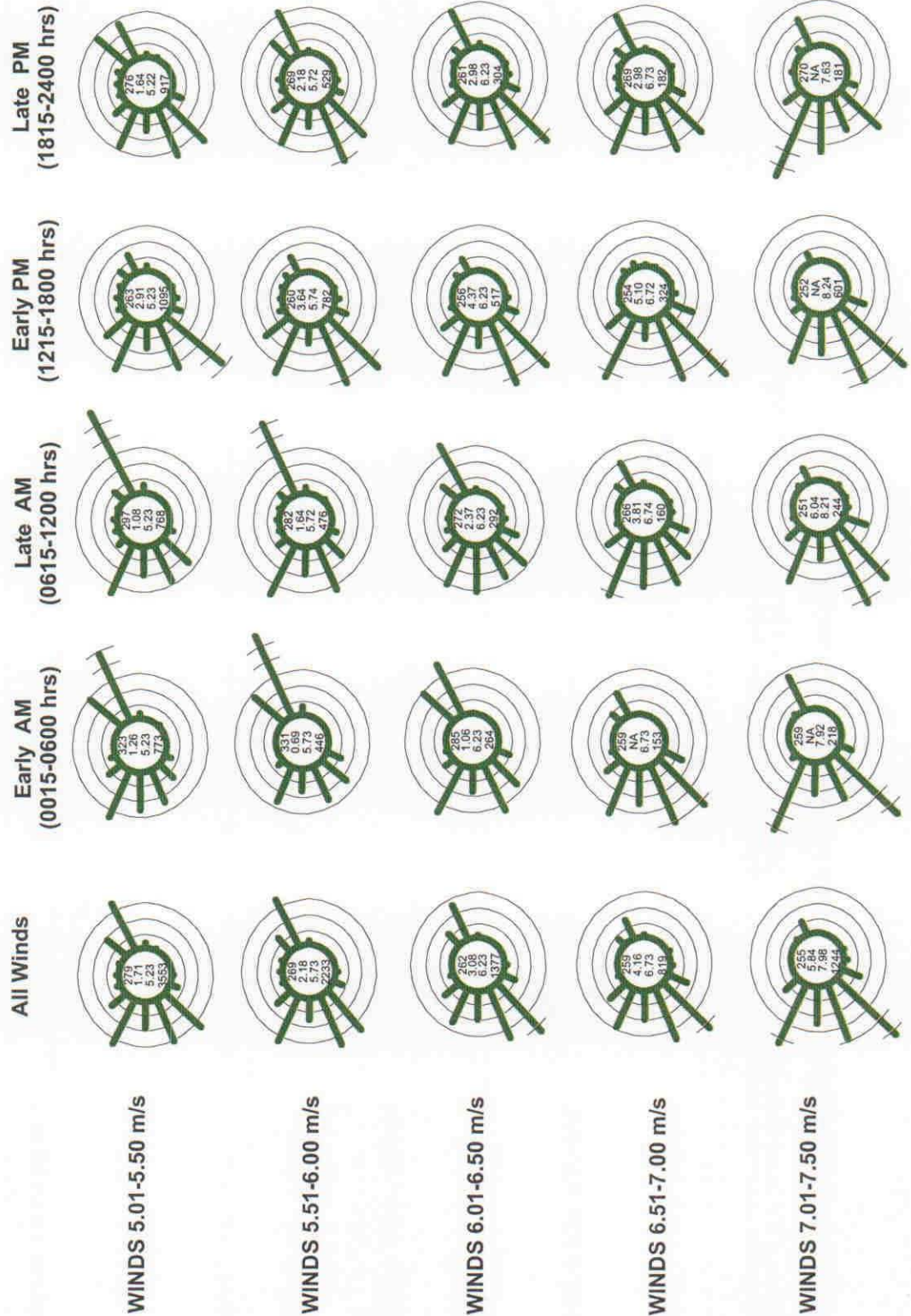


Part 1: Analysis of Wind Rose Change with Respect to Low Wind Speeds



Section: ETOS (Southern Appalachians)
 Topographic Zone: Ridge Top

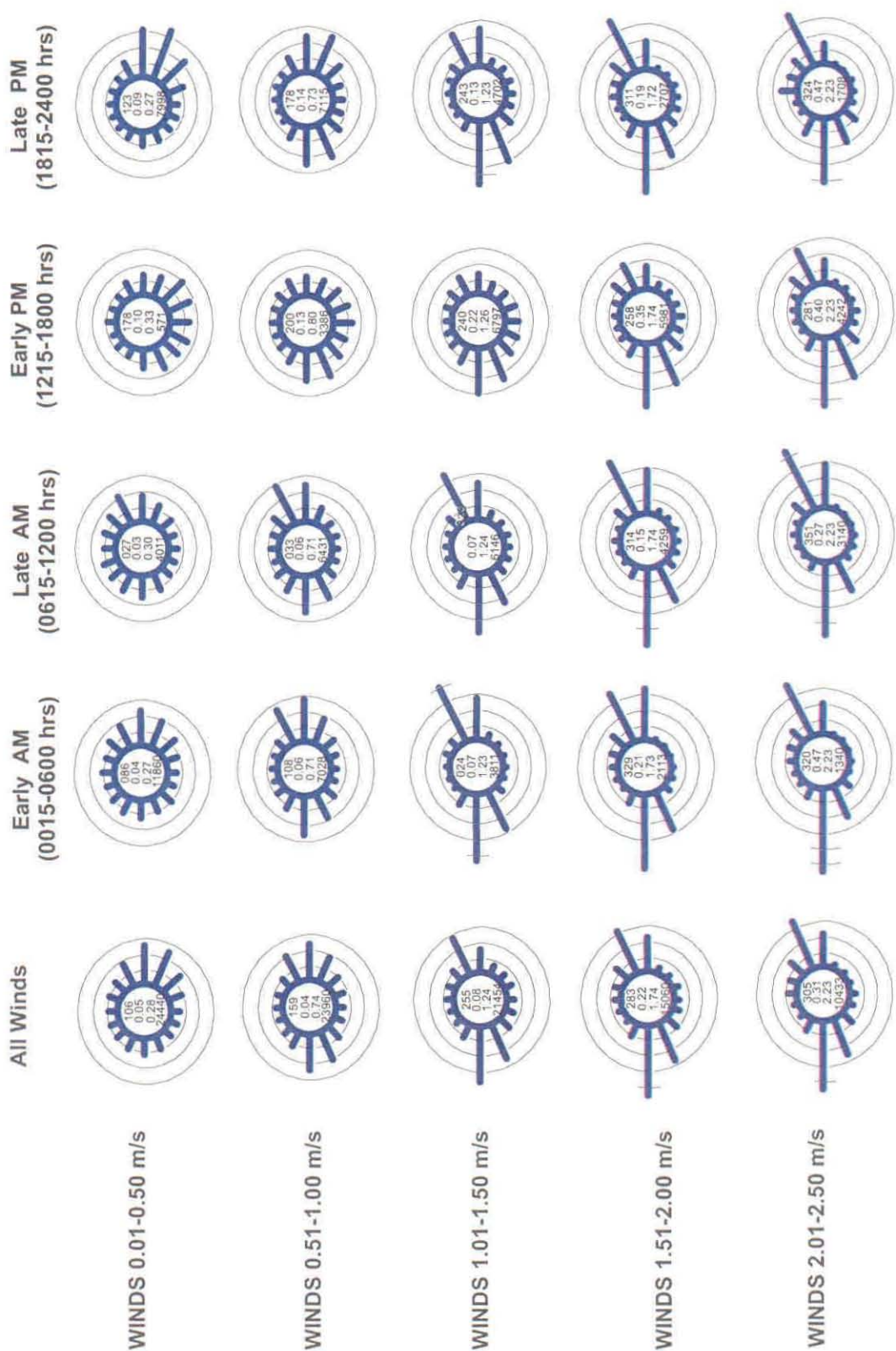
Site: T119, Walker Branch, Lat 35 58 N, Long 84 17 W, Altitude 340 m, Tower Ht 45 m
 Period of Record: January 1994 - June 1997





Part 1: Analysis of Wind Rose Change with Respect to Low Wind Speeds

Section: ETOS (Southern Appalachians) Site: T001, NOAA Office, Lat 36 00 N, Long 84 15 W, Altitude 267 m, Tower Ht 17 m
 Topographic Zone: Valley Bottom Period of Record: January 1994 - March 1997

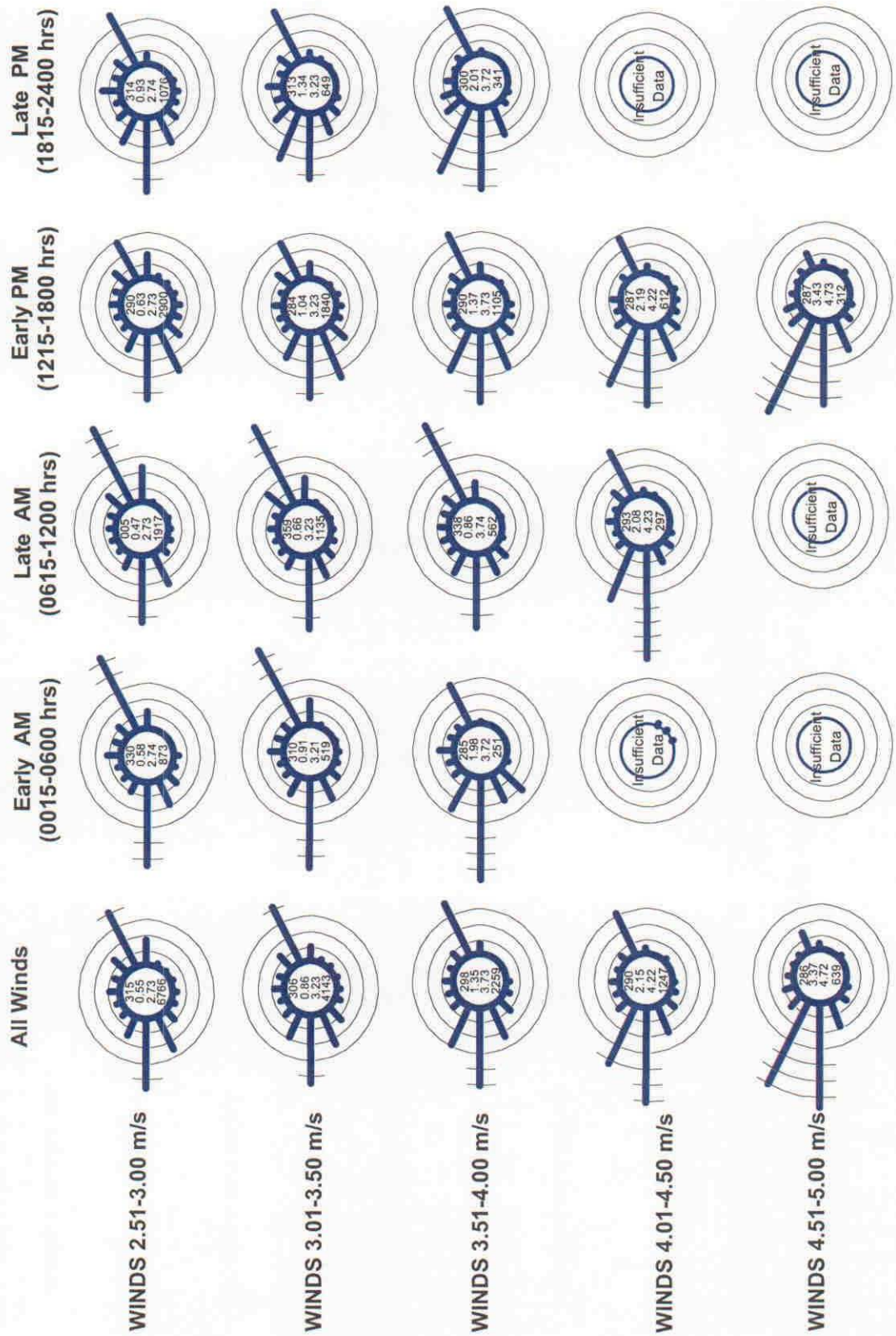


Part 1: Analysis of Wind Rose Change with Respect to Low Wind Speeds



Section: ETOS (Southern Appalachians)
 Topographic Zone: Valley Bottom

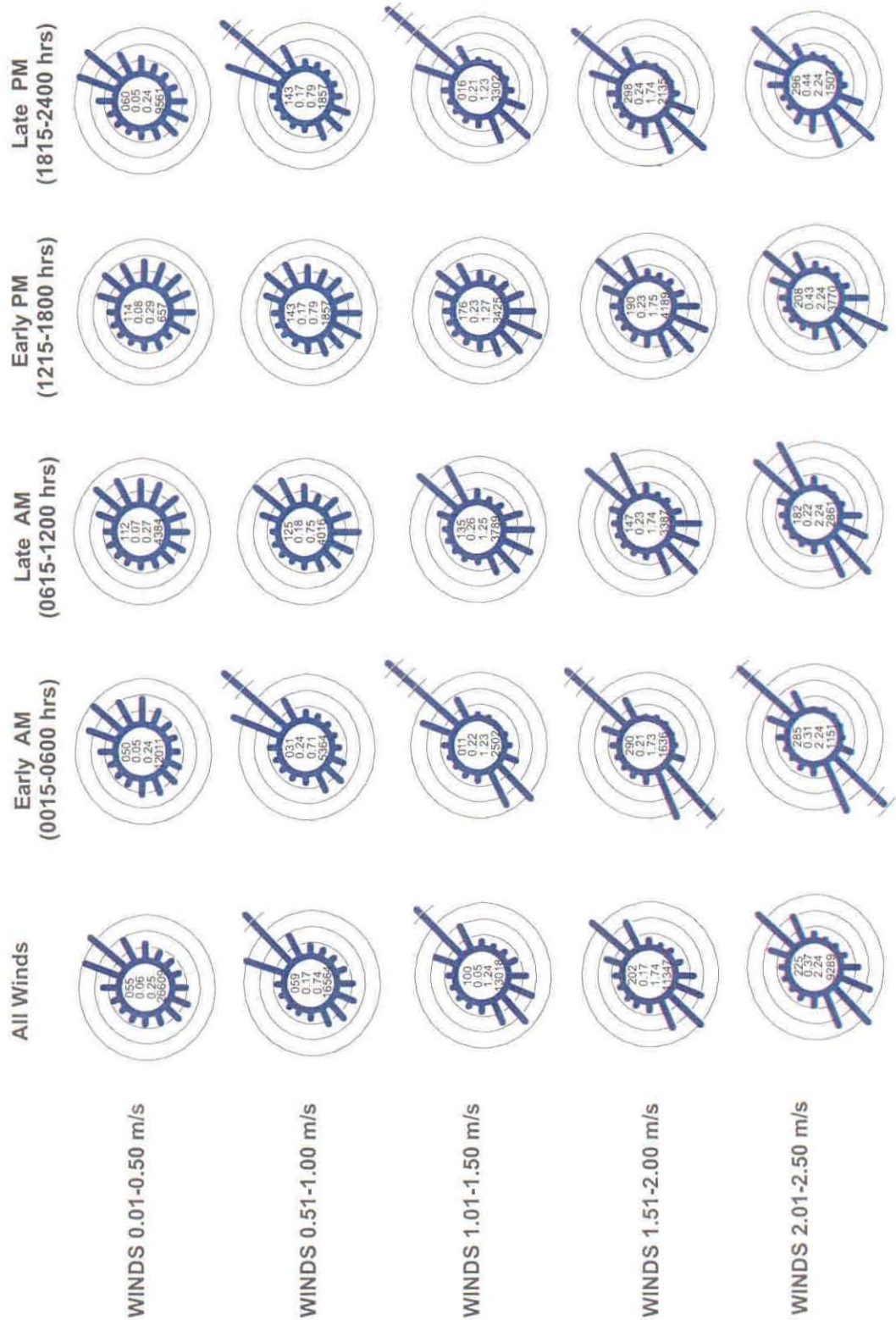
Site: T001, NOAA Office, Lat 36 00 N, Long 84 15 W, Altitude 267 m, Tower Ht 17 m
 Period of Record: January 1994 - March 1997





Part 1: Analysis of Wind Rose Change with Respect to Low Wind Speeds

Section: ETOS (Southern Appalachians) Site: T004, Scarboro, Lat 35 59 N, Long 84 13 W, Altitude 248 m, Tower Ht: 10 m
 Topographic Zone: Valley Bottom Period of Record: March 1994 - June 1996, January 1997 - September 1997

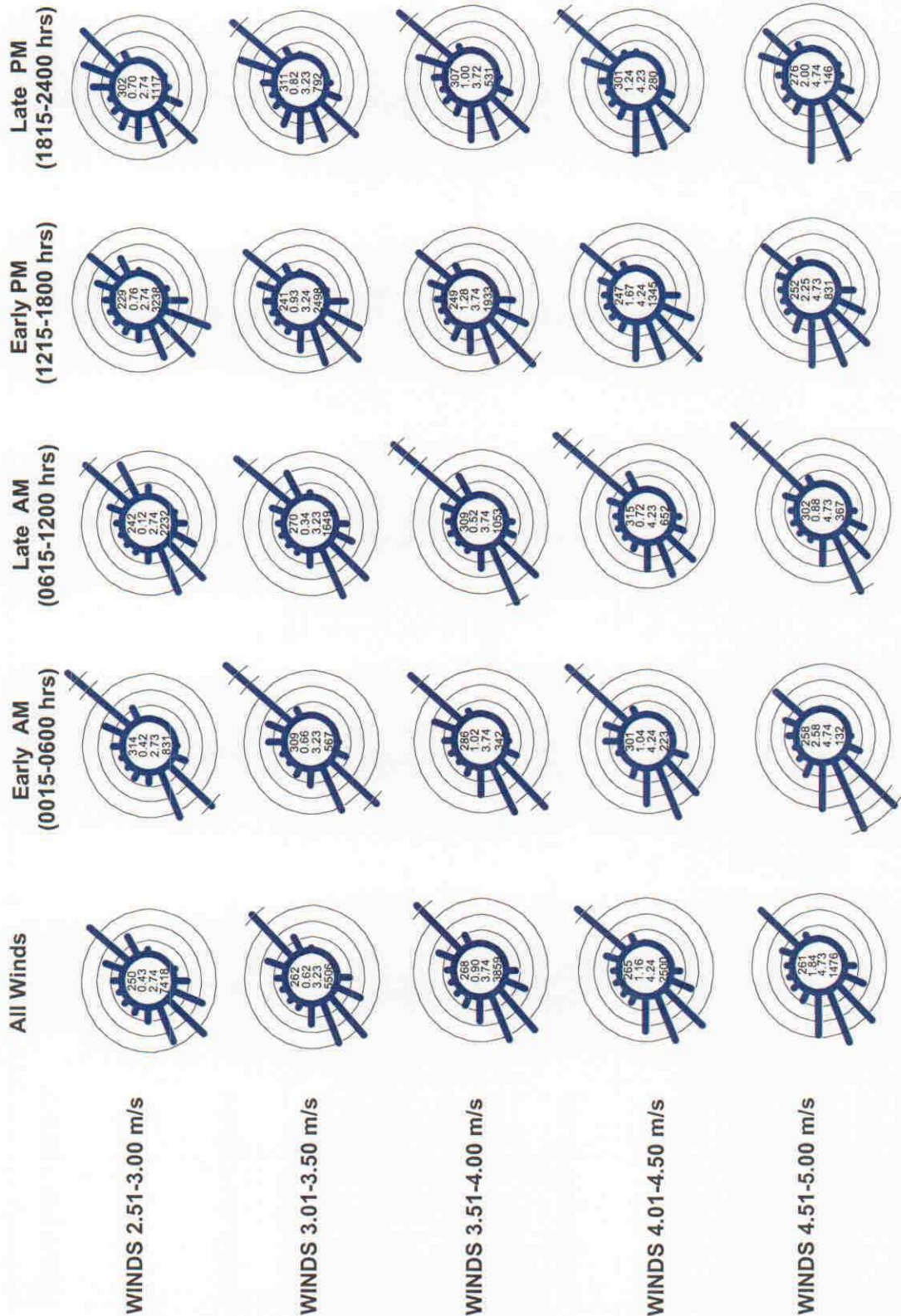


Part 1: Analysis of Wind Rose Change with Respect to Low Wind Speeds



Section: ETOS (Southern Appalachians)
 Topographic Zone: Valley Bottom

Site: T004, Scarboro, Lat 35 59 N, Long 84 13 W, Altitude 248 m, Tower Ht 10 m
 Period of Record: March 1994 - June 1996, January 1997 - September 1997

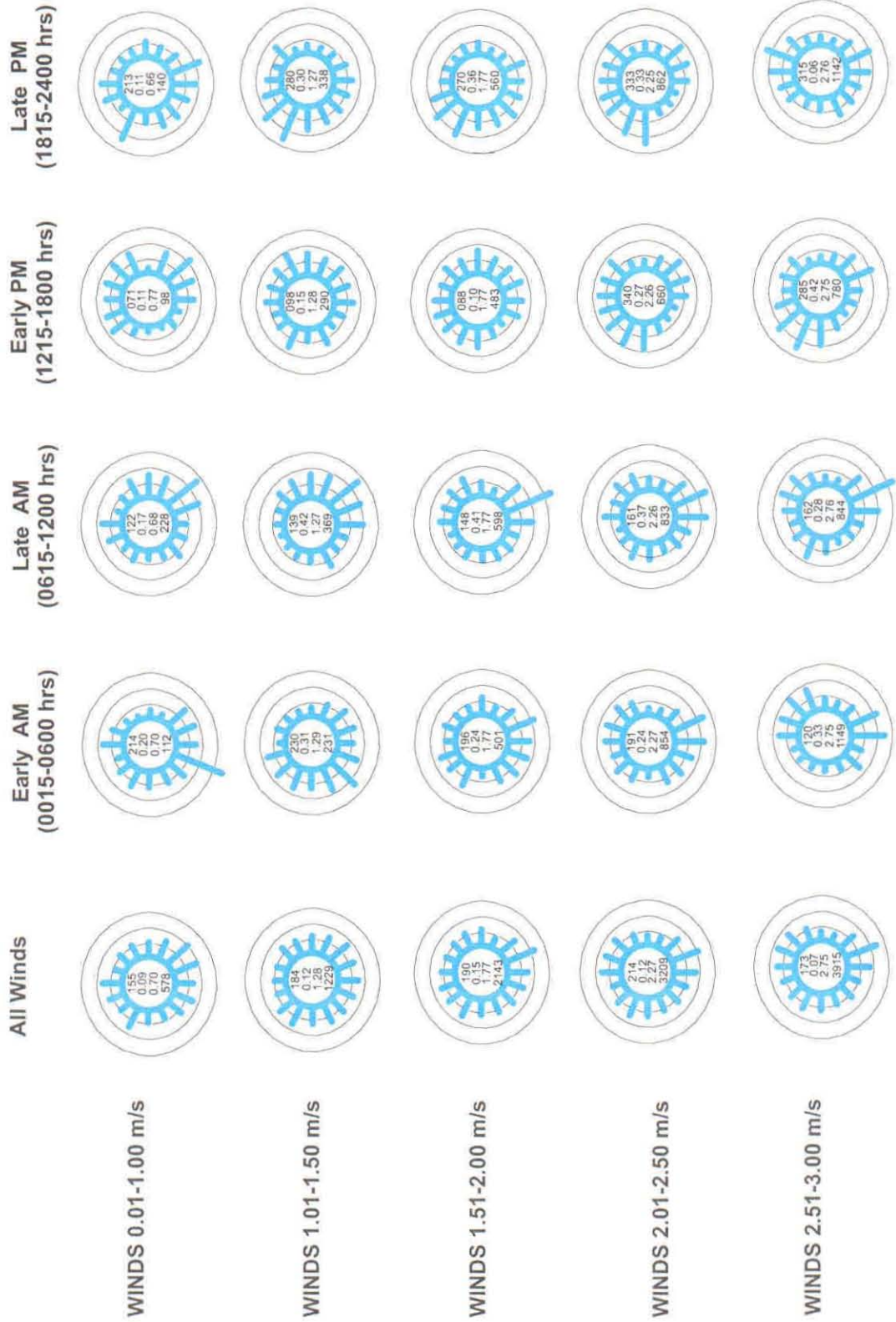


Part 1: Analysis of Wind Rose Change with Respect to Low Wind Speeds



Section: ETOS (Southern Appalachians)
 Topographic Zone: Plateau

Site: T330, Allardt, Lat 36 23 N, Long 84 54 W, Altitude 520 m, Tower Ht 25 m
 Period of Record: May 1999 - February 2000

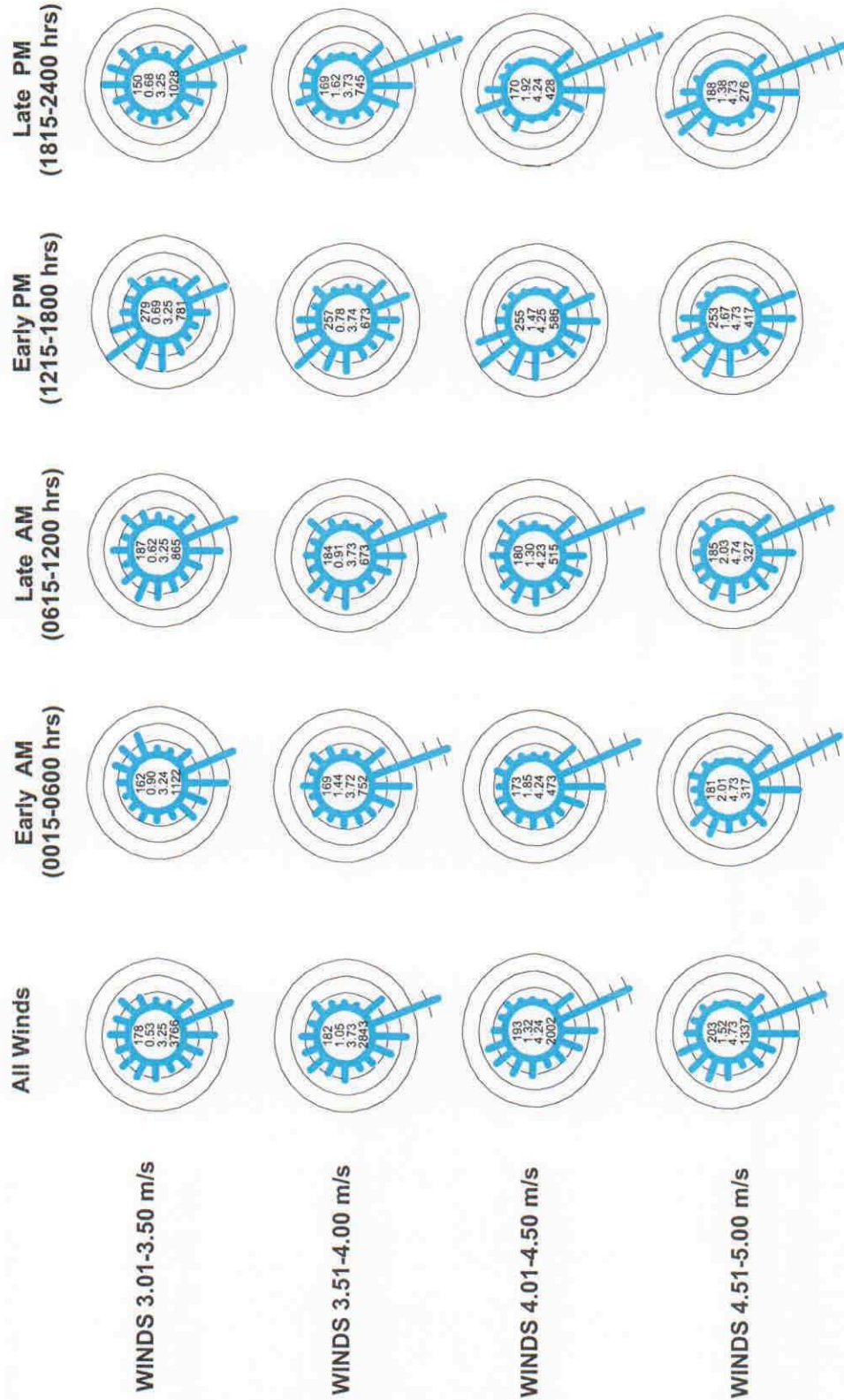




Part 1: Analysis of Wind Rose Change with Respect to Low Wind Speeds

Section: ETOS (Southern Appalachians)
 Topographic Zone: Plateau

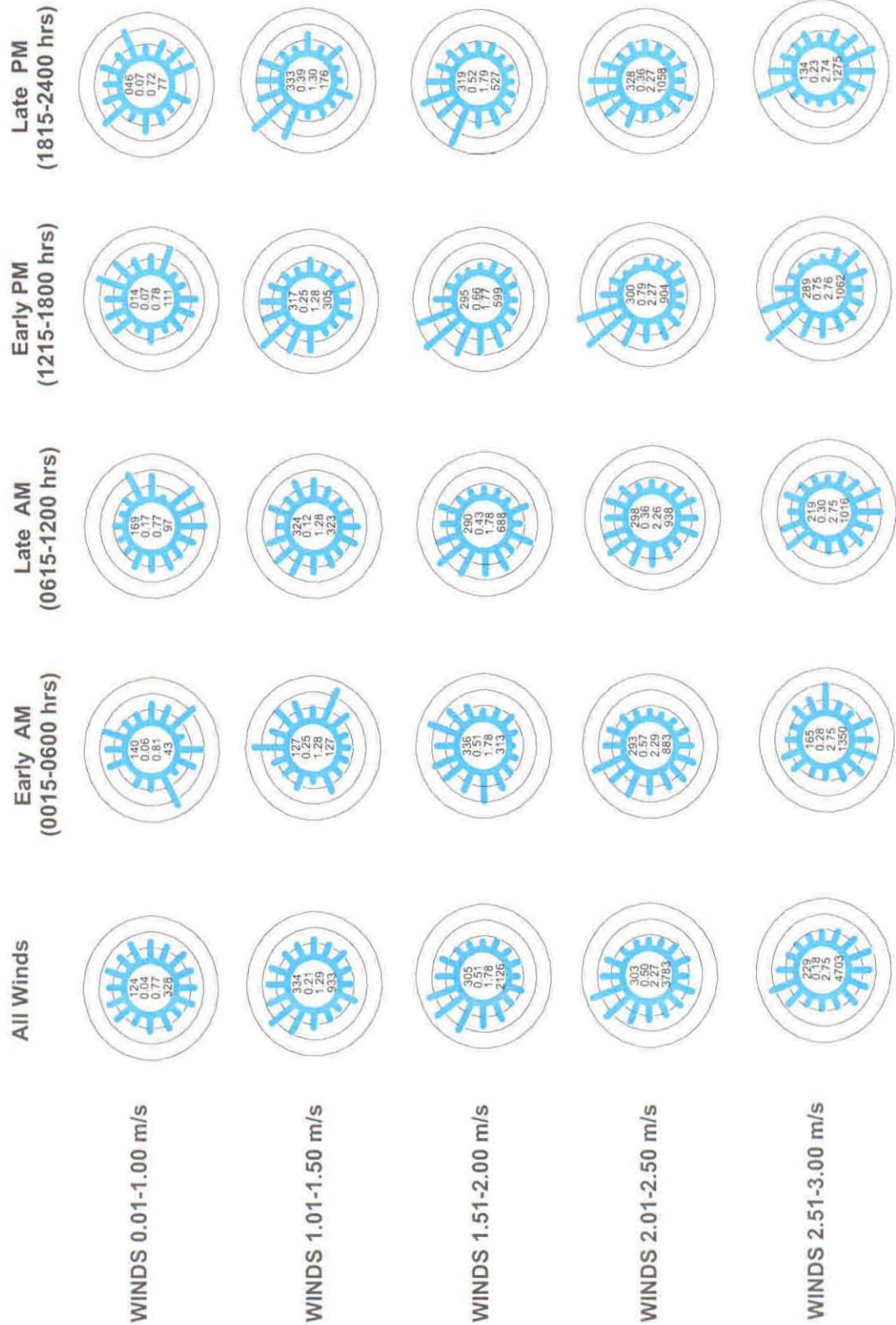
Site: T330, Allardt, Lat 36 23 N, Long 84 54 W, Altitude 520 m, Tower Ht 25 m
 Period of Record: May 1999 - February 2000



Part 1: Analysis of Wind Rose Change with Respect to Low Wind Speeds



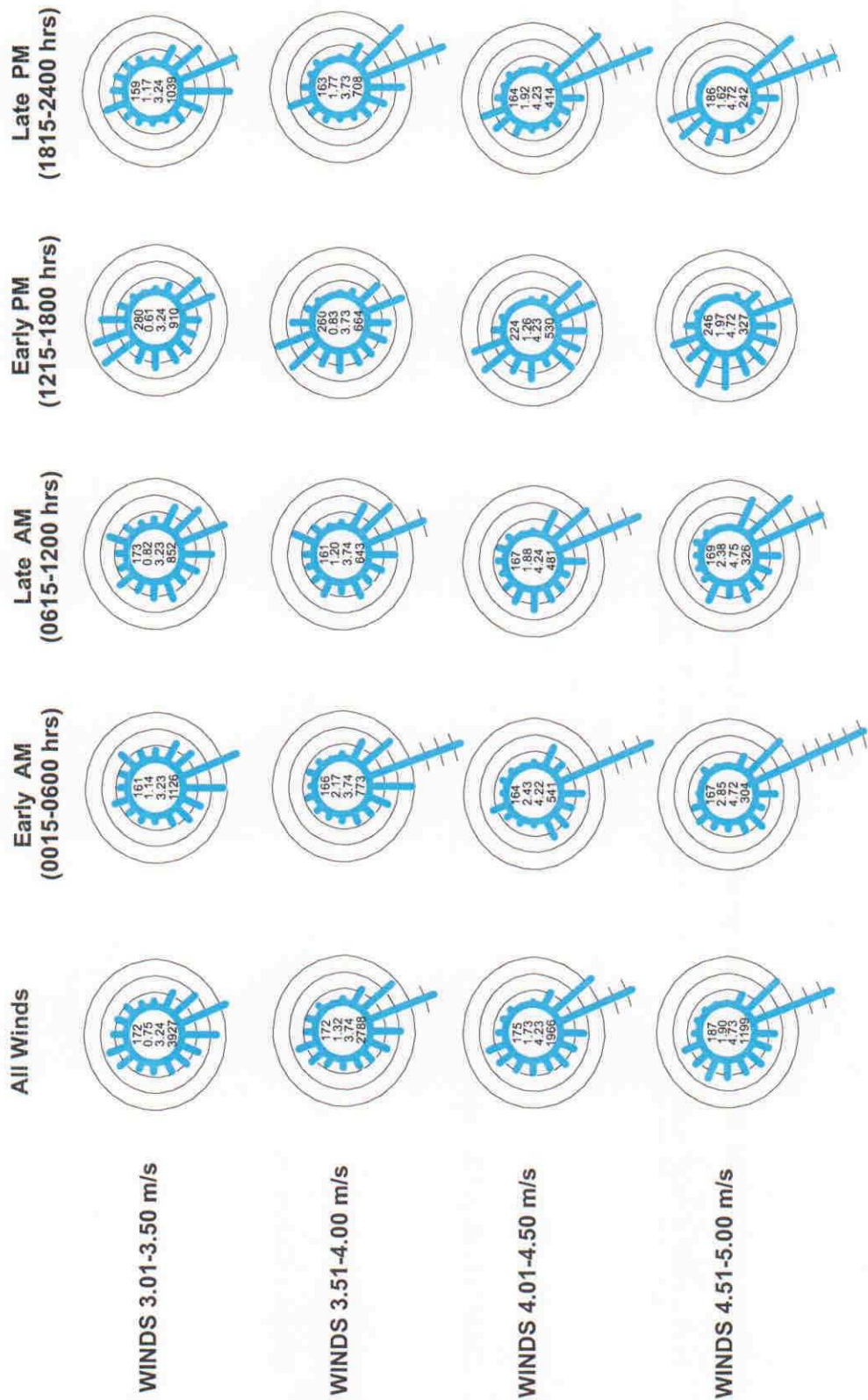
Section: ETOS (Southern Appalachians)
 Topographic Zone: Plateau
 Site: T331, Spencer, Lat 35.40 N, Long 85.29 W, Altitude 572 m, Tower Ht 25 m
 Period of Record: May 1999 - February 2000



Part 1: Analysis of Wind Rose Change with Respect to Low Wind Speeds



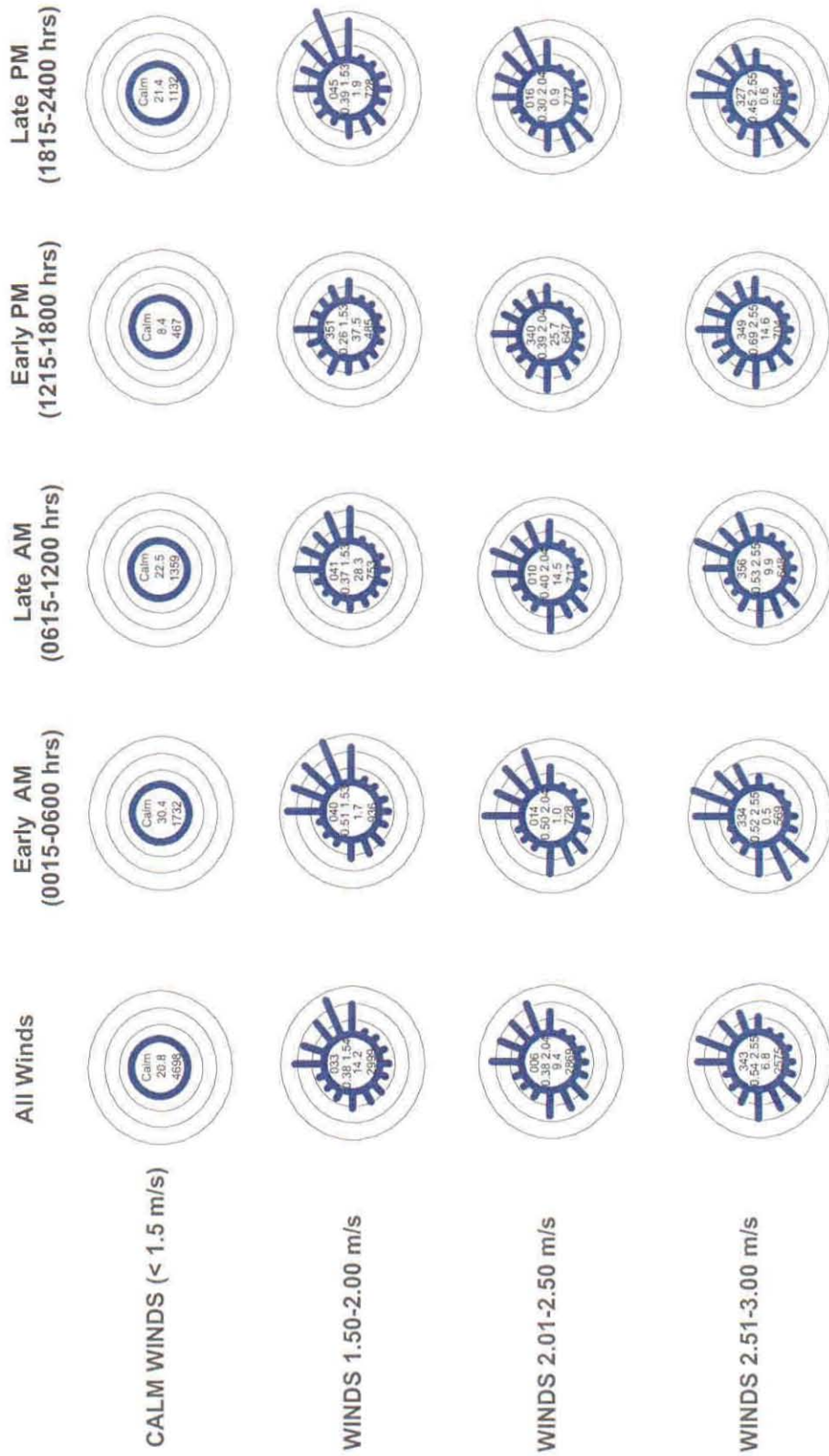
Section: ETOS (Southern Appalachians)
 Topographic Zone: Plateau
 Site: T331, Spencer, Lat 35 40 N, Long 85 29 W, Altitude 572 m, Tower Ht 25 m
 Period of Record: May 1999 - February 2000





Part 1: Analysis of Wind Rose Change with Respect to Low Wind Speeds

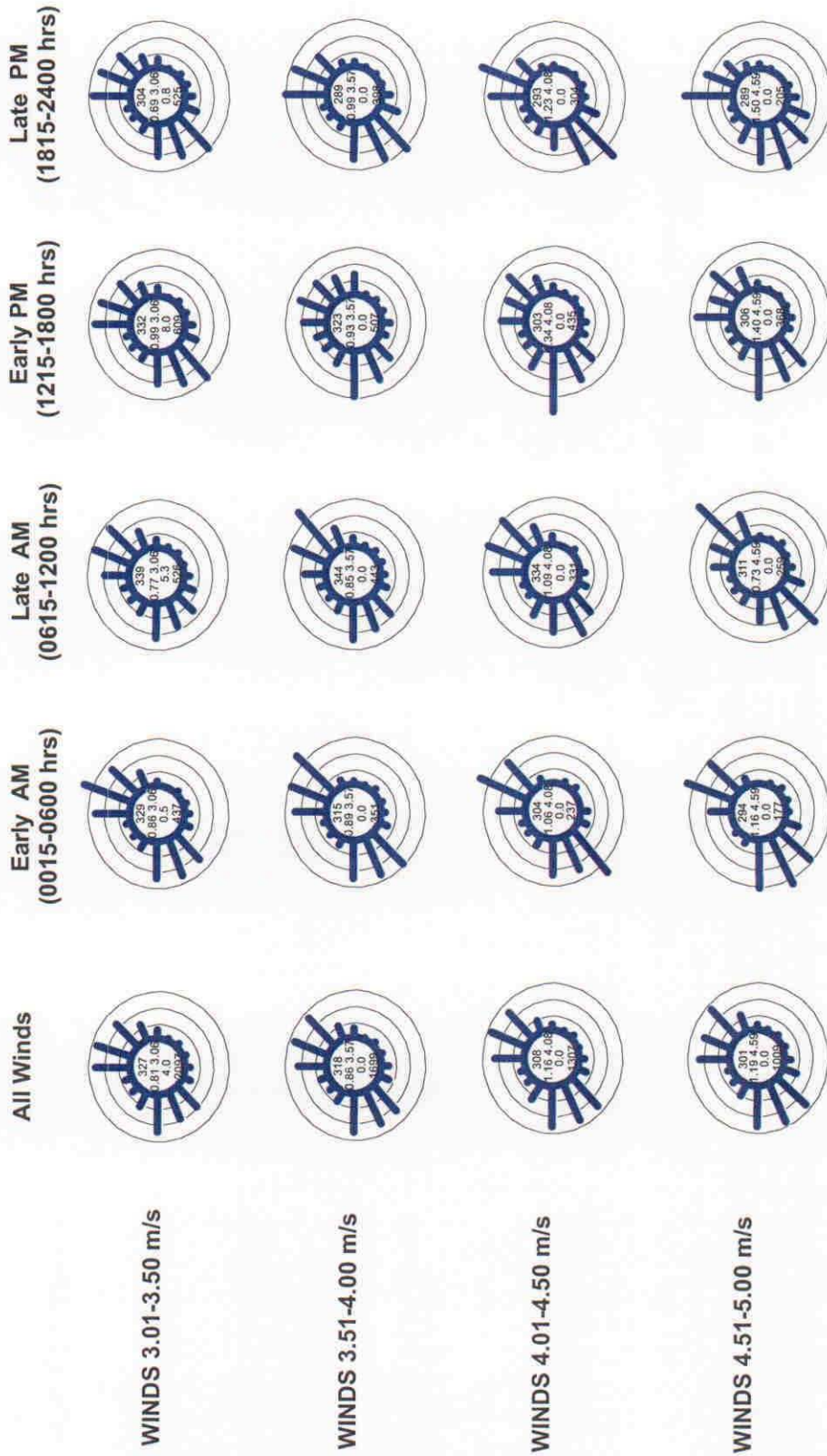
Section: ASOS (Southern Appalachians) Site: Knoxville McGhee-Tyson Airport, Lat 35 49 N, Long 83 59 W, Altitude 293 m, Tower Ht 9 m
 Topographic Zone: Valley Bottom Period of Record: January 1998 - February 2000



Part 1: Analysis of Wind Rose Change with Respect to Low Wind Speeds



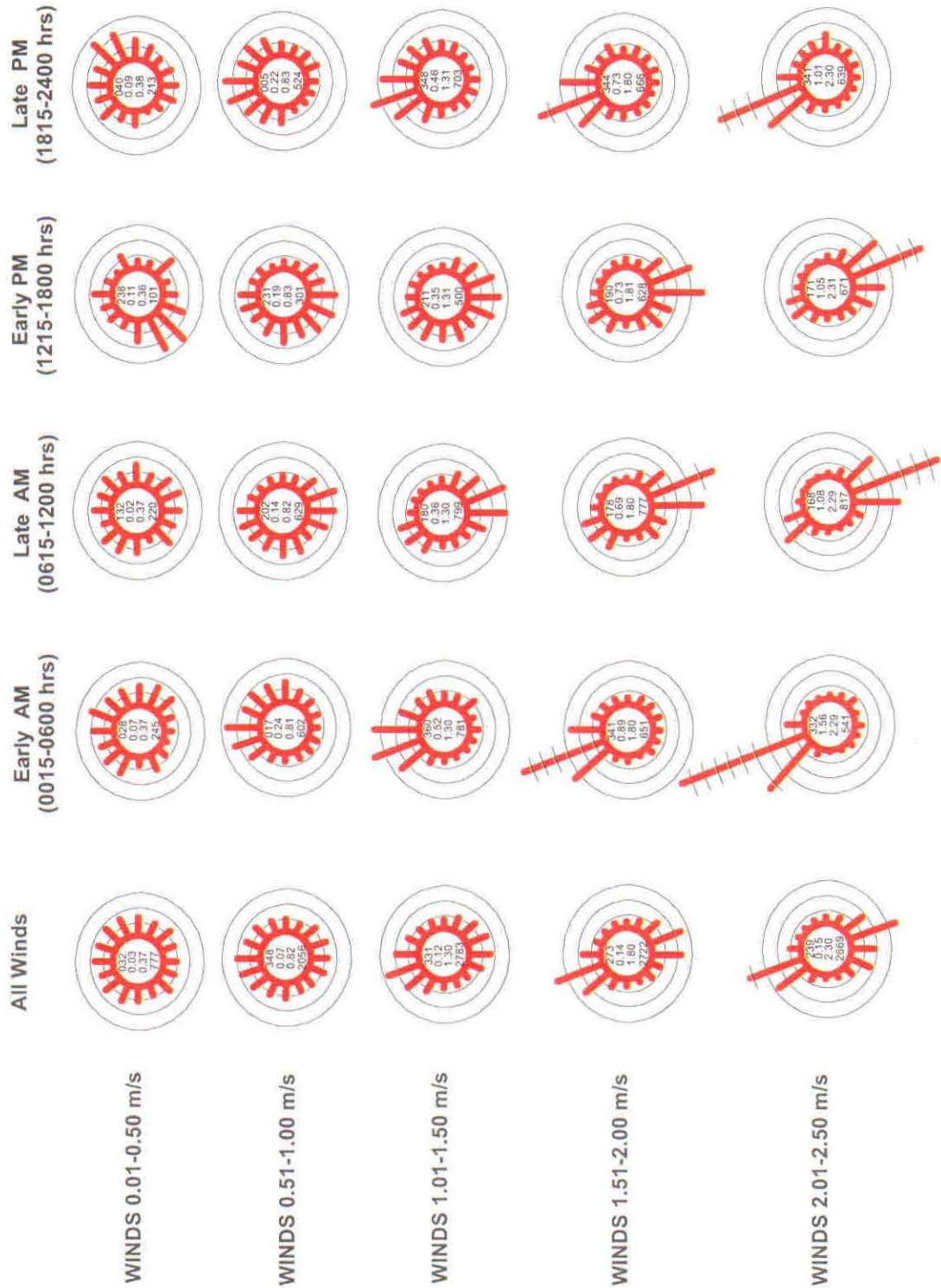
Section: ASOS (Southern Appalachians) Site: Knoxville McChessee-Tyson Airport, Lat 35 49 N, Long 83 59 W, Altitude 293 m, Tower Ht 9 m
 Topographic Zone: Valley Bottom Period of Record: January 1998 - February 2000



Part 1: Analysis of Wind Rose Change with Respect to Low Wind Speeds

Section: INEEL (Snake River Basin)
 Topographic Zone: Mountain Valley

Site: BLU, Blue Dome, Lat 44.04 N, Long 112.50 W, Altitude 1750 m
 Period of Record: January 1994 - December 1997

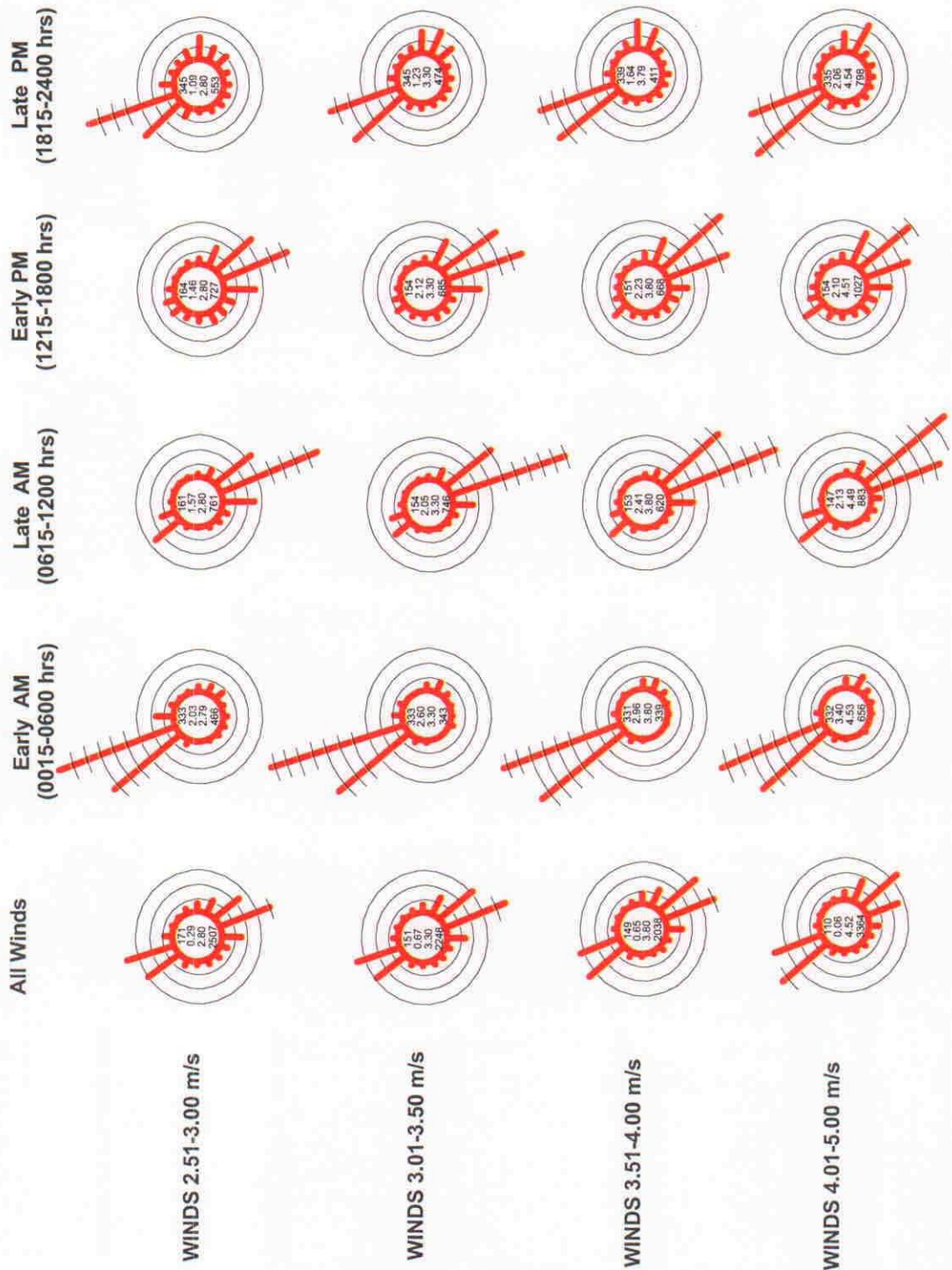


Part 1: Analysis of Wind Rose Change with Respect to Low Wind Speeds



Section: INEEL (Snake River Basin)
 Topographic Zone: Mountain Valley

Site: BLU, Blue Dome, Lat 44 04 N, Long 112 50 W, Altitude 1750 m
 Period of Record: January 1994 - December 1997

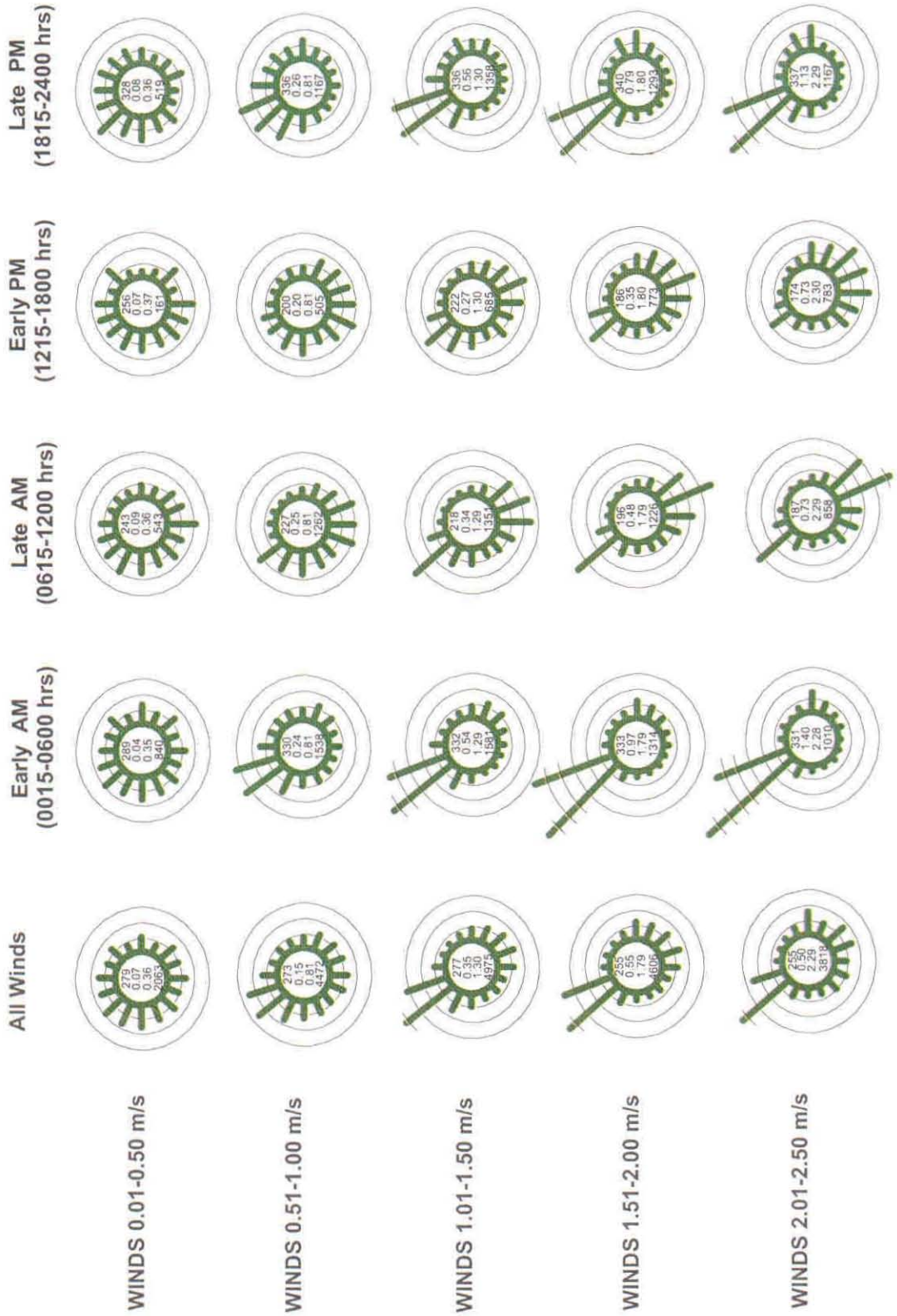


Part 1: Analysis of Wind Rose Change with Respect to Low Wind Speeds



Section: INEEL (Snake River Basin)
 Topographic Zone: High Valley

Site: ARC, Arco, Lat 43 38 N, Long 113 18 W, Altitude 1637 m
 Period of Record: January 1994 - December 1997

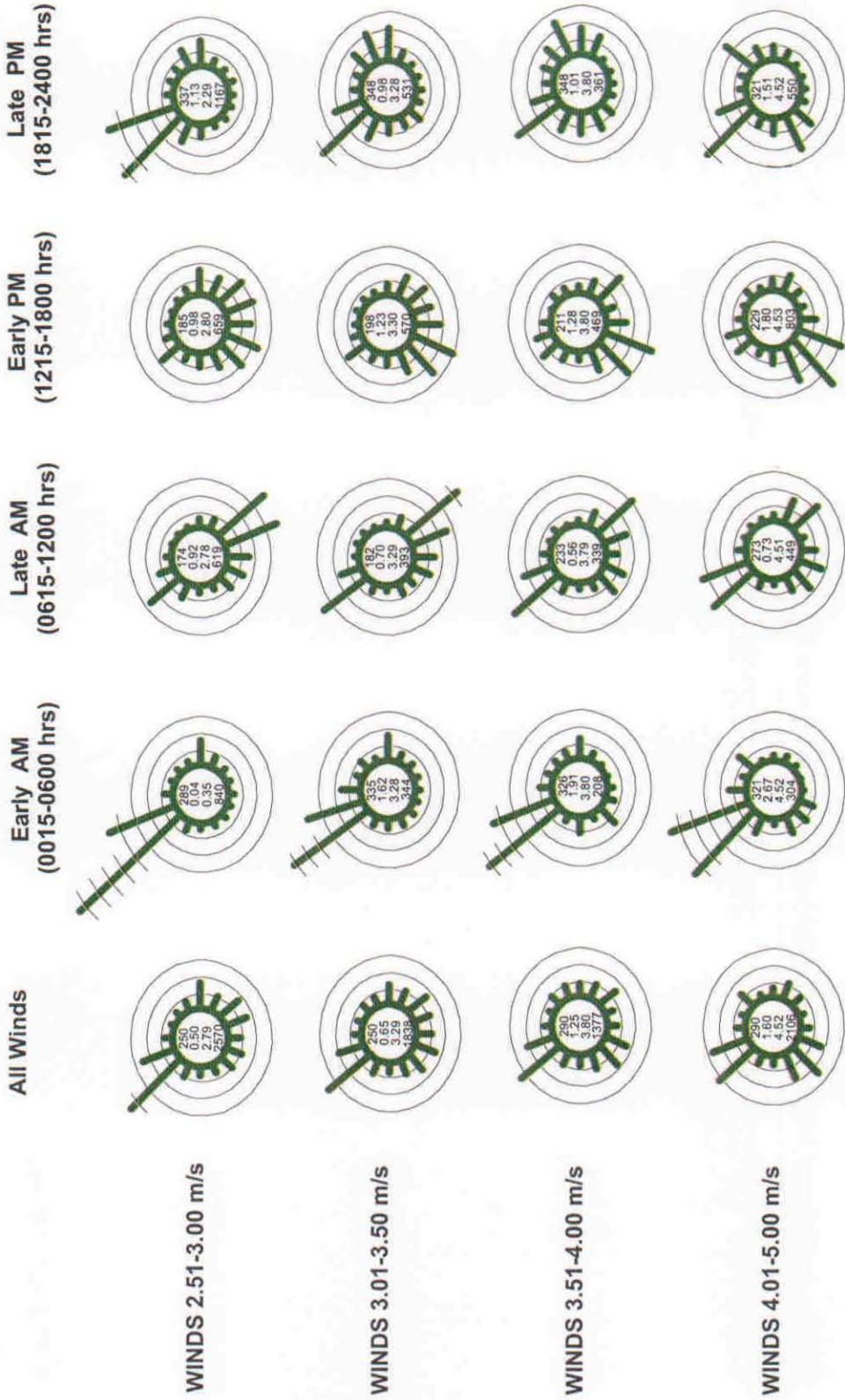




Part 1: Analysis of Wind Rose Change with Respect to Low Wind Speeds

Section: INEEL (Snake River Basin)
 Topographic Zone: High Valley

Site: ARC, Arco, Lat 43 38 N, Long 113 18 W, Altitude 1637 m
 Period of Record: January 1994 - December 1997

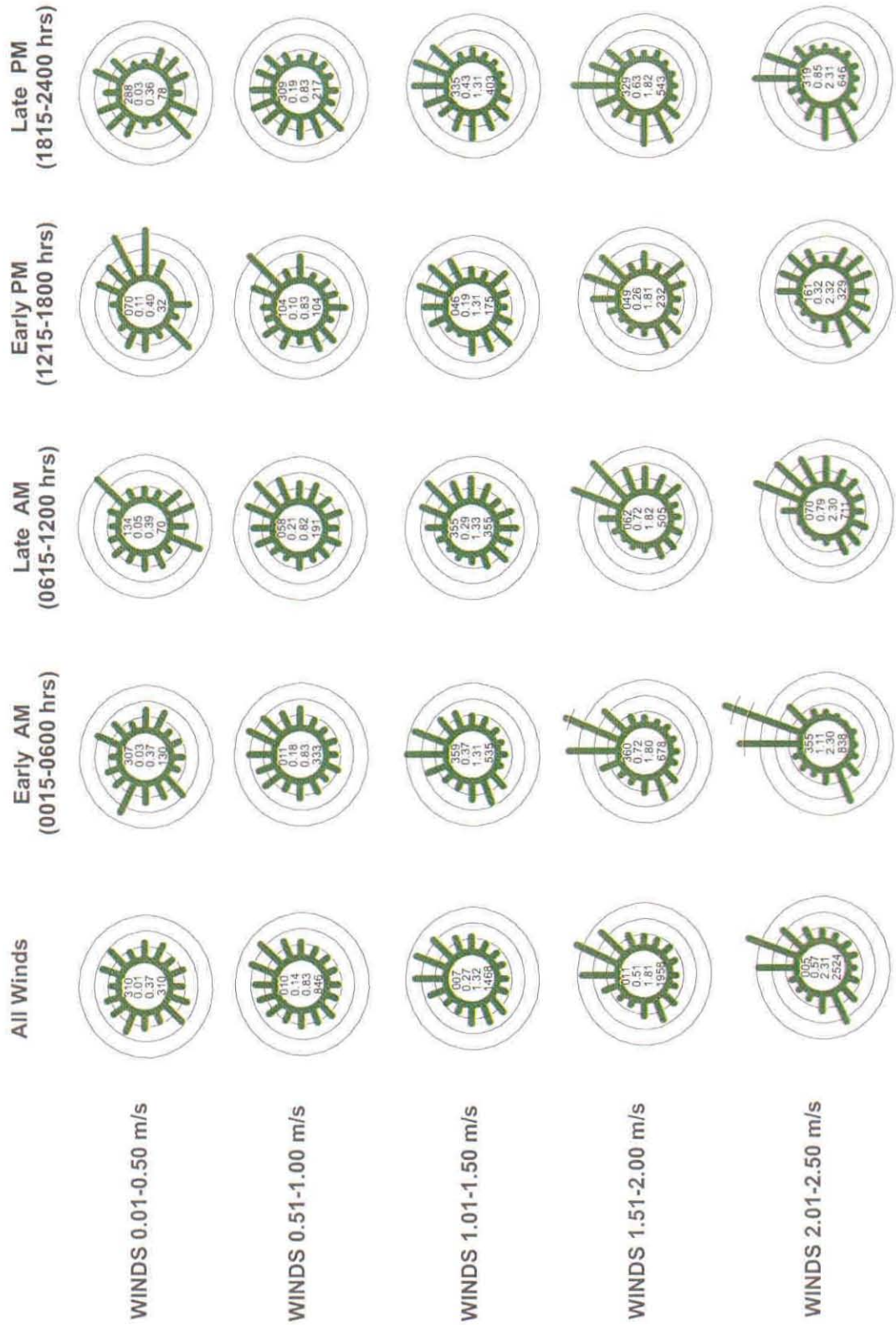




Part 1: Analysis of Wind Rose Change with Respect to Low Wind Speeds

Section: INEEL (Snake River Basin)
 Topographic Zone: High Valley

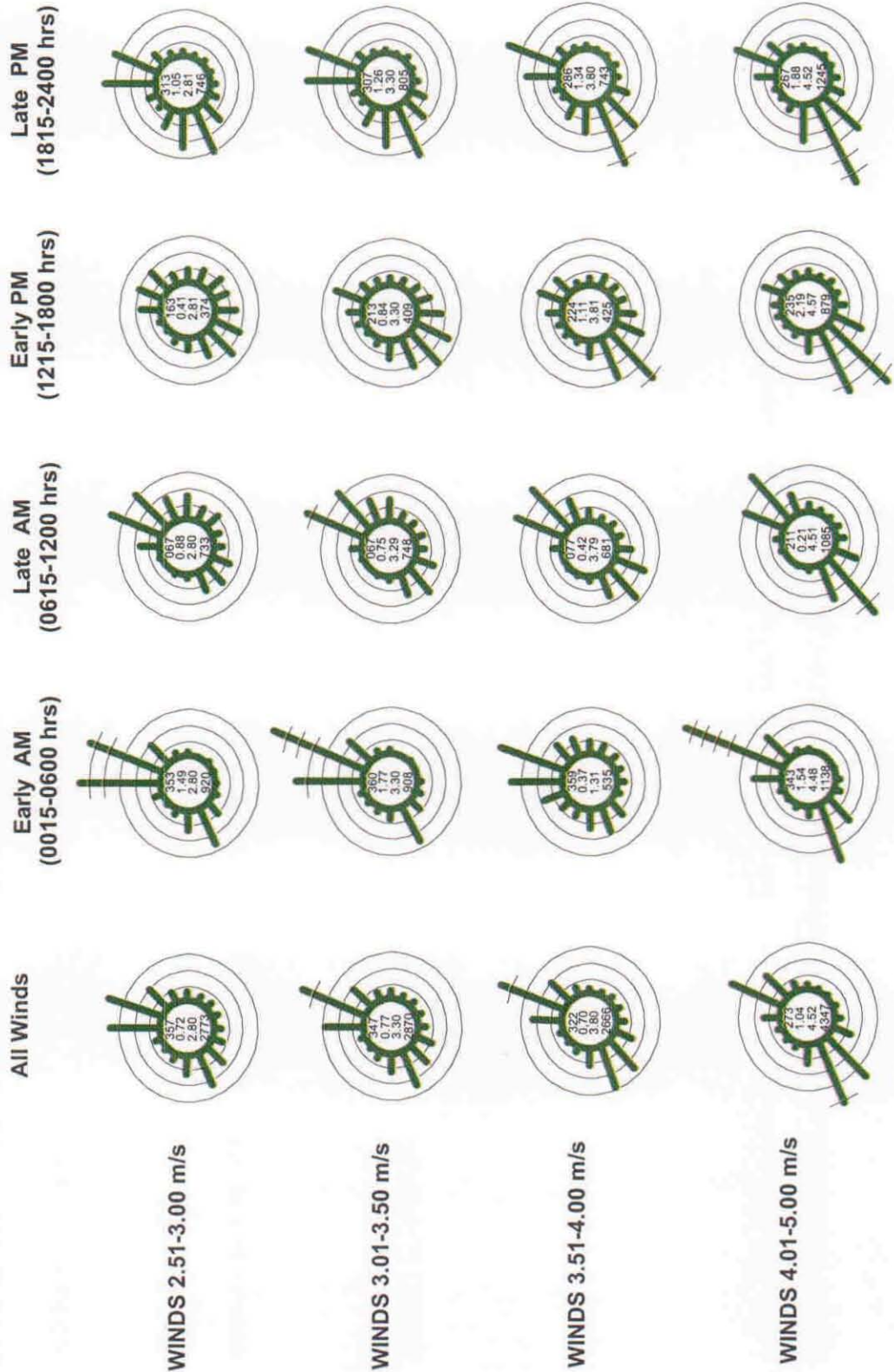
Site: CRA, Craters of Moon Monument, Lat 43 25 N, Long 115 33 W, Altitude 1817 m
 Period of Record: January 1994 - December 1997



Part 1: Analysis of Wind Rose Change with Respect to Low Wind Speeds



Section: INEEL (Snake River Basin)
 Topographic Zone: High Valley
 Site: CRA, Craters of Moon Monument, Lat 43 25 N, Long 115 33 W, Altitude 1817 m
 Period of Record: January 1994 - December 1997

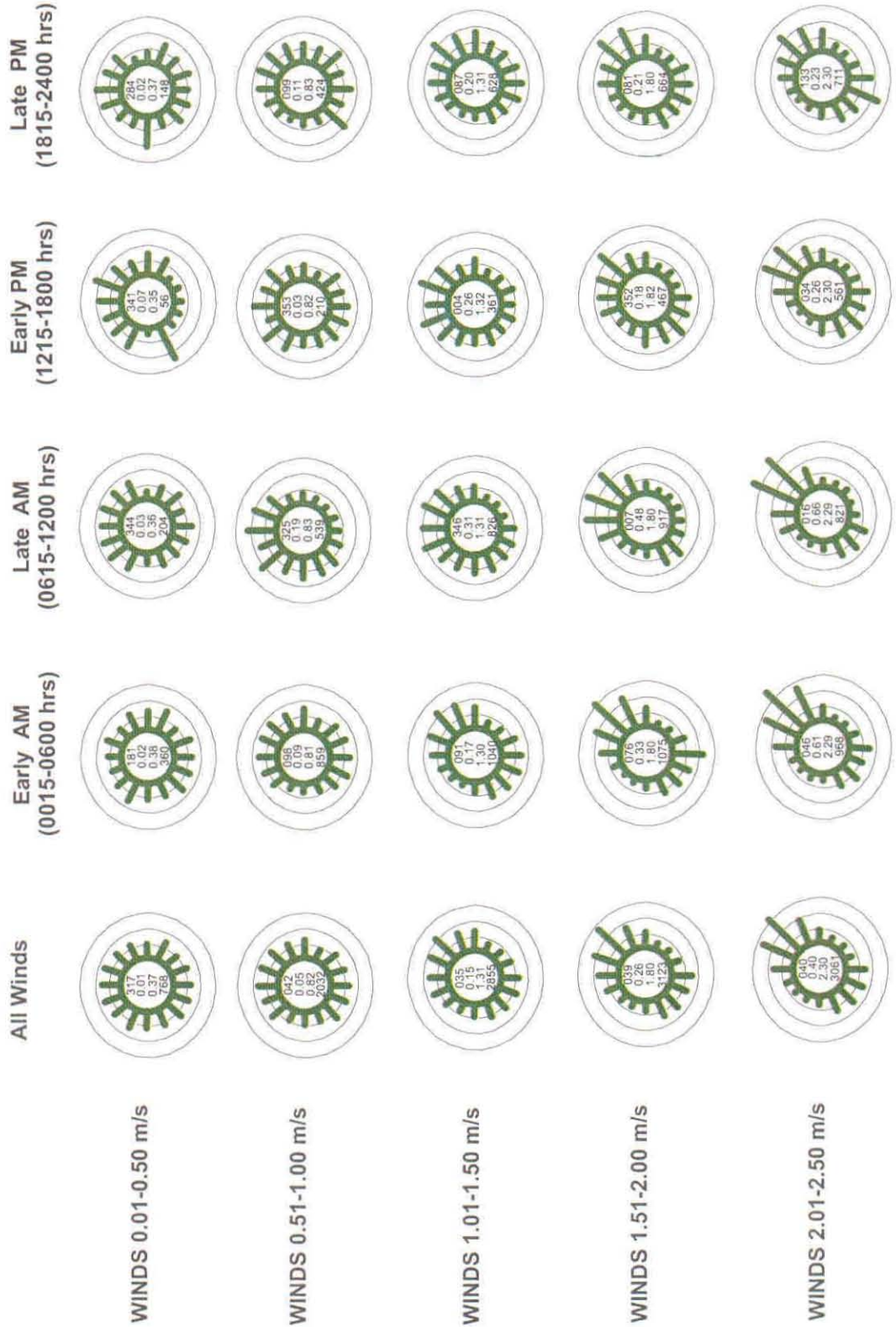




Part 1: Analysis of Wind Rose Change with Respect to Low Wind Speeds

Section: INEEL (Snake River Basin)
 Topographic Zone: High Valley

Site: EBR, Lava Zone, Lat 43.36 N, Long 112.39 W, Altitude 1561 m
 Period of Record: January 1994 - December 1997

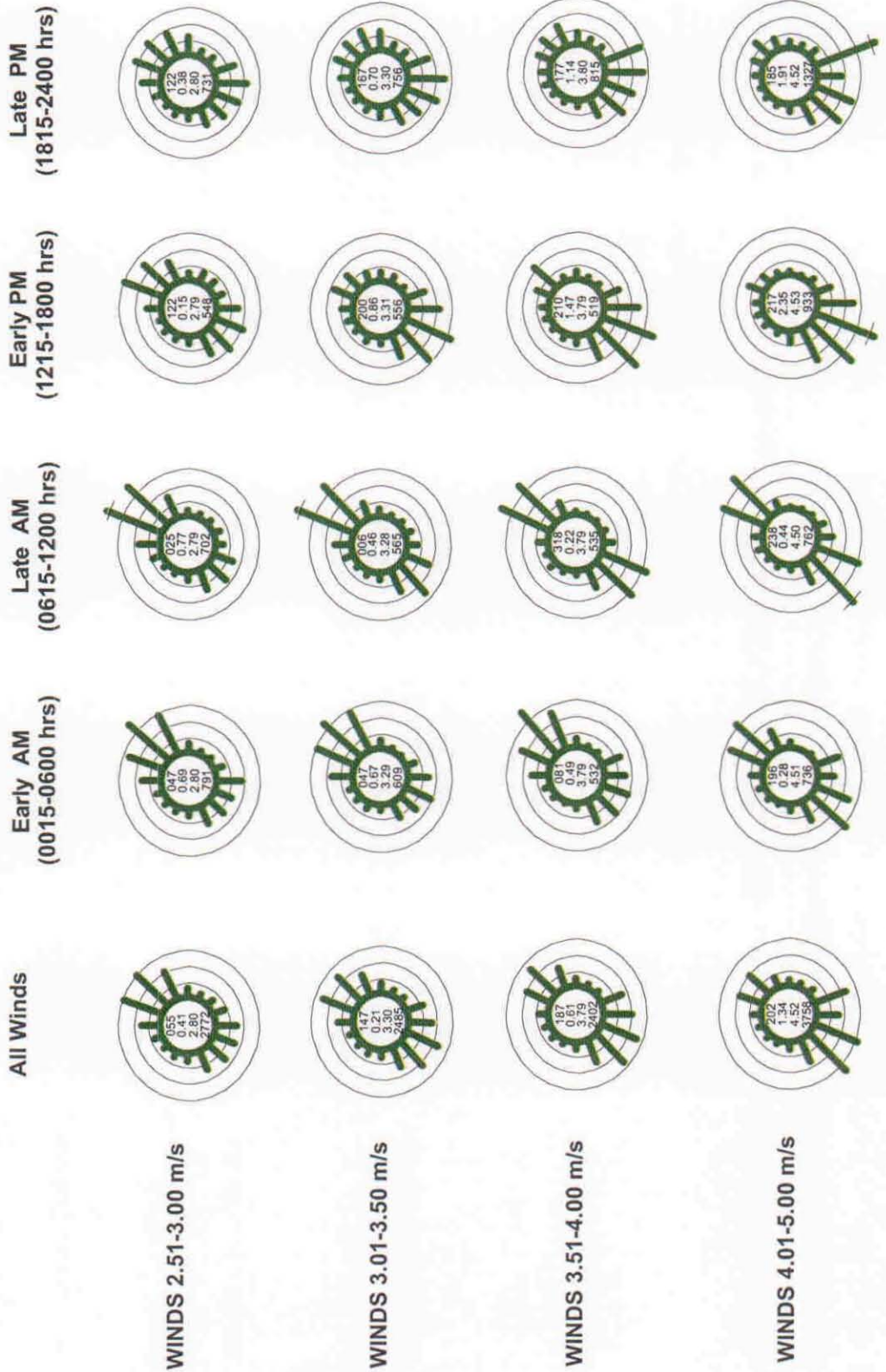




Part 1: Analysis of Wind Rose Change with Respect to Low Wind Speeds

Section: INEEL (Snake River Basin)
 Topographic Zone: High Valley

Site: EBR, Lava Zone, Lat 43 36 N, Long 112 39 W, Altitude 1561 m
 Period of Record: January 1994 - December 1997

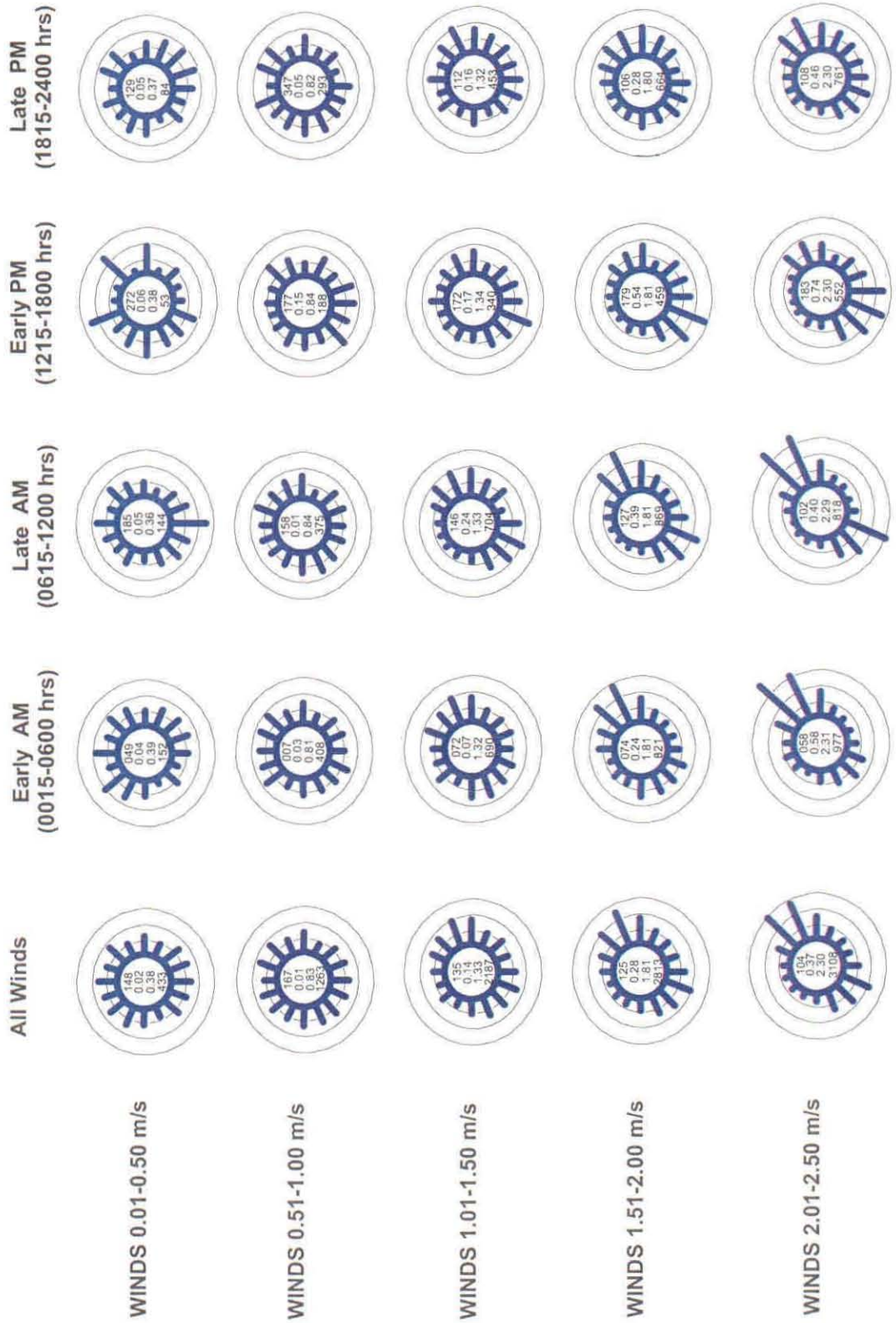




Part 1: Analysis of Wind Rose Change with Respect to Low Wind Speeds

Section: INEEL (Snake River Basin)
 Topographic Zone: Low Valley

Site: BLA, Blackfoot, Lat 43 16 N, Long 112 24 W, Altitude 1369 m
 Period of Record: January 1994 - December 1997

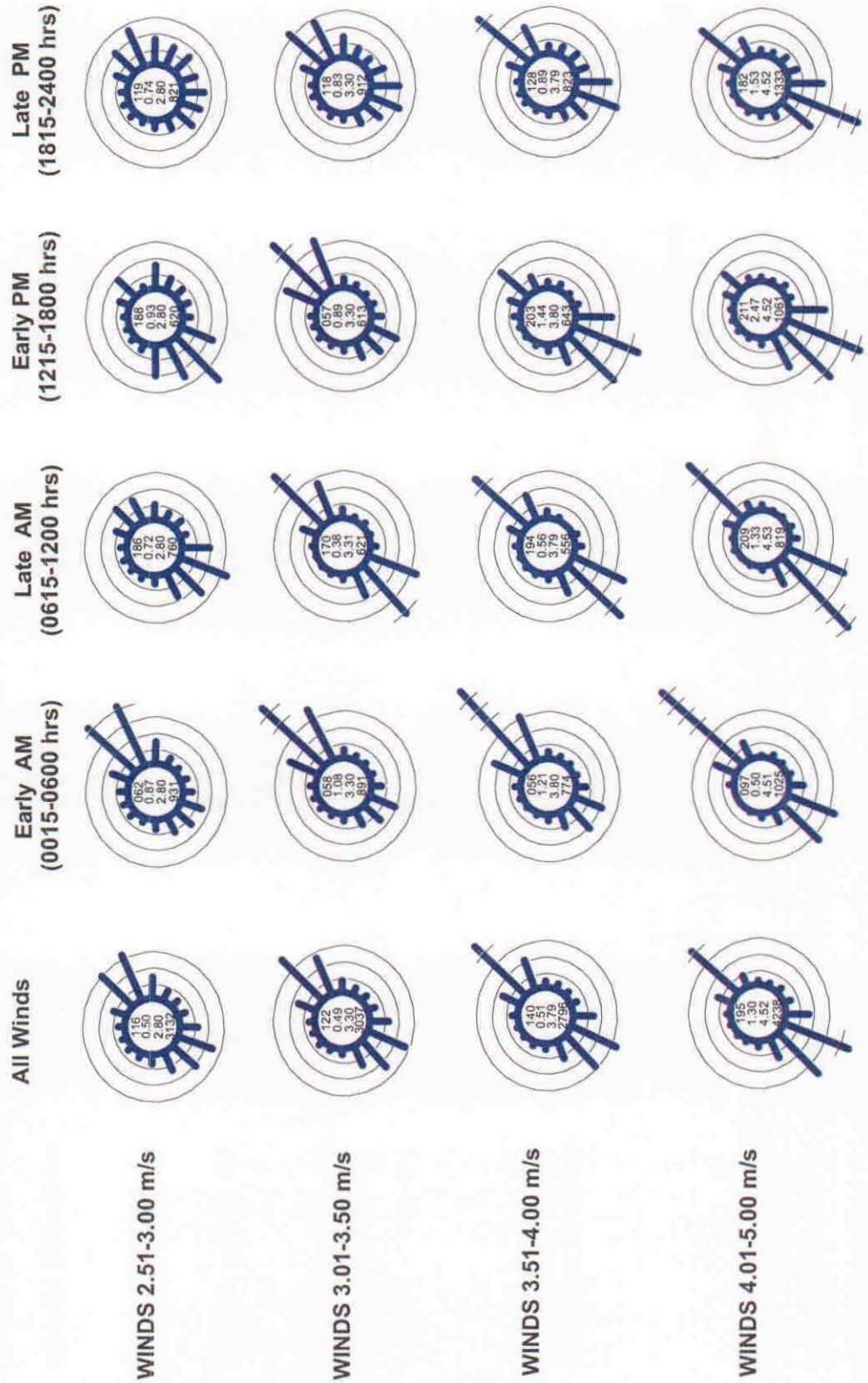




Part 1: Analysis of Wind Rose Change with Respect to Low Wind Speeds

Section: INEEL (Snake River Basin)
 Topographic Zone: Low Valley

Site: BLA, Blackfoot, Lat 43 16 N, Long 112 24 W, Altitude 1369 m
 Period of Record: January 1994 - December 1997

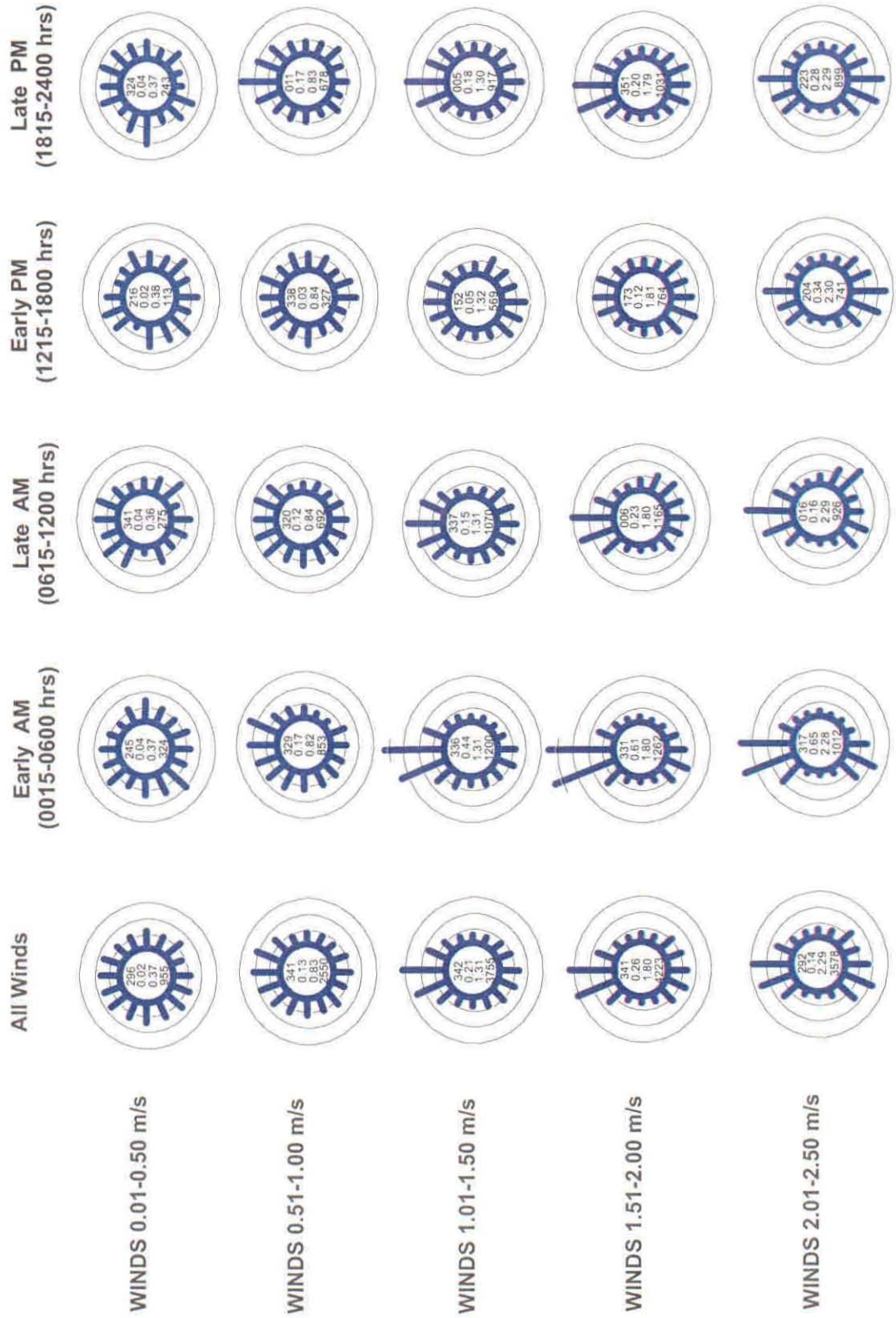




Part 1: Analysis of Wind Rose Change with Respect to Low Wind Speeds

Section: INEEL (Snake River Basin)
 Topographic Zone: Low Valley

Site: IDA, Idaho Falls, Lat 43 31 N, Long 112 04 W, Altitude 1438 m
 Period of Record: January 1994 - December 1997

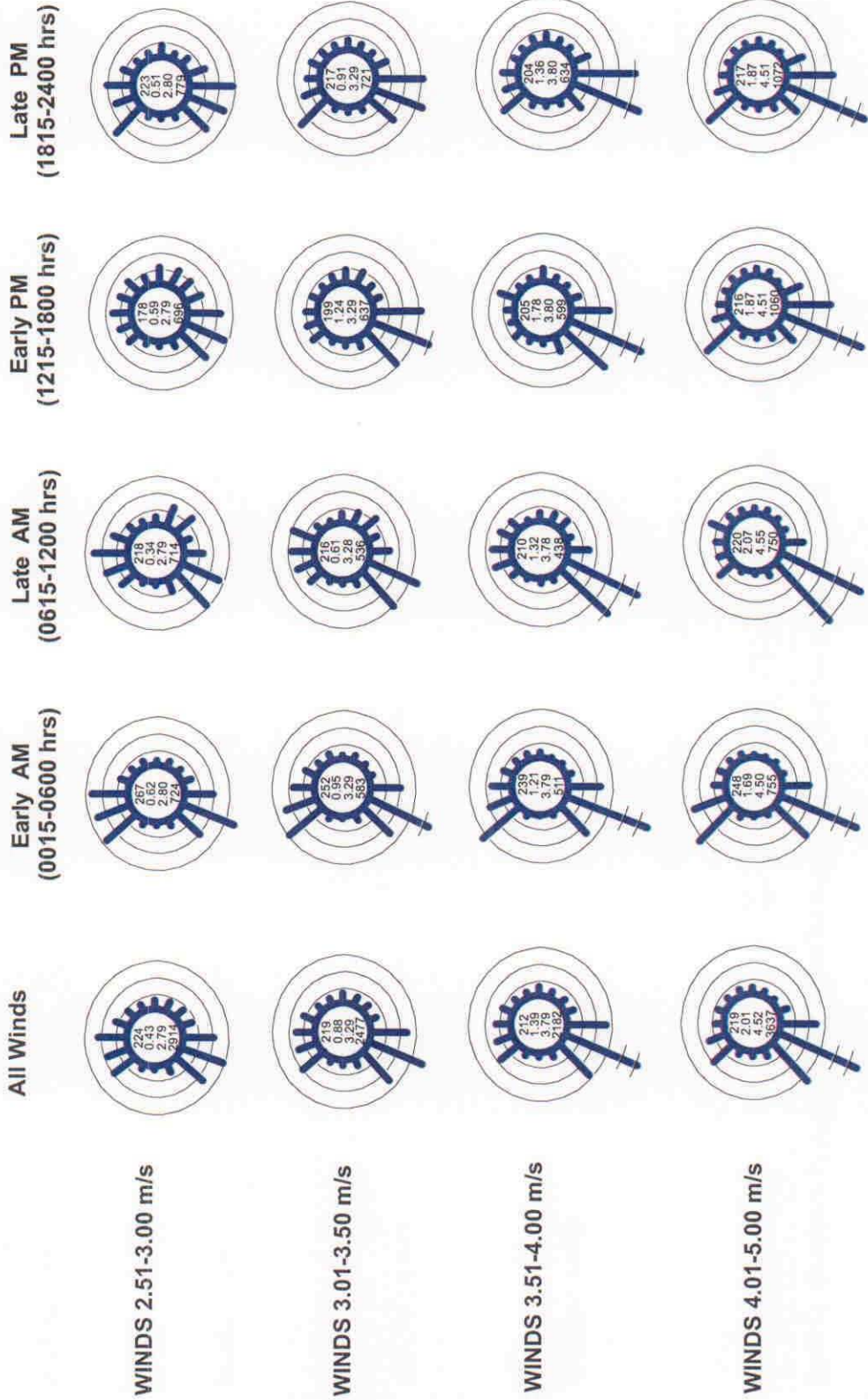


Part 1: Analysis of Wind Rose Change with Respect to Low Wind Speeds



Section: INEEL (Snake River Basin)
Topographic Zone: Low Valley

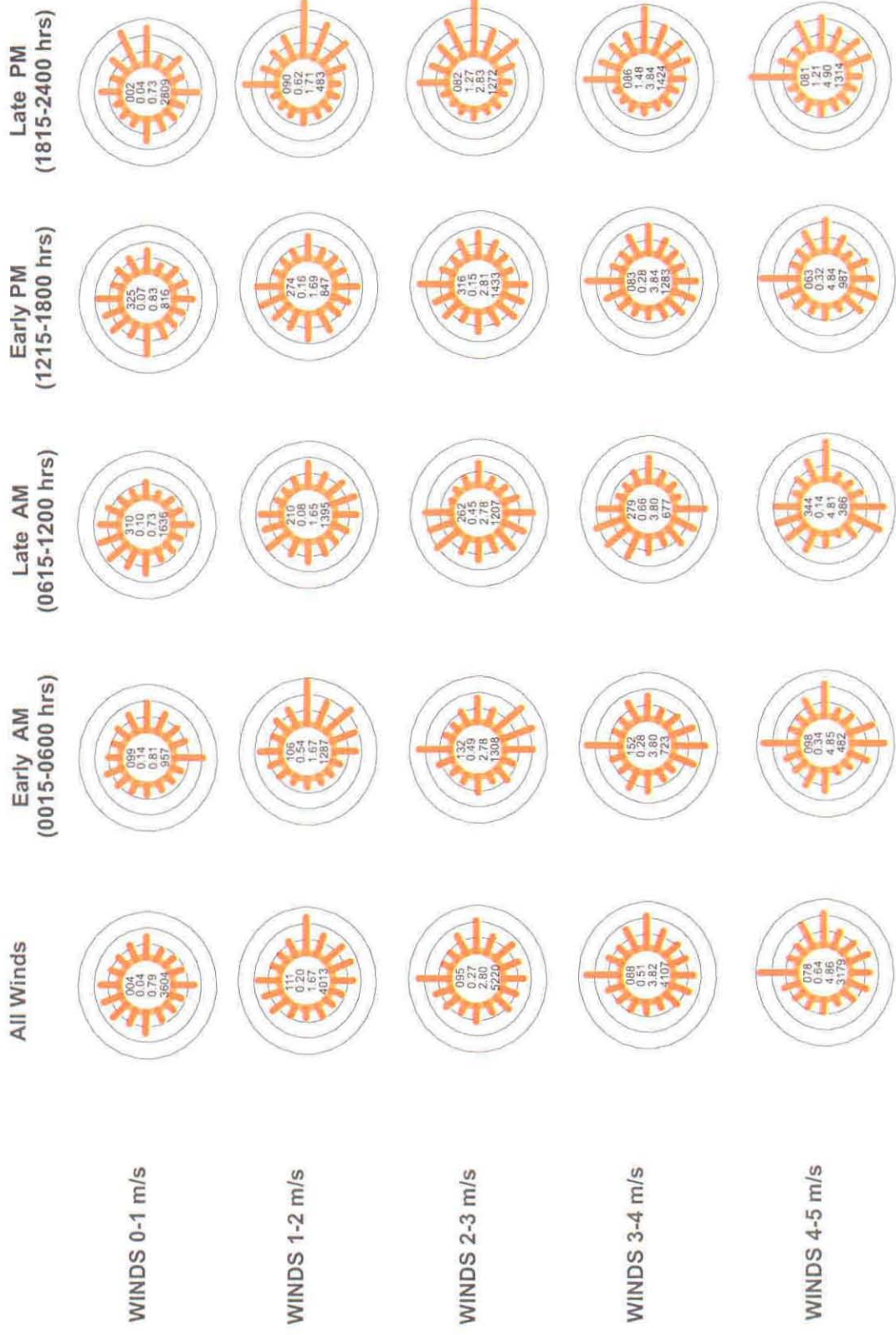
Site: IDA, Idaho Falls, Lat 43 31 N, Long 112 04 W, Altitude 1438 m
Period of Record: January 1994 - December 1997





Part 1: Analysis of Wind Rose Change with Respect to Low Wind Speeds

Section: CAPE
 Topographic Zone: Coast
 Site: Cape Canaveral, FL, Lat 28 30 N, Long 80 36 W, Altitude 3 m
 Period of Record: January 1991 - August 1993



Appendix B

Wind Rose Analysis With Respect to Low Wind Speeds

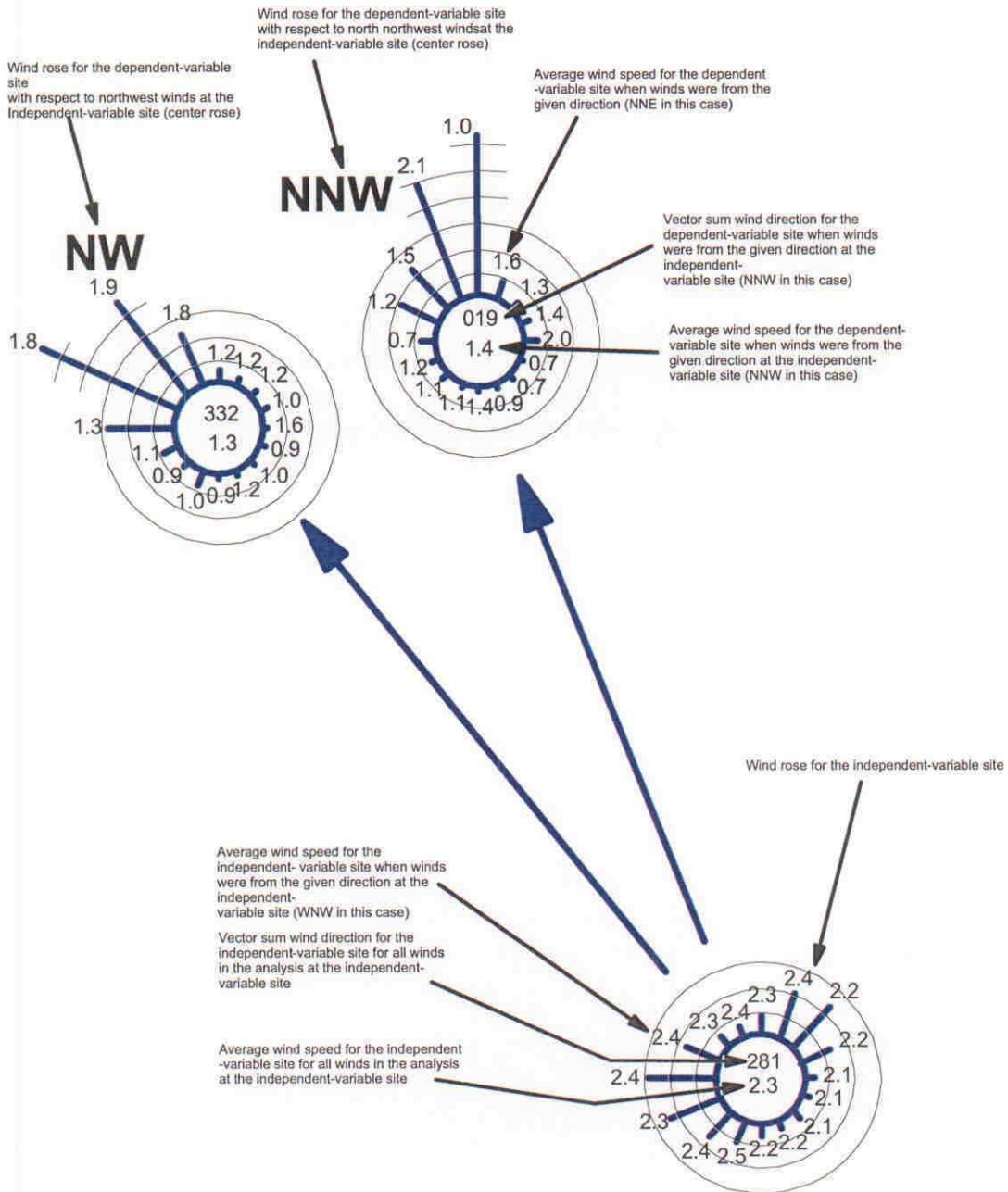
Part 2: Changes in Wind Direction and Speed with Respect to Winds Aloft Plots

Part 2: Change in Wind Direction and Speed with Respect to Winds Aloft



KEY TO WIND ROSE INTERPRETATION (Partial Chart Shown for Illustration)

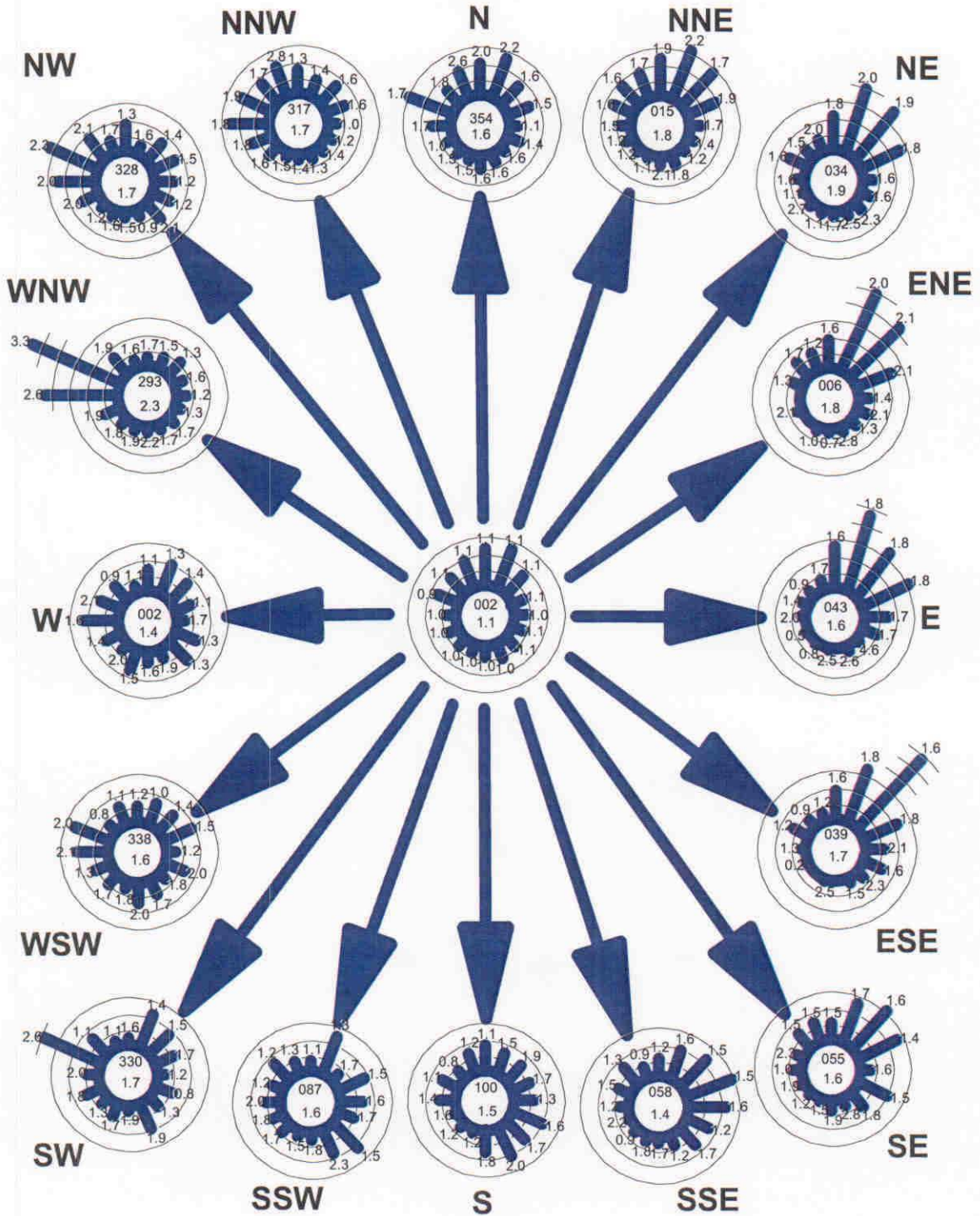
All wind direction measurements are given in degrees (0 to 360)
 All wind speed measurements are given in meters per second (m/s)
 Each ring equals 5% frequency of wind direction for all wind roses



Part 2: Change in Wind Direction and Speed with Respect to Winds Aloft



Resultant Winds at Pine Ridge (Outer Wind Roses) for Light Winds (< 1.5 m/s) at Buffalo Mountain (Center Wind Rose)

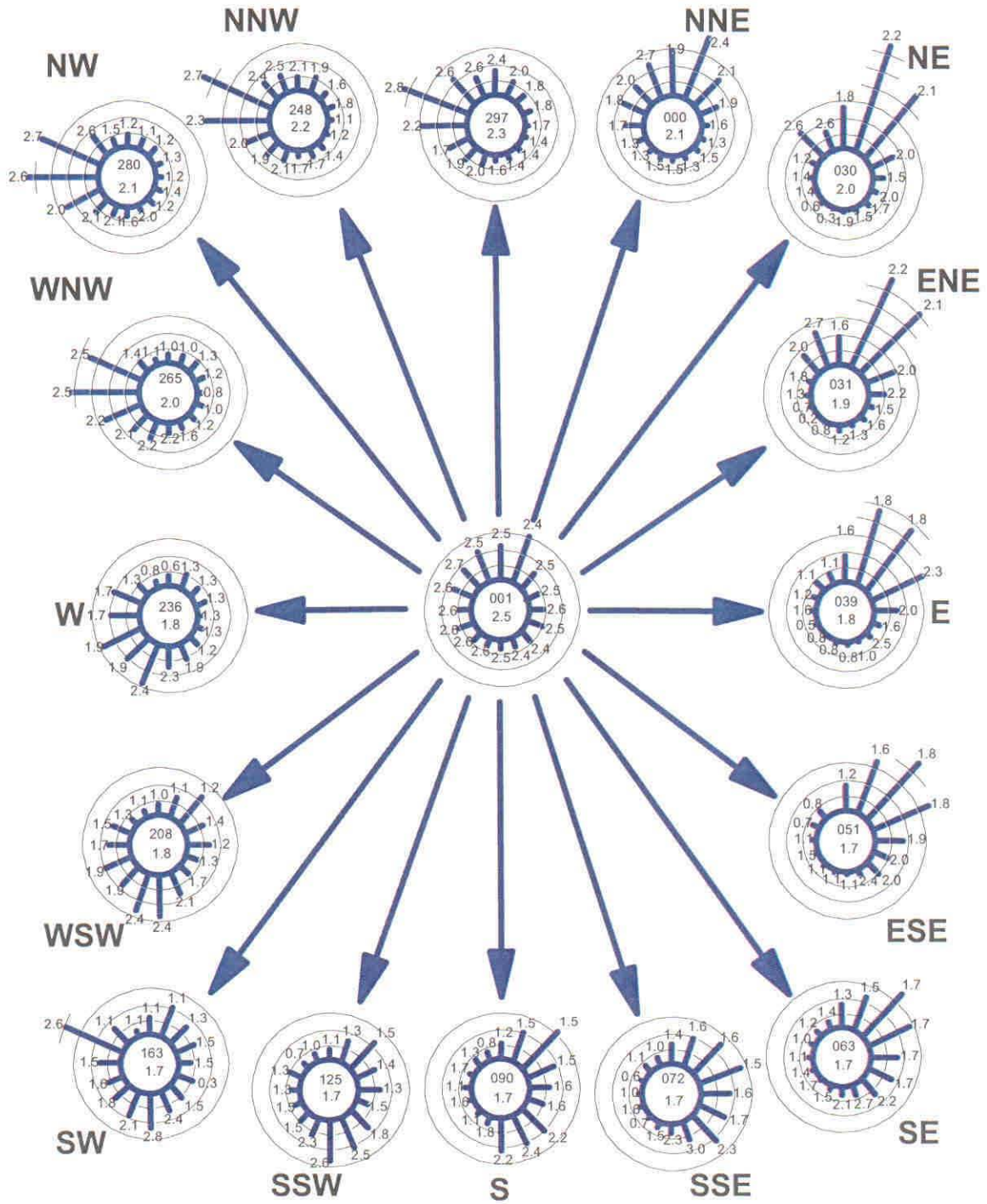


Part 2: Change in Wind Direction and Speed with Respect to Winds Aloft



Resultant Winds at Pine Ridge (Outer Wind Roses) for Moderate Winds (1.5 - 3.5 m/s) at Buffalo Mountain

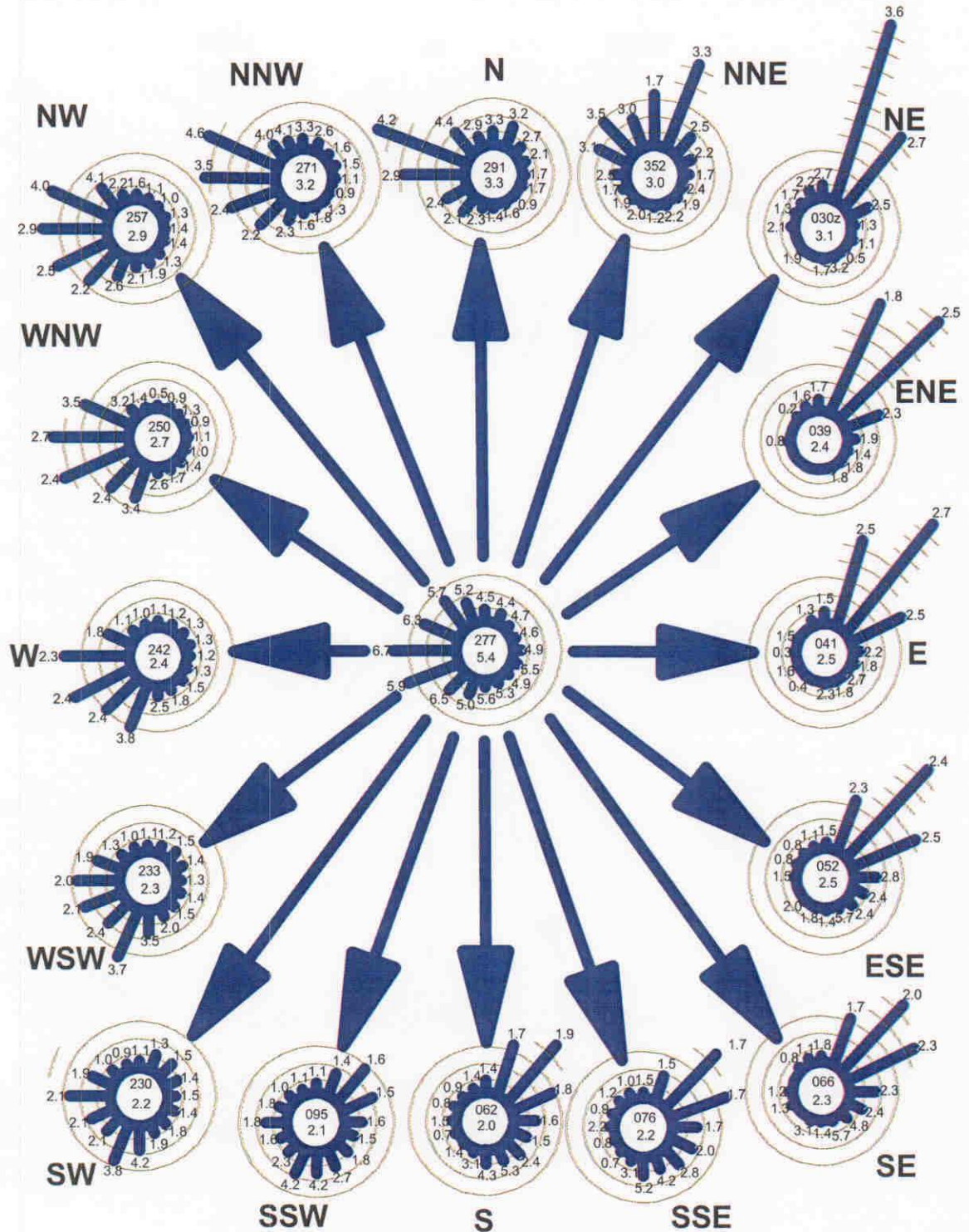
(Center Wind Rose)



Part 2: Change in Wind Direction and Speed with Respect to Winds Aloft



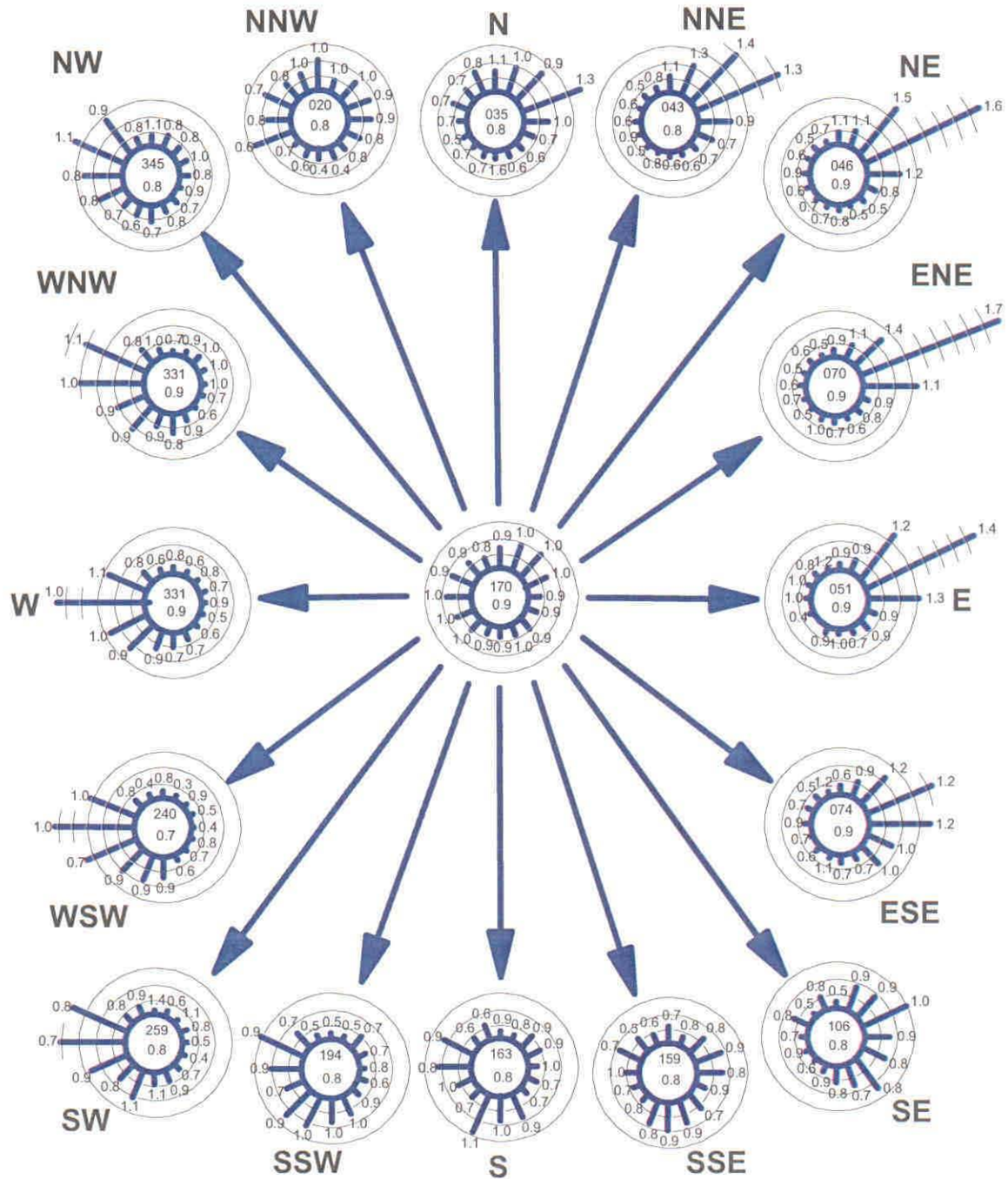
Resultant Winds at Pine Ridge (Outer Wind Roses) for Strong Winds (> 3.5 m/s) at Buffalo Mountain (Center Wind Rose)
(Center Wind Rose)



Part 2: Change in Wind Direction and Speed with Respect to Winds Aloft



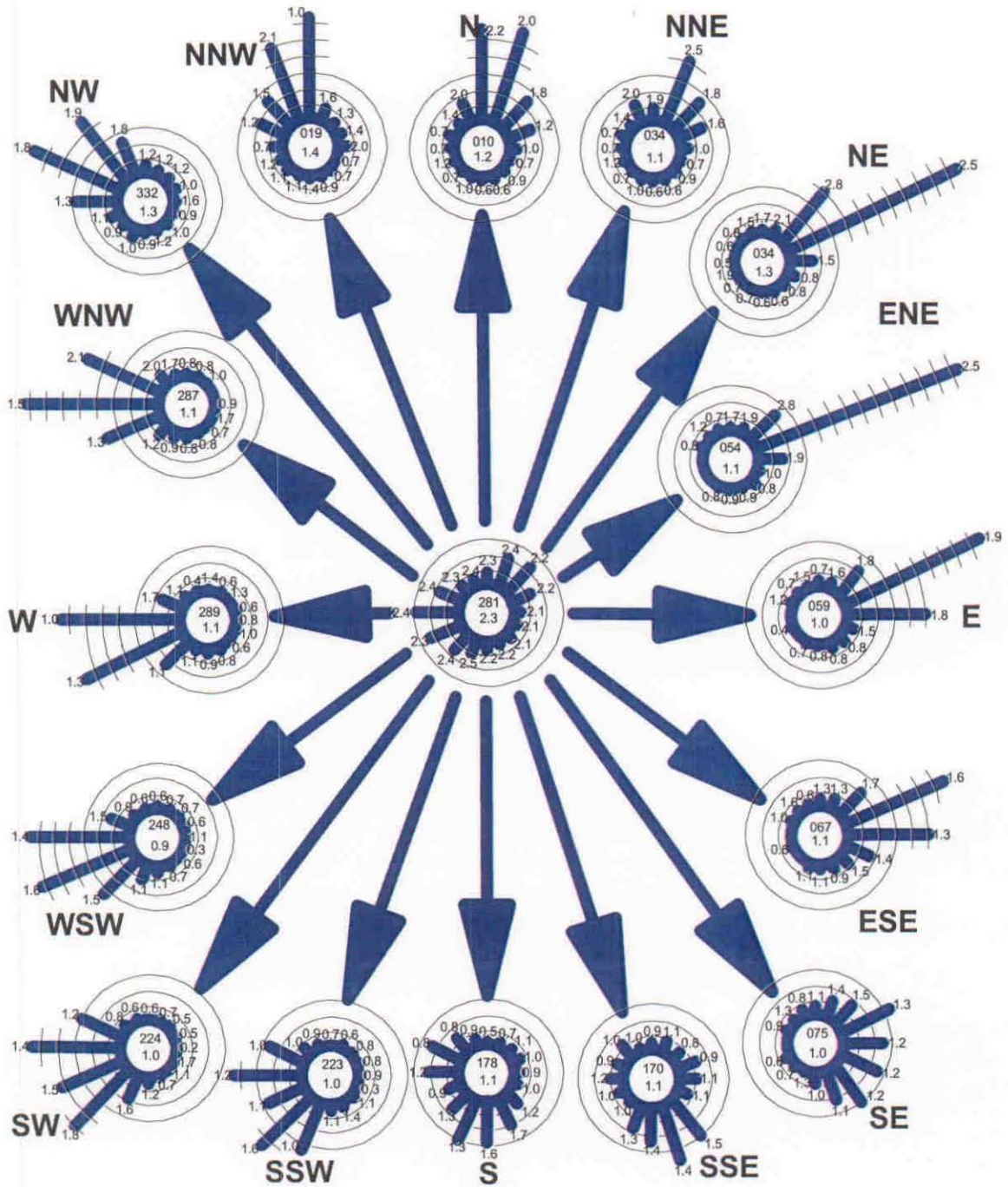
Resultant Winds at Oak Ridge Municipal Building (Outer Wind Roses) for Light Winds (< 1.5 m/s) at Pine Ridge (Center Wind Rose)



Part 2: Change in Wind Direction and Speed with Respect to Winds Aloft



Resultant Winds at Oak Ridge Municipal Building (Outer Wind Roses) for Moderate and Strong Winds (= or > 1.5 m/s) at Pine Ridge (Center Wind Rose)



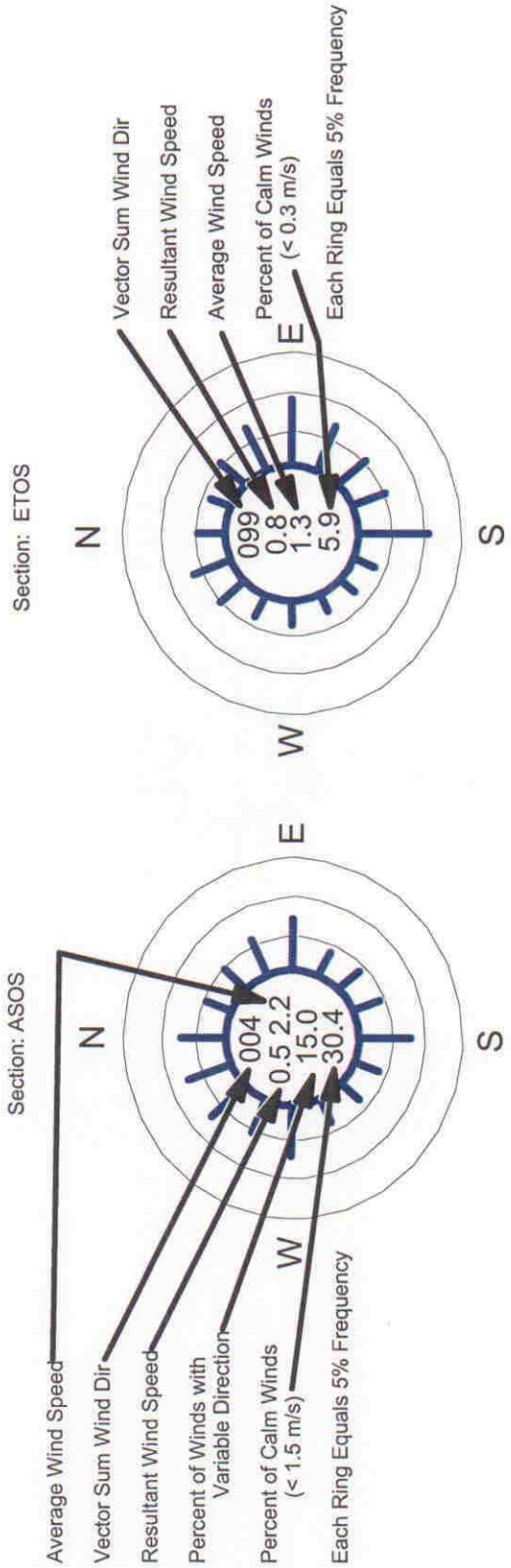
Appendix C

Wind Rose Analysis With Respect to Low Wind Speeds

Part 3: Wind Rose Computation by Site and Time of Day and Subsequent Site to Site Comparison Plots

Part 3: Wind Rose Computation by Site and Time of Day and Subsequent Site to Site Comparisons

KEY TO WIND ROSE INTERPRETATION



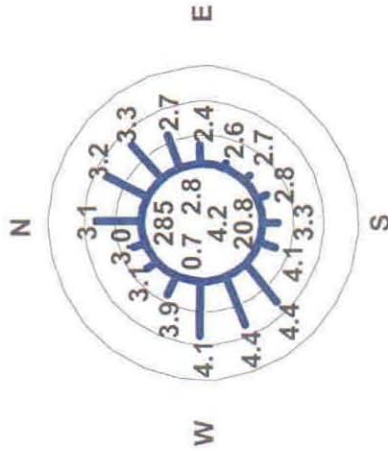
All Wind Direction measurements are given in degrees (0 to 360)
 All Wind Speed measurements are given in meters per second (m/s)

Part 3: Wind Rose Computation by Site and Time of Day and Subsequent Site to Site Comparisons

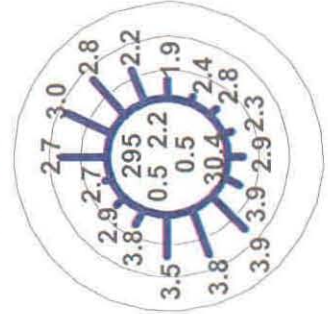


Section: ASOS
 Topographic Zone: Valley Bottom
 Site: Knoxville McGhee-Tyson Airport, Lat 35 49 N, Long 83 59 W, Altitude 293 m, Tower Ht 9 m
 Period of Record: January 1998 - February 2000

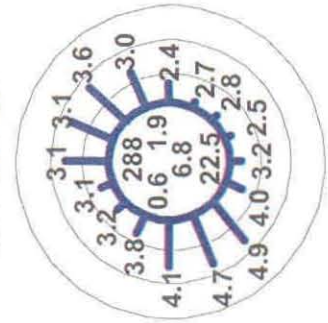
ALL WINDS



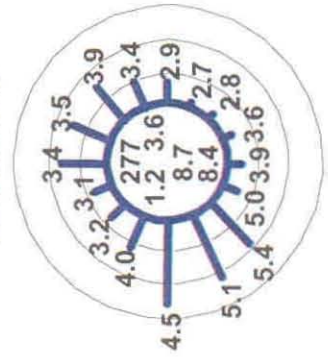
EARLY AM WINDS 0001-0600 hrs



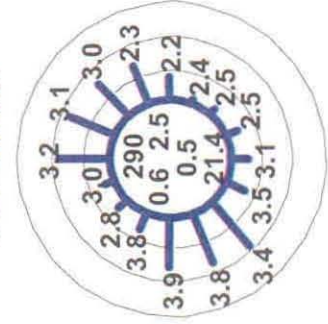
LATE AM WINDS 0601-1200 hrs



EARLY PM WINDS 1201-1800 hrs



LATE PM WINDS 1801-2400 hrs

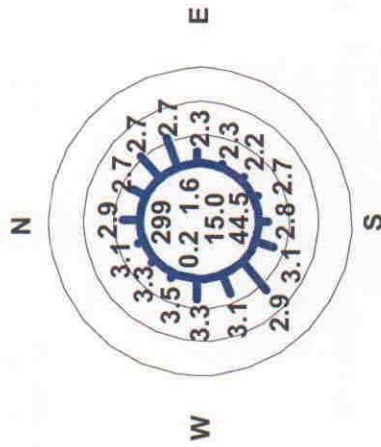


Part 3: Wind Rose Computation by Site and Time of Day and Subsequent Site to Site Comparisons

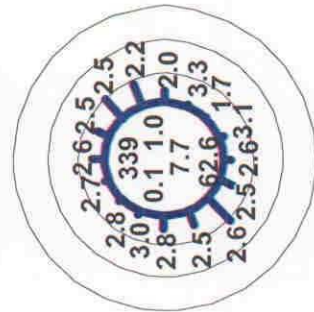


Section: ASOS
 Topographic Zone: Valley Bottom
 Site: Oak Ridge, TN; Lat 36 01 N, Long 84 14 W, Altitude 277 m, Tower Ht 9 m
 Period of Record: January 1998 - February 2000

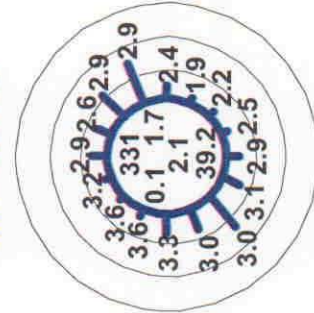
ALL WINDS



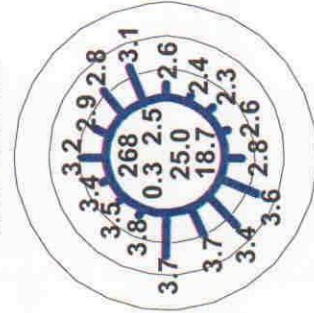
**EARLY AM WINDS
 0001-0600 hrs**



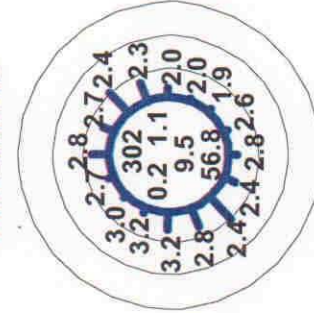
**LATE AM WINDS
 0601-1200 hrs**



**EARLY PM WINDS
 1201-1800 hrs**



**LATE PM WINDS
 1801-2400 hrs**

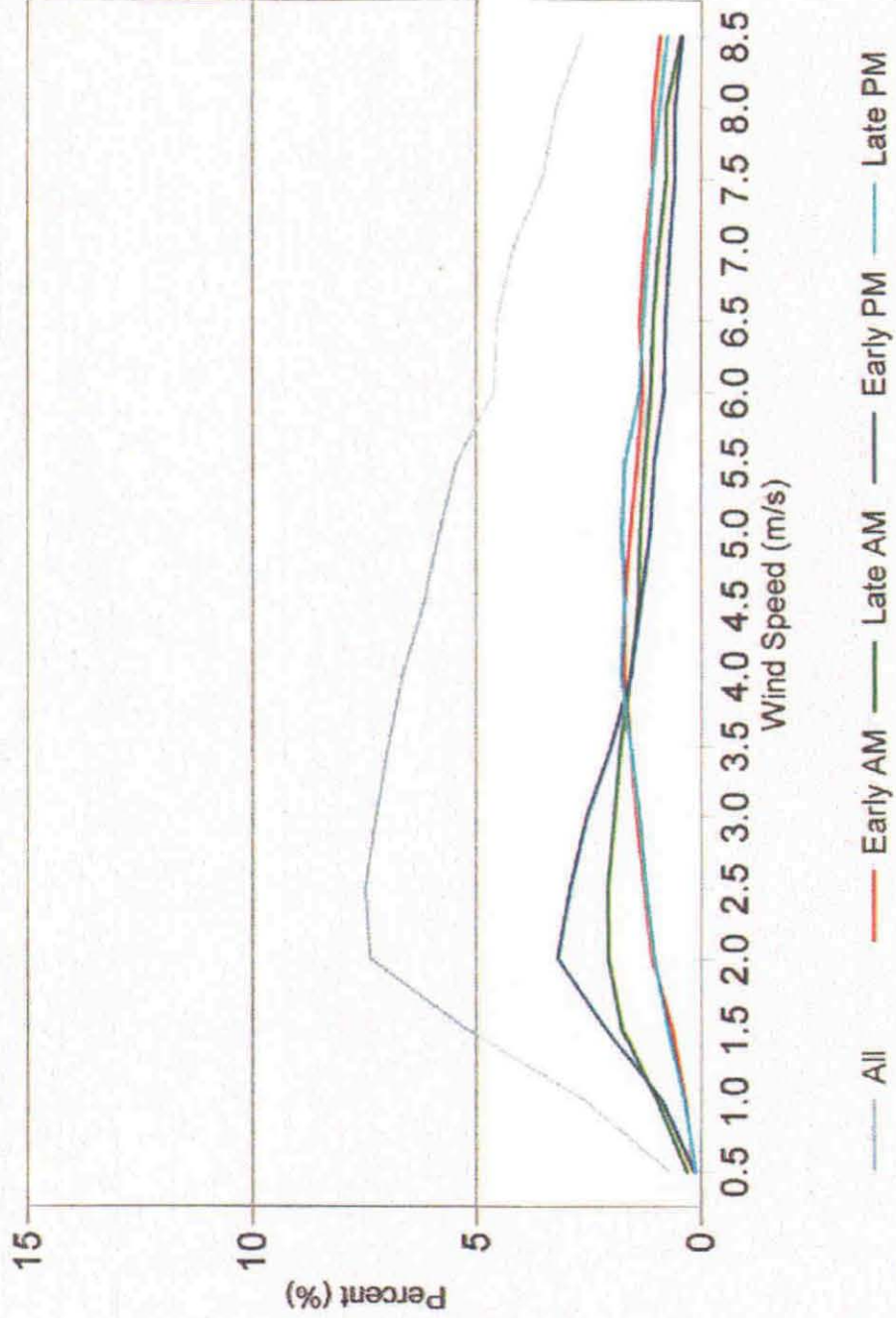


Appendix D

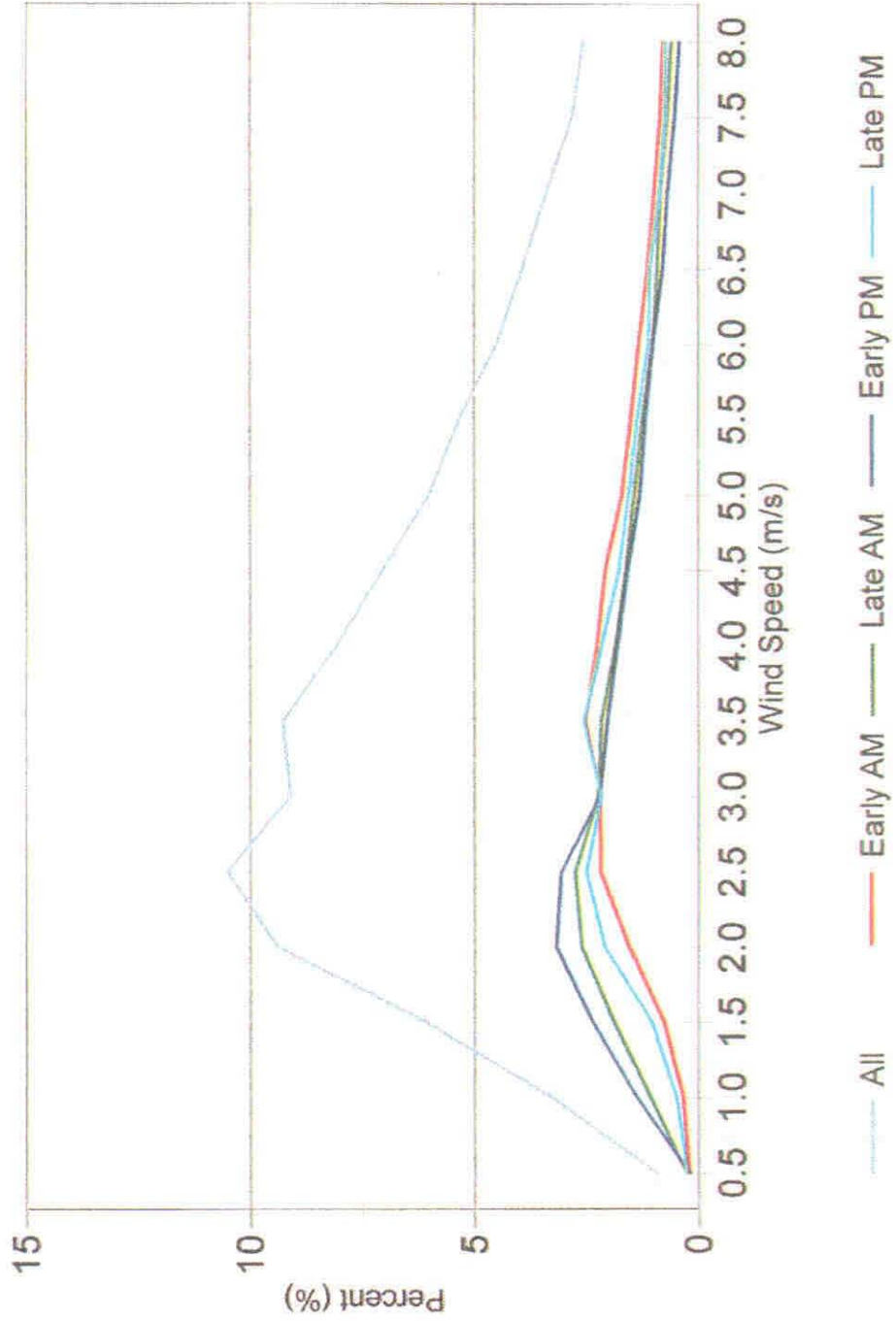
Wind Rose Analysis With Respect to Low Wind Speeds

Part 4: Wind Speed Distribution with Respect to Time of Day Plots

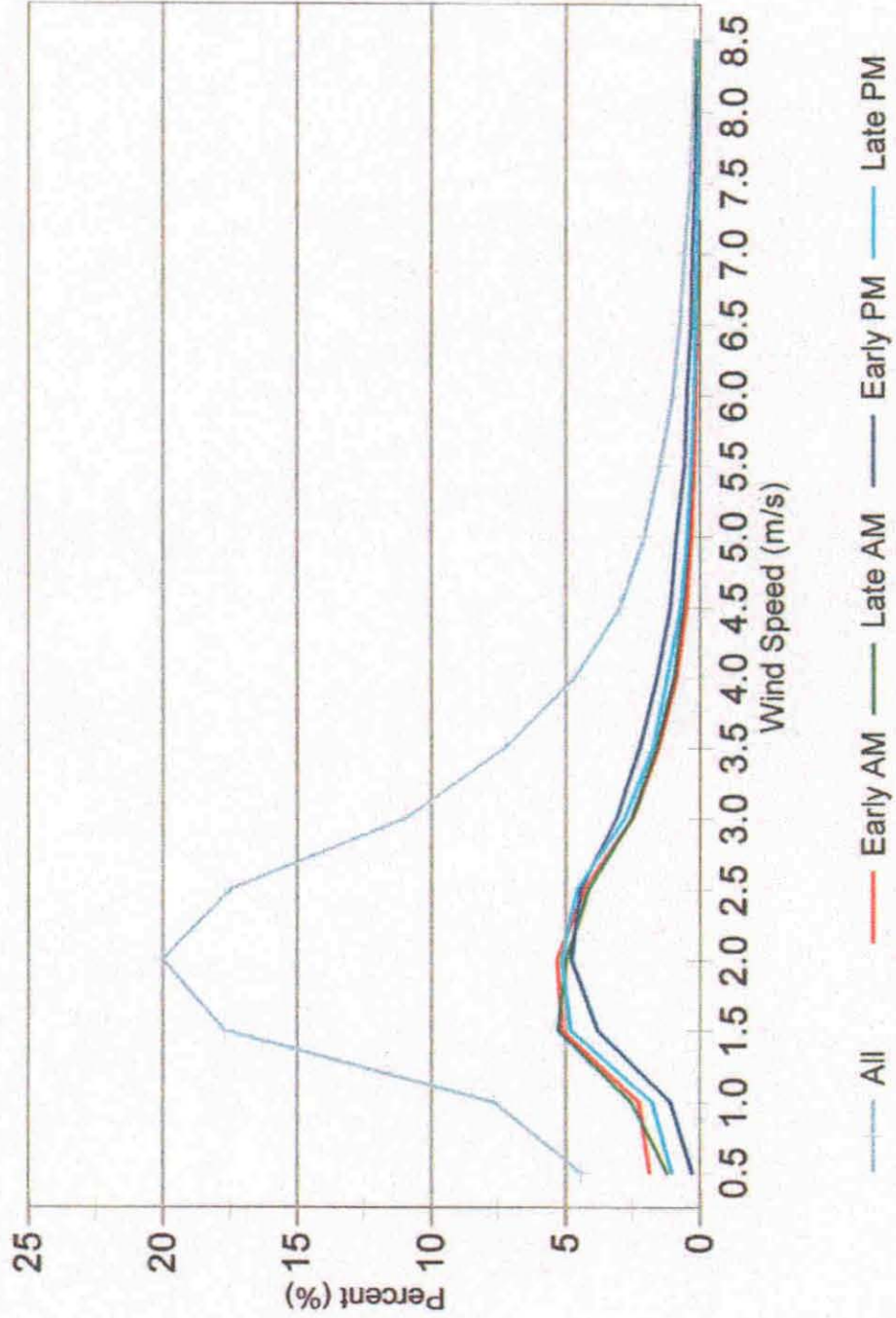
Site T223: Cove Mountain
Wind Speed Distribution



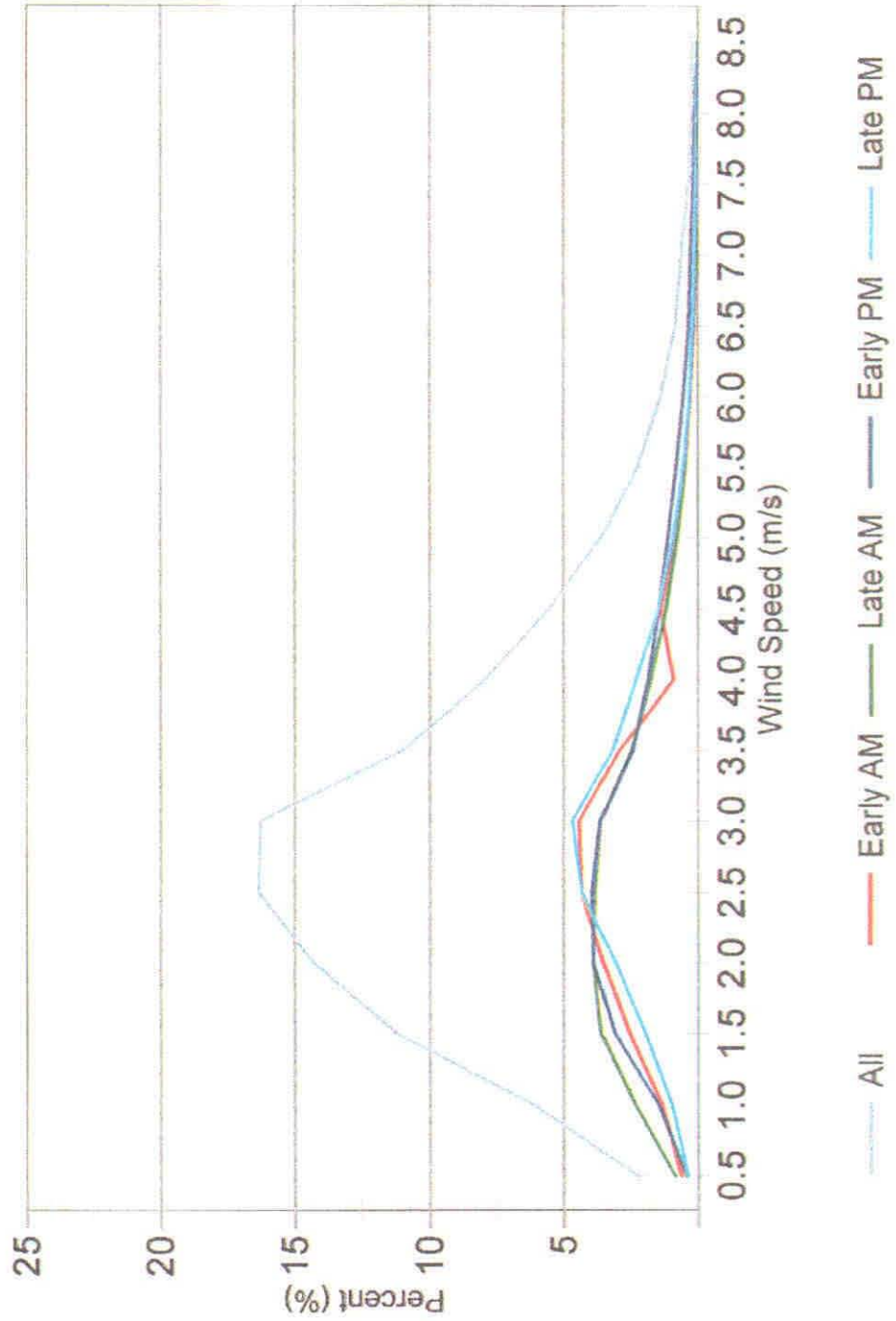
Site T224: Buffalo Mountain
Wind Speed Distribution



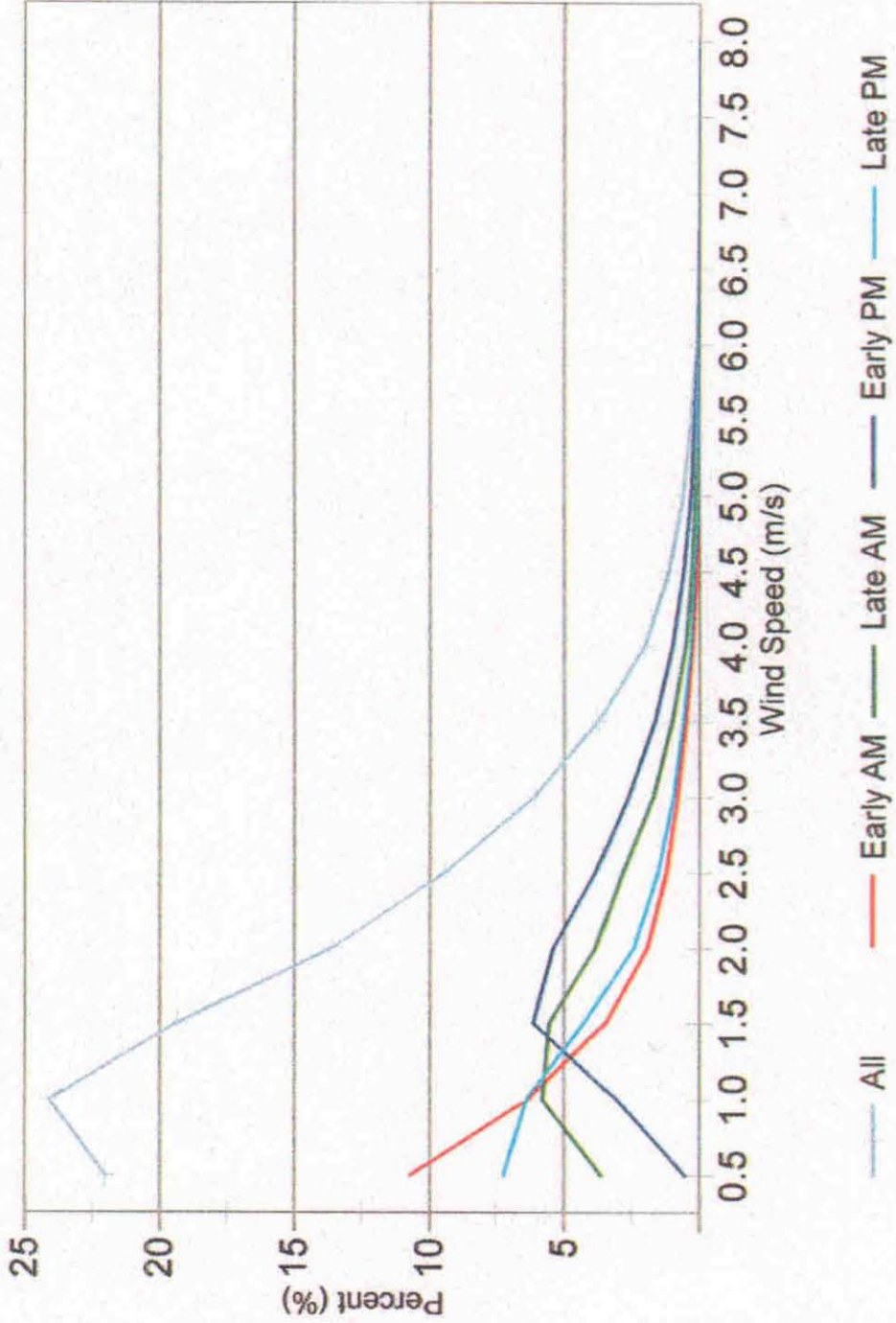
Site T110: Pine Ridge
Wind Speed Distribution



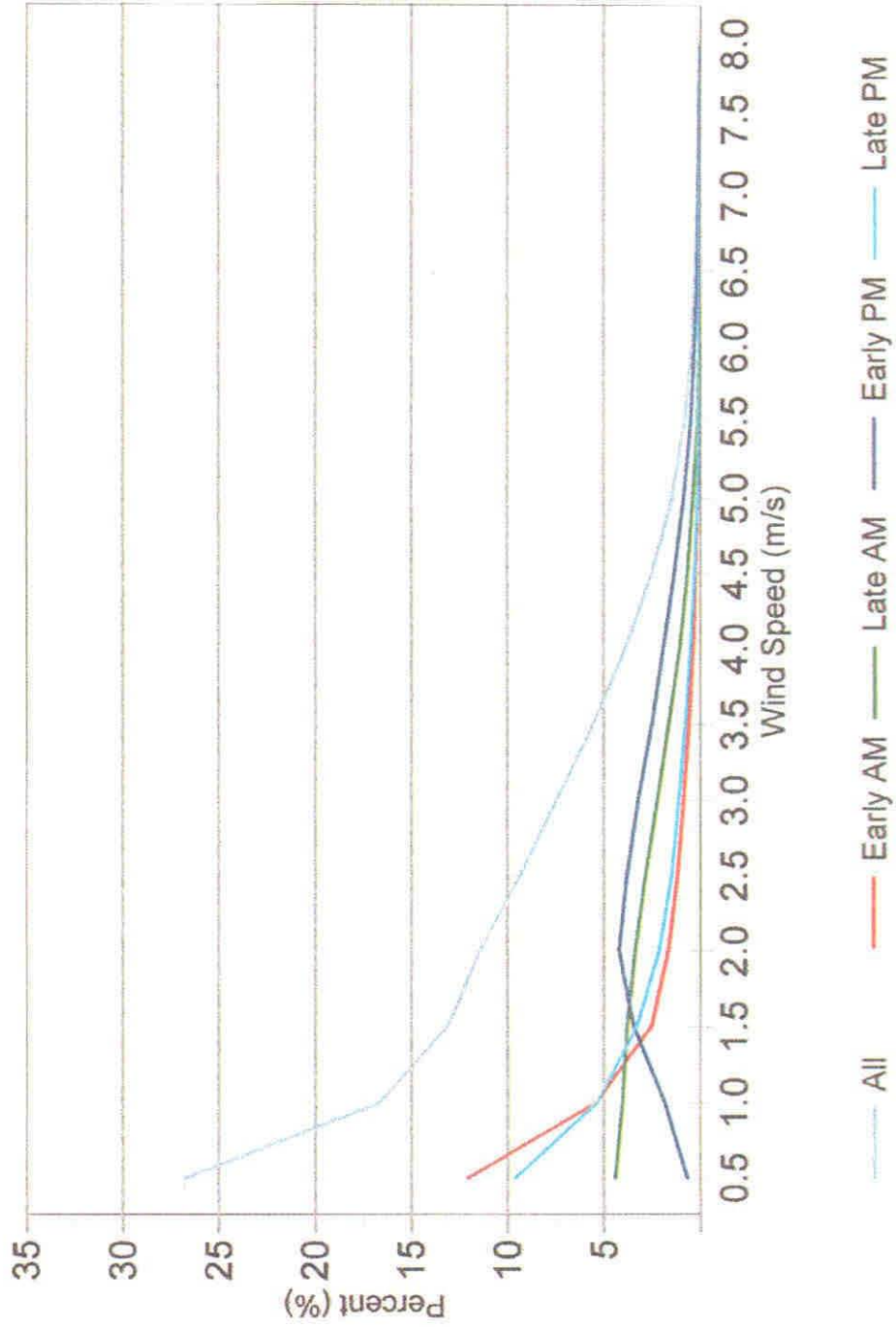
Site T119: Walker Branch
Wind Speed Distribution



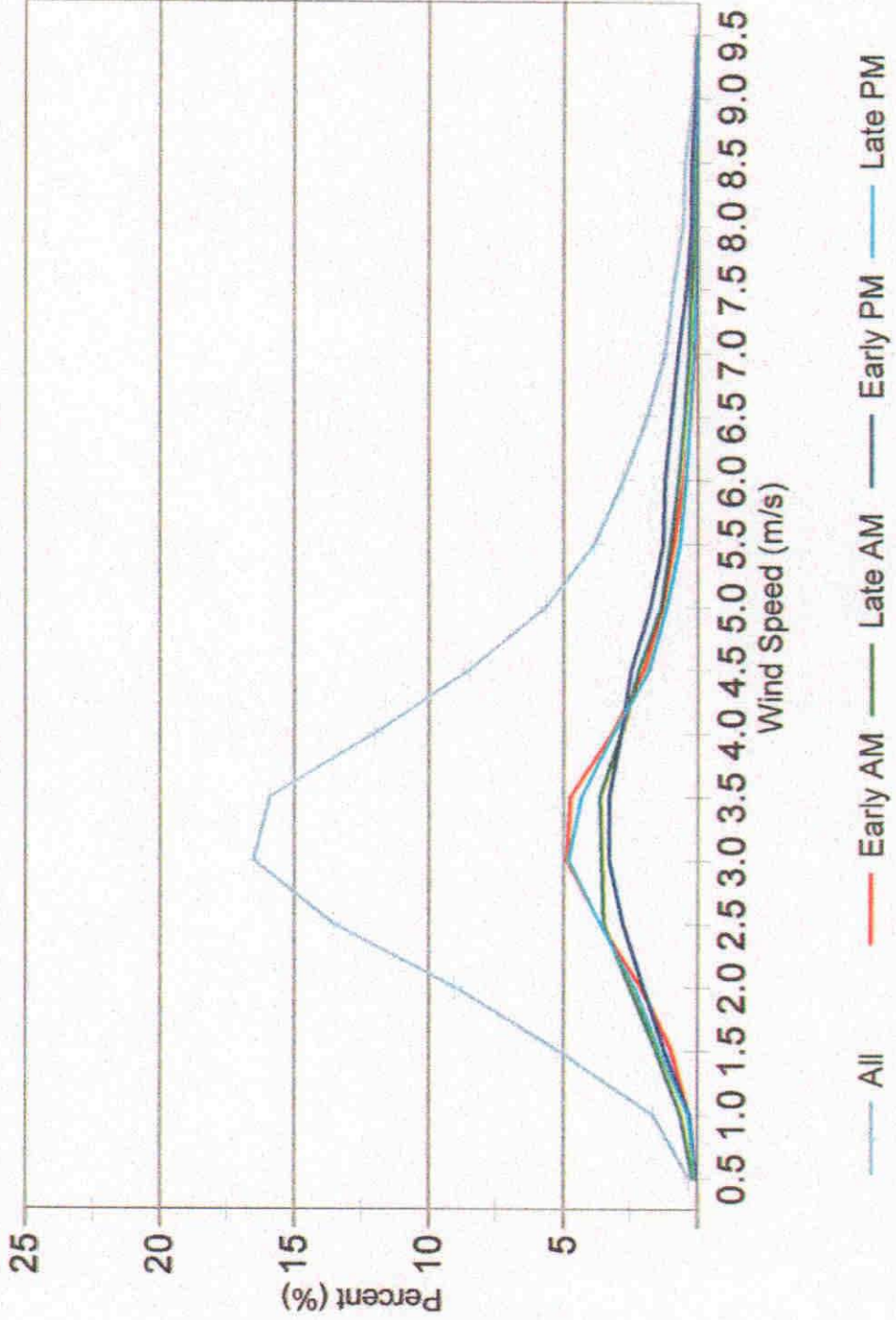
Site T001: NOAA Office
Wind Speed Distribution



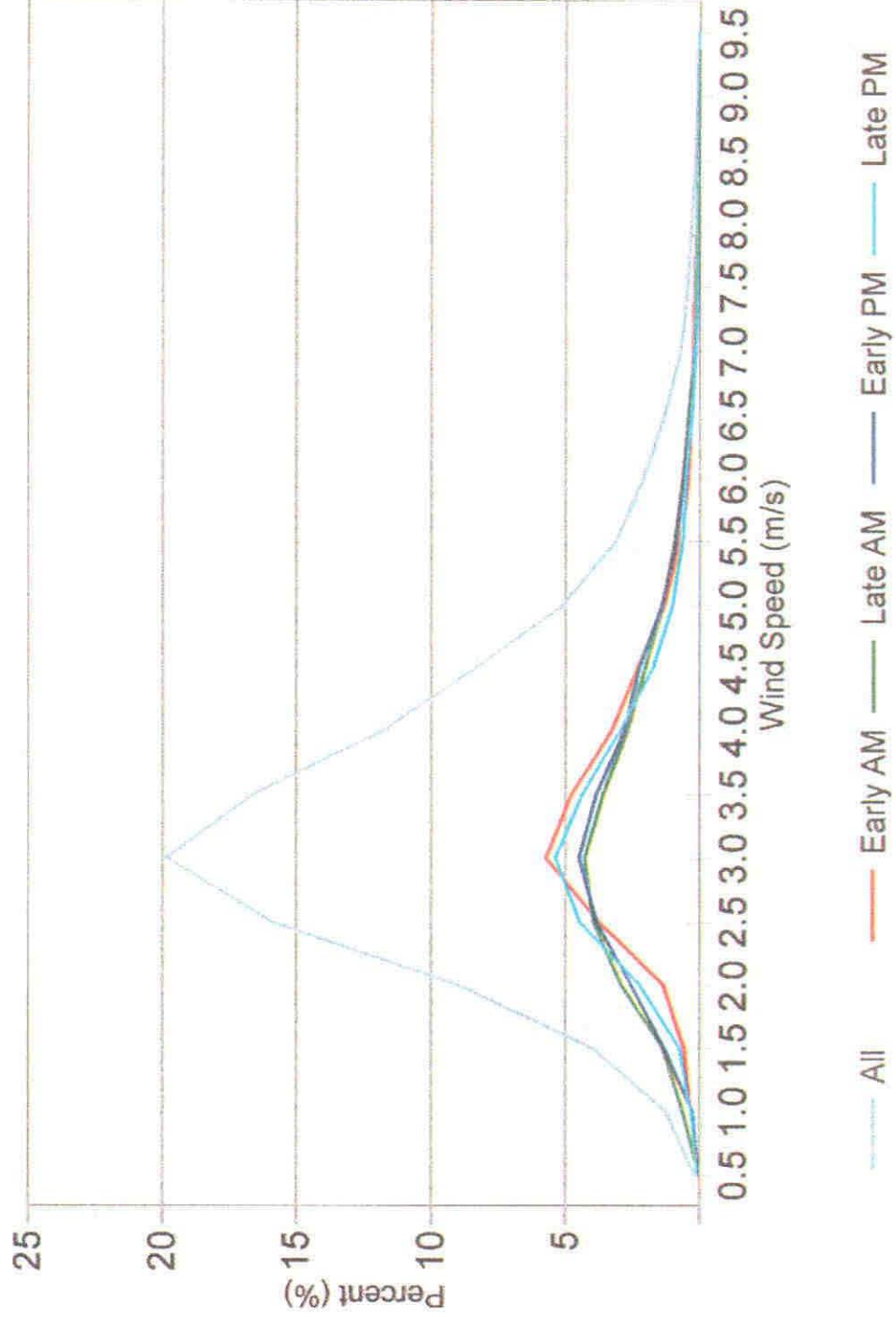
Site T004: Scarborough
Wind Speed Distribution



Site T330: Allardt
Wind Speed Distribution



Site T331: Spencer
Wind Speed Distribution

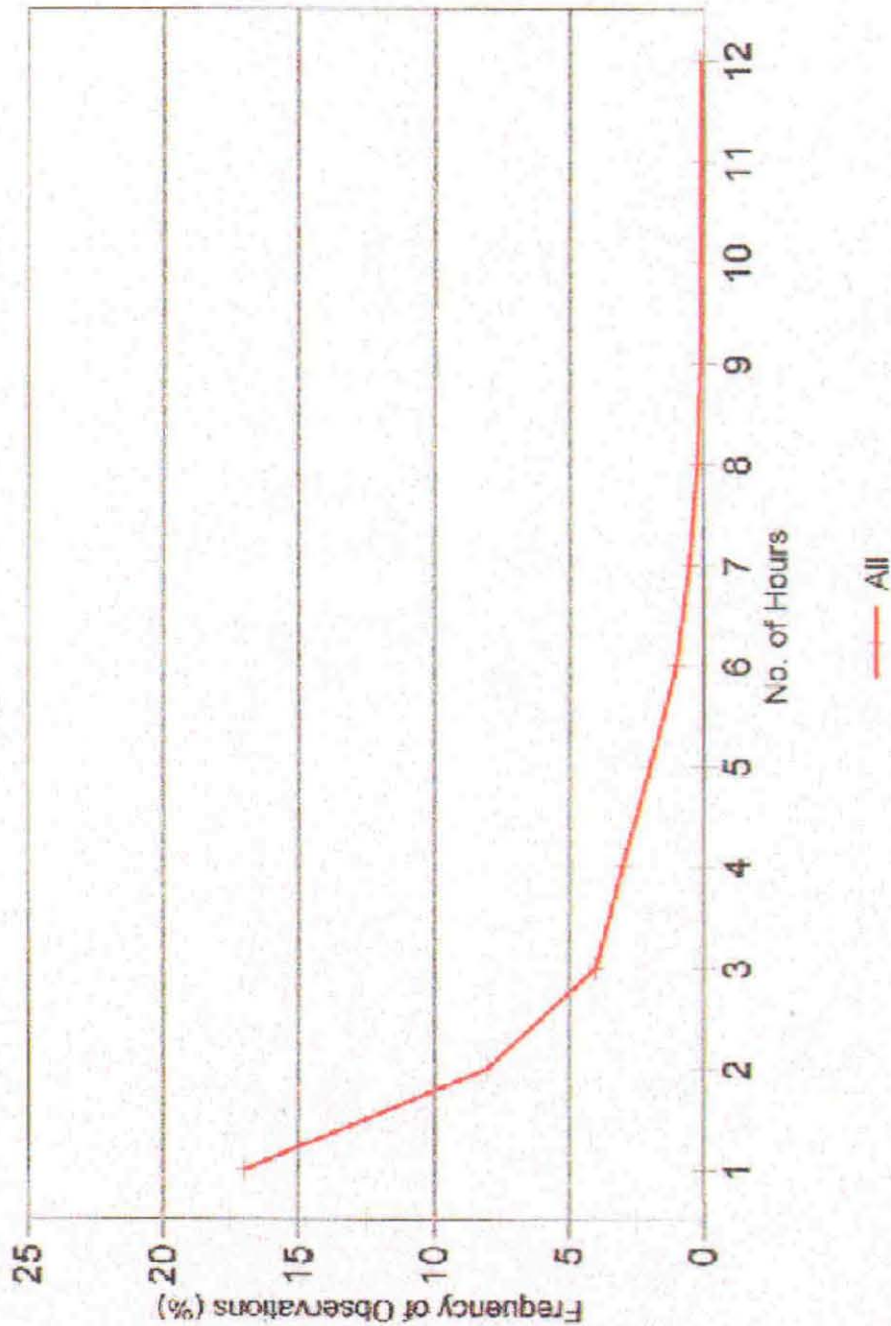


Appendix E

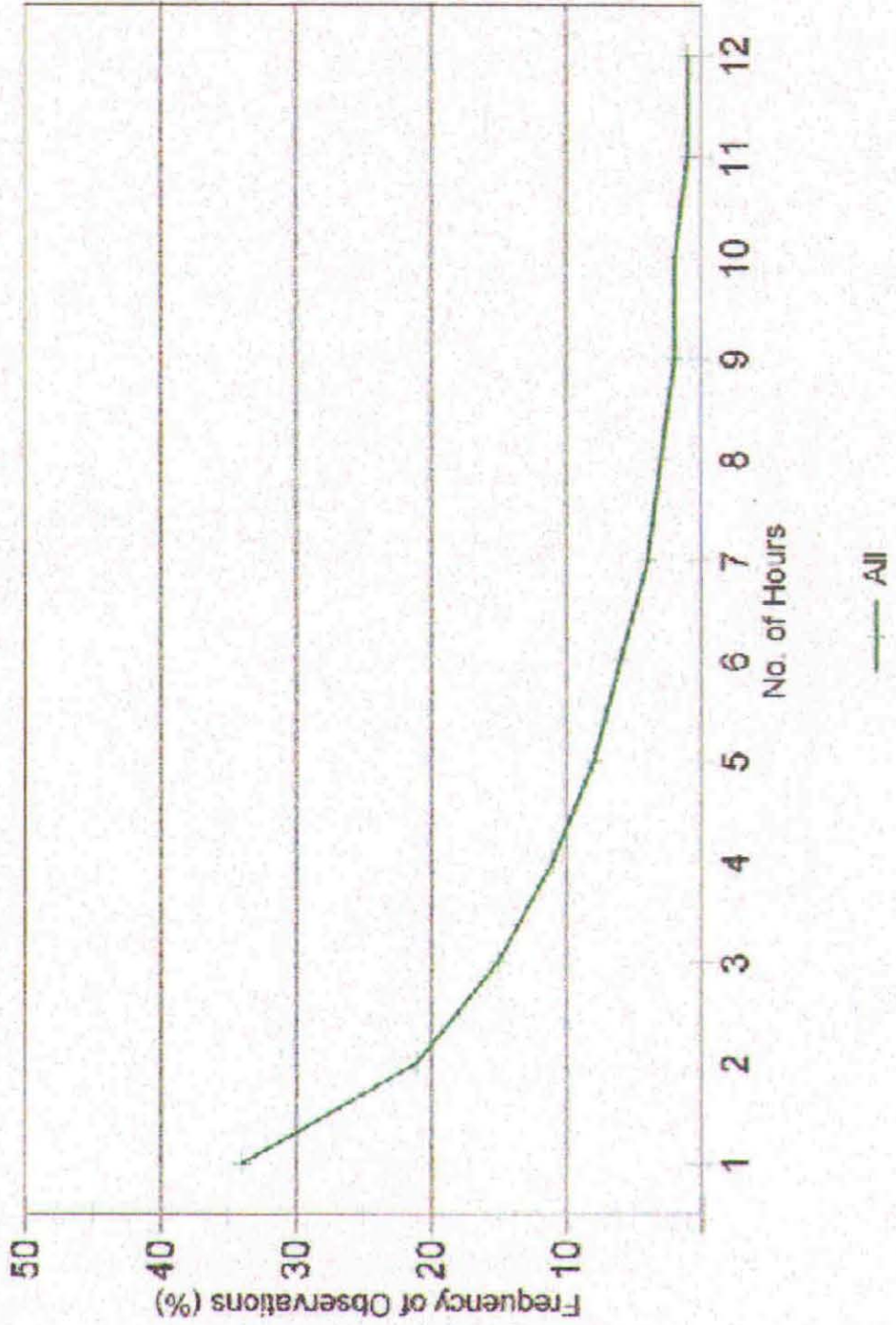
Wind Rose Analysis With Respect to Low Wind Speeds

Part 5: Duration of Calm and Light Winds Plots

Knoxville McGhee-Tyson Airport
Duration of Winds < 0.5 m/s 1961-1993



Knoxville McGhee-Tyson Airport
Duration of Winds < 2.0 m/s 1991-1993



Knoxville McGhee-Tyson Airport

Duration of Winds < 3.5 m/s 1991-1993

